3-ACETAMIDO-5-ACETYLFURAN FROM *N*-ACETYL-D-GLUCOSAMINE: ITS SYNTHESIS, PROPERTIES AND APPLICATIONS

by

© Yi Liu

A thesis submitted to the

School of Graduate Studies

in partial fulfillment of the requirements for the degree of

Doctor of Philosophy

Department of Chemistry

Memorial University of Newfoundland

July, 2017

St. John's Newfoundland

ABSTRACT

In recent years, biomass has been developed as a resource for production of biofuels and renewable chemicals. 5-Hydroxymethylfurfural (5-HMF) is an important platform compound for a variety of value-added chemicals. 5-HMF can be obtained from the dehydration of lignocellulosic biomass such as fructose, glucose, sucrose and cellulose. There have been numerous studies on the synthesis of 5-HMF, among which many were focused on the mechanisms. The tools and approaches used for mechanistic studies on the transformation of biomass to 5-HMF were reviewed, showing that both lab techniques (e.g. NMR spectroscopy, kinetic studies) and computational calculations can be used for intermediate detection and mechanism investigation. It is proposed that the methods used with this class of renewable feedstock will be valuable in studying the reactions of related nitrogen-containing carbohydrates.

N-Acetyl-D-glucosamine (NAG) is an amino sugar and the monomer of chitin, which occurs abundantly in the shells of crustaceans. The dehydration of NAG produces a renewable amide, 3-acetamido-5-acetylfuran (3A5AF). When ionic liquids (ILs) were used as solvents, the 3A5AF yield was influenced by the acidity of the ILs. The addition of boric acid ($B(OH)_3$) and sodium chloride (NaCl) improved the 3A5AF yield. Ethyl acetate (EtOAc) was added for in situ extraction of 3A5AF during the reaction, and an optimum yield of 55.6% was achieved. Kinetic studies were performed for the dehydration of NAG and its two isomers (NAGal, NAMan) in the presence of $B(OH)_3$. Chromogen I and III were proposed as important intermediates in the mechanism, as their characteristic peaks

were observed in the ^{1}H NMR spectra of NAG dehydration. ^{11}B NMR spectroscopy was performed to study the role of $B(OH)_3$ in the dehydration of NAG. The reusability of [Bmim]Cl in the conversion of NAG to 3A5AF was studied.

The pK_a of 3A5AF was determined through both computational calculations and experimental measurements. The solubility of 3A5AF in supercritical carbon dioxide ($scCO_2$) was low, mainly due to the strong intermolecular forces between 3A5AF molecules. Dimerization energies of 3A5AF were calculated, and IR and NMR analyses were performed to investigate the hydrogen bonding. The highest occupied molecular orbital, lowest unoccupied molecular orbital, electrostatic potential and atomic charges of 3A5AF were determined through molecular orbital calculations. A reaction between 3A5AF and a methyl Grignard reagent was performed to study the reactivity of the two carbonyl carbons towards a nucleophile.

Hydrolysis of 3A5AF was performed via sodium hydroxide (NaOH) catalysis and an amino-substituted furan product was obtained. Reduction of the acetyl group in 3A5AF was achieved using sodium borohydride ($NaBH_4$) or catalytically via transfer-hydrogenation using an iridium (Ir) catalyst. 3A5AF and the hydrolysis product were tested for CO_2 capture, but no reaction was observed because of their inherent acidity. Tautomerism of 3A5AF was observed in methanol-d_4 (CD_3OD) as evidenced by H-D exchange within the acetyl group.

DEDICATION

To my husband, Hui, for his patience, understanding and support during my PhD program.

To my parents and my sister, for all their unconditional support and encouragement in my life.

ACKNOWLEDGEMENTS

I would like to acknowledge my supervisor, Prof. Francesca M. Kerton, for giving me the opportunity to study in the group and offering me all kinds of guidance, encouragement, understanding and support. Thanks for her trust and patience in my work. Her revisions and helpful comments during my thesis writing are greatly appreciated. I am also grateful that she shared my happiness and gave me support when I was sad in my life. I would also like to thank my supervisory committee members, Prof. Christopher M. Kozak and Prof. Travis D. Fridgen, for their valuable suggestions during the annual meetings and kind comments on my thesis. Thank you to all the Green Chemistry and Catalysis Group members, past and present, for the shared knowledge and help. Special thanks to the visiting undergraduate German students, Karen Strassel and Cosima Stähler, for their help in my research. My deep gratitude to Prof. Christopher N. Rowley, for his guidance and support in the computational work. Thanks to Prof. Kelly Hawboldt for her advice on CO_2 capture and funding via a Mitacs internship cluster with Suncor Energy. Thank you to Prof. Ning Yan (National University of Singapore) for the nice collaboration with us. I also extend my thanks to Dr. Céline Schneider, Dave Davidson and Linda Winsor for their help in analysis in C-CART (Centre for Chemical Analysis, Research and Training). Thanks to Nick Ryan for his help with IR experiments. All staff in the Chemistry Department's main office are deeply thanked. Finally, I would like to express thanks to Department of Chemistry, School of Graduate Studies (SGS), Graduate Students' Union (GSU) and Memorial University for the services and financial support.

Table of Contents

List of Tables

Chapter 2

Chapter 3

List of Figures

Chapter 1

Chapter 2

Chapter 3

Chapter 4

Chapter 5

List of Schemes

Chapter 1

Chapter 2

Chapter 3

Chapter 4

Chapter 5

List of Equations

List of Symbols, Nomenclature or Abbreviations

A: pre-exponential factor

ATR-IR: attenuated total reflection infrared

ca.: approximately (Latin *circa*)

cf.: compare (Latin *confer*)

CN: coordination number

CP: cross polarization

CPMD-MTD: Car-Parrinello based ab initio molecular dynamics coupled with metadynamics

δ: chemical shift in parts per million downfield from a standard

DEPT: distortionless enhancement by polarization transfer

E_a: activation energy

E-factor: environmental factor

e.g.: for example (Latin *exempli gratia*)

equiv.: equivalent

ESI-MS/MS: electrospray ionization tandem mass spectrometry

ESP: electrostatic potential

et al.: and others (Latin *et alii*)

etc.: and so forth (Latin *et cetera*)

EXAFS: extended X-ray absorption fine structure

ε: extinction coefficient

FCM: functional carbon material

FD: factorial design

GES: Gibbs energy surface

FT-IR: fourier transform infrared

GC-MS: gas chromatography-mass spectrometry

HOMO: highest occupied molecular orbital

HPLC: high-performance liquid chromatography

HR ESI-MS: high resolution electrospray ionization mass spectrometer

ICP-MS: inductively coupled plasma mass spectrometry

i.e.: that is (Latin *id est*)

IL: ionic liquid

IR: infrared spectroscopy

k: rate constant

KIE: kinetic isotope effect

λ: wavelength

LUMO: lowest unoccupied molecular orbital

MD: molecular dynamics

mol%：mole percent of a substance

MW: microwave

m/z: mass to charge ratio

NBO: natural bond orbital

NCW: near-critical water

NMR: nuclear magnetic resonance

NOE: nuclear overhauser enhancement

ν: IR frequency

OECD: Organization for Economic Cooperation and Development

PCM: polarizable continuum model

QM/MM MD: quantum mechanics/molecular mechanics molecular dynamics

R: gas constant

RDF: radial distribution functions

RISM-SCF-SEDD: reference interaction site model self-consistent field spatial electron density distribution

$scCO_2$: supercritical carbon dioxide

SCFs: supercritical fluids

SCW: supercritical water

SMD: solvation model based on density

TD-DFT: time-dependent density functional theory

TLC: thin-layer chromatography

US DOE: the United States Department of Energy

UV-Vis: ultraviolet-visible

VOCs: volatile organic compounds

v/v: volume ratio

wt%: weight per weight percentage

% yield: percent yield

Chapter 1

Introduction and Overview

1.1 Green Chemistry and Renewable Feedstocks

Green chemistry is a philosophy of chemical research and engineering which encourages minimal use and generation of hazardous substances during reactions and other chemical processes.[1] The guiding principle of green chemistry, as Anastas said, is "the design of environmentally benign products and processes".[1, 2] The twelve principles of green chemistry have been condensed into one twelve-character word, PRODUCTIVELY, by Tang et al.,[3] as shown in Figure 1-1. Through the use of these principles, chemists can play an important role in sustainable development.

P: Prevent wastes
R: Renewable materials
O: Omit derivatization steps
D: Degradable chemical products
U: Use safe synthetic methods
C: Catalytic reagents
T: Temperature, pressure ambient
I: In-process monitoring
V: Very few auxiliary substances
E: E-factor, maximize feed in product
L: Low toxicity of chemical products
Y: Yes, it is safe

Figure 1-1. Twelve condensed principles of green chemistry.

Among the twelve principles of green chemistry, there is one that encourages "the use of renewable feedstocks",[2] meaning that feedstocks or raw materials used should be renewable instead of depleting if possible. Renewable feedstocks refer to resources that can

renew themselves after being used by humans for products and/or in the energy industry.[4] These include sunlight, wind, and wood, the latter being a source of biomass.

Biomass is a general term used to describe biological material generated by a living organism.[5] Biomass can be obtained from agricultural waste, forest products, and aquatic materials, and then converted to a variety of useful chemicals. The United States Department of Energy (US DOE) has reviewed the field of renewable chemicals and identified twelve molecules (platform chemicals) with significant potential for the synthesis of other compounds (Figure 1-2).[6]

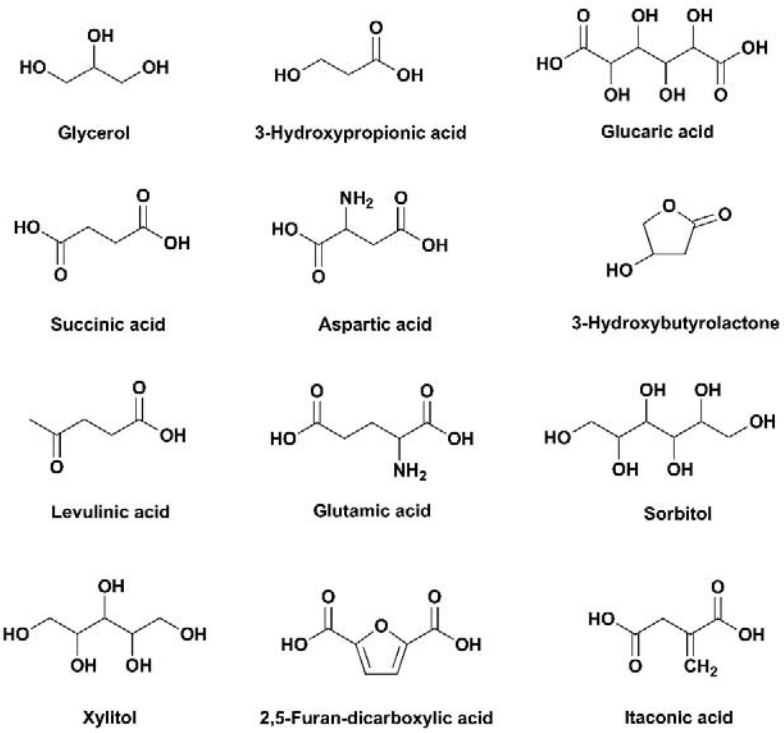

Figure 1-2. Top twelve platform chemicals identified by US DOE.

The use of biomass for fuels and chemicals is a significant research area, mainly because of the potential crisis surrounding the depletion of fossil fuels in the coming decades. In terms of biomass utilization, as a replacement for or supplement to petroleum, the established conversion of corn or sugarcane to bioethanol via fermentation is far from enough, and new processes using lignocellulosic biomass (cellulose, hemi-cellulose and lignin) are needed.[7] Currently the whole world faces the serious problem of high CO_2 emissions. The use of biomass may relieve this, since the CO_2 produced during the conversion of biomass to chemicals or materials can be balanced by the CO_2 consumed in the growth of biomass.[8] However, carbon neutrality is not guaranteed as growth, processing and transport of biomass all use energy and so release CO_2 into the environment.

Accounting for 71% of the earth's surface, oceans are great resources of biomass such as algae and waste from shellfish processing and other food industries.[9] Figure 1-3 shows the potential products obtained from oceanic biomass. The crustacean waste annually generated worldwide from shrimp, squid, crabs and krill is estimated to be 1.15 million tons.[10] If not disposed appropriately, this waste will cause serious environmental and health problems. The perishability of the waste will cause eutrophication in the sea, which will consume a lot of oxygen; while on land it will lead to the growth of pathogens and other bacteria.[11, 12]

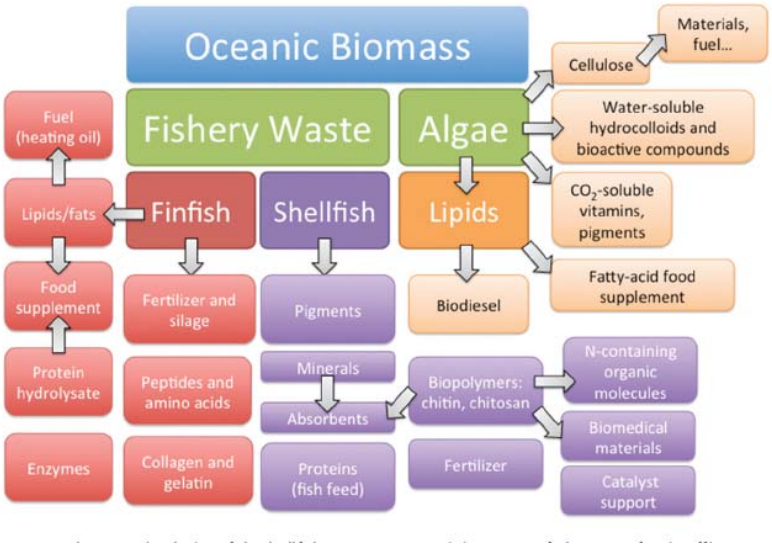

Figure 1-3. Potential products obtained from oceanic biomass.[9] (F. M. Kerton, Y. Liu, K. W. Omari and K. Hawboldt, *Green Chem.*, 2013, **15**, 860-871. Reproduced with permission of the Royal Society of Chemistry. All rights reserved.)

1.2 *N*-Acetyl-D-glucosamine (NAG)

N-Acetyl-D-glucosamine (NAG) is the monomer of chitin (Scheme 1-1). The amino polysaccharide chitin is the second most abundant biopolymer after cellulose on earth, and the most abundant biopolymer in the ocean.[13] An important difference between chitin and cellulose is that the former has an acetamido functional group while in the latter all groups are hydroxyls. The average content of chitin in crustacean shell waste is 20% - 30%.[14] Chitin can be extracted using either chemical or biological methods. There are three configurations of chitin based on the arrangement of the chains, and the one most often seen in crustacean shells is α-chitin.[15]

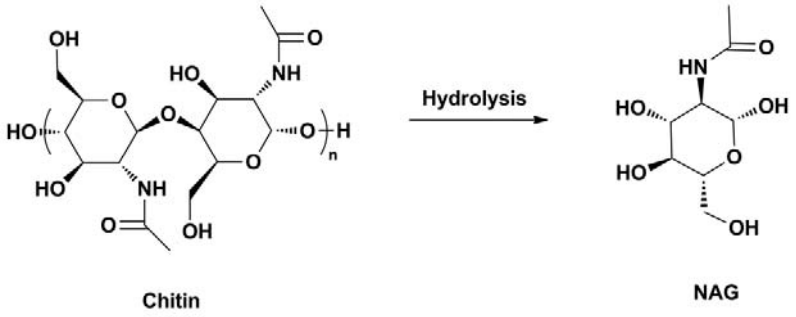

Scheme 1-1. Conversion of chitin to NAG.

1.2.1 Production

A lot of studies have been performed on the production of NAG from chitin, among which acid hydrolysis and enzymatic hydrolysis are the two main methods. Acid hydrolysis of chitin was applied earlier, and is used commercially in industry. Hydrochloric acid (HCl) is the acid used in this process most frequently. Under acidic conditions, the glycosidic bonds of chitin are cleaved to give the monomer NAG. The reaction rate in this acid-catalyzed process is related to the concentration of protons in the solution.[16] The Sukwattanasinitt group used microwave irradiation and ultrasound to promote the hydrolysis of α-chitin in shrimp shells.[17] It was found that thirty minutes of pre-sonication increased the solubility of chitin in the HCl solution at a low temperature, thus improving the selectivity of the hydrolysis to produce NAG. According to the analysis using an electrospray ionization mass spectrometer (ESI-MS), higher reaction temperatures produced NAG more quickly, but deacetylation to give D-glucosamine (GlcN) and acetic acid also occurred more easily. In industry, high temperatures are commonly used. Therefore, the NAG produced deacetylates to generate GlcN in situ, which is then isolated

and re-acetylated to form NAG.[18] In addition to the unsatisfactory yields of NAG, this method has some other "not green" issues as well. Usually highly concentrated acids and high temperatures are needed, therefore the economic and energy costs are high and acidic waste is generated.[19] In recent years the production of NAG from chitin using enzymes has been more studied. Chitinases refer to the hydrolytic enzymes that can degrade chitin. During the reaction, the chitin polymer is degraded to chitin oligosaccharides first, which then undergo further cleavage to yield NAG and other saccharides.[20, 21] Many chitinases can be found in natural sources, such as bacteria, fungi, plants and animals. For instance, the Jadhav group used *Penicillium ochrochloron* to produce chitinase from agriculture residue, and this chitinase was applied in chitin hydrolysis.[22] Results from thin-layer chromatography (TLC) and high-performance liquid chromatography (HPLC) indicated that NAG was obtained as the main product within a reaction time of 3 h. In the studies by Giuliano Garisto Donzelli et al. and Jamialahmadi et al. the yields of NAG approached 78% - 79%.[21, 23]

1.2.2 Application

To date, the use of NAG as a chemical reagent or a drug has not been widely studied. It has the potential to be a useful material both in chemistry and pharmacy areas because of the *N*-acetyl group. In 2012, Stallforth and co-workers synthesized sialic acid (Figure 1-4) from NAG using the enzyme macrophomate synthase.[24] Sialic acid plays an important role in many biological processes, such as cell to cell communication. In 2013, Chen et al. successfully synthesized the anti-influenza drugs, oseltamivir and tamiphosphor (Figure 1-

4), from NAG.[25] NAG can be used for oral administration drugs because of its sweet taste. The significant anti-tumor activity of NAG oligomers was discovered by Masuda et al. on a mouse model.[26] In addition, NAG can efficiently suppress Rheumatoid Arthritis according to the study by the Osaki group on mouse models.[27] These potential applications show that NAG is a promising biomass feedstock from a commercial perspective.

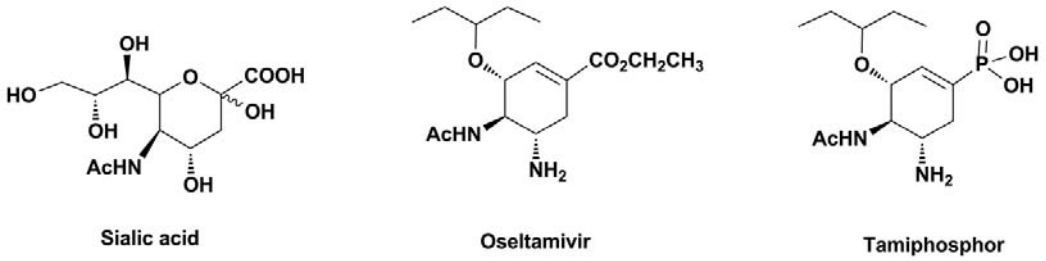

Figure 1-4. Structures of sialic acid, oseltamivir and tamiphosphor in the study of Stallforth and co-workers[24] and Chen et al.[25]

1.3 Carbohydrates

In the ocean of biomass utilization research, a large portion focuses on biomass-derived carbohydrates. A carbohydrate molecule is normally composed of C, H and O atoms as $C_m(H_2O)_n$. Some derivatives containing heteroatoms can also be considered as carbohydrates, such as NAG (a derivative of glucose), which is the key feedstock in this thesis. The other name of carbohydrates is "saccharide". Typically there are four kinds of saccharides: monosaccharides, disaccharides, oligosaccharides and polysaccharides.[28]

1.3.1 Monosaccharides

Monosaccharides are the simplest carbohydrates. The general formula for monosaccharides is $(CH_2O)_n$, where n is at least three. A typical monosaccharide is composed of several hydroxyl groups and one carbonyl group (an aldehyde or ketone). The simplest monosaccharides are dihydroxyacetone and glyceraldehyde when n is three (Figure 1-5). Some monosaccharides are the units forming more complicated saccharides. For example, starch consists of many glucose units.

Dihydroxyacetone Glyceraldehyde

Figure 1-5. Structures of dihydroxyacetone and glyceraldehyde (the simplest monosaccharides).

Among various monosaccharides, the most common ones are glucose and fructose. They are two hexoses that are naturally derived from fruits, vegetables and plants. They have both straight chain and cyclic forms, of which the latter have five-membered and six-membered ring isomers (Scheme 1-2 and Scheme 1-3). These sugars are closely related to human health and daily life. In particular, glucose is essential to provide energy to the human brain and body. Fructose is widely used as a sweetener because of its cheap price and very sweet taste.

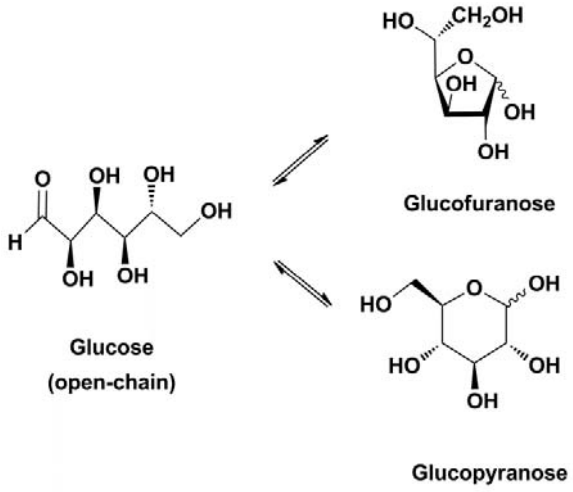

Scheme 1-2. Structures of glucose in straight-chain and cyclic forms.

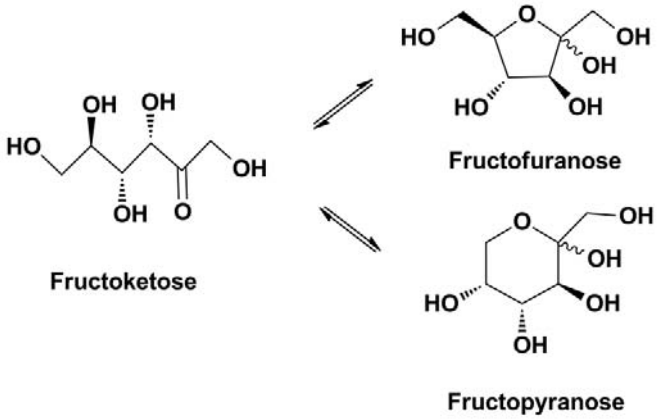

Scheme 1-3. Structures of fructose in straight-chain and cyclic forms.

1.3.2 Disaccharides

When two monosaccharides come together in a dehydration reaction, the carbohydrate formed is a disaccharide. The bond formed by the hydroxyl groups through dehydration is a glycosidic bond. As there are multiple possible combinations of hydroxyl groups from

two monosaccharides that can form glycosidic bonds, a variety of disaccharides can be generated. For example, two glucose units can form maltose, trehalose and cellobiose based on different bond arrangements. Common disaccharides include sucrose, lactose and maltose. Sucrose (Figure 1-6) is composed of glucose and fructose, and can be extracted from sugar cane and beets. It is the main component of table sugar.

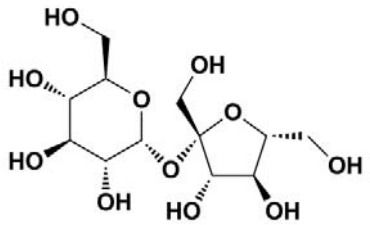

Sucrose

Figure 1-6. Structure of sucrose.

1.3.3 Oligosaccharides and Polysaccharides

The small polymer generated through dehydration of three to nine monosaccharides is an oligosaccharide. If more monosaccharides are involved, the sugar is labelled a polysaccharide. Oligosaccharides and polysaccharides are biological polymers that can be widely found in nature. Fox example, oligofructose, which is composed of fructose units, exists in many vegetables and fruits. Cellulose (Figure 1-7) is the most common polysaccharide. It consists of hundreds to thousands of D-glucose units.[29] Cellulose is a fundamental component of the cell wall in green plants, and is used in the paper industry.

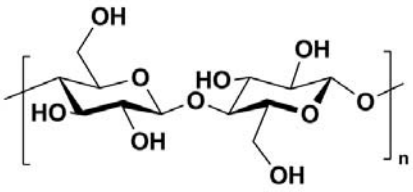

Cellulose

Figure 1-7. Structure of cellulose.

1.4 Useful Chemicals Converted from Renewable Feedstocks

1.4.1 5-Hydroxymethylfurfural (5-HMF)

In research on the conversion of biomass to chemicals and biofuels, reactions using sugars as reactants form a large proportion of the studies to date. Among these, the conversion of saccharides to 5-HMF (Figure 1-8) via dehydration reactions has been studied extensively.

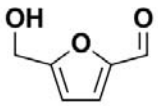

5-HMF

Figure 1-8. Structure of 5-hydroxymethylfurfural (5-HMF).

1.4.1.1 Production

5-HMF seldom exists in fresh food, but it can be easily found in heated sugar-containing foods, such as dried fruits. It is a product of the Maillard reaction that occurs between amino acids and reducing sugars. The first synthesis of 5-HMF was conducted by Dull in 1895 by heating inulin in oxalic acid solution under pressure.[30] In the same year,

Kiermayer also managed to obtain 5-HMF from sugar cane using a similar method.[31] From then on, studies related to 5-HMF began to develop, and are still quite popular today. Reports on the dehydration of hexoses into 5-HMF are mainly focused on the conversion of fructose, glucose, sucrose and cellulose.

As water is a perfectly green solvent (see **1.5.2**), many researchers have tried to use it in 5-HMF synthesis.[32] For instance, Omari et al. performed the hydrolysis of chitosan in water at 200 °C for 30 min under microwave irradiation.[33] Several Lewis acids were used as catalysts, and tin(IV) chloride pentahydrate ($SnCl_4 \cdot 5H_2O$) gave the best result with 10.0 wt% 5-HMF produced when dilute conditions (20 mL water) were applied. Under more concentrated conditions (4 mL water) there was less 5-HMF but a large amount of levulinic acid (LA) (23.9 wt%) obtained. It is proposed that in more concentrated reaction environment 5-HMF tends to react to form LA. One effective way to suppress the formation of LA and other side-products is the use of activated carbon as absorbent for 5-HMF, as Vinke et al. did in their research.[34]

A biphasic system is a reaction system composed of two immiscible solvents. Usually the reactants and catalysts are soluble in one layer, while the products are extracted into the other layer once generated. This approach encourages the reaction to proceed and prevents side-reactions from occurring (Figure 1-9). 5-HMF dissolves well in many organic solvents, so studies using aqueous media with organic solvents to form biphasic systems have been reported.[35] Román-Leshkov et al. applied a water-methyl isobutyl ketone (MIBK) system with HCl as the catalyst to synthesize 5-HMF. Without any phase modifiers, the conversion

of fructose could reach 91% but the selectivity of 5-HMF was only 60%.[36] When the aqueous phase was modified with the addition of a polar aprotic solvent (dimethyl sulfoxide or 1-methyl-2-pyrrolidinone) and a hydrophilic polymer (poly(1-vinyl-2-pyrrolidinone)), and the organic phase was modified with 2-butanol, the fructose conversion reached 92% with 5-HMF selectivity of 77%.

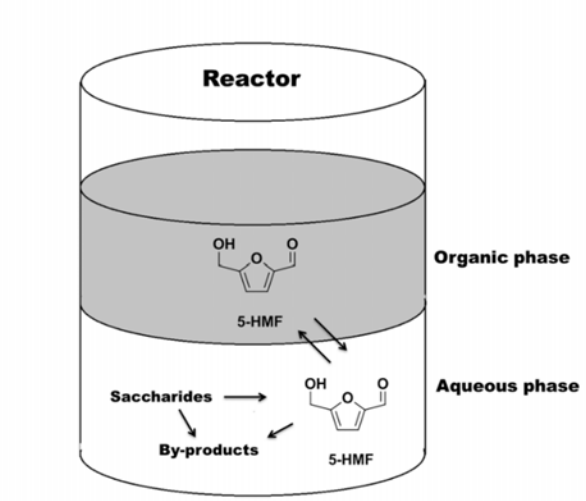

Figure 1-9. A biphasic system used in 5-HMF synthesis.

With the development of ionic liquids (ILs) in recent years, their use as solvents and/or catalysts in 5-HMF synthesis has also been extensively developed, and good results have been achieved.[32, 37, 38] The first IL used in this area was pyridinium chloride by Fayet and Gelas in 1983.[39] The yield of 5-HMF from fructose conversion was as high as 70% at 120 °C for 30 min. Unfortunately, this good performance did not raise scientists' strong interest until 2003 when Lansalot-Matras and Moreau converted fructose to 5-HMF using two ILs: 1-butyl-3-methyl imidazolium tetrafluoroborate ([Bmim][BF_4]) and 1-butyl-3-methyl

imidazolium hexafluorophosphate ([Bmim][PF_6]).[40] Their study used Amberlyst-15 sulfonic ion-exchange resin as the catalyst, with dimethyl sulfoxide (DMSO) as a co-solvent since fructose did not dissolve well in the hydrophobic [Bmim][PF_6]. The best 5-HMF yield was nearly 80% using [Bmim][PF_6] at 80 °C after 24 h. When [Bmim][BF_4] was used, the highest yield was 87% at 80 °C after 32 h. In the work by Qi et al. on the conversion of fructose, 1-butyl-3-methylimidazolium chloride ([Bmim]Cl) was used together with co-solvents (DMSO, EtOAc, $scCO_2$, ethanol, etc.) and Amberlyst-15 acidic ion-exchange resin was the catalyst.[41] The fructose was predissolved in the IL to form a gel-like solution, and then the catalyst and co-solvent were added. The reaction could be conducted at room temperature (25 °C) with conversions of fructose around 90% and yields of 5-HMF around 80%. With longer reaction time, 5-HMF underwent self-polymerization or cross-polymerization with fructose to form humins, therefore the yield decreased.

As the dehydration process is acid-facilitated, a system with proper acidity would be very helpful to stimulate the generation of 5-HMF. Therefore, many studies have been focused on the use of acidic ILs. In a 2006 study by Moreau et al., 1-H-3-methylimidazolium chloride ([Hmim]Cl), a Brønsted acidic IL (see **1.5.4.4**), was used as the solvent as well as the catalyst for the dehydration of fructose and sucrose in a microbatch reactor at 90 °C.[42] The 5-HMF yield from the dehydration of fructose reached 92% after 45 min. It was proposed that sucrose was split to fructose and glucose first via hydrolysis with crystallization water from the reagents. Then the fructose was converted to 5-HMF with a 100% yield while the glucose had negligible reaction (Scheme 1-4). After

5-HMF extraction using diethyl ether (Et_2O), the IL was dried and subsequently reused. By removing the water from the IL, 5-HMF yields had only slight fluctuations during five runs.

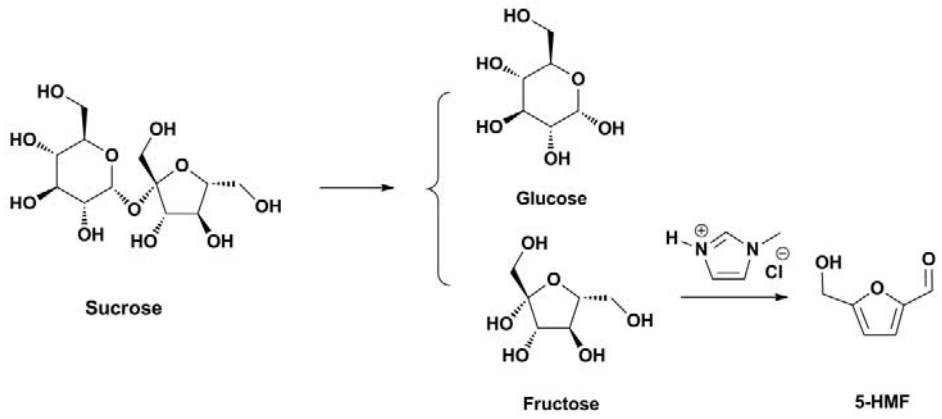

Scheme 1-4. Cleavage of sucrose and conversion of fructose in [Hmim]Cl.[42]

Although water is one product in the dehydration reactions and its generation may hinder yields, some studies have shown that an appropriate amount of water could increase the yield of 5-HMF. In the work by Ding et al., 5-HMF was synthesized from microcrystalline cellulose using a series of acidic ILs (Figure 1-10) as the catalysts in the solvent 1-ethyl-3-methylimidazolium acetate ([Emim][OAc]).[43] With 1-(4-sulfonic acid)butyl-3-methylimidazolium hydrogen sulfate ([Bmim-SO_3H][HSO_4]) as the acid catalyst and copper(II) chloride ($CuCl_2$) as a co-catalyst, the maximum yield of 5-HMF reached 62.6% in the conversion of 0.35 g cellulose when the dosage of water was 0.2 mL, but more water led to the decomposition of 5-HMF to side-products. The main function of water here is to hydrolyze the cellulose to glucose.

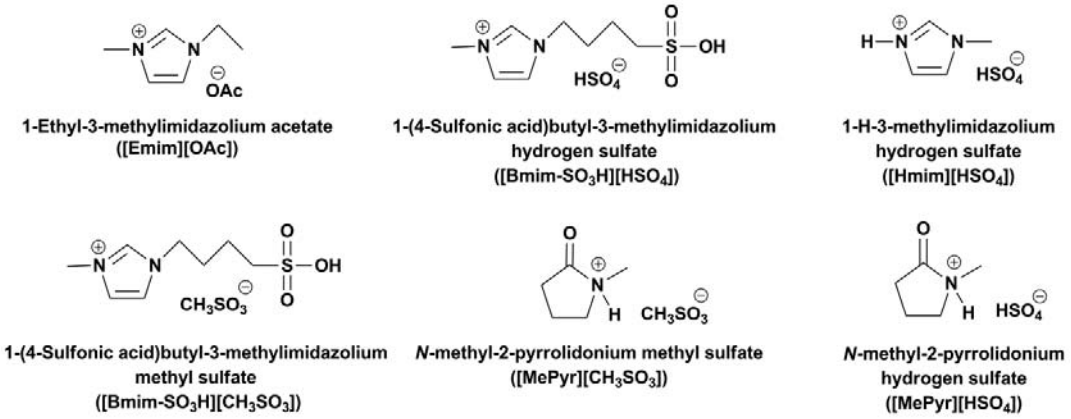

Figure 1-10. ILs used in the work by Ding et al. of cellulose conversion to 5-HMF.[43]

According to Ståhlberg et al., the addition of boric acid ($B(OH)_3$) was effective in improving 5-HMF yields in hexose dehydration without metal catalysts.[44] For glucose, a maximum 5-HMF yield of 42% was obtained at 120 °C after 3 h in 1-ethyl-3-methylimidazolium chloride ([Emim]Cl) as the solvent. Among other sugars tested, sucrose was converted to 5-HMF with the yield as high as 66%. In related research, Caes et al. applied a variety of ortho-carboxyl-substituted phenylboronic acids as organocatalysts in glucose and cellulose conversion.[45] A decent 5-HMF yield of 57% from glucose could be achieved using 200 mol% 2-methoxycarbonylphenylboronic acid (Figure 1-11) and magnesium chloride hexahydrate ($MgCl_2 \cdot 6H_2O$) in dimethylacetamide (DMA) at 120 °C after 4 h. The dehydration of cellulose was conducted at 105 °C in [Emim]Cl and sulfuric acid (H_2SO_4) using 120 mol% 2-methoxycarbonylphenylboronic acid and $MgCl_2 \cdot 6H_2O$ as catalysts. After 1 h, the 5-HMF yield reached 41%. Although the loadings of the boronic acid catalysts were high, the recovery of the catalysts was realized and the catalysts could be reused for four reaction cycles.

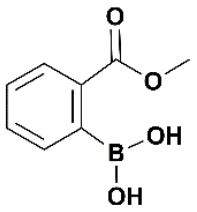

Figure 1-11. Structure of 2-methoxycarbonylphenylboronic acid used in the study by Caes et al. of glucose/cellulose conversions to 5-HMF.[45]

Sodium chloride (NaCl) is another additive commonly used in 5-HMF studies. According to Román-Leshkov et al., when salts are added to a biphasic system the number of 5-HMF molecules dissolved in the reaction layer will be decreased because of the salting-out effect, and they will move to the extraction layer.[46] However, the yield will not be increased significantly in this way. The work by Hansen et al. suggested that salts stabilized the intermediates formed in the $B(OH)_3$-catalyzed reaction, thus the acidity of the system was strengthened and the yield increased.[47] Among all salts they tested, halide salts gave better 5-HMF yields than sulfates and nitrates, indicating that the anions in the reaction system play an important role.

The dehydration of hexoses to 5-HMF is a process in which three water molecules are lost. So far there have been a variety of mechanisms raised, but none of them have stood out among the rest. In **Chapter 2**, a review is presented about the mechanistic studies on the transformations of biomass to 5-HMF and the tools and approaches used for the research.

1.4.1.2 Applications of 5-HMF

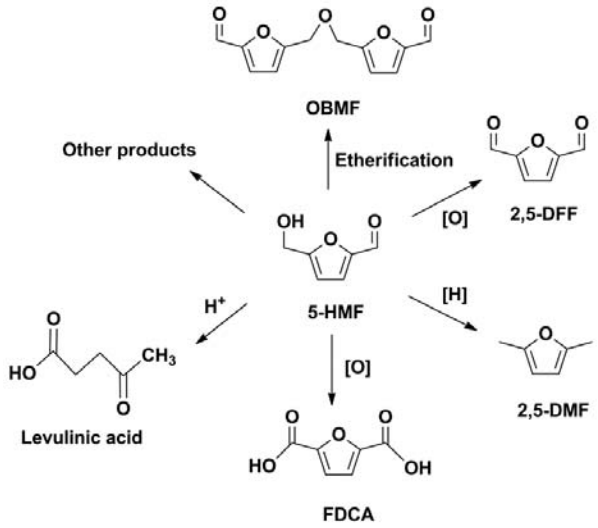

Scheme 1-5. 5-HMF as a platform chemical in the synthesis of various useful products.

As "a sleeping giant",[48] 5-HMF is an important platform chemical accessible from biomass. With several functionalities, it can be an intermediate for many useful products and promising biofuels. Not only cyclic compounds, such as furan products, can be obtained, but also acyclic chain chemicals such as LA. Reactions that can be used in its conversion include hydrogenation, oxidation and hydrogenolysis (Scheme 1-5).[49]

5-HMF can react with hydrogen gas to produce 2,5-dimethylfuran (2,5-DMF).[50, 51] 2,5-DMF is an alternative fuel for transportation because of its satisfactory properties in ignition, emission and combustion compared with traditional gasoline.[52] 5-HMF can also be converted to 2,5-diformylfuran (2,5-DFF), which is widely used in the produce of furan-urea resins,[53] furanic biopolymers,[54] fungicides[55] and pharmaceutical precursors.[56] Another important compound from 5-HMF transformation, 2,5-furandicarboxylic acid (FDCA), is

listed as one of the twelve top platform chemicals from biomass (Figure 1-2) and can replace terephthalic acid in the synthesis of polyesters, polyamides and polyurethanes.[57] Selective etherification of 5-HMF gives the product of 5,5'-oxy(bis-methylene)-2-furaldehyde (OBMF), which is significant in the preparation of some imine-based polymers, heterocyclic ligands and hepatitis antiviral precursors.[57, 58]

1.4.2 3-Acetamido-5-acetylfuran (3A5AF)

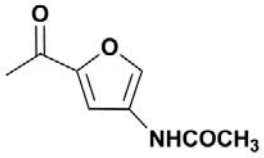

3A5AF

Figure 1-12. Structure of 3-acetamido-5-acetylfuran (3A5AF).

As far as the Kerton group is aware, 3A5AF (Figure 1-12) is the first nitrogen-containing product obtained from the dehydration of a hexose in solution, and it is hoped to be a building block for amines and other chemicals. So far there are only a limited number of studies on 3A5AF, mainly because it is not commercially available in large quantities at a reasonable price. This may be due to the difficulty in achieving high 3A5AF yields in its synthesis.

1.4.2.1 Production

In 1984, 3A5AF was first obtained from NAG by Franich et al. using a pyrolysis method.[59] A large-scale pyrolysis of 2 g NAG was conducted with products isolated through a silica gel column, and a 2% molar yield of 3A5AF was obtained. In 1998, Ho et

al. pyrolyzed a NAG/anhydrous sodium phosphate/quartz sand mixture at 200 °C for 30 min.[60] The reaction mixture was extracted and concentrated for Gas Chromatography-Mass Spectrometry (GC-MS) analysis. 3A5AF was obtained as the main product with a yield of 288 mg per kilogram NAG. The products were isolated using a preequilibrated silica gel column, and the ^{1}H NMR data of 3A5AF was given (acetone-d_6 as the solvent).

In recent research by Omari et al., the yield of 3A5AF was increased to 60%.[61] DMA was chosen as the best solvent because of its relatively mild physical properties (boiling point, flash point and acute toxicity) and good performance in 3A5AF yield. Inductively coupled plasma mass spectrometry (ICP-MS) analysis determined that boron and chlorine contents in NAG from different commercial sources varied and that these two elements in large quantities were useful in improving 3A5AF yields. An optimal 3A5AF yield of 57.7% was achieved with 1 equivalent of $B(OH)_3$ and 2 equivalents of NaCl. Nevertheless, DMA is still a high boiling organic solvent, which is not favored in green chemistry.[62, 63] In a follow-up study by Drover et al., ionic liquids were tried as solvents in this conversion.[64] Initially, a series of neutral ILs were tested without any additives and [Bmim]Cl gave the highest 3A5AF yield of 25.5%. Subsequently, various acidic and basic additives were added to the reaction system with [Bmim]Cl as the solvent, aiming to improve the yield. When heated at 180 °C for 1 h, the system containing $B(OH)_3$ gave a yield of 3A5AF as high as 60%. The addition of NaCl also increased the yield, but only to 38.3%. Other acidic catalysts (e.g. HCl, $CrCl_2$) did not increase the yield significantly.

In 2014, the Yan group conducted the direct conversion of chitin to 3A5AF.[65] With 3 mL *N*-methyl-2-pyrrolidone as the solvent, a mixture of 100 mg chitin, 122 mg $B(OH)_3$ and 58 mg NaCl was heated in an oil bath at 215 °C for 2 h and a 3A5AF yield of 7.5% was obtained. The water content was controlled below 1% to prompt the hydrolysis of chitin and avoid inhibiting the dehydration process. In 2015, the same group switched to ionic liquids to conduct the same reaction.[66] Cl-containing ILs were superior and gave relatively higher 3A5AF yields compared with other ILs. A series of additives were screened, and the combination of $B(OH)_3$ and HCl gave the best performance. The main function of HCl was to improve the hydrolysis of chitin. After being heated at 180 °C for 1 h, a mixture of 1 g [Bmim]Cl, 80 mg chitin, 4 equivalents of $B(OH)_3$ and 1 equivalent of HCl gave a 3A5AF yield of 6.2%. A collaboration with this group focusing on the conversion of NAG to 3A5AF was performed, which will be discussed in **Chapter 3**.

1.4.2.2 Mechanism

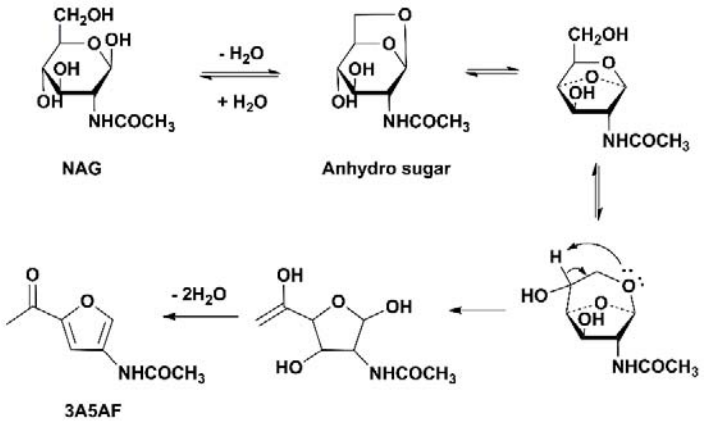

Scheme 1-6. Proposed mechanism of NAG conversion into 3A5AF.[59]

In the study by Franich et al., the generation of 3A5AF was proposed to result from the thermal rearrangement and dehydration of an important intermediate: 2-acetamido-1,6-anhydro-2-deoxy-β-D-glucopyranose (anhydro-sugar) (Scheme 1-6).[59]

In the thermal degradation study by Ho et al., they proposed both cyclic and acyclic pathways to 3A5AF starting from the open chain aldose form of NAG (Scheme 1-7).[60]

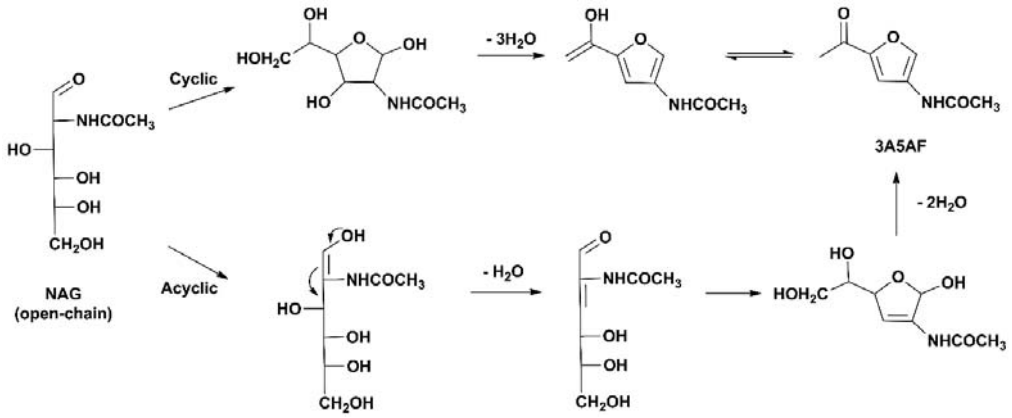

Scheme 1-7. Proposed mechanism of NAG conversion into 3A5AF.[60]

In the study by Drover et al.,[64] acidic protons from the IL cations were proposed to react with the hydroxyl oxygen in NAG to give the aldose form of NAG, which undergoes intramolecular nucleophilic attack to form a five-membered ring product. Subsequent loss of water and enolization was proposed to give the final product of 3A5AF (Scheme 1-8). In the study on chitin conversion by Chen et al.,[65] a similar reaction pathway was proposed starting from the hydrolysis of chitin to NAG (Scheme 1-8).

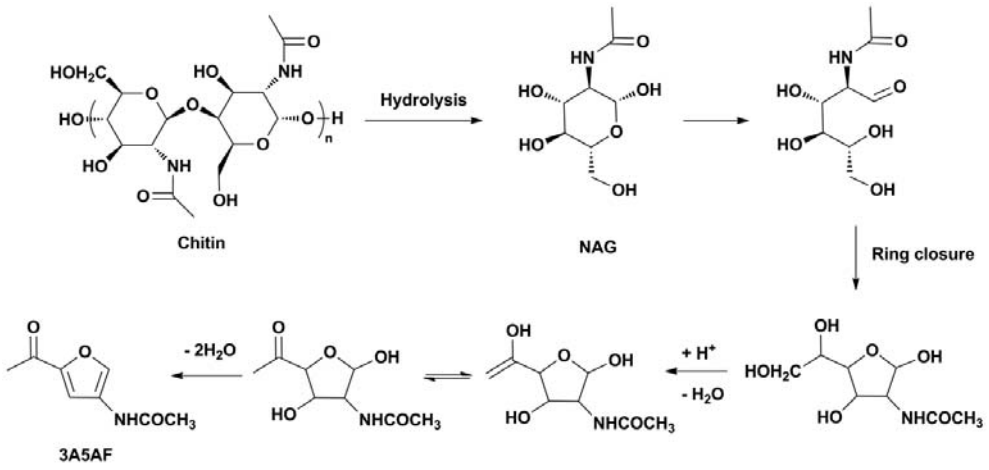

Scheme 1-8. Proposed mechanism of chitin conversion into 3A5AF.[64, 65]

1.4.2.3 Possible Applications of 3A5AF

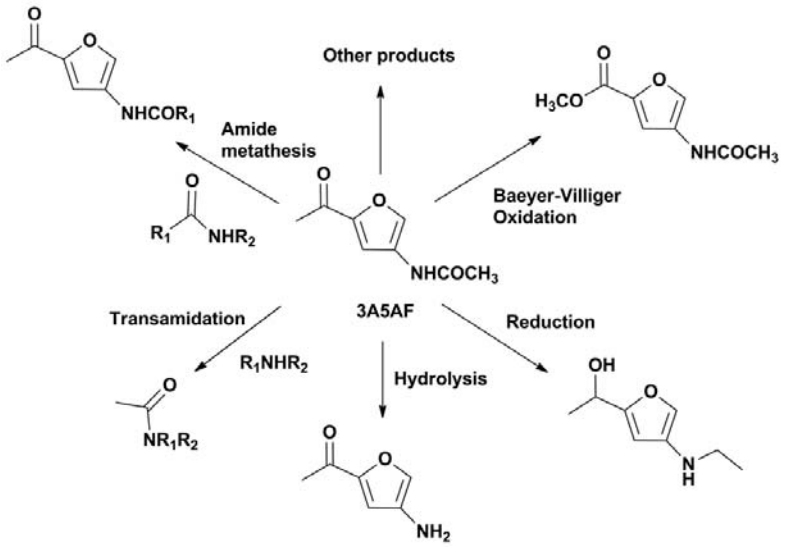

Scheme 1-9. Proposed applications of 3A5AF.

As a promising platform for many useful compounds (Scheme 1-9), the efficient synthesis of 3A5AF should be studied further to make it cheap and widely available to

chemists. To that effect, one goal of this research was to improve the efficiency of producing 3A5AF from NAG. Physical and chemical properties of 3A5AF were studied in order to design better synthesis routes that give higher yields. Another part of the presented research was to utilize 3A5AF in some simple applications, for example, as a CO_2-capture solvent.

1.5 Solvents

Solvents are frequently used in reaction systems. Functions of solvents include heat and mass transfer, and separations and purifications. Some solvents are acidic or basic, so they are able to adjust the acidities or basicities of the reaction systems and thus influence the reaction rates and/or yields. Traditional solvents are often volatile organic compounds (VOCs), which have serious detrimental environmental and health effects. VOCs can lead to ozone depletion and smog formation. Most VOCs are flammable and toxic. Health hazards range from headaches and eye irritation through to very serious concerns including cancers. For instance, dichloromethane (DCM) is a good solvent widely used in both lab research and industrial processes. However, it is a suspected human carcinogen.[67] Because of these concerns, "safer solvents and auxiliaries" is listed as one of the twelve principles of green chemistry. Ideal solvents should have low toxicity, low volatility and little influence on the environment and human bodies. In recent years, scientists have been devoting themselves to looking for alternative solvents to VOCs. Water, supercritical fluids and ionic liquids have all been developed as greener choices for solvent use.[68]

1.5.1 Solvent-free Systems

The greenest solvent is "solvent-free", which means no solvent is used.[69] In some studies higher product yields and/or reaction rates can be obtained in solvent-free conditions compared with those when solvents are used.[70, 71] In some reactions, a reagent or product is in its liquid phase, so it can act as the solvent to promote heat and mass transfer.[72, 73] In organic synthesis, a variety of reactions can be conducted in the solid-state or vapor-state. For example, cerium(IV) oxide has been reported as an efficient solid catalyst in the transformation of amines to amides, which was a solvent-free process with high yields of *N*-alkyl amides obtained.[74] Mechanochemistry, in which reagents are mixed with ball mills and shaken at high speed, is a way to perform solvent-free reactions between two or more solid reagents. It has already been successfully applied in industry.[75, 76] One thing that needs to be realized is that in many cases, although the synthesis can be conducted in the absence of a solvent, the subsequent extraction and purification of products may still involve solvent use. However, the total need for solvents has been significantly decreased compared with traditional routes, so these approaches are considered to be green and favored.

1.5.2 Water

When solvents are inevitable, water is the greenest choice. Water is non-toxic and non-flammable. It can be easily obtained from nature, thus being cheap and renewable. Water has no color or odor, so the contamination will be easy to recognize when it happens. The high polarity of water and the density of 1g/mL make its separation from many organic

solvents realizable, and biphasic systems can be formed. Water has a high dielectric constant (78.30), which makes ionic reactions favored in aqueous systems. In addition, water has a high heat capacity, so exothermic reactions can be more safely controlled in aqueous systems. Because of these merits, endeavours have been made to replace VOCs with water for solvent use in both lab research and industry.

However, there are still some disadvantages of water. For example, the high heat capacity of water may be a drawback since it will be time and energy consuming to heat or cool the aqueous reaction system. Many organic reagents or products do not dissolve well in water, so water cannot play an efficient role as a solvent. Furthermore, although biphasic systems can be well formed between water and many organic solvents, most organic solvents have a certain degree of solubility in water. This will cause the contamination of the aqueous phase and thus subsequent treatment is needed to avoid its discharge into nature. Some reagents and catalysts are moisture-sensitive or water-insoluble, so the aqueous system will inhibit the reaction process. For instance, aluminum chloride, a frequently used catalyst, is very hygroscopic, so it will be deactivated in the reaction system if water exists.

Despite these challenges, water is a very promising solvent. Scientists have tried to optimize its use through status modifications. Superheated water, also known as subcritical water or near-critical water (NCW), is water under pressure at high temperatures between its boiling point (100 °C) and its critical temperature (374 °C). Being this status, some properties of NCW are different from the normal water below 100 °C. It has lower polarity, density, viscosity and surface tension. Many organic compounds are soluble in NCW, so it

can be used as an alternative to organic solvents in some processes such as extraction. In 2014, Reddy et al. used NCW in the extraction of lipids from wet algae.[77] Both conventional-heated and microwave-assisted NCW extractions were tried. 100% lipid extraction efficiency was achieved using microwave at 205 °C after 25 min. In this process, the drying of the wet raw materials was eliminated compared with conventional organic solvent extractions, so it is more energy efficient.

1.5.3 Supercritical Fluids (SCFs)

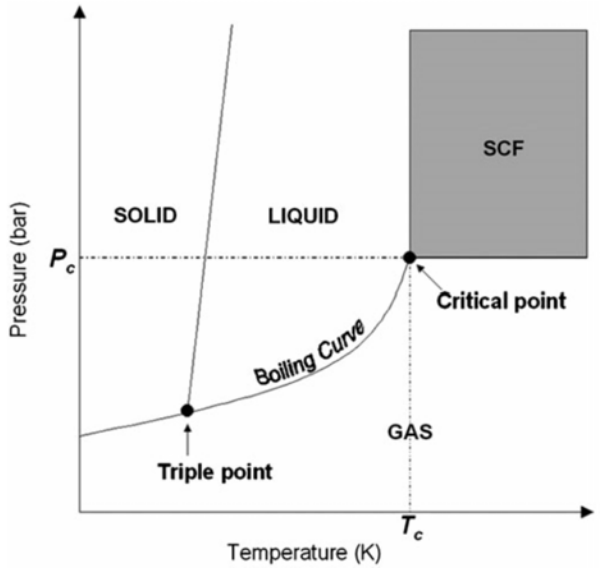

Figure 1-13. A single-component phase diagram for a typical substance.[67] (F. M. Kerton and R. Marriott, *Alternative Solvents for Green Chemistry*, Royal Society of Chemistry, Cambridge, UK, 2nd edn., 2013. Reproduced with permission of the Royal Society of Chemistry. All rights reserved.)

SCFs are substances which are at temperatures and pressures above their critical points (Figure 1-13). Supercritical water (SCW) and supercritical carbon dioxide ($scCO_2$) are much more studied than others, mainly because of their easy access and environmentally friendly properties. As a kind of solvent, SCFs have a number of advantages. Most gases have high solubilities in SCFs, so reactions involving gaseous reagents are favored. The solvation interactions between the solutes and the solvent are weaker in SCFs than in conventional solvents. The cage effects in radical reactions are also lower in SCFs. Therefore reaction rates can be highly promoted. However, exothermic reactions having faster rates means more heat will be let out in a short time, and this can cause serious problems because of the heat transfer limitations. In addition, pressure vessels are needed in order to use SCFs. They are more expensive than glassware, and must be handled safely. Based on the current situation, improvement in SCF technology is needed for better application.

So far, $scCO_2$ is the most widely used SCF, even more than SCW. This mainly results from its superior properties. CO_2 is non-flammable and non-toxic. It is widely available, so the cost to obtain it is low. There is no liquid waste using $scCO_2$ as the solvent. Products can be simply isolated from the solvent by reducing the pressure to convert CO_2 to a gas, which is then collected for recycling. CO_2 is inert to free-radicals and cannot be oxidized, so radical reactions and oxidations can be safely performed in $scCO_2$. Nevertheless, CO_2 reacts with nucleophiles (such as Grignard reagents), which limits its use in this area. In addition, CO_2 is relatively non-polar, so the dissolution of polar compounds with high

molecular weight will need modifications or co-solvents. A great number of reactions have been studied in $scCO_2$, including hydrogenations, hydroformylations, and polymerizations.[78, 79] Industrially, $scCO_2$ is extensively used in extraction, especially for beverage, food and flavor, cosmetic and skin care products. The low temperature in the extraction avoids the evaporation and degradation of volatile compounds, so high product yields can be achieved.

1.5.4 Ionic Liquids (ILs)

1.5.4.1 History

ILs are ionic compounds made of organic cations and inorganic or organic anions (Figure 1-14). The "ILs" people usually refer to are room-temperature ILs with melting points below 100 °C. The first room-temperature IL is ethylammonium nitrate ($[EtNH_3][NO_3]$), found by Paul Warden in 1914.[80] However, in the following decades this sort of compound did not inspire many scientists to study them in detail. Only approximately 100 articles about ILs had been published by 1999.[81] From then on, with the publication of some reviews on ILs,[82-85] the enthusiasm about ILs began to increase. A variety of research has been performed about modified IL synthesis, their properties, and their applications as electrolytes, catalysts and solvents. In 2002, Swatloski et al. found that cellulose could be dissolved in some imidazolium ILs.[86] Since then many studies on solubilities of cellulose and other carbohydrates in ILs have been reported, thus broadening the application of ILs in the field of biomass utilization.[87-89]

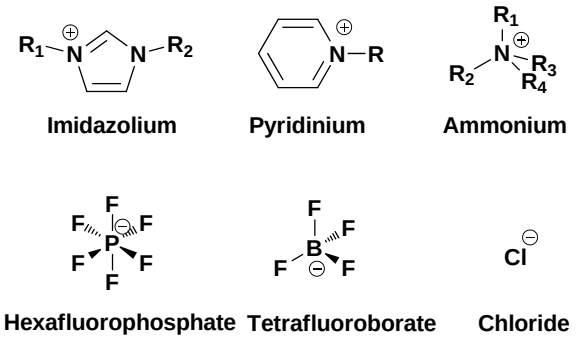

Figure 1-14. Some typical cations and anions of ionic liquids.

1.5.4.2 Synthesis

There are many methods to synthesize ILs, among which two basic reactions are frequently involved as the last steps: Mentschukin reaction and Finkelstein reaction.[90] Generally, the former is an alkylation between a precursor (e.g. 1-methylimidazole) and an alkyl halide or alkyl methanesulfonate. The ILs generated via this route can be used as the precursors for the second reaction, to synthesize some other types of ILs through the metathesis of the halide or methanesulfonate anions (Scheme 1-10).

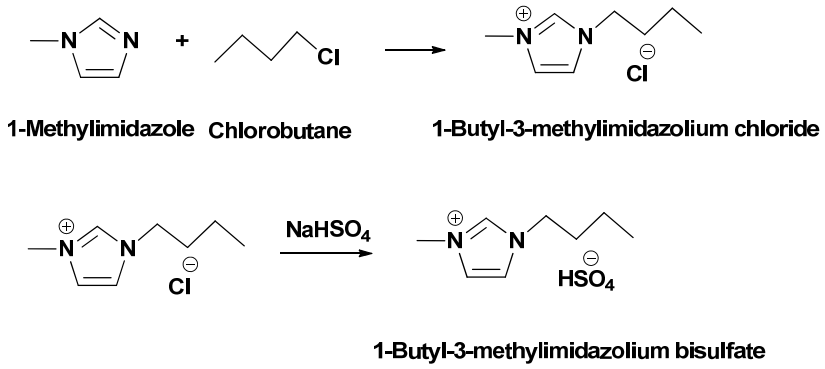

Scheme 1-10. Frequent synthesis routes of ionic liquids. (Top: Mentschukin reaction; bottom: Finkelstein reaction).

1.5.4.3 Properties

ILs have advantages that make them potentially ideal solvents. Firstly, most ILs are non-volatile and non-flammable, so they do not vaporize and have little risk of causing fire, as opposed to VOCs. Based on this feature, separation of volatile products from ILs can be realized through distillation. Secondly, ILs are thermally stable. Therefore, when ILs are used as solvents the reactions can be performed at higher temperatures without worrying about solvent decomposition. In the study by Kamimura et al., waste fiber-reinforced plastics were depolymerized under microwave irradiation in ILs.[91] The reaction temperature could reach above 300 °C in *N*-methyl-*N*-propylpiperidinium bis(trifluoromethylsulfonyl)imide ([PP13][NTf_2]), and the best yield of the product (phthalic anhydride) was 83%.

As the cations and anions of ILs can be adjusted, many properties of ILs are tunable. For example, [Bmim][PF_6] is hydrophobic, but the switch of the anion to $[BF_4]^-$ makes the new IL hydrophilic. This is a convenient way to adjust the reaction environment and broaden the application of ILs.

Nevertheless, ILs also have some shortcomings. In general, they are more expensive than common organic solvents, and have higher viscosities. The room temperature viscosities for organic solvents are usually 0.2 to 10 cP (centipoise), while for ILs the range is wider from 10 to 10^5 cP.[92] The high viscosity of ILs increases the difficulties of handling as well as the energy and economic cost for efficient mass transfer. Viscosity adjustments can be made through the modification of cations and/or anions of the ILs, and the use of

co-solvents. According to the study by Seddon et al., the viscosities of [Bmim][BF_4] and [Bmim][PF_6] decreased as the amount of the mixed organic solvents and water increased.[93]

Despite their fast development, the toxicities of ILs are still a concern which people pay much attention to. ILs may lead to aquatic and soil contamination because of their miscibility with water and persistence in the environment. They can also have serious toxic impacts on aquatic organisms.[94] So far a general conclusion about the toxicities of the common ILs (imidazolium, pyridinium and quaternary ammonium based ones) is that the influence of cations is more significant than anions, and longer alkyl chain length in cations can lead to increasing toxicity.[95]

If an IL has a good biodegradability, it can be converted to CO_2 and non-toxic biomass by active microorganisms, and thus its toxicity will be less of a problem. Biodegradation is the breakdown of materials through biochemical methods. According to the standard of Organization for Economic Cooperation and Development (OECD), if a chemical can reach 60% theoretical CO_2 removal in a 10-day window within a 28-day test period, it is regarded as "readily biodegradable".[96] It should be noted that an IL is composed of two parts: a cation and an anion. Therefore the degradation should be related with both components. Perfluorinated anions, such as $[PF_6]^-$ and $[BF_4]^-$, are recalcitrant to breakdown, so ILs containing them are harder to biodegrade. The biodegradation of ILs with halide anions is only based on the cations since halides are already mineralized. Many anions from organic acids, sugar acids and amino acids show high levels of biodegradation when paired with proper cations.[97] Among various cations, a lot of studies indicated that most

imidazolium-based ILs have poor biodegradabilities, except some with octyl sulfate anions.[98, 99] The alkyl chain length in cations can also influence the biodegradabilities of ILs (like it does to the toxicities of ILs as mentioned above), but the trend is opposite: ILs with longer alkyl chains are more biodegradable than shorter ones.[100] Modification of cations or anions can make changes to this feature. For example, in the study by the Gathergood group in 2012, the introduction of amide groups in the side chains of imidazolium ILs increased their biodegradabilities to be above 60%.[101]

1.5.4.4 Acidic ILs

Acidic ILs, an important branch of ILs, are often used in acid-facilitated reactions. Acidic ILs obtain their acidities from cations or anions or both. They are divided into Brønsted acidic ILs, Lewis acidic ILs, and dual acidic ILs (Figure 1-15).[102]

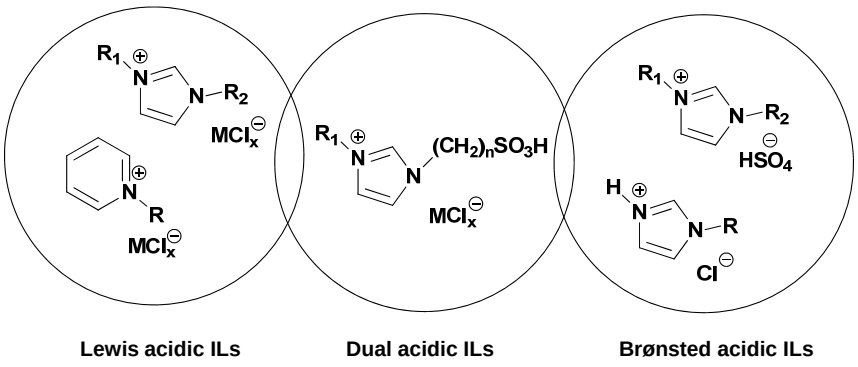

Figure 1-15. Types of acidic ionic liquids.

Brønsted acidic ILs act as proton donors, and the acidity can be obtained from either cations (e.g. $[Bmim\text{-}SO_3H]^+$, $[Hmim]^+$) or proton donor anions (e.g. $[HSO_4]^-$, dihydrogen phosphate $[H_2PO_4]^-$). ILs with protonated acidic groups on cations or with protons on the

quaternary N atoms of the cations are also called protic ILs, which are usually highly polar solvents.[103] Lewis acidic ILs act as electron pair acceptors, such as 1-butyl-3-methylimidazolium aluminum chloride ([Bmim]Cl-$AlCl_3$), and 1-ethyl-3-methylimidazolium chromium(Ⅱ) chloride ([Emim]Cl-$CrCl_2$). They are prepared by the addition of an appropriate amount of Lewis acid to a neutral IL. The mole fraction of the Lewis acid [$\chi(MCl_x)$] in a Lewis acidic IL is an important factor, and different fractions may lead to differences in acidities, physical and chemical properties of the IL. Take [Bmim]Cl-$AlCl_3$ as an example, the system is Lewis basic when $\chi(AlCl_3)$ is smaller than 0.5, neutral when $\chi(AlCl_3)$ is equal to 0.5, and Lewis acidic when $\chi(AlCl_3)$ is larger than 0.5.[104] The viscosity of the system increases with the decrease of $\chi(AlCl_3)$.[105] Dual and multi-functionalized acidic ILs are composed of cations from protic ILs and anions from Lewis acidic ILs, and usually have both Brønsted and Lewis acidic features.

1.5.4.5 Applications

1.5.4.5.1 Solvents and Extraction Media

So far a large part of the studies of carbohydrate solubilities in ILs are about cellulose. The study by the Rogers group in 2002 gave several significant findings,[86] which have been further confirmed in their later researches.[106, 107] Anions of ILs have greater influence than cations on cellulose solubilities in ILs because they can break the inter- and intra-molecular hydrogen bonding in cellulose and form new ones with the hydroxyl protons in the polysaccharide. Chloride (Cl^-) is more effective than bromide (Br^-), thiocyanate ($[SCN]^-$), $[PF_6]^-$ and $[BF_4]^-$. When heated in a microwave oven for 3 - 5 s pulses at full power, up to

25 wt% cellulose was dissolved in [Bmim]Cl. High-resolution ^{13}C NMR spectra showed that the structure of cellulose was disordered in the dissolution process.[106] ^{13}C and $^{35/37}Cl$ NMR analysis indicated that the Cl^- anion formed extensive hydrogen bonding with the hydroxyl protons in a 1:1 stoichiometry.[107] The increase of alkyl chain length in cations led to the decrease of cellulose solubility because of the drop of effective chloride concentration in the system. In 2006, Fukaya et al. found that because of their stronger hydrogen-bond basicities, 1,3-dialkylimidazolium formates performed better to dissolve cellulose than 1-allyl-3-methylimidazolium chloride ([Amim]Cl) with lower temperatures needed.[108] For example, cellulose started to dissolve in [Amim][HCOO] at 60 °C and at 85 °C approximately 22 wt% cellulose was dissolved; while in [Amim]Cl the dissolution started at 80 °C and only 2.5 wt% was dissolved at 85 °C. In 2014, the Esposito group successfully synthesized a series of ILs through hydrothermal decarboxylation of amino acid-derived imidazolium zwitterions,[109] which were prepared in their previous work.[110] The advantage of this study is that the starting materials from the beginning are amino acids, water, hydrogen peroxide and acetic acid, which are all quite green. The solubility of microcrystalline cellulose reached as high as 16.9 wt% at 100 °C by conventional heating in 1,3-diethyl-4-methylimidazolium acetate.

ILs can also act as reaction and extraction media. As mentioned in many examples in the 5-HMF application section (see **1.4.1.2**), ILs have been widely used as powerful solvents in the conversion of monosaccharides to 5-HMF, resulting in good yields. Recently, Jiao et al. used a series of imidazolium-based ILs for indole extraction from wash

oil.[111] When the volume ratio of [Bmim][BF_4] to model wash oil was 1 : 1, an indole extraction efficiency of 91.52% and a distribution coefficient of 9.51 were obtained after extraction at 40 °C for 60 min. The [Bmim][BF_4] can be separated from indole using Et_2O, and was reused three times without significant decrease in extraction efficiency.

1.5.4.5.2 Catalysts

ILs play an important role in catalysis, not only in lab reactions but also in industrial processes.[112, 113] In the transformations of biomass, especially cellulose, acidic ILs are quite often used since acidic systems usually promote the reactions. Take the study by Xu et al. as an example, a series of heteropolyanion-based ILs with sulfonic acid group (-SO_3H) functionalized cations and molybdovanadophosphoric acid anions ($H_{4-N}PMo_{11}VO_{40}^{N-}$) were synthesized and used in the conversion of microcrystalline cellulose to formic acid (FA).[114] At 180 °C under an oxygen pressure of 1.0 MPa, the IL with 1-(4-sulfonic acid) propyl-3-methylimidazolium cation ([Pmim-SO_3H]$_3$[$HPMo_{11}VO_{40}$]) gave the best FA yield of 51.3%. It was proposed that the Brønsted acidic cation was responsible for the catalysis of cellulose hydrolysis to glucose, while the anion accelerated the conversion of glucose to FA. The IL can be reused at least three times with little decrease in cellulose conversion and FA yield.

Biodiesel was made via the transesterification of waste cooking oil with methanol by the Lin group in 2013.[115] An IL, 4-allyl-4-methylmorpholin-4-ium bromine ([MorMeA]Br) was used together with sodium hydroxide (NaOH) as the catalysts. When the mass ratio of the IL to NaOH was 1:0.75, the best biodiesel yield of 98.1% was achieved after the system

(the molar ratio of methanol to waste oil was 9:1) was heated at 70 °C under microwave irradiation for 6 min. The IL was reused seven times with biodiesel yields around 98%.

Besides these two main aspects, there are many other areas in which ILs are widely used, such as in electrochemistry and transition metal catalysis. Due to their benign properties, ILs have great potential and a promising future. However, during their development, attention should be paid to their toxicities and environmental persistence, and steps should be taken to decrease their harm to the environment. Only through this can ILs become truly green solvents.

1.5.4.6 IL Recovery

Because of toxicity concerns, the treatment of ILs after experiments is quite important. As already seen in many cases discussed above, ILs are often recycled, aiming to make the process as green as possible. Generally, the used ILs are recovered from the reaction mixture first to make them pure enough for reuse. There are various methods for IL recovery based on the properties of ILs.[116] Since ILs are low-volatile and thermally stable, distillation is the first choice for their separation from volatile and thermally stable products. However, when products are non-volatile or thermally sensitive, extra solvents are needed for extraction. If the ILs are hydrophobic while products are hydrophilic, then water can be properly used. Otherwise, organic solvents are usually applied in the separation. CO_2 is soluble in ILs, but ILs are not soluble in CO_2.[117] In addition, many organic compounds have good solubilities in $scCO_2$. Therefore, $scCO_2$ can be used to extract compounds from ILs. If trace of $scCO_2$ is left in the ILs, it is easy to remove through a temperature increase or

pressure decrease, thus avoiding IL contamination. Scurto et al. performed a study of the separation of [Bmim][PF_6] and methanol by CO_2 addition.[118] Without CO_2, the IL and methanol were totally miscible. By adding CO_2 gas to the pressure of its low critical endpoint, a second liquid layer began to form, which was mainly methanol. With the continuous increase of CO_2 pressure to another critical point (K-point), the methanol layer merged with the gas phase. In this scCO_2/methanol layer no [Bmim][PF_6] was detected by ultraviolet-visible (UV-Vis) spectroscopy. An explanation was given that the addition of CO_2 decreased the solvent strength of methanol so it did not dissolve ionic species any more. The two critical points were closely related to the initial IL concentration and temperature. If the IL concentration was too high (49.3 mol%), the addition of CO_2 would not lead to a phase split.

A large number of ILs are very hydrophilic. They absorb water so easily and it is quite energy intensive and time consuming to do a distillation to remove residual water. Therefore, other methods have been investigated such as adsorption. Qi et al. prepared a kind of functional carbon material (FCM) loaded with carboxylic groups through the hydrothermal carbonization of cellulose.[119] The obtained FCM was used to adsorb [Bmim]Cl from its aqueous solution with the adsorption capacity (0.171 mmol/g) comparable to a commercial activated carbon (0.206 mmol/g). The absorbed [Bmim]Cl can be desorbed in acidic solutions with a maximum stripping rate of 76.8%. The regenerated FCM absorbent can be reused for at least three runs without significant decreases in its adsorption capacity.

Although ILs are quite useful, not many of them have been commercialized for industrial use. One main reason for this is their high cost and difficult subsequent treatment. Therefore, efficient recycling and reuse of ILs will be crucial to more abundant and greener applications of ILs.

1.6 Summary

Due to the potential crisis surrounding the depletion of fossil fuels and the need to reduce CO_2 emissions, the transformation of biomass into chemicals and fuels has been studied intensively over recent years. Current research is mainly focused on the conversion of carbohydrates which can be obtained on land, such as fructose, glucose and cellulose. Studies of oceanic biomass are limited despite its high abundancy. As an important platform chemical converted from renewable feedstocks, 5-HMF was discussed from two aspects: production and applications. There have been a large number of mechanistic studies on 5-HMF synthesis, which are presented in **Chapter 2**. NAG can be obtained from chitin, which abundantly exists in shells of crustaceans. The transformation of NAG or chitin to 3A5AF was presented from production methods and mechanistic features, followed by the possible applications of 3A5AF. Compared with 5-HMF, there is still significant scope to study the chemistry of 3A5AF. Solvents play an important role in chemical reactions. Different kinds of solvents including water, SCFs and ILs were introduced, among which ILs were discussed in detail from synthesis, properties, applications and recovery.

1.7 Objectives of Thesis

The essential objective of this thesis was to investigate the transformation of renewable feedstocks, develop efficient reaction routes for 3A5AF synthesis, and perform property and application studies of 3A5AF. To this end in **Chapters 2** to **5**, the following objectives were targeted: (1) A review and understanding of the tools and approaches used to study the transformations of carbohydrates of relevance to the field of green chemistry. (2) Further optimize the process for producing 3A5AF from NAG and develop an understanding of the factors that influence this process especially in ionic liquids. (3) Propose a mechanism for the conversion of NAG to 3A5AF based on experimental data. (4) Determine key physical and chemical properties of 3A5AF experimentally and computationally in order to better target future applications and improved processes for its production. (5) Develop and optimize the first reactions of 3A5AF and characterize the resulting products.

In **Chapter 2**, mechanistic studies on the transformation of biomass into 5-HMF were reviewed, mainly focused on the tools and approaches used (NMR spectroscopy, computational calculations, etc.). This review gives an insight into how certain instruments and techniques were applied to detect reaction intermediates and explore potential mechanisms. This detailed review was performed in order to place the mechanistic studies described in Chapter 3 into context. In **Chapter 3**, studies of 3A5AF production from NAG in ILs were discussed. 3A5AF yields were improved via the use of additives, in situ extraction and multiple runs (repeated microwave heating and extraction cycles) of a single

reaction mixture. Kinetic and mechanistic studies were performed to investigate the reaction process. In **Chapter 4**, computational calculations and lab experiments were combined to study the physical and chemical properties of 3A5AF. In **Chapter 5**, hydrolysis and reduction reactions of 3A5AF were performed, which are the most detailed reactivity studies on this molecule to date. The scientific data presented in **Chapters 4 and 5** constitute the first descriptions of the chemical and physical properties of 3A5AF.

1.8 References

1. P. T. Anastas and J. C. Warner, *Green Chemistry: Theory and Practice*, Oxford University Press, New York, 2000.

2. P. T. Anastas, L. G. Heine and T. C. Williamson, *Green Chemical Syntheses and Processes*, American Chemical Society, Washington DC, 2000.

3. S. L. Y. Tang, R. L. Smith and M. Poliakoff, *Green Chem.*, 2005, **7**, 761-762.

4. P. Anastas and N. Eghbali, *Chem. Soc. Rev.*, 2010, **39**, 301-312.

5. Biomass Energy Centre, http://www.biomassenergycentre.org.uk/, (accessed January 26, 2017).

6. J. E. Holladay, J. J. Bozell, J. F. White and D. Johnson, *Top Value Added Chemicals from Biomass*, U. S. DOE Report PNNL-16983, Pacific Northwest National Laboratory, the United States of America, 2007.

7. F. Cherubini and A. H. Strømman, *Biofuels, Bioprod. Biorefin.*, 2011, **5**, 548-561.

8. J. N. Chheda, G. W. Huber and J. A. Dumesic, *Angew. Chem. Int. Ed.*, 2007, **46**, 7164-7183.

9. F. M. Kerton, Y. Liu, K. W. Omari and K. Hawboldt, *Green Chem.*, 2013, **15**, 860-871.

10. S.-K. Kim, *Marine Cosmeceuticals: Trends and Prospects*, CRC Press, Boca Raton, 2011.

11. W. Bruck, J. Slater and B. Carney, *Chitin and Chitosan from Marine Organisms* in *Chitin, Chitosan, Oligosaccharides and Their Derivatives*, ed. S. Kim, CRC Press, New York, 2010, pp. 11-23.

12. M. S. Islam, S. Khan and M. Tanaka, *Mar. Pollut. Bull.*, 2004, **49**, 103-110.

13. C. Jeuniaux and M. F. Voss-Foucart, *Biochem. Syst. Ecol.*, 1991, **19**, 347-356.

14. K. Kurita, *Mar. Biotechnol.*, 2006, **8**, 203-226.

15. D. E. Hunt, D. Gevers, N. M. Vahora and M. F. Polz, *Appl. Environ. Microbiol.*, 2008, **74**, 44-51.

16. N. Dolgopyatova, V. Y. Novikov, I. Konovalova and N. Putintsev, *Russ. J. Appl. Chem.*, 2013, **86**, 986-991.

17. A. Ajavakom, S. Supsvetson, A. Somboot and M. Sukwattanasinitt, *Carbohydr. Polym.*, 2012, **90**, 73-77.

18. P. Aloise, A. L. Creagh and C. A. Haynes, *Process for Producing N-Acetyl-D-glucosamine*, U. S. Patent 5.998.173, Dec 7, 1999.

19. H. Sashiwa, S. Fujishima, N. Yamano, N. Kawasaki, A. Nakayama, E. Muraki, M. Sukwattanasinitt, R. Pichyangkura and S.-i. Aiba, *Carbohydr. Polym.*, 2003, **51**, 391-395.

20. W. Suginta, P. Robertson, B. Austin, S. C. Fry and L. A. Fothergill‐Gilmore, *J. Appl. Microbiol.*, 2000, **89**, 76-84.

21. B. Giuliano Garisto Donzelli, G. Ostroff and G. E. Harman, *Carbohydr. Res.*, 2003, **338**, 1823-1833.

22. N. S. Patil and J. P. Jadhav, *Int. Biodeterior. Biodegrad.*, 2014, **91**, 9-17.

23. K. Jamialahmadi, J. Behravan, M. F. Najafi, M. T. Yazdi, A. Shahverdi and M. Faramarzi, *Biotechnology*, 2011, **10**, 292-297.

24. P. Stallforth, S. Matthies, A. Adibekian, D. G. Gillingham, D. Hilvert and P. H. Seeberger, *Chem. Commun.*, 2012, **48**, 11987-11989.

25. C.-A. Chen and J.-M. Fang, *Org. Biomol. Chem.*, 2013, **11**, 7687-7699.

26. S. Masuda, K. Azuma, S. Kurozumi, M. Kiyose, T. Osaki, T. Tsuka, N. Itoh, T. Imagawa, S. Minami, K. Sato and Y. Okamoto, *Carbohydr. Polym.*, 2014, **111**, 783-787.

27. K. Azuma, T. Osaki, T. Wakuda, T. Tsuka, T. Imagawa, Y. Okamoto and S. Minami, *Inflammation*, 2012, **35**, 1462-1465.

28. R. V. Stick, *Carbohydrates: the Sweet Molecules of Life*, Academic press, London, 2001.

29. D. M. Updegraff, *Anal. Biochem.*, 1969, **32**, 420-424.

30. G. Dull, *Chem. Zeit.*, 1895, **19**, 166 and 216-167.

31. J. Kiermayer, *Chem. Zeit.*, 1895, **19**, 1003-1005.

32. J. Song, H. Fan, J. Ma and B. Han, *Green Chem.*, 2013, **15**, 2619-2635.

33. K. W. Omari, J. E. Besaw and F. M. Kerton, *Green Chem.*, 2012, **14**, 1480-1487.

34. P. Vinke and H. Van Bekkum, *Starch/Staerke*, 1992, **44**, 90-96.

35. T. Wang, M. W. Nolte and B. H. Shanks, *Green Chem.*, 2014, **16**, 548-572.

36. Y. Román-Leshkov, J. N. Chheda and J. A. Dumesic, *Science*, 2006, **312**, 1933-1937.

37. M. E. Zakrzewska, E. Bogel-Łukasik and R. Bogel-Łukasik, *Chem. Rev.*, 2011, **111**, 397-417.

38. S. Dutta and S. Pal, *Biomass Bioenergy*, 2014, **62**, 182-197.

39. C. Fayet and J. Gelas, *Carbohydr. Res.*, 1983, **122**, 59-68.

40. C. Lansalot-Matras and C. Moreau, *Catal. Commun.*, 2003, **4**, 517-520.

41. X. Qi, M. Watanabe, T. M. Aida and R. L. Smith Jr, *ChemSusChem*, 2009, **2**, 944-946.

42. C. Moreau, A. Finiels and L. Vanoye, *J. Mol. Catal. A: Chem.*, 2006, **253**, 165-169.

43. Z. Ding, J. Shi, J. Xiao, W. Gu, C. Zheng and H. Wang, *Carbohydr. Polym.*, 2012, **90**, 792-798.

44. T. Ståhlberg, S. Rodriguez‐Rodriguez, P. Fristrup and A. Riisager, *Chem. Eur. J.*, 2011, **17**, 1456-1464.

45. B. R. Caes, M. J. Palte and R. T. Raines, *Chem. Sci.*, 2013, **4**, 196-199.

46. Y. Román-Leshkov and J. A. Dumesic, *Top. Catal.*, 2009, **52**, 297-303.

47. T. S. Hansen, J. Mielby and A. Riisager, *Green Chem.*, 2011, **13**, 109-114.

48. M. Bicker, D. Kaiser, L. Ott and H. Vogel, *J. Supercrit. Fluids*, 2005, **36**, 118-126.

49. A. Corma, S. Iborra and A. Velty, *Chem. Rev.*, 2007, **107**, 2411-2502.

50. Y. Roman-Leshkov, C. J. Barrett, Z. Y. Liu and J. A. Dumesic, *Nature*, 2007, **447**, 982-985.

51. A. S. Nagpure, A. K. Venugopal, N. Lucas, M. Manikandan, R. Thirumalaiswamy and S. Chilukuri, *Catal. Sci. Technol*, 2015, **5**, 1463-1472.

52. S. Zhong, R. Daniel, H. Xu, J. Zhang, D. Turner, M. L. Wyszynski and P. Richards, *Energy Fuels*, 2010, **24**, 2891-2899.

53. A. S. Amarasekara, D. Green and L. D. Williams, *Eur. Polym. J.*, 2009, **45**, 595-598.

54. A. Gandini and N. M. Belgacem, *Polym. Int.*, 1998, **47**, 267-276.

55. M. Del Poeta, W. A. Schell, C. C. Dykstra, S. K. Jones, R. R. Tidwell, A. Kumar, D. W. Boykin and J. R. Perfect, *Antimicrob. Agents Chemother.*, 1998, **42**, 2503-2510.

56. K. T. Hopkins, W. D. Wilson, B. C. Bender, D. R. McCurdy, J. E. Hall, R. R. Tidwell, A. Kumar, M. Bajic and D. W. Boykin, *J. Med. Chem.*, 1998, **41**, 3872-3878.

57. C. Moreau, M. N. Belgacem and A. Gandini, *Top. Catal.*, 2004, **27**, 11-30.

58. O. Casanova, S. Iborra and A. Corma, *J. Catal.*, 2010, **275**, 236-242.

59. R. A. Franich, S. J. Goodin and A. L. Wilkins, *J. Anal. Appl. Pyrolysis*, 1984, **7**, 91-100.

60. J. Chen, M. Wang and C.-T. Ho, *J. Agric. Food. Chem.*, 1998, **46**, 3207-3209.

61. K. W. Omari, L. Dodot and F. M. Kerton, *ChemSusChem*, 2012, **5**, 1767-1772.

62. K. Alfonsi, J. Colberg, P. J. Dunn, T. Fevig, S. Jennings, T. A. Johnson, H. P. Kleine, C. Knight, M. A. Nagy, D. A. Perry and M. Stefaniak, *Green Chem.*, 2008, **10**, 31-36.

63. P. G. Jessop, *Green Chem.*, 2011, **13**, 1391-1398.

64. M. W. Drover, K. W. Omari, J. N. Murphy and F. M. Kerton, *RSC Adv.*, 2012, **2**, 4642-4644.

65. X. Chen, S. L. Chew, F. M. Kerton and N. Yan, *Green Chem.*, 2014, **16**, 2204-2212.

66. X. Chen, Y. Liu, F. M. Kerton and N. Yan, *RSC Adv.*, 2015, **5**, 20073-20080.

67. F. M. Kerton and R. Marriott, *Alternative Solvents for Green Chemistry*, Royal Society of Chemistry, Cambridge, UK, 2nd edn., 2013.

68. F. M. Kerton, *Solvent Systems for Sustainable Chemistry* in *Encyclopedia of Inorganic and Bioinorganic Chemistry*, John Wiley & Sons, Ltd, 2016.

69. K. Tanaka and F. Toda, *Chem. Rev.*, 2000, **100**, 1025-1074.

70. A. Orita, L. Jiang, T. Nakano, N. Ma and J. Otera, *Chem. Commun.*, 2002, 1362-1363.

71. F. Fringuelli, R. Girotti, F. Pizzo, E. Zunino and L. Vaccaro, *Adv. Synth. Catal.*, 2006, **348**, 297-300.

72. Y. Zhao, J. Li, C. Li, K. Yin, D. Ye and X. Jia, *Green Chem.*, 2010, **12**, 1370-1372.

73. M. M. Mojtahedi, E. Akbarzadeh, R. Sharifi and M. S. Abaee, *Org. Lett.*, 2007, **9**, 2791-2793.

74. M. Tamura, T. Tonomura, K.-i. Shimizu and A. Satsuma, *Green Chem.*, 2012, **14**, 717-724.

75. B. Rodriguez, A. Bruckmann, T. Rantanen and C. Bolm, *Adv. Synth. Catal.*, 2007, **349**, 2213-2233.

76. G. Kaupp, *CrystEngComm*, 2006, **8**, 794-804.

77. H. K. Reddy, T. Muppaneni, Y. Sun, Y. Li, S. Ponnusamy, P. D. Patil, P. Dailey, T. Schaub, F. O. Holguin and B. Dungan, *Fuel*, 2014, **133**, 73-81.

78. P. Pollet, E. A. Davey, E. E. Ureña-Benavides, C. A. Eckert and C. L. Liotta, *Green Chem.*, 2014, **16**, 1034-1055.

79. B. Subramaniam, R. V. Chaudhari, A. S. Chaudhari, G. R. Akien and Z. Xie, *Chem. Eng. Sci.*, 2014, **115**, 3-18.

80. P. Walden, *Bull. Acad. Imper. Sci.*, 1914, **8**, 405-422.

81. J. P. Hallett and T. Welton, *Chem. Rev.*, 2011, **111**, 3508-3576.

82. T. Welton, *Chem. Rev.*, 1999, **99**, 2071-2084.

83. D. Bradley, P. Dyson and T. Welton, *Chem. Rev.*, 2000, **9**, 18-21.

84. M. J. Earle and K. R. Seddon, *Pure Appl. Chem.*, 2000, **72**, 1391-1398.

85. J. F. Brennecke and E. J. Maginn, *AIChE J.*, 2001, **47**, 2384-2389.

86. R. P. Swatloski, S. K. Spear, J. D. Holbrey and R. D. Rogers, *J. Am. Chem. Soc.*, 2002, **124**, 4974-4975.

87. N. Sun, M. Rahman, Y. Qin, M. L. Maxim, H. Rodríguez and R. D. Rogers, *Green Chem.*, 2009, **11**, 646-655.

88. P. Mäki-Arvela, I. Anugwom, P. Virtanen, R. Sjöholm and J.-P. Mikkola, *Ind. Crops Prod.*, 2010, **32**, 175-201.

89. A. A. Rosatella, L. C. Branco and C. A. Afonso, *Green Chem.*, 2009, **11**, 1406-1413.

90. O. A. El Seoud, A. Koschella, L. C. Fidale, S. Dorn and T. Heinze, *Biomacromolecules*, 2007, **8**, 2629-2647.

91. A. Kamimura, S. Yamamoto and K. Yamada, *ChemSusChem*, 2011, **4**, 644-649.

92. R. L. Gardas and J. A. P. Coutinho, *Fluid Phase Equilib.*, 2008, **266**, 195-201.

93. K. R. Seddon, A. Stark and M.-J. Torres, *Pure Appl. Chem.*, 2000, **72**, 2275-2287.

94. D. J. Couling, R. J. Bernot, K. M. Docherty, J. K. Dixon and E. J. Maginn, *Green Chem.*, 2006, **8**, 82-90.

95. M. C. Bubalo, K. Radošević, I. R. Redovniković, J. Halambek and V. G. Srček, *Ecotoxicol. Environ. Saf.*, 2014, **99**, 1-12.

96. OECD Guidelines for the Testing of Chemicals, http://www.oecd.org/chemicalsafety/testing/oecdguidelinesforthetestingofchemicals.htm (accessed February 10, 2017)

97. A. Jordan and N. Gathergood, *Chem. Soc. Rev.*, 2015, **44**, 8200-8237.

98. N. Gathergood, M. T. Garcia and P. J. Scammells, *Green Chem.*, 2004, **6**, 166-175.

99. N. Gathergood, P. J. Scammells and M. T. Garcia, *Green Chem.*, 2006, **8**, 156-160.

100. K. M. Docherty, J. K. Dixon and C. F. Kulpa Jr, *Biodegradation*, 2007, **18**, 481-493.

101. D. Coleman, M. Spulak, M. T. Garcia and N. Gathergood, *Green Chem.*, 2012, **14**, 1350-1356.

102. C. Chiappe and S. Rajamani, *Eur. J. Org. Chem.*, 2011, **2011**, 5517-5539.

103. T. L. Greaves and C. J. Drummond, *Chem. Rev.*, 2008, **108**, 206-237.

104. L. Y. Piao, X. Fu, Y. L. Yang, G. H. Tao and Y. Kou, *Catal. Today*, 2004, **93-95**, 301-305.

105. P. Wasserscheid and W. Keim, *Angew. Chem. Int. Ed.*, 2000, **39**, 3772-3789.

106. J. S. Moulthrop, R. P. Swatloski, G. Moyna and R. D. Rogers, *Chem. Commun.*, 2005, 1557-1559.

107. R. C. Remsing, R. P. Swatloski, R. D. Rogers and G. Moyna, *Chem. Commun.*, 2006, 1271-1273.

108. Y. Fukaya, A. Sugimoto and H. Ohno, *Biomacromolecules*, 2006, **7**, 3295-3297.

109. S. Kirchhecker, M. Antonietti and D. Esposito, *Green Chem.*, 2014, **16**, 3705-3709.

110. D. Esposito, S. Kirchhecker and M. Antonietti, *Chem. Eur. J.*, 2013, **19**, 15097-15100.

111. T. Jiao, X. Zhuang, H. He, L. Zhao, C. Li, H. Chen and S. Zhang, *Green Chem.*, 2015, **17**, 3783-3790.

112. A. M. da Costa Lopes and R. Bogel-Łukasik, *ChemSusChem*, 2015, **8**, 947-965.

113. T. Welton, *Coord. Chem. Rev.*, 2004, **248**, 2459-2477.

114. J. Xu, H. Zhang, Y. Zhao, Z. Yang, B. Yu, H. Xu and Z. Liu, *Green Chem.*, 2014, **16**, 4931-4935.

115. Y.-C. Lin, P.-M. Yang, S.-C. Chen and J.-F. Lin, *Fuel Process. Technol.*, 2013, **115**, 57-62.

116. N. L. Mai, K. Ahn and Y.-M. Koo, *Process Biochem.*, 2014, **49**, 872-881.

117. L. A. Blanchard, Z. Gu and J. F. Brennecke, *J. Phys. Chem. B*, 2001, **105**, 2437-2444.

118. A. M. Scurto, S. N. V. K. Aki and J. F. Brennecke, *J. Am. Chem. Soc.*, 2002, **124**, 10276-10277.

119. X. Qi, L. Li, T. Tan, W. Chen and R. L. Smith, *Environ. Sci. Technol.*, 2013, **47**, 2792-2798.

1.9 Co-Authorship Statement

This PhD thesis includes results of joint research that have been published in or submitted to peer reviewed journals in the form of four full papers, as follows:

Chapter 2: Tools and Approaches Used for Mechanistic Studies on the Transformation of Biomass into 5-Hydroxymethylfurfural

Authors: Yi Liu and Francesca M. Kerton

Journal: *GreenChem.*

The principle author (Yi Liu) contributed to all aspects of the project as the main researcher including: literature review, collecting and analyzing the data, presenting and discussing the data with the corresponding author, writing the manuscript (first and final drafts) and preparing answers to the questions and comments of the peer reviewers.

The corresponding author (Dr. Francesca M. Kerton) proposed the initial topic of the review and contributed to several aspects of the project including: revision of the draft manuscript and submission to the journal, and supervision of the principal author (Y. L.).

Chapter 3: Synthesis of 3-Acetamido-5-acetylfuran from *N*-Acetyl-D-glucosamine in Ionic Liquids and Mechanistic Studies in a Range of Solvents

Aspects of this chapter (approx. 15-20% of its contents) have been published in the paper described below. However, over 80% of the contents of **Chapter 3** remain unpublished currently. A manuscript containing the NMR and mechanistic studies of NAG conversion is currently in preparation. Karen Strassel (a visiting undergraduate researcher from Germany) assisted in studying the conversion of *N*-acetylmannosamine and *N*-acetylgalactosamine, as part of the mechanistic work described. All other work in **Chapter 3** is my own. The aspects of the journal article (*RSC Adv.*, 2015, **5**, 20073-20080) performed by others are not included in my thesis.

Article: Conversion of Chitin and *N*-Acetyl-D-glucosamine into a *N*-Containing Furan Derivative in Ionic Liquids

Authors: Xi Chen, Yi Liu, Francesca M. Kerton and Ning Yan

Journal: *RSC Adv.*, 2015, **5**, 20073-20080

The principle author (Xi Chen) contributed to all aspects of the project as the main researcher including: literature review, performing 80% of the experiments, collecting and analyzing the data, designing new experiments, presenting and discussing the data with the corresponding authors, writing the manuscript (first and final drafts) and preparing answers to the questions and comments of the peer reviewers.

The co-first-author (Yi Liu) contributed to around 20% of the experiments and data analysis, mainly on the conversion of *N*-acetyl-D-glucosamine.

The corresponding author (Dr. Francesca M. Kerton) proposed the initial experiments and contributed to several aspects of the project including: data analysis, design of new experiments, revision of the draft manuscript and supervision of the co-first-author (Y. L.).

The corresponding author (Dr. Ning Yan) proposed the initial experiments and contributed to several aspects of the project including: data analysis, design of new experiments, revision of the draft manuscript and submission to the journal, and supervision of the principal author (X. C.).

Chapter 4: Combined Experimental and Computational Studies on the Physical and Chemical Properties of the Renewable Amide, 3-Acetamido-5-acetylfuran

Authors: Yi Liu, Christopher N. Rowley and Francesca M. Kerton

Journal: *ChemPhysChem*, 2014, **15**, 4087-4094

The principle author (Yi Liu) contributed to all aspects of the project as the main researcher including: literature review, performing all the experiments, collecting and analyzing the data, designing new experiments, presenting and discussing the data with the corresponding authors, writing the manuscript (first and final drafts) and preparing answers to the questions and comments of the peer reviewers.

The corresponding author (Dr. Christopher N. Rowley) helped in the design of the computational calculations and contributed to several aspects of the project including: analysis of the computational data and revision of the draft manuscript.

The corresponding author (Dr. Francesca M. Kerton) proposed the initial experiments and contributed to several aspects of the project including: data analysis, design of new experiments, revision of the draft manuscript and submission to the journal, and supervision of the principal author (Y. L.).

Chapter 5: Formation of a Renewable Amine and an Alcohol via Transformations of 3-Acetamido-5-acetylfuran

Authors: Yi Liu, Cosima Stähler, Jennifer N. Murphy, Brandon J. Furlong and Francesca M. Kerton

Journal: *ACS Sustainable Chemistry and Engineering*, 2017, **5**, 4916-4922

The principle author (Yi Liu) contributed to all aspects of the project as the main researcher including: literature review, performing 70% of the experiments, collecting and analyzing the data, designing new experiments, training the co-authors (Cosima Stähler and Brandon J. Furlong) to perform experiments and assisting in analyzing their data, presenting and discussing the data with the corresponding author, writing the manuscript (first and final drafts) and preparing answers to the questions and comments of the peer reviewers.

The co-second-author (Cosima Stähler) ran around 10% of the experiments and data analysis, mainly concerning the reduction of 3A5AF using $NaBH_4$. *The co-second-author (Jennifer N. Murphy)* ran around 10% of the data analysis, mainly on factorial design of experiments. *The third-author (Brandon J. Furlong)* ran about 10% of the experiments and data analysis, mainly running Ir-catalyzed reduction of 5-HMF and 3A5AF.

The corresponding author (Dr. Francesca M. Kerton) proposed the initial experiments and contributed to several aspects of the project including: data analysis, design of new experiments, revision of the draft manuscript and submission to the journal, and supervision of the principal author (Y. L.) and co-authors (C.S, J. N. M. and B. J. F.).

Chapter 2

Tools and Approaches Used for Mechanistic Studies on the Transformation of Biomass into 5-Hydroxymethylfurfural

A version of this chapter has been submitted for publication.

Yi Liu, and Francesca M. Kerton*

Tools and Approaches Used for Mechanistic Studies on the Transformation of Biomass into 5-Hydroxymethylfurfural, *GreenChem*.

2.1 Introduction

With the rapid development of industry in response to the dramatic increases in human population, the world is currently experiencing a great demand for energy, which is leading to a potential crisis surrounding fossil fuel depletion. In addition, the large emissions of carbon dioxide and other flue-gases (nitrogen oxides and sulfur dioxide) from fossil fuel combustion have caused environmental problems such as climate change and acid rain. The use of biomass as an alternative resource for both fuels and chemicals has been regarded as a promising and effective solution to the current situation. Some chemicals produced from biomass can play the role of platforms for the synthesis of a series of other compounds. Among biomass studies in recent decades, 5-hydroxymethylfurfural (5-HMF, Figure 2-1) is a quite popular platform chemical which can be obtained from lignocellulosic biomass transformations. In this tutorial review, we will provide an introduction to scientific efforts to date that attempt to reveal the mechanism of 5-HMF synthesis from saccharides using a range of tools.

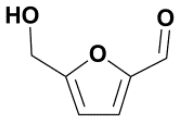

5-HMF

Figure 2-1. Structure of 5-hydroxymethylfurfural (5-HMF).

As "a sleeping giant",[1] 5-HMF is one of the important building block chemicals that has become the focus of research during the past decade. Dehydration of sugars to 5-HMF is a significant reaction in the field of biomass conversion, and reported results have mainly

focused on the conversion of fructose, glucose and cellulose.[2-4] With both hydroxyl and aldehyde functional groups, 5-HMF can be an intermediate for a variety of value-added products and promising biofuels. For example, 2,5-furandicarboxylic acid (FDCA) can be obtained from the oxidation of 5-HMF. FDCA has been listed among the twelve top platform chemicals from biomass by the US Department of Energy.[5] It can replace terephthalic acid in the synthesis of polyesters, polyamides and polyurethanes.[6] It can also be an intermediate in the production of other polymers or pharmaceutical and photography chemicals.[7] Moreover, the hydrogenation of 5-HMF can produce 2,5-dimethylfuran (2,5-DMF), which is an alternative fuel for transportation because of its satisfactory performance in ignition, emission and combustion compared with traditional gasoline.[8]

Because of its valuable applications, numerous efforts have been conducted on the effective synthesis of 5-HMF, and within these studies many chemists have explored the reaction mechanisms. Mechanistic studies are quite helpful in revealing what happened during the course of a multi-step reaction on a molecular level. Through such efforts, chemists should be able to design more effective reaction pathways and higher product yields could potentially be achieved. However, most mechanisms in this field have been proposed based on chemical intuition and there are only a few that have been developed based on computational calculations and experimental results. Herein we aim to present an overview of the tools and approaches used in mechanistic studies of 5-HMF synthesis from biomass. Instead of focusing on reaction pathways, the main purpose of this review is to give an insight into how certain instruments and techniques were applied to detect reaction

intermediates and explore mechanisms. We hope this tutorial is a good starting point for researchers who are interested in pursuing mechanistic studies of biomass transformations.

2.2 Fructose

Fructose is a simple hexose found in plants, fruits and vegetables. The fructose normally used in the research efforts described herein is D-fructose. It has five isomers including both straight chain and cyclic forms (Scheme 2-1). Besides its traditional use as a sweetener in industry, the dehydration of fructose has been extensively studied because of its cheap price, fast conversion and high 5-HMF yields.

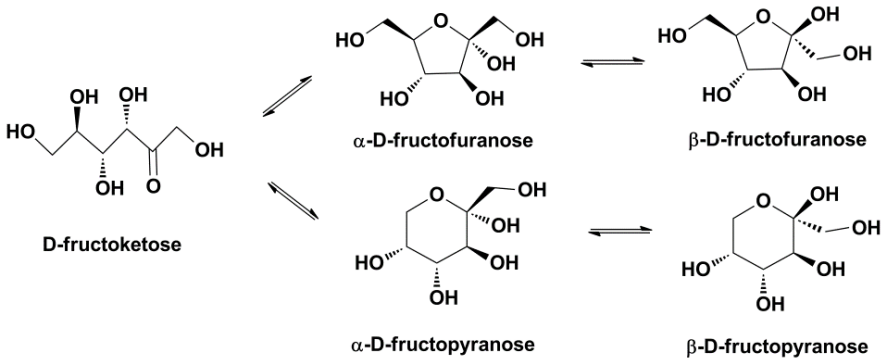

Scheme 2-1. Five isomers of D-fructose.

So far two reaction pathways have mainly been proposed for the dehydration of fructose to 5-HMF. It can proceed via a cyclic or acyclic (open-chain) route (Scheme 2-2).[9] In 1910, Nef first came up with the cyclic route for 5-HMF formation from fructose involving a fructofuranosyl cationic intermediate.[10] In the acyclic route, the key intermediate was 3-deoxy-hexosulose, which was first introduced by Anet in 1960 in a communication article about the importance of 3-deoxyhexosones as intermediates in sugar

transformations.[11] In 1965, several 3-deoxyhexosones were detected during the dehydration of fructose to 5-HMF, supporting the assumption about their role in the transformations of carbohydrates.[12] Both mechanisms have been discussed in many studies since they were raised. However, evidence from lab experiments and computational calculations is still scarce, and neither of these two routes has stood out as the definitive pathway, and of course either or both routes may occur dependent on the exact reaction conditions.

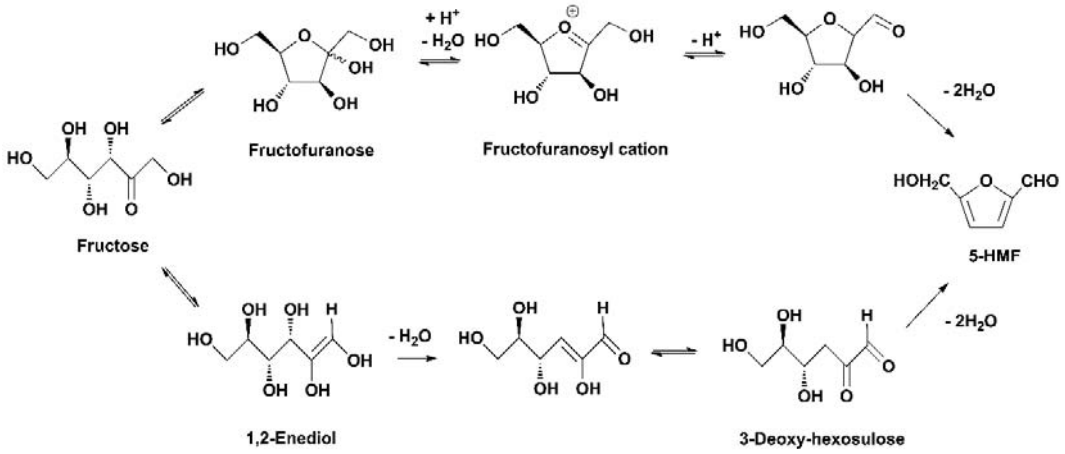

Scheme 2-2. Cyclic (top) and acyclic (bottom) pathways of fructose conversion to 5-HMF.[11, 13-15]

2.2.1 Nuclear Magnetic Resonance (NMR) Spectroscopy

NMR spectroscopy is a tool frequently used in mechanistic studies. It is quite useful since it can offer a variety of information via both the commonly studied ^{1}H and ^{13}C NMR spectroscopies. NMR spectra of some other elements can also be obtained by doing specific NMR analyses such as ^{17}O and ^{11}B NMR spectroscopy. Isotopic labelling techniques are

also often used as a powerful tool in gaining mechanistic insights. For example, if several carbon atoms in fructose are ^{13}C labelled (Figure 2-2), the ^{13}C proportion of these carbon atoms is higher than for the other carbon atoms. Consequently, these enriched carbon atoms have much higher intensities than the others in ^{13}C NMR spectra so their resonances are easier to track. This can be used to trace the locations of these carbons in the products, and to analyze the structures of compounds.

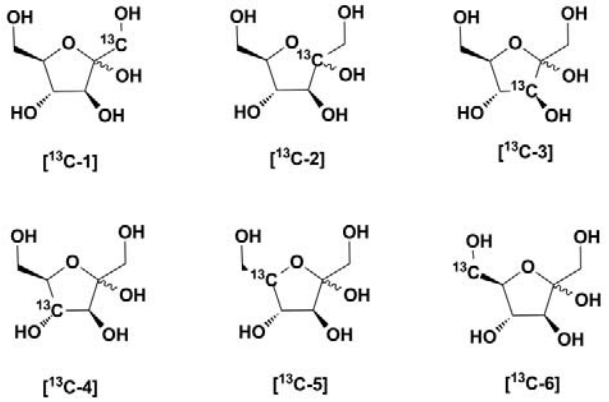

Figure 2-2. Fructose molecules with different ^{13}C labelled carbon atoms.

Because of its useful properties (high boiling point, high decomposition temperature, rare proton/deuterium exchange) and ability to dissolve many compounds, dimethyl sulfoxide-d_6 (DMSO-d_6) is a widely-used solvent in NMR-assisted mechanistic studies. In a typical experiment, the starting materials (fructose and catalysts if applicable) are dissolved in DMSO-d_6. The solution is allowed to equilibrate at room temperature for a certain time (at least 12 h) to stabilize, and ^{1}H and ^{13}C NMR spectra are then recorded. The solution is subsequently heated to a desired temperature, and ^{1}H and ^{13}C NMR spectra are taken periodically over the course of the reaction. In the studies by Amarasekara et al.[16]

and Zhang et al.,[17] biphenyl was used as an internal standard for quantification purpose. The Horváth group also used DMSO-d_6 or methylsulfonylmethane for quantitative measurements as an alternative to biphenyl.[18] As shown in the studies by the groups of Horváth,[18] Zhang,[17, 19] and Kimura,[20] ^{13}C-labelled fructose has been used to evaluate the tendencies of intermediates to form and identify their structures from a common fructofuranose starting point through to the product 5-HMF.

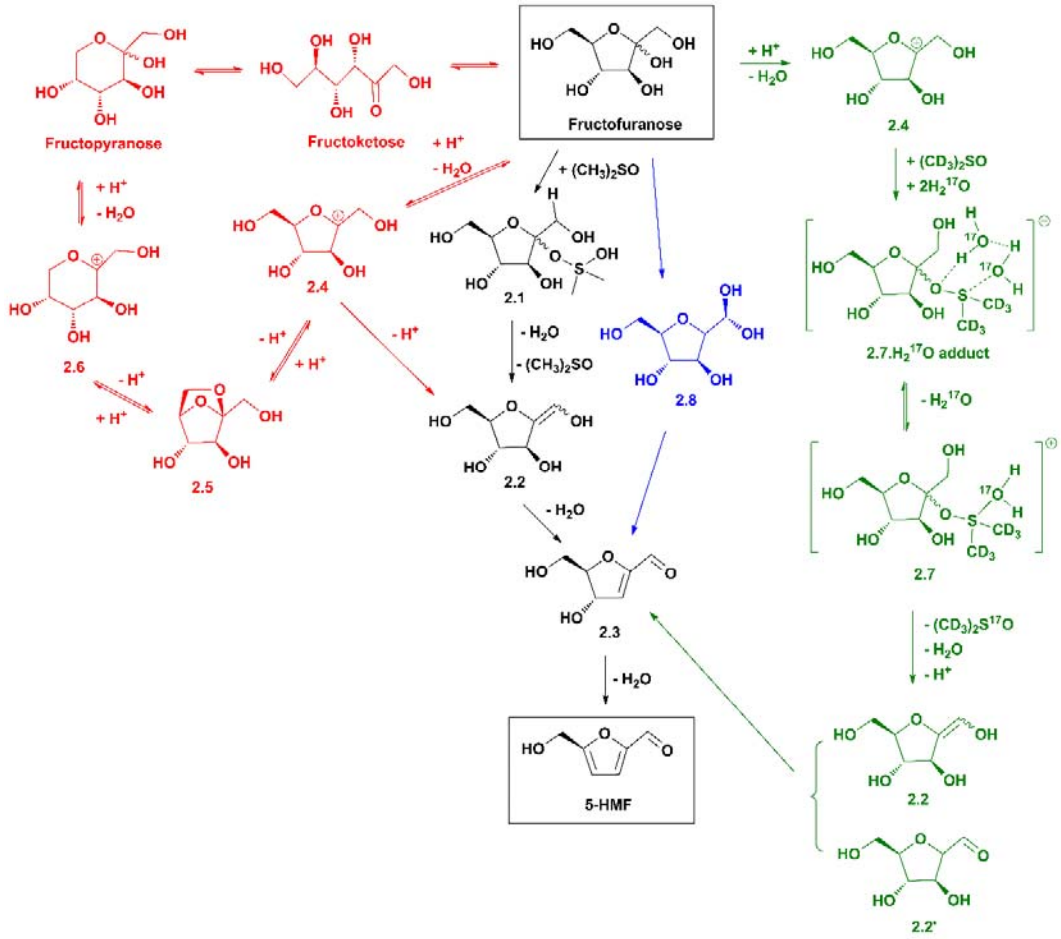

Scheme 2-3. Reaction pathways of the dehydration of fructose to 5-HMF proposed by Horváth[18] (red), Amarasekara[16] (black), Kimura[20] (blue) and Zhang (green)[17, 19].

Table 2-1. ^{1}H and ^{13}C NMR data of the intermediates in Scheme 2-3 and 5-HMF.

Compound	Solvent	δ_H (ppm)	δ_C (ppm)	Ref
2.2	DMSO-d_6	5.57 (d, H1), 4.11 (dd, H3), 3.74 (H4), 3.83 (H5), 3.55 (H6), 3.44 (H6')	118.9 (C1), 139.1 (C2), 75.2 (C3), 76.3 (C4), 86.4 (C5), 61.5 (C6)	18
2.3	DMSO-d_6	9.47 (s, H1), 6.25 (d, H3), 4.81 (dd, H4), 4.26 (td, H5), 3.46 (m, H6)	184.3 (C1), 156.4 (C2), 122.3 (C3), 73.6 (C4), 90.3 (C5), 61.3 (C6)	18
	DMSO-d_6	6.23 (d, H3), 9.46 (s)	184.9 (C1), 156.9, 122.8,	16
	DMSO-d_6	-	186 (C1), 157 (C2), 129 (C3), 85 (C4), 90 (C5), 62 (C6)	20
	DMSO-d_6	9.47 (s, H1), 6.25 (d, H3), 4.81 (dd, H4), 4.26 (td, H5), 3.46 (m, H6)	184.0 (C1), 156.4 (C2), 122.5 (C3), 73.4 (C4), 90.1 (C5), 61.1 (C6),	17
2.5	DMSO-d_6	3.59 (m, H1), 3.68 (dt, H3), 3.51 (d, H4), 4.38 (dd, H5), 3.53 (d, H6), 3.41 (dd, H6')	57.6 (C1), 108.3 (C2), 81.2 (C3), 78.3 (C4), 82.6 (C5), 65.9 (C6)	18
2.7	DMSO-d_6	-	57.4 (C1), 108.0 (C2), 78.1, 81.0, 82.4, 65.6 (C6),	17
2.8	DMSO-d_6	-	63 (C1), 109 (C2), 78 (C3), 78 (C4), 85 (C5), 66 (C6)	20
5-HMF	DMSO-d_6	9.52 (s, H1), 7.48 (d, H3), 6.59 (dt, H4), 4.49 (s, H6)	177.9 (C1), 151.6 (C2), 124.5 (C3), 109.9 (C4), 162.0 (C5), 56.0 (C6)	18
	DMSO-d_6	6.57 (d), 7.46 (d), 9.51 (s)	178.7, 152.4, 125.0, 110.4, 162.8, 58.6,	16
	DMSO-d_6	4.47 (s), 6.50 (d), 7.40 (d), 9.49 (s)	178.3 (C1), 151.8 (C2), 110.0, 124.6, 162.0, 56.5 (C6),	17, 19
	D_2O	-	183.2 (C1), 154.5, 113.7, 164.0, 58.2 (C6),	19

Scheme 2-3 shows the putative reaction maps of fructose dehydration to 5-HMF discussed in **2.2.1**. Table 2-1 lists the ^{1}H and ^{13}C NMR data of the main intermediates and 5-HMF. The ^{1}H and ^{13}C NMR spectra of fructose in DMSO-d_6 show that at room temperature the five isomers have chemical shifts ranging from 3.0 - 4.5 ppm and 50 - 220 ppm.[19] The NMR analysis of [^{13}C-2] fructose further revealed that the cyclic isomers have resonances of their C2 atoms within 95 - 110 ppm and the open-chain fructose has its carbonyl resonance at 215 ppm.[18, 20]

In 2008 Amarasekara et al. performed the dehydration of fructose at 150 °C in DMSO-d_6.[16] ^{1}H and ^{13}C NMR data showed that after 6 min an intermediate (**2.3**) appeared. With the increase of 5-HMF signals, the intensity of **2.3** started to decrease from t = 24 min and finally disappeared. In the mechanism proposed in this study, DMSO was proposed to act as a Lewis base and interact with fructose to form some intermediates (**2.1** and **2.2**). However, no NMR evidence was given to support their existence possibly because of their fast conversions to **2.3** in the reaction process.

In 2012, the Horváth group mapped the dehydration of fructose catalyzed by sulfuric acid (H_2SO_4) in different solvents through isotopic labelling experiments.[18] After the solution of the starting materials was equilibrated at room temperature for one week or heated at 150 °C for 5 min, the five isomers of fructose were detected to be in equilibria by ^{13}C NMR spectroscopy. A solution of [^{13}C-2] fructose in DMSO-d_6 was heated at 150 °C for 4 h, and ^{13}C NMR spectra were recorded during the reaction. From t = 2 min, three peaks at 108.3 (**2.5**), 139.2 (**2.2**) and 156.5 ppm (**2.3**) started to increase. Peaks of 5-HMF

appeared at t = 4 min and kept increasing. By t = 25 min, resonances of **2.5** and **2.2** had decreased to very low intensities, and by the end of the reaction all three intermediates vanished. [^{13}C-1] to [^{13}C-6] fructose were respectively used to perform the reaction, and ^{13}C NMR spectra were analyzed to identify the structures of **2.5**, **2.2**, and **2.3**. In addition, a certain amount of deuterium oxide (D_2O) was added to the starting materials. No deuterium incorporation into 5-HMF indicated that the three steps from **2.4** towards 5-HMF were irreversible (otherwise 5-HMF-D1 would be produced). This means that 5-HMF formation catalyzed by H_2SO_4 is not via fructoketose (the open-chain form of fructose) i.e. the acyclic pathway is not followed (otherwise 5-HMF-D3 would be produced). A reaction mechanism was proposed based on the analysis of their NMR results. **2.5** was believed to be an intermediate in the equilibrium between two fructosyl oxocarbenium ions, **2.4** and **2.6**, which were derived from the furanose and pyranose isomers respectively. **2.2** was produced from the deprotonation of **2.4**, and then dehydrated to form **2.3**. Finally, 5-HMF was obtained by loss of one water molecule from **2.3**. This study elegantly applied isotopic labelling techniques to analyze the different reaction pathways from the fructose isomers and the structures of possible intermediates. It is significant as it clearly showed for the first time that the often proposed fructoketose pathway is not followed.

In 2012 Zhang et al. performed in situ ^{13}C and ^{1}H NMR studies of fructose conversion using different catalysts in both DMSO-d_6 and water (10 wt% deuterium oxide (D_2O) added).[19] The ^{1}H and ^{13}C NMR results in DMSO-d_6 indicated that 5-HMF was the only product from fructose transformation in all experiments. In the ^{13}C NMR spectra of the

reaction catalyzed by Amberlyst 70 at 95 °C, the signals of three fructose cyclic isomers (β-pyranose, α- and β-furanose) were detected at the beginning of the reaction, and decreased in intensity with the increase of the 5-HMF peaks over time. Correspondingly, the ^{1}H NMR spectra showed the same trend.

In the experiments with water as the solvent, when phosphate anion/niobic acid catalyst was used, the intermediate **2.3**, 5-HMF and furfural were clearly identified in the ^{13}C NMR spectra by t = 40 min. When Amberlyst 70 was used as the catalyst, 5-HMF signals were detected in the ^{13}C and ^{1}H NMR spectra within 4 h, and started to decrease afterwards because of the decomposition of 5-HMF to levulinic acid (LA) and formic acid (FA). When H_2SO_4 was used, 5-HMF was formed within 1 h and then started to convert to LA and FA after this time.

Afterwards, [^{13}C-1] and [^{13}C-6] fructose were used as the reactants to track the locations of the carbon atoms in the product. In DMSO-d_6, with increasing reaction time, the three signals of the ^{13}C-1 atoms in the fructose isomers (63.3, 64.0, 64.6 ppm) decreased in intensity and a corresponding signal at 178.3 ppm increased, belonging to the C1 atom of 5-HMF. Similarly, the peaks of C6 atoms in the fructose isomers (61.2, 63.0, 63.2 ppm) decreased in intensity along with increasing signal strength for the C6 atom in 5-HMF (56.5 ppm) over time. These results revealed that the C1 and C6 in 5-HMF were derived from C1 and C6 in fructose. The same conclusion was obtained when water was used as the solvent. Nevertheless, in this work the authors didn't give detailed information about the pathway of the transformation of fructose to 5-HMF. The ^{13}C-labelling study in this case

was not used to identify intermediates and based on the positions of the labelled carbons in the starting material and final product either pathway could have been followed.

In 2016, the same group presented their further study of fructose dehydration using the same catalysts with a more specific mechanism determined.[17] Firstly, two intermediates (**2.7** and **2.3**) were identified in the ^{13}C NMR spectra recorded during the reaction process. Six signals from **2.7** appeared at t = 1 h, and increased in intensity during the following 4 h. Their intensities started to decrease with the increase in intensity of the 5-HMF peaks, and finally disappeared after 24 h. Meanwhile, another set of six peaks (**2.3**) were detected at t = 2 h, which kept increasing in intensity till t = 6 h and then decreased until hardly visible at t = 12 h. Through intensity normalized ^{13}C NMR spectra, **2.3** was ensured to be different from **2.7** because of their different appearance times and time dependences of their signal amplitudes. Moreover, they showed via intensity-time plots for **2.7** compared with **2.3** that **2.7** was generated before **2.3** en route to 5-HMF formation.

Next, the group identified the structures of the intermediates through the analysis of distortionless enhancement by polarization transfer (DEPT) 135 ^{13}C NMR spectra, ^{13}C NMR spectra of different ^{13}C labelled fructose and high resolution electrospray ionization mass spectra (HR ESI–MS). Comparison of the DEPT 135 ^{13}C NMR spectra with the normal ^{13}C NMR result at t = 6 h indicated that **2.7** had two secondary carbons (same phase), three tertiary carbons (opposite phase) and one quaternary carbon (undetectable). **2.3** had one secondary carbon, four tertiary carbons and one quaternary carbon. Afterwards, reactions of [^{13}C-1], [^{13}C-2] and [^{13}C-6] fructose were carried out and analyzed using ^{13}C

NMR spectroscopy. The analysis successfully located the signals of C1, C2 and C6 from fructose in **2.7**, **2.3** and 5-HMF. HR ESI-MS analysis was performed for a reaction mixture (80 °C, 6 h) and a control sample (fructose dissolved in DMSO at room temperature). Comparison between the results revealed the existence of three intermediates in the reaction mixture, corresponding to $[Fructose\text{-}OH]^+$ (*m/z* 163.0600), $[Fructose\text{-}H_2O+Na]^+$ (*m/z* 185.0420) and $[Fructose\text{-}2H_2O+H]^+$ (*m/z* 145.0494) in the HR ESI-MS spectra. They were assigned to **2.7**, **2.2** (or **2.2'**) and **2.3** respectively.

Besides ^1H and ^{13}C NMR analysis, ^{17}O NMR spectroscopy was also applied for further confirmation of the structure of **2.7**. The fructose and the catalyst were dissolved in DMSO-d_6 with 0.5% $H_2{}^{17}O$ (20.0% at ^{17}O) added. In situ ^{17}O NMR spectra were recorded at room temperature first. Then the solution was heated at 80 °C for 24 h, and analyzed by in situ ^{17}O NMR spectroscopy periodically. From t = 2 h, two peaks appeared at 60 ppm and 580 ppm. The latter was assigned to the aldehyde oxygen in 5-HMF. Its appearance in ^{17}O NMR spectra resulted from the exchange with the ^{17}O in $H_2{}^{17}O$, as the fructose used was not labelled. The signal at 60 ppm decreased from t = 2 h to t = 8 h with the increase of 5-HMF peak, indicating that it was from an intermediate. Comparing its appearance and disappearance time with ^{13}C NMR data this peak was assigned to **2.7**. During the reaction, the signal at 12.4 ppm from the naturally occurring ^{17}O in DMSO-d_6 was found to increase, indicating that ^{17}O from $H_2{}^{17}O$ was incorporated into DMSO-d_6. A control experiment of $H_2{}^{17}O$ (0.5%) in DMSO-d_6 under the same condition without fructose addition showed no change in the peak intensity at 12.4 ppm. Hence DMSO was believed to participate in the

reaction process and consequently caused the incorporation of ^{17}O. This study is therefore interesting as it further confirms the involvement of DMSO in the reaction mechanism, and also suggests that water can act to influence mechanisms in this field too.

Based on all experimental work accomplished and previous findings by others,[16, 18, 20] the group proposed a mechanism involving DMSO participation. This is the first study that offered experimental evidence for DMSO interaction with the reaction species. It needs to be noted that the intermediate during the conversion of **2.7** to **2.3** has two possible forms, enol (**2.2**) or aldehyde (**2.2'**), but this study was not able to detect either one experimentally, probably because of its low concentration under the reaction conditions applied.

In the study by Kimura et al. in 2013,[20] they found one new intermediate (**2.8**) in the dehydration of fructose in DMSO-d_6 but the participation of DMSO was not seen in the reaction mechanism. At t = 15 min, two new peaks appeared at 109 ppm and 157 ppm, and were assigned to two intermediates (**2.8** and **2.3**). During the reaction progress, the signal of **2.3** kept increasing till t = 45 min, and then the signal of 5-HMF at 152 ppm appeared and started to increase in intensity. At the end of the reaction (330 min), 5-HMF was the only product and both intermediates had disappeared. The plots of the reactant and product concentrations versus time showed that **2.8** appeared slightly earlier than **2.3**, and 5-HMF concentration increased coupled with the decrease in concentrations of these two species, which further indicated that they were the precursors for 5-HMF generation. NMR chemical shift calculations of the two intermediates in polarizable continuum model (PCM) of DMSO as the solvent were performed using the Gaussian 09 program at the B3LYP

level of theory with the augmented cc-pVDZ (aug-cc-pVDZ) basis set. The experimental values and calculation results were in acceptable agreement. The structures of the two intermediates were identified using [^{13}C-1], [^{13}C-2], [^{13}C-5], [^{13}C-6] and [^{13}C-1, 2, 3, 4, 5, 6] fructose for reactions and analyzing the corresponding ^{13}C NMR spectra obtained. **2.8** was assigned to 3,4-dihydroxy-2-dihydroxymethyl-5-hydroxymethyltetrahydrofuran. This study claimed to be the first one that discovered the existence of this intermediate in the fructose dehydration process. **2.8** is different from the DMSO-substituted (**2.1**) or the enol intermediate (**2.2**) in the mechanism previously proposed by Amarasekara.[16] Therefore a different reaction pathway was proposed in this study. However, it should be noted that **2.8** was possibly formed before or after the generation of other intermediates (**2.1** or **2.2**) and may be present in low (undetectable) concentrations in reactions studied by others.

2.2.2 Computational Studies

In recent years, computational chemistry has become increasingly important for investigating reaction mechanisms. The advantages of computational calculations include their convenience to operate and that they can be performed at the same time as lab work. A variety of information can be obtained such as electrostatic potential of molecules and Gibbs energies of activation for chemical reactions. More and more researchers prefer to apply both experimental and computational work in their studies. The theoretical data can provide predictions and explanations for the experimental results, while the lab results provide factual support to the calculations. In the area of biomass transformations, computational studies are normally used to calculate the activation energies of every single

step of a putative reaction pathway, analyze their endo- or exo-thermic properties and investigate the stabilities of proposed intermediates.

In order to do mechanistic studies through computational calculations, the first step is to optimize the geometries of the models i.e. find the most stable atomic arrangements of the molecules with the lowest energies. Afterwards a series of calculations can be implemented including vibrational frequencies, molecular energy and NMR spectra prediction. Since in actual lab experiments solvents are often used, the solvation effect should be considered in calculations. In Density Functional Theory (DFT) modelling, usually the Gibbs energies of the species in the gas phase are calculated first, and then the implicit (continuum) solvent models are included for the calculation of solvation energies via electronic structures. However, this approach neglects some factors that are significant in real reaction circumstances such as solvent dynamic effects. Therefore, simulations based on molecular dynamics (MD) methods using explicit solvent models have been developed in some studies in order to get more accurate reaction pathways, which are closer to the actual mechanisms. Nevertheless, DFT modelling is still a good starting point for people interested in computational mechanistic studies because of its easy operation and good accuracy. The engine used most widely in DFT calculations is Gaussian. B3LYP is the most commonly used level of theory with several basis sets supported (e.g. 6-31G, 6-311+G, cc-PVTZ). For higher accuracy requirements, Gaussian-*n* methods (G1, G2, G2MP2, G3, G3MP2, G3B3, G3MP2B3, G4, and G4MP2) are good to use.

In the work by Zhang et al. in 2016 as discussed in **2.2.1**, after experimental studies they performed Gibbs energy calculations of the Brønsted acid-catalyzed dehydration of fructose in the gas phase using Gaussian 09 software with G4MP2 level of theory.[17] For species in which DMSO was incorporated, the solvation energies were calculated using the solvation model based on density (SMD) at the B3LYP/6-31G(2df,p) level of theory with DMSO as the solvent. The authors believed that the entropic effects from association and dissociation were less significant in the solution where DMSO had interaction with the solutes than in the gas phase, therefore the entropies from gas-phase Gibbs energy calculations were neglected in the calculations of the species involving DMSO participation. The obtained Gibbs energy surface showed that the fructose molecule absorbed energy (52.3 kJ/mol) during protonation at the tertiary hydroxyl site (O2H) first. Afterwards, the calculation results indicated that the interaction between DMSO and the protonated fructose was quite exergonic (-71.5 kJ/mol) and led to the formation of **2.7** (Scheme 2-3). Then **2.7** lost the DMSO molecule and one water molecule to produce **2.5**, the intermediate found in the study by the Horváth group. This resulted in the generation of **2.2**. Two pathways from **2.2** to **2.3** were given. One was the protonation, dehydration and deprotonation of **2.2**; while the other one involved the acid-catalyzed tautomerization of **2.2** to **2.2'** first, and **2.2'** underwent protonation, dehydration and deprotonation. The process from **2.2** to **2.3** was exergonic (-70.3 kJ/mol), which supported the fact that the stable species **2.3** was detected in experimental work. Finally, the conversion of **2.3** to 5-HMF was also very exergonic (-95.4 kJ/mol), so 5-HMF was favored as the final product.

Besides **2.7**, the geometry of **2.7** with one water molecule added was also optimized. It was found that this water molecule could provide hydrogen bonding and strengthen the bond between C2 from fructose and O from DMSO (bond length decreased from 1.47 Å to 1.46 Å). This calculation supported the deduction about the incorporation of ^{17}O atom into DMSO-d_6, which was postulated from the ^{17}O NMR analyses.

In order to investigate the function of DMSO as a prominent solvent in the dehydration of fructose, the Vlachos group[21] performed MD simulations of fructose and 5-HMF under ambient conditions. Water or a water-DMSO mixture was used as the solvent system and the calculation results were compared to study the solvation effect of DMSO. In order to detect the local organization of the solvent molecules and their interactions with fructose and 5-HMF molecules, radial distribution functions (RDF) between solute-solvent atom pairs and volumetric maps of the local three-dimensional structural arrangement of the solvent around the solute were calculated. As shown in Table 2-2, in the first solvation shell, the average RDF values of fructose carbon atoms with the oxygen atom from DMSO (C-OS) were higher than with the water oxygen atom (C-OW), and the number of water molecules per fructose carbon atom coordinates with (coordination number) was lower in water-DMSO mixture than in pure water. In the volumetric maps of the solvated fructose, the isosurfaces of the density of water oxygen and DMSO oxygen atoms around the fructose molecule showed that the addition of DMSO broke the continuous solvation-ring structure of water molecules around the fructose molecule.

Table 2-2. The RDF values and coordination numbers calculated for fructose in water or a water-DMSO mixture in the study by the Vlachos group.[21]

			Water + DMSO	Water
3% Fructose	RDF at 3.6 Å (R)	C-OS	1.44	-
		C-OW	1.07	0.99
	Coordination number	DMSO-fructose	0.73	-
		Water-fructose	3.0	5.2
25% Fructose	RDF at 3.6 Å (R)	C-OS	1.46	-
		C-OW	1.32	1.11
	Coordination number	DMSO-fructose	0.72	-
		Water-fructose	4.0	5.2

All these results indicated that DMSO was more strongly coordinated with the fructose than water. The coordination of fructose carbon atoms was explained to be related to the hydrogen bonding between fructose and water or DMSO (Figure 2-3). As both a hydrogen bond donor and acceptor, water molecules tended to stay around the oxygen atoms of the hydroxyl groups of fructose to lower the threshold of acid-catalyzed dehydration of fructose (the proton transfer from a hydronium ion to a hydroxyl group on C2, C3 or C4 of fructose). By contrast, DMSO is only a hydrogen bond acceptor, so it competed with water to form hydrogen bonds with the hydrogen atoms of fructose's hydroxyl groups, especially around C2, C3 and C4. This helped to eliminate side reactions during fructose dehydration such as polymerization, by preventing the hydrogen atoms from removing the hydroxyl groups and forming glycosidic linkages with other fructose molecules. Furthermore, DMSO also had stronger coordination with 5-HMF carbon atoms than water, especially with C1, indicated

by the simulation results of RDFs and the three-dimensional arrangement of water and DMSO molecules around a 5-HMF molecule. This strong interaction between DMSO molecules and C1 of 5-HMF inhibited the cleavage of the C1-C2 bond of 5-HMF which leads to the hydration of 5-HMF to FA and LA. Therefore, this work provided further evidence to support the use of hydrogen-bond acceptor solvents (especially DMSO) in the transformations of fructose.

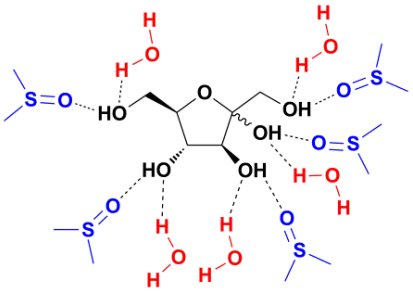

Figure 2-3. The hydrogen bonding between a fructose molecule and water (red, as a hydrogen bond donor) and DMSO (blue, as a hydrogen bond acceptor) molecules.[21]

During 2011 and 2012, four groups respectively published their achievements on the computational calculations of the Brønsted acid-catalyzed dehydration of fructose in water.[22-26] Caratzoulas and Vlachos performed their studies using the hybrid Quantum Mechanics/Molecular Mechanics Molecular Dynamics (QM/MM MD) simulation and established a first-principles-based microkinetic model of the acid-catalyzed dehydration of fructose for a simulation accuracy test.[22, 23] In the study by Assary et al. in 2011, Gaussian 03, Gaussian 09 and NWCHEM programs were used for the calculations.[24] The B3LYP/6-31G(2df,p) level of theory was applied first for geometry optimization and calculation of

frequencies and zero-point energies. Then a more accurate method, Gaussian-4 level of theory, was used to calculate molecular energies of fructose, 5-HMF, the intermediates and transition state models. In their subsequent study in 2012, the G4MP2 level of theory was applied for all calculations using Gaussian 09 program.[25] The Pidko group performed the calculations using the Gaussian 09 software and the B3LYP/6-311+G(d,p) level of theory to study the production of 5-HMF from both fructose and glucose and its subsequent transformation to LA.[26] The solvation effect of water was considered in all studies. The way to simulate the reaction proceeding with acid catalysis was to develop a protonated fructose model as the reactant. In all these studies, the comparison between the calculation results of all possible protonation sites indicated that protonation at the tertiary hydroxyl group (O2H) was the thermodynamically optimum one because 1) this model had the lowest gas-phase Gibbs energy; 2) the removal of the first water molecule had the lowest activation Gibbs energy; 3) the reaction pathway would have led to ring opening or fragmentation if the protonation happened on either of the other two hydroxyl groups.

The cyclic pathway of fructose conversion which involved fructofuranosyl intermediates was supported by all these studies (Scheme 2-4) and the findings from the NMR studies described in **2.2.1** were confirmed. In the simulation of fructose dehydration in water at 90 °C performed by Caratzoulas and Vlachos in 2011,[22] the Gibbs energy of activation for the loss of the first water molecule was quite low (25.1 kJ/mol) and a C2 carbonium intermediate (**2.4**) was generated. The removal of the second water molecule was more difficult (73.6 kJ/mol). Before the second dehydration, the proton transfer from

O1 to O3 occurred and produced an oxonium ion (**2.11→2.12**). The participation of one water molecule was found to promote this proton transfer through decreasing the energy barrier by 55.6 kJ/mol, but more water molecules led to an increase of the activation energy back to high values. The C3 carbonium intermediate (**2.13**) obtained after the second dehydration was not stable and a hydride transfer from C4 to C3 immediately happened (**2.14**). Two possibilities for the required hydride transfer before the third dehydration were calculated and the one from C5 to C4 was more favored, resulting in a furanic oxonium ion (**2.15**), which subsequently had a proton transfer and the exothermic loss of the third water molecule. The use of water as the solvent caused the higher energy barrier in hydride transfer via the reorganization of the polar solvent environment and the consequent solvation of the asymmetrical charge distribution. This group furthered their research and announced more achievements in 2012.[23] An improved Gibbs energy profile was given with more reasonable estimates for the hydride transfer and the second dehydration. A microkinetic model for the acid-catalyzed dehydration of fructose was established and the accuracy of molecular simulations was tested. The hydride transfer from C1 to C2 (**2.4** to **2.4'**) was found to be the rate-limiting step. The results were claimed to be in good agreement with experimental results.[27]

At almost the same time as Caratzoulas and Vlachos performed their studies in 2011, Assary et al. also conducted their calculations on the conversion of fructose to 5-HMF in both neutral water and an acidic environment.[24] In the neutral environment at 25 °C, the comparison of entropies and Gibbs energies between the four intermediates and four

transition states in the reaction process showed that the inclusion of a water molecule in the system decreased the activation energies for each step. However, the activation barriers were still quite high (above 160 kJ/mol), indicating that the dehydration of fructose in neutral water at room temperature was not favored. The same procedure was simulated at 225 °C, and the activation energies for all steps reduced drastically compared with the values at 25 °C. This was attributed to the more significant ionization of water molecules at higher temperatures, which resulted in a reaction environment more amenable to acid-catalysis. In the acid-catalyzed simulation, a reaction route similar to Caratzoulas' but with more detailed intermediates and transition states was given. The highest enthalpy of activation barrier was 162.3 kJ/mol, from the loss of the second water molecule (**2.12** →**2.13**). This result was claimed to be in agreement with some reported experimental results using mineral or Lewis acids as catalysts, which were in a range of 129.7 - 142.2 kJ/mol.[13, 28-30] The conclusion was made that protonated intermediates from acid-catalyzed reaction systems would promote the conversion of fructose to 5-HMF.

In the following year, the same group performed another computational study on the acid-catalyzed dehydration of fructose and glucose in water at 25 °C.[25] During the transformation of fructose to 5-HMF, three possible paths were proposed for the conversion of **2.4'** to **2.2** (Scheme 2-4). Compared with the generation of **2.19** through a hydride shift (17.6 kJ/mol), this study showed that the deprotonation of **2.4'** to form **2.2** directly (-7.9 kJ/mol) or via **2.5** as an intermediate (-39.3 kJ/mol) was more thermodynamically favored, especially the latter one. Afterwards, **2.2** underwent the loss of two water molecules

through the protonation at O3H and O4H. Since the proton affinity of O3H was 50.2 kJ/mol higher than O4H, the protonation was proposed to occur at O3H first in this mechanism. It was believed that water promoted the conversion of **2.2** to **2.3** by acting as a proton mediator to form an eight-membered transition state (**2.20**).

In the study by the Pidko group,[26] an astonishing twenty-four possible routes for fructose conversion were calculated, among which nine involved the formation of 5-HMF before the final product LA was obtained. On the most thermodynamically favored route, the dehydration of fructose to 5-HMF was -156 kJ/mol exergonic with **2.3** modeled as an intermediate (Scheme 2-4, blue). According to the authors, the formation of a conjugated π system within the furan ring and the entropy increase during the dehydration were the main forces driving the conversion of fructose towards LA via 5-HMF formation.

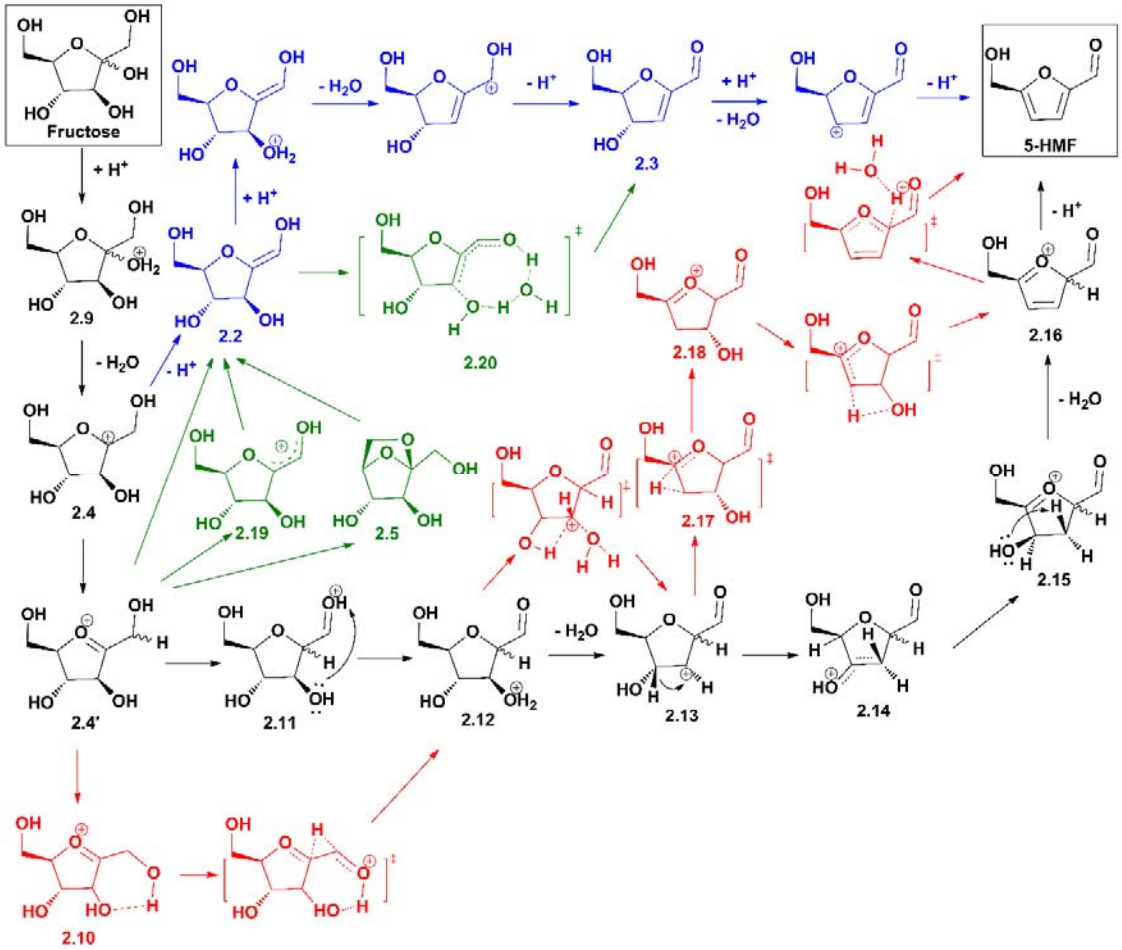

Scheme 2-4. The reaction pathways of the dehydration of fructose to 5-HMF proposed by Caratzoulas and Vlachos and coworkers[22, 23] (black), Assary et al.[24, 25] (red: 2011; green: 2012) and the Pidko group (blue)[26].

As a promising kind of solvent and catalyst, the application of ionic liquids in the transformation of carbohydrates has also been studied extensively. In the work by Arifin et al. in 2016, the dehydration of glucose was studied using the reference interaction site model self-consistent field spatial electron density distribution (RISM-SCF-SEDD) method

in a modified GAMESS program package.[31] The geometry optimizations were performed with B3LYP functional and 6-31+G(d,p) basis set, and the energy calculations were implemented at CCSD(T)/aug-cc-pVDZ level of theory. The reaction was simulated in water or 1,3-dimethylimidazolium chloride (MmimCl) and catalyzed by HCl. Two mechanisms were proposed for the isomerisation of glucose (see **2.3.2**). Afterwards, the transformation of fructose to 5-HMF was simulated in the same pathway proposed by Assary (Scheme 2-4, highlighted in green),[30] in which **2.2** was directly obtained from **2.4'**. In both solvents, the rate-limiting step was the conversion of **2.4'** to **2.2**.

In 2015, the Zhang group investigated the dehydration of glucose in BmimCl catalyzed by a Brønsted acid-functionalized ionic liquid, 1-butyl sulfonic acid-3-methylimidazolium chloride ([BmimSO$_3$H]Cl), through a DFT study.[32] The Gaussian 09 program with meta GGA BB95 functional and 6-31G(d,p) basis set was used, and the solvation effect was considered by applying SMD. Two mechanisms were proposed (see **2.3.2**), in which path **I** involved the dehydration of fructose to 5-HMF after the isomerisation of glucose to fructose (Scheme 2-5). The glucose-fructose isomerization process will be discussed in more detail later in **2.3.2**, as the focus here is on transformations of fructose. During the removal of the first water molecule from fructose, O2H hydroxyl group is removed because of the interaction between it and the proton from the sulfonic acid group (-SO$_3$H) in the ionic liquid cation, and an oxocarbenium intermediate (**2.21**) was produced. Afterwards, it was proposed that **2.21** had interaction with -SO_3^- and a water molecule (**2.22**) and then **2.2** was formed. The loss of the second water molecule was

achieved through the ten-membered transition state (**2.23**), in which -SO_3H acted as a proton shuttle to accept the proton at O1H and transfer its own proton to O3. The role of -SO_3H here is similar to the water molecule in the conversion of **2.2** to **2.3** in the study by Assary (Scheme 2-4, highlighted in green). The third water molecule removal proceeded at O4H in a similar route to the first dehydration. In this study the -SO_3H group is the key portion of the ionic liquid that catalyzes the dehydration of fructose.

In the study by Li et al. about imidazolium ionic liquid-promoted dehydration of fructose, the use of 1-butyl-3-methylimidazolium bromide (BmimBr) resulted in a maximum 5-HMF yield of 92% with almost 100% fructose conversion.[33] The in situ Fourier transform infrared (FT-IR) spectra showed the OH stretching frequency of fructose decreased in the presence of BmimBr. The resonances of H1 and H6 of fructose had upfield shift in the ^{1}H NMR spectra, and the split of fructose signals in the ^{13}C NMR spectra was observed during the reaction. These changes were caused by the hydrogen bonding of fructose with BmimBr. A DFT study was performed using Gaussian 09 program with the B3PW91 functional and the 6-311++G(d,p) basis set to gain insight into these experimental observations. A mechanism was proposed in which the removal of all three water molecules was triggered by the hydrogen bonding between fructose and Br^- (Scheme 2-5).

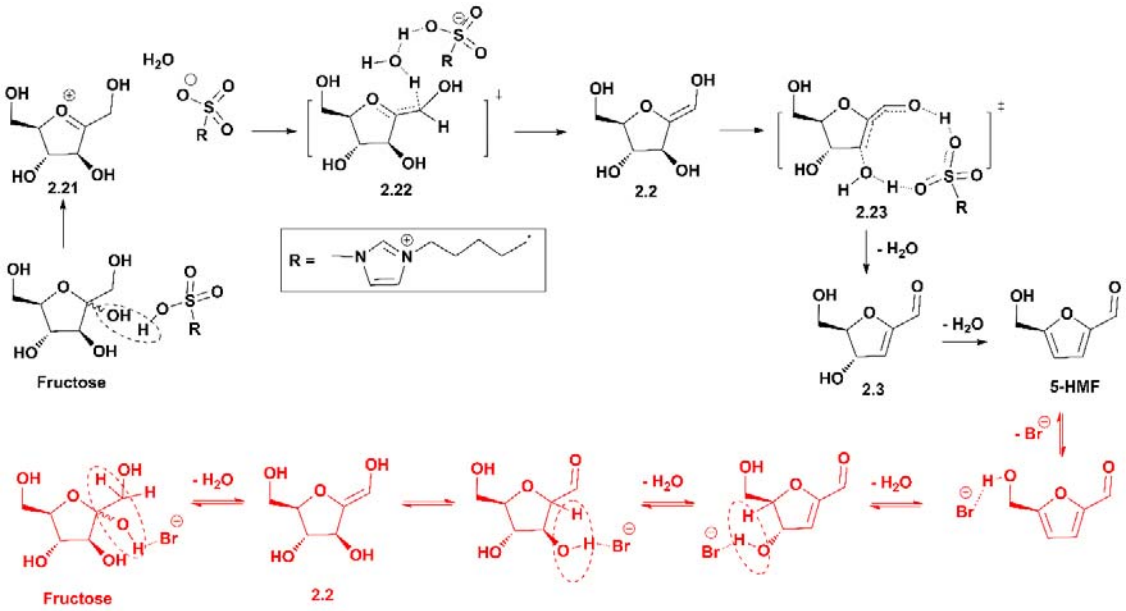

Scheme 2-5. Mechanisms of fructose dehydration in ionic liquids proposed by Zhang[32] (black) and Li[33] (red) (the cation or anion of the ionic may be omitted for clarity).

Most of the studies discussed above are about the transformation of fructose catalyzed by a Brønsted acid. In 2011, Guan et al. performed DFT studies of glucose and fructose dehydration catalyzed by trivalent metal chlorides ($CrCl_3$, $MoCl_3$, WCl_3 and $FeCl_3$) in BmimCl.[34] The calculations were carried out in the gas phase using Gaussian 03 program with B3LYP theory. The LANL2DZ basis set was used for the metal elements while the 6-31G+(d,p) was used for the other elements. The natural bond orbital (NBO) analysis was performed using the NBO program in the Gaussian 03 package. The metal chlorides were proposed to form four-coordinate complexes after their dissolution in the ionic liquid, with three Cl^- and one $[Bmim]^+$ ligands (Scheme 2-6). The first part of the study concerned the isomerisation of glucose to fructose (see **2.3.2**). Afterwards, the dehydration of fructose

was proposed to start from the coordination of fructose to the metal complex at O1 and O2. The water molecule removed became a ligand of the metal complex. After the loss of the third water molecule, hydrogen bonding was observed between O6 and the proton of the water ligand (**2.27**). The overall conversion of fructose to 5-HMF was thermodynamically favored using the four metal chlorides studied, and the overall activation barrier (the first water removal) increased in the order of WCl_3 (106.7 kJ/mol) < $MoCl_3$ (131.8 kJ/mol) < $CrCl_3$ (147.7 kJ/mol) < $FeCl_3$ (165.7 kJ/mol). The explanation about their different performances will be discussed in **2.3.2**.

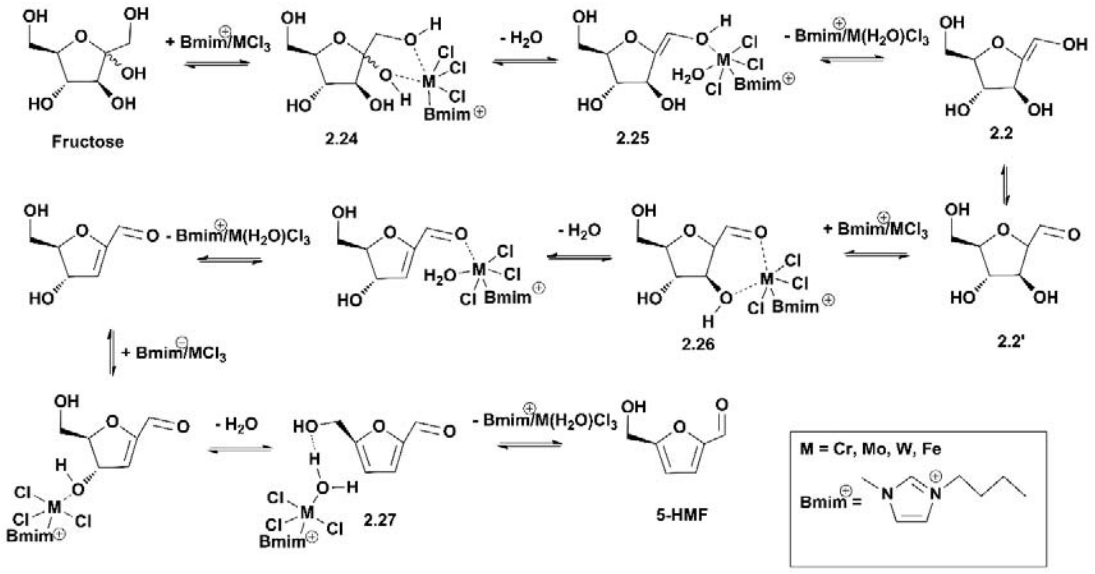

Scheme 2-6. The mechanism of metal chloride-catalyzed fructose dehydration to 5-HMF proposed by Guan et al.[34]

As can be seen from the discussion above, **2.2**, **2.3** and **2.4** are significant intermediates in mechanisms proposed from both NMR studies and calculations. In NMR studies (Scheme 2-4), **2.3** is a common intermediate detected in almost all works; **2.2** is proposed

in three studies and **2.4** is in two. Therefore, the results of mechanistic studies from computational calculations and lab experiments are in reasonable agreement and can support each other. These structures and intermediates are therefore key species for others working in this field to detect and measure in order to understand their reaction pathways, and they may also act as clues towards possible pathways in transformations of other saccharide molecules.

2.2.3 Other Methods

2.2.3.1 Kinetic Studies

To the best of my knowledge, the earliest research trying to determine the reaction mechanism for the dehydration of fructose through experiments was performed by Antal et al.[14] in 1990. After analyzing a variety of previous studies, they concluded that under weakly acidic conditions a small amount of 3-deoxyglycosuloses were probably generated which led to the generation of 5-HMF via an acyclic mechanism; with higher acidity and/or higher temperatures applied, the cyclic route involving fructofuranosyl intermediates was favored (Scheme 2-2). Afterwards, the authors performed kinetic studies for the fructose dehydration in water with and without acid catalysts. A system of supercritical flow-reactors was applied to conduct reactions at high temperatures (maximum 500 °C) and pressures (maximum 34.5 MPa). The compounds produced during the reaction were analyzed using high performance liquid chromatography (HPLC) and gas chromatograph-mass spectrometry (GC-MS). The kinetic evidence to support the cyclic mechanism was discussed from three aspects. Firstly, the detection of a very small amount of glucose and

no mannose in the reaction mixture indicated that during the process the Lobry de Bruyn-van Ekenstein transformation between fructose and glucose was very slow under applied conditions. Therefore the enolization of fructose, a key step in this transformation, must be slow. Consequently, the enols which are significant intermediates in the acyclic mechanism were actually present in negligible amounts and had little influence in the conversion of fructose. Secondly, if the 3-deoxyglycosulose intermediate in the acyclic route was generated during the reaction process, it should have undergone a benzylic acid rearrangement under the reaction conditions to produce glucometasaccharinic acids or lactones, which were not found via GC-MS analysis. Finally, sucrose was used as the reactant in the dehydration reaction under similar conditions. The first step of this process is the hydrolysis of sucrose into a fructofuranosyl cation and glucose.[35, 36] The yield of 5-HMF from the fructose part (the fructofuranosyl cation) in the dehydration of sucrose was higher than from pure fructose, either with or without acid catalysts. This result was in accordance with the hypothesis that the fructofuranosyl cation was an important intermediate in the cyclic pathway of fructose dehydration to yield 5-HMF. This work is a milestone in the area of sugar transformations, and has been referenced by numerous studies later on.

In the study by Caratzoulas and Vlachos as mentioned in **2.2.2**, the hydride transfer from C1 to C2 (**2.4'→2.11**) was recognized as the rate-limiting step via QM/MM MD simulations.[22, 23] In order to evaluate the accuracy of this conclusion, Vlachos and co-workers performed isotopic-labelling experiments in 2013 based on the kinetic isotope

effect (KIE).[37] The labelled fructose of which the proton on C1 was replaced by deuterium was used in the dehydration reaction. A decrease in the fructose disappearance rate and 5-HMF appearance rate compared with normal fructose conversion confirmed that the hydride transfer from C1 to C2 was indeed the rate-limiting step (Scheme 2-7).

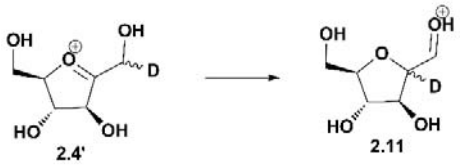

Fructose conversion $k_H/k_D = 1.20$
5-HMF yield $k_H/k_D = 2.20$

Scheme 2-7. The hydride transfer from **2.4'** to **2.11** and the rate ratios of fructose conversion and 5-HMF yield for unlabelled fructose (k_H) and labelled fructose (k_D) in the study by Vlachos and co-workers.[37]

2.3 Glucose

Glucose, also known as "grape sugar", is an aldose which can be found in plants and animals. Naturally existing glucose is D-glucose. Similar to fructose, glucose also has five isomers, including both ring and open-chain forms (Scheme 2-8). In the field of biomass transformation, glucose has been extensively studied alongside fructose for the production of 5-HMF. Despite the comparable lower 5-HMF yields compared with fructose, the low cost of glucose is a significant advantage in its use as the reactant.[38]

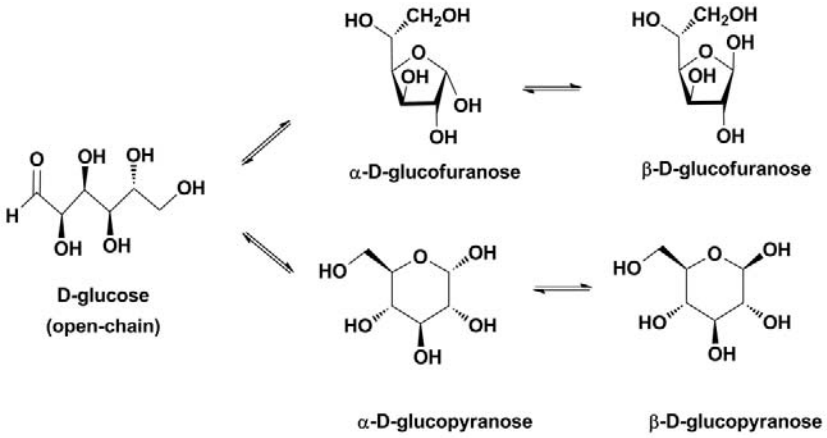

Scheme 2-8. Five isomers of D-glucose.

There have been two mechanisms generally proposed for the conversion of glucose to 5-HMF. As shown in Scheme 2-9, route **A** is the direct dehydration of glucose through several furan aldehyde intermediates;[39, 40] while in route **B** the isomerisation of glucose to fructose is a crucial step, and 5-HMF is obtained via dehydration of the generated fructose. Among the numerous studies on the transformation of glucose in the past one hundred years, most of them have focused on route **B**. Two mechanisms have been proposed for the isomerisation of glucose to fructose (**B1** and **B2**, Scheme 2-9). **B1** is through an enolization and **B2** is through a 1,2-hydride shift. Both mechanisms have been supported experimentally and computationally in various researches with a range of catalysts used.

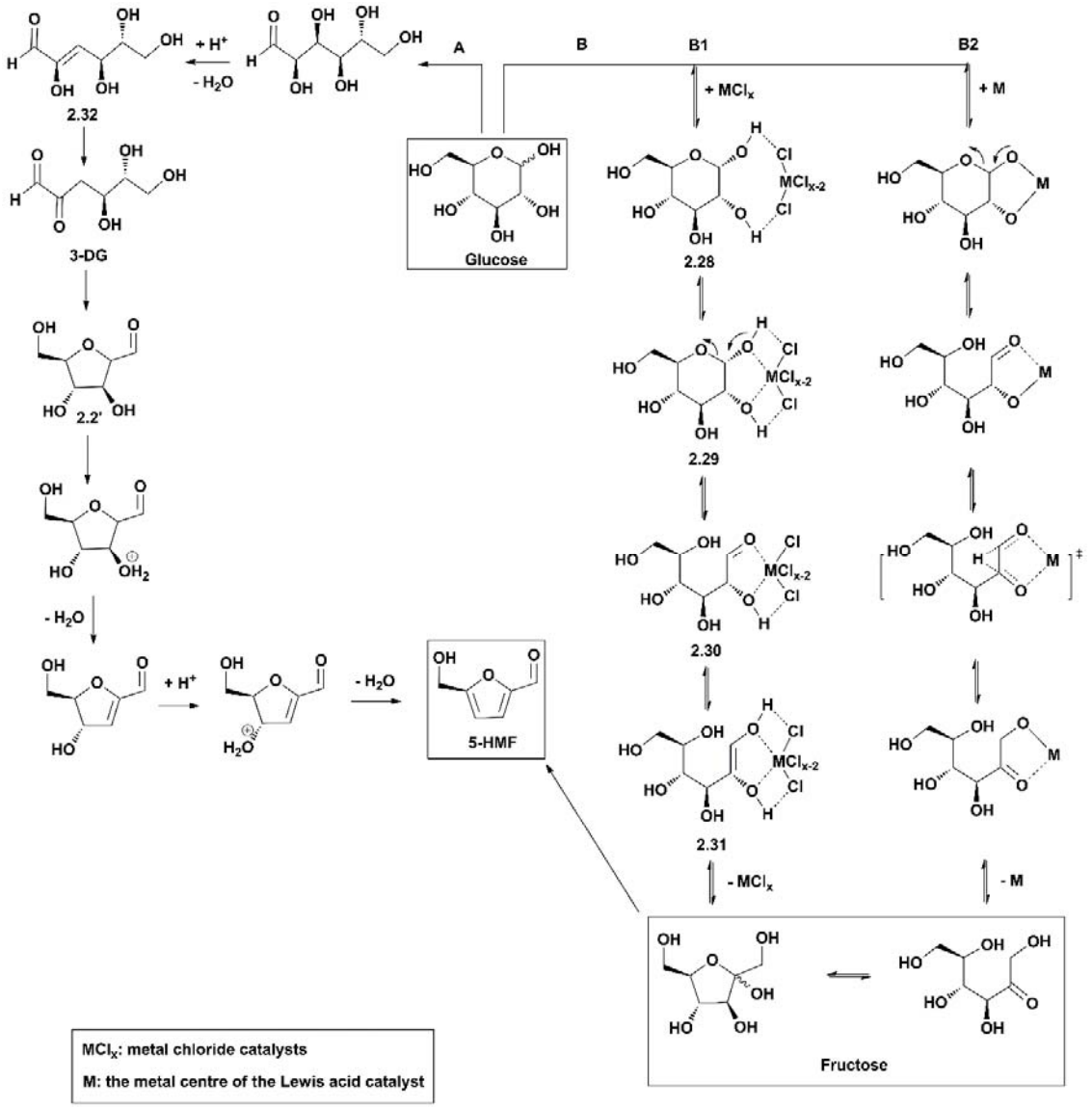

Scheme 2-9. Proposed mechanisms of glucose conversion to 5-HMF.

2.3.1 NMR Spectroscopy

In 2011 Matubayasi and co-workers managed to detect all the straight chain and ring isomers of both glucose and fructose through in situ ^{13}C NMR analysis of unlabelled and

[^{13}C-1] glucose (Figure 2-4) in D_2O, after the solution was equilibrated for 20 h and heated to a particular temperature (100 °C or 160 °C) for a certain time.[41] This result indicated that during the isomerisation all isomeric forms of glucose and fructose were formed and therefore may play important roles in the mechanism for 5-HMF formation.

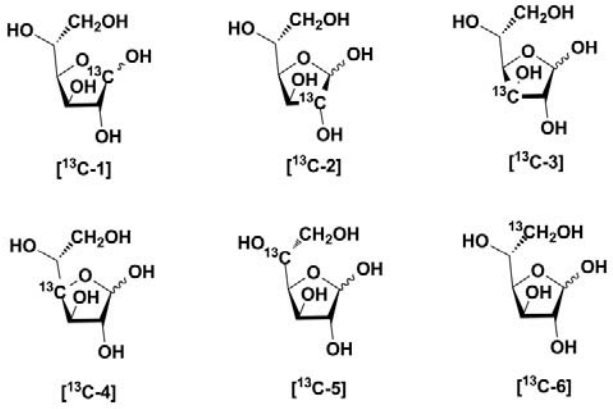

Figure 2-4. Glucose molecules with different ^{13}C labelled carbon atoms.

Table 2-3. ^{1}H and ^{13}C NMR data of glucose, fructose, the intermediates in **2.3.1** and 5-HMF.

Compound	Solvent	δ_H (ppm)	δ_C (ppm)	Ref
Glucose	D_2O	-	Open-chain: 205.0 (C1); α-glucopyranose: 92.5 (C1); β-glucopyranose: 97.4 (C1); α-glucofuranose: 97.7 (C1); β-glucofuranose: 102.8 (C1)	41
	DMSO-d_6	-	α-glucopyranose: 97.35 (C1), 75.25 (C2); β-glucopyranose: 92.62 (C1), 72.80 (C2); α-glucofuranose: 104.37 (C1), 80.35 (C2); β-glucofuranose: 102.73 (C1), 72.21 (C2)	42
	Solid-state	-	Open-chain: 205 ppm (C1)	43
Fructose	D_2O	-	Open-chain: 213.1 (C1); α-fructopyranose: 66.2 (C1); β-fructopyranose: 65.6 (C1); α-fructofuranose: 64.4 (C1); β-fructofuranose: 64.8 (C1)	41
	DMSO-d_6	-	Open-chain: 71.17 (C1), 205.54 (C2)	42
	DMSO-d_6	-	103.6	44
	Solid-state	-	Open-chain: 214 ppm (C1)	43
3-DG	Solid-state	-	^{13}C CP/MAS NMR: 110 ppm (C2, absorbed on TiO_2); 118 ppm (C2, absorbed on phosphate/TiO_2)	45
2.29 (MCl_x = $SnCl_4$)	DMSO-d_6	4.90 (s)	-	46
2.29 (MCl_x = $GeCl_4$)	DMSO-d_6	-	76.4	44
2.42	DMSO-d_6	5.33 (H1), 3.85 (H2), 3.77 (H3), 3.51 (H4), 3.49 (H5), 2.92 & 2.81 (H6)	101.7 (C1), 83.6 (C2), 73.7 (C3), 70.6 (C4), 73.6 (C5)61.3 (C6)	47
2.43	DMSO-d_6	-	Two isomers: 72.58 & 74.15 (C1), 189.88 & 192.40 (C2)	42
2.2	DMSO-d_6	-	147.60 (C1), 136.30 (C2)	42
5-HMF	D_2O	-	180.9 (C1)	41
	DMSO-d_6	-	178.44 (C1), 152.16 (C2)	42
	DMSO-d_6	9.49 (s, H1)	-	48
	DMSO-d_6	-	152.1 (C2), 124.3 (C3), 110.9 (C4), 56.1 (C6)	44

The study by Zhao et al. in 2007 is a milestone because for the first time it revealed the interaction of metal halide catalysts with glucose.[49] The role of the interaction in the mutarotation of glucose isomers and the isomerisation of glucose to fructose was explored in an ionic liquid solvent (1-ethyl-3-methylimidazolium chloride, [Emim]Cl). The ^{13}C NMR spectra showed that before the addition of the catalyst (copper(II) chloride, $CuCl_2$, or chromium(II) chloride, $CrCl_2$) the main component in the solution was α-glucopyranose. After the catalyst was added, another set of peaks belonging to β-glucopyranose was detected. This implied the occurrence of mutarotation, which led to the interconversion of α- and β-glucopyranose isomers. Correspondingly, in the ^{1}H NMR spectra, the six sharp peaks of the hydroxyl groups of glucose broadened and shifted upfield after catalyst addition, suggestive of an interaction with the catalyst. Furthermore, competition studies using glycerol or glyceraldehyde together with glucose as starting materials were performed, in order to locate the portion in glucose interacting with the catalyst. The NMR analysis showed that glyceraldehyde existed as a hemiacetal dimer in [Emim]Cl. Therefore, in [Emim]Cl glucopyranose contains functional groups reminiscent of both glycerol and glyceraldehyde. The competition reaction results implied that glycerol had no effect on the dehydration of glucose; while glyceraldehyde led to a drop in both glucose conversion and 5-HMF yield. This result indicated that it was the hemiacetal portion of glucopyranose instead of the polyalcohol portion that interacted with the catalyst. It was proposed that the metal centre interacted with the oxygen atoms of the hydroxyl groups to cause the mutarotation of glucose and the subsequent isomerisation (Scheme 2-10), but no

experimental work was performed to verify this. However, these findings were supported by Zhang et al. in 2011.[50] They performed the synthesis of 5-HMF from glucose using hydroxyapatite supported chromium chloride (Cr-HAP) as the catalyst in 1-butyl-3-methylimidazolium chloride ([Bmim]Cl) as the solvent. The ^{13}C NMR analysis provided evidence for the mutarotation of glucose isomers, and traces of fructose were detected during the dehydration of glucose.

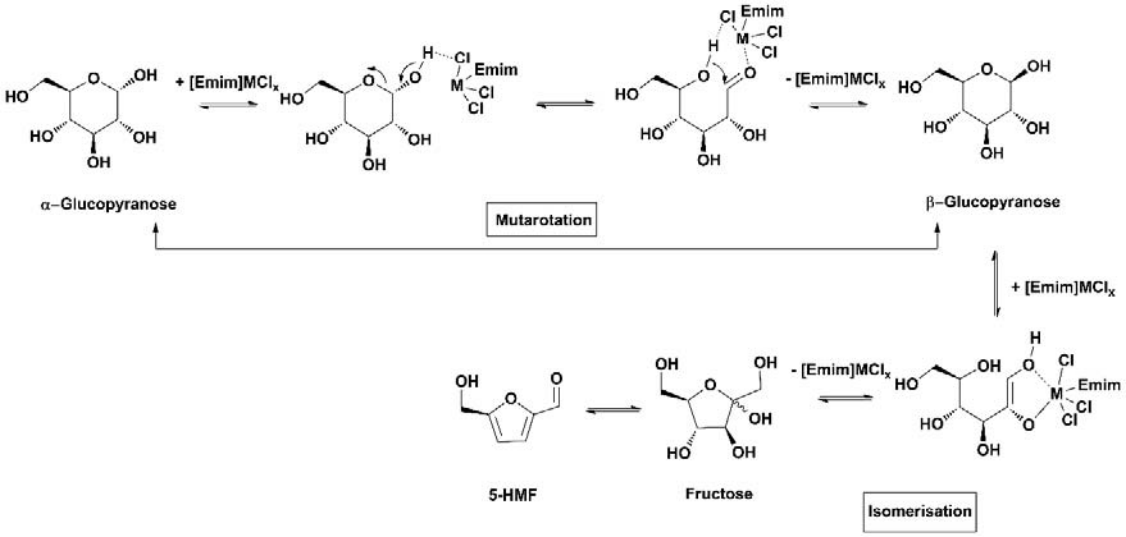

Scheme 2-10. The mechanism of glucose mutarotation and isomerisation proposed by Zhao et al.[49]

After Zhao's work, several researchers used similar methods (NMR analysis and competition studies) to explore the mechanisms of glucose dehydration to 5-HMF.[44, 46, 48] Different Lewis acids were used as catalysts and ionic liquids or water were used as solvents. In the study by Han and co-workers using tin(IV) chloride ($SnCl_4$), during the screening of solvents it was found that the 5-HMF yield was low if the anion of the ionic

liquid had a strong coordination ability, such as chloride (Cl^-) and trifluoroacetate (TFA^-).[46] It was explained that these Lewis basic anions would compete with glucose to interact with the Sn centre and thereby inhibit the dehydration process. 1-Ethyl-3-methylimidazolium tetrafluoroborate ([Emim][BF_4]) was chosen as the solvent for further experiments. Ethanol, ethylene glycol and 1,3-propanediol were used for competition studies. The glucose conversion and 5-HMF yield decreased drastically with the addition of ethylene glycol but did not change upon ethanol or 1,3-propanediol addition. This indicated that during the conversion of glucose, a five-membered ring chelate complex forms as an intermediate and the presence of ethylene glycol, which can form a similar complex, inhibits the catalyst. ^{1}H NMR spectra showed that both α- and β-glucopyranose were detected in the absence of the catalyst. After $SnCl_4$ was added, broadening of the resonances of the hydroxyl groups was observed, and the compound formed was assigned to be an intermediate resulting from the interaction between the Cl^- ions and the protons from the hydroxyl groups (Scheme 2-9, **2.28,** MCl_x = $SnCl_4$). A new peak at 4.90 ppm was found upon heating the mixture to 80 or 100 °C for 2 min, and was assigned to a new intermediate (**2.29**), which was the five-membered ring chelate complex resulting from the interaction of the Sn centre with the oxygen atoms from the 1,2-dihydroxy group of glucose. Afterwards **2.29** ring opened to form an open-chain intermediate (**2.30**), which then produced an enediol intermediate (**2.31**). 5-HMF was proposed to be generated either directly from **2.31** or through the fructose produced from **2.31**. In a study by De et al. in 2011, they briefly carried out a ^{1}H NMR study on glucose dehydration using aluminum(III) chloride ($AlCl_3$) as the catalyst in DMSO-d_6.[48] A similar observation was made regarding broadening of hydroxyl peaks and

was attributed to the hydrogen bonding between the chloride ions and the protons from the hydroxyl groups. However, a 1,2-hydride shift mechanism was proposed for the subsequent isomerisation of glucose, which was different from Han's work.

In a study by Zhang et al. in 2011, [^{13}C-2] glucose was used as the reactant with germanium(IV) chloride ($GeCl_4$) as the catalyst and [Bmim]Cl as the solvent.[44] The ^{13}C NMR spectra showed that both α- and β-glucopyranose were detected before the addition of $GeCl_4$. A new peak at 76.4 ppm appeared after the Lewis acid was added, and decreased in intensity as the temperature and amount of 5-HMF increased. It was assigned to an intermediate formed between the Ge centres and two neighbouring oxygen atoms of 1,2-dihydroxy group of glucopyranose (Scheme 2-9, **2.29,** $MCl_x = GeCl_4$). A competition study was performed using phenylfluorone, which contains a diol moiety, and both the glucose conversion and 5-HMF yield decreased significantly because of competitive complexation of phenylfluorone with $GeCl_4$. An enolization pathway similar to Han's was proposed for the subsequent conversion of **2.29** to fructose.

Compared with Zhao's work, these studies took further steps to identify the intermediates of metal complexation in the isomerisation process. However, it would be ideal if more specific NMR data could be obtained for the thorough identification of the intermediates or model compounds for intermediates isolated.

It needs to be noted that all the studies discussed above were focused on confirming the complexation of the Lewis acid catalyst with glucose. None of them provided experimental evidence to support the proposed enolization or 1,2-hydride shift mechanisms

of glucose isomerisation. From 2011 to 2013, four groups used glucose deuterated at C2 (glucose-D2) as the reactant for the dehydration reaction and studied mechanisms via ^{1}H and ^{13}C NMR spectroscopy.[51-54] As is shown in Scheme 2-11, if a 1,2-hydride shift occurs in the isomerisation, the deuterium at the C2 will transfer to C1 of the fructose or 5-HMF obtained. In ^{1}H NMR spectra, the percentage of deuterium incorporation can be calculated from the integration of the resonances. Theoretically, if a 1,2-hydride shift occurs the fructose should contain 100% deuterium at C1 and the 5-HMF should be 50% deuterated at C1. In ^{13}C NMR spectra, because of disruption of the nuclear overhauser enhancement (NOE) caused by the deuterium atoms, ^{13}C resonance intensities of ^{13}C-^{1}H pairs will be doubly enhanced while the resonance intensities of ^{13}C-^{2}H pairs will remain unchanged.[55] Also, the resonances resulting from ^{13}C-^{2}H couplings should appear as triplets with relatively lower intensities than other ^{13}C resonances from carbons having protons rather than deuterium attached. If enolization happens in the isomerisation, the deuterium will be expelled into the solvent so in theory no deuterium will be in the produced fructose and 5-HMF. However, it should be noted that a small amount of deuterium incorporation might be seen because of the proton/deuterium exchange. Conversely, if a deuterated solvent, such as D_2O, is used, 50% deuterium incorporation at C1 of fructose or 5-HMF is expected for an enolization pathway but nor for a 1,2-hydride shift mechanism.

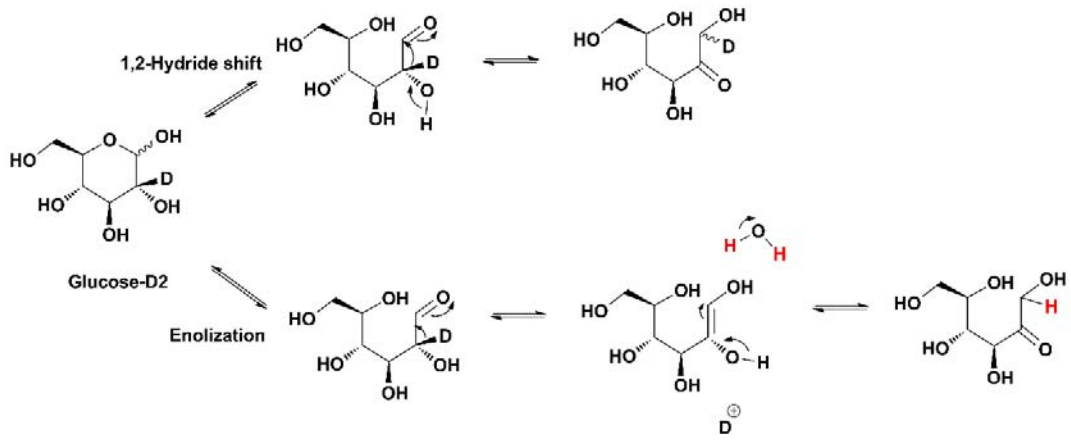

Scheme 2-11. Two putative routes of glucose-D2 isomerisation.

In 2010, Raines and co-workers performed a mechanistic study on the conversion of glucose to 5-HMF through ^{1}H and ^{2}H NMR analysis.[51] The reaction was accomplished in dimethylacetamide (DMA) with chromium(III) chloride ($CrCl_3$) or $CrCl_2$ as the catalyst. One equivalent D_2O or water (to glucose) was added into the starting materials. When D_2O was the deuterium source, less than 5% deuterium incorporation was detected at C1 of the 5-HMF produced. When glucose-D2 was used as the deuterium source, approximately 33% deuterium was incorporated at C1 of 5-HMF, and a signal of the aldehydic deuteron was observed in the ^{2}H NMR spectrum. These results indicated that the isomerisation of glucose went along the 1,2-hydride shift pathway instead of the enolization route. A similar study using D_2O was performed on mannose (a C2 epimer of glucose) and also less than 5% deuterium incorporation was detected, thus confirming the conclusion about the 1,2-hydride shift mechanism under the applied conditions.

During the same year, the Davis group studied the mechanism of glucose-D2 isomerisation using a tin-containing zeolite (Sn-Beta) in water.[52] After the aqueous glucose solution containing Sn-Beta was heated for 15 min at 110 °C, the fructose product was separated from the glucose by HPLC and analyzed using ^{1}H and ^{13}C NMR spectroscopy. Compared with the standard NMR spectra of unlabelled fructose in D_2O, the fructose product did not produce a signal at 3.45 ppm (the proton at C1) in the ^{1}H spectrum, and the resonances at 63.8 ppm (C1 of β-fructopyranose) and 62.6 ppm (C1 of β-fructofuranose) in the ^{13}C spectrum appeared as triplets with low intensities. These results indicated that the deuterium at C2 of glucose-D2 transferred to C1 of the fructose intermediate, thus leading to the lack of expected signal for the proton at C1 in the ^{1}H NMR spectrum and the NOE effect in the ^{13}C NMR spectrum. Therefore, a 1,2-hydride shift mechanism was also proposed for the isomerisation of glucose when this heterogeneous Lewis acid catalyst was used. A KIE was observed with a $k_H/k_D = 1.98$ in the initial reaction rate, further revealing that the hydride shift was the rate-limiting step. In addition, the group performed a similar mechanistic study of glucose isomerisation with a base catalyst (sodium hydroxide, NaOH). The fructose generated had the same ^{1}H and ^{13}C NMR spectra as the unlabeled fructose, indicating that no deuterium was incorporated during the isomerisation process. Hence a proton transfer mechanism was proposed, in which the deuterium at C2 of glucose-D2 was transferred into the solution and a proton from the solution was incorporated into the fructose.

The use of Sn-Beta as the catalyst in glucose isomerisation was further investigated by Bermejo-Deval et al. in 2013.[43] Initially, the ring opening of sugars was studied using ^{13}C solid state NMR and IR spectroscopy. The ^{13}C NMR spectra showed that immediately after the ^{13}C-labelled fructose was absorbed into Sn-Beta, a peak at 214 ppm was observed, which was assigned to C2 of open-chain fructose. This peak was verified through cross polarization (CP) experiments. The IR spectra also revealed the signal of the keto carbonyl of open-chain fructose at 1728 cm^{-1}. For the ^{13}C-labelled glucose absorbed into Sn-Beta, the resonance of C1 of open-chain glucose at 205 ppm was not observed because of its low concentration. However, the appearance of a peak at 214 ppm indicated that a certain amount of glucose was ring-opened and converted to open-chain fructose. Furthermore, a broad band at 1730 - 1720 cm^{-1} was seen in the IR spectra, which was assigned to the combination of the keto carbonyl of open-chain fructose (1728 cm^{-1}) and the aldehyde carbonyl of open-chain glucose (1720 cm^{-1}). The kinetic studies of the isomerisation of glucose implied that KIEs ($k_H/k_D \approx 2$) were observed for both Sn-Beta- and Ti-Beta-catalyzed reactions, hence the 1,2-hydride shift was proposed as the rate-limiting step. Finally, a DFT study was performed using Gaussian 09 program with the B3LYP and MP2 levels of theory. The cc-pVDZ-pp, Aldrich's VTZ and 6-31+G(d) basis sets were respectively used for Sn, Ti and Si atoms, and the 6-311+G(d) basis set was for the other elements. The solvation effect in water was considered using the SMD solvation model. A mechanism through a 1,2-hydride shift was proposed (Scheme 2-12) and the energies of all intermediates and transition states were calculated. The isomerisation catalyzed by a Sn-Beta open-site with one adjacent silanol group had an enthalpy of activation of 92.5 kJ/mol,

which was in good agreement with the experimental value (88.7 ± 2.9 kJ/mol). For a Sn-Beta closed-site, an activation barrier of approximately 125.5 kJ/mol was calculated, thus it was claimed not to be the primary reaction pathway.

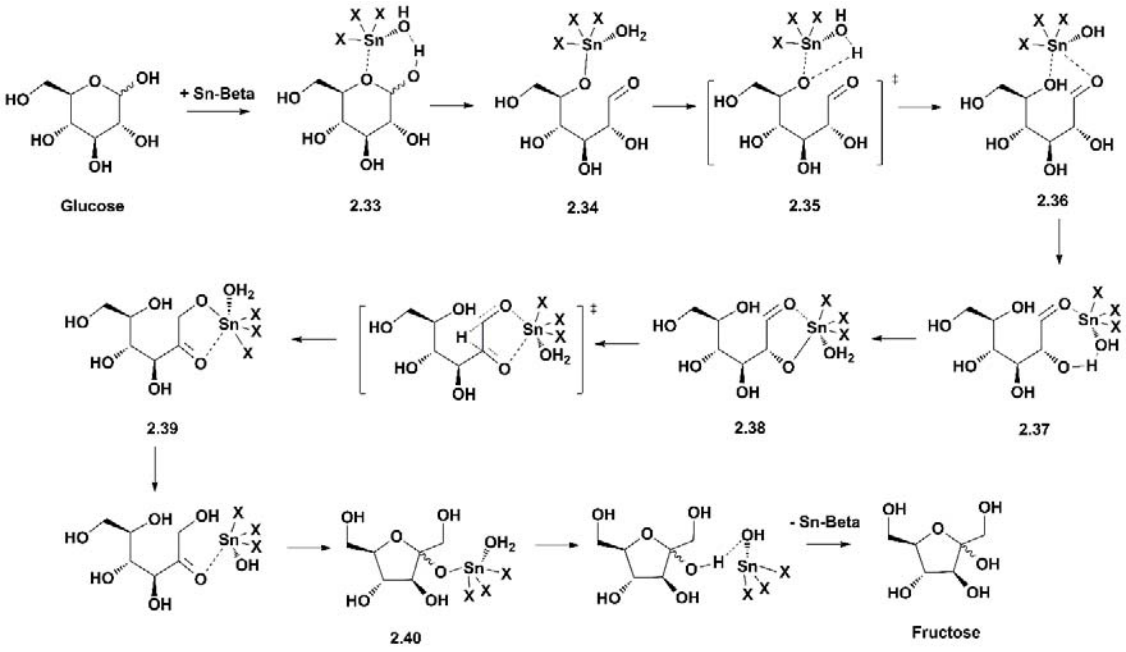

Scheme 2-12. The mechanism of Sn-Beta-catalyzed isomerisation of glucose proposed by Bermejo-Deval et al.[43]

In 2013, Choudhary et al. performed the isomerisation of glucose in aqueous solution using both homogeneous ($CrCl_3$, $AlCl_3$) and heterogeneous (Sn-Beta) Lewis acid catalysts and investigated the mechanisms.[56] When glucose-D2 was used as the reactant, KIEs were observed for the reactions catalyzed by $CrCl_3$ ($k_H/k_D = 1.77 \pm 0.11$) and $AlCl_3$ ($k_H/k_D = 1.71 \pm 0.10$) at 40 °C, indicating that the hydride shift was the rate-limiting step, which is the same conclusion as in the studies by the Davis group and Bermejo-Deval et al. Afterwards,

^{1}H and ^{13}C NMR spectra were recorded for the glucose-D2 reactions catalyzed by the three catalysts, and the same observations were obtained for the fructose product as in the study by the Davis group (lack of the proton at C1 in ^{1}H NMR spectrum and the NOE effect of C1 in ^{13}C NMR spectrum), confirming a 1,2-hydride shift mechanism. In addition, ^{2}H NMR spectroscopy was used in the glucose-D2 conversion catalyzed by $CrCl_3$. At the beginning of the reaction, resonances at 3.04 ppm and 3.33 ppm were detected and were assigned to D2 of β- and α-glucopyranose respectively. As the reaction proceeded, two signals at 3.51 ppm and 3.40 ppm appeared, belonging to the deuterium at C1 of β-fructopyranose and β-fructofuranose. Finally, a peak at 9.29 ppm was observed and was assigned to the deuterium at C1 of 5-HMF. Therefore, it can be validated that the deuterium at C2 of glucose was transferred to C1 of fructose and then C1 of 5-HMF during the whole process.

3-Deoxyglucosone (3-DG, Scheme 2-9, route **A**) was proposed as an intermediate in the dehydration of carbohydrates to 5-HMF by Anet in 1960s.[11, 12, 39] In a study by the Bols group in 2011, this mechanism was verified through a combination of experiments and calculations (see **2.3.2**).[40] In 2015, the Hara group performed the dehydration of glucose catalyzed by titanium oxide (TiO_2) and phosphate-immobilized TiO_2 (phosphate/TiO_2) in water.[45] A mechanism through 3-DG without the isomerisation to fructose was proposed and studied using ^{2}H and ^{13}C NMR spectroscopy. The reaction was also performed using scandium triflate ($Sc(OTf)_3$) as the catalyst for comparison. When glucose-D2 and glucose-D1 were respectively used as the reactant, the ^{2}H NMR spectra showed that 55% and 54% deuterium incorporation were detected in the 5-HMF produced with $Sc(OTf)_3$ catalysis.

With the catalysis of TiO_2 and phosphate/TiO_2, no deuterium incorporation was detected in the 5-HMF generated from glucose-D2, and incorporation much higher than 54% was observed for the reaction of glucose-D1 (TiO_2: 74%; phosphate/TiO_2: 98%). Combining these results, the $Sc(OTf)_3$-catalyzed reaction was believed to proceed through the isomerisation route via a 1,2-hydride shift; while for TiO_2 and phosphate/TiO_2 catalysis the mechanism through 3-DG was more reasonable (Scheme 2-13). The ^{13}C cross-polarization/magic angle spinning (CP/MAS) NMR spectroscopy was used to detect the existence of 3-DG. The ^{13}C CP/MAS NMR spectra of [^{13}C-2] glucose absorbed on TiO_2 and phosphate/TiO_2 at room temperature showed two resonances at 110 ppm and 118 ppm respectively, which were assigned to C2 of 3-DG.

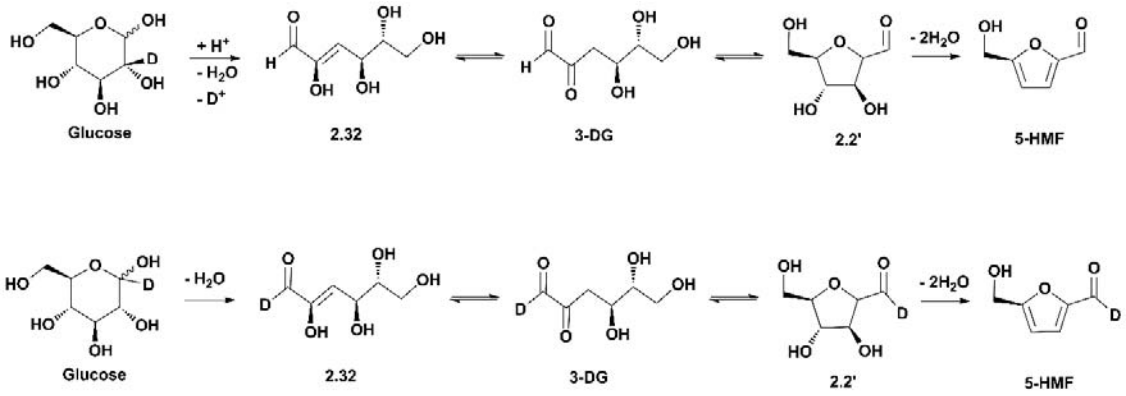

Scheme 2-13. The transformations of glucose-D2 (top) and glucose-D1 (bottom) to 5-HMF through 3-DG.[45]

Boric acid ($B(OH)_3$) and its derivatives have been found to be able to form chelate complexes with carbohydrates,[57-61] and catalyze the isomerisation of aldohexoses to ketohexoses.[62, 63] In 2011, the Riisager group achieved the first metal-free dehydration of

glucose using $B(OH)_3$ as the catalyst in ionic liquids.[53] A 5-HMF yield of 42% was obtained. The mechanism was briefly probed using glucose-D2 as the reactant. The ^1H NMR analysis revealed less than 5% deuterium incorporation, thus the isomerisation of glucose catalyzed by $B(OH)_3$ was proposed to proceed via an enolization mechanism (Scheme 2-14), which was different from the reactions catalyzed by the metal Lewis acid catalysts described above. In 2013, Caes et al. applied a series of phenylboronic acids in the transformation of glucose and cellulose to 5-HMF.[54] Glucose-D2 and D_2O were used in mechanistic study. The ^1H NMR spectra showed that the deuterium from D_2O instead of glucose-D2 was incorporated at C1 of the 5-HMF obtained, further indicating an enolization route similar to that proposed in Riisager's work.

The mechanism of glucose isomerisation catalyzed by boron species was further investigated by Lukamto et al. in 2013.[64] They synthesized a series of boronic acids and used them to catalyze the dehydration of glucose and cellulose. A sophisticated mechanistic study was performed including stereochemical considerations and competition reactions besides NMR analyses. Firstly, the stereochemical studies showed that the *trans*-vicinal diol at the 3,4-position of glucose was the most likely site to interact with the boronic acid. The *trans*-vicinal diol at 3,4-position is *anti* to the ring, so the approach by the boronic acid towards it is encouraged by steric effects. Moreover, complexation of the *trans*-vicinal diol with the boronic acid would lead to distortion of the stable pyranose ring, thus facilitating the ring opening needed for isomerisation. Afterwards, competition studies were performed and 1,3-dipropanol was found to lead to a more significant 5-HMF yield decrease than 1,2-

dipropanol. Combined with the findings from a previous study,[65] it was claimed that the formation of 4,6-boroglucopyranose was significant in the mechanism. Finally, two glucose derivatives in which the hydroxyl group at C6 was replaced by a proton or another functional group were reacted under similar conditions. The product yields (10% and 15%) were much lower compared with the 5-HMF yield from glucose (44%), further confirming the important role of the 4,6-diol moiety. Both ^{1}H and ^{13}C NMR spectra showed that the resonances of glucose shifted upfield (0.165 ppm in ^{1}H NMR spectrum and 0.02 ppm in ^{13}C NMR spectrum), indicating the ring had expanded after catalyst addition because of its complexation with the boronic acid.[66] This study proposed a mechanism with one more step: the boronic acid complexed with the 4,6-diol first and then repositioned to form the 3,4-boroglucopyranose (Scheme 2-14, highlighted in red), which was supported in Riisager's work by computational studies (see **2.3.2**). However, they did not make any efforts to verify the enolization pathway proposed for the isomerisation process.

In 2012, Ananikov and co-workers performed the conversion of carbohydrates to 5-HMF using boron trioxide (B_2O_3) as the catalyst in ionic liquids, and analyzed the reaction mixture through the ^{1}H, ^{13}C and ^{11}B NMR analysis.[47] Their initial attempt to analyze the NMR sample failed because of microheterogeneity within the reaction mixture that led to low resolution NMR spectra with quite broad spectral lines. The problem was likely caused by the high viscosity, the conductive ionic nature and the absorption of radiofrequencies by the ionic liquid solvent.[67] It was solved by using a NMR tube equipped with a stirrer as the reactor, thus NMR spectra could be recorded directly after the reaction was done with

adequate stirring, and the microheterogeneity of the sample was decreased to below the spectroscopic influence level. The NMR analysis of fructose in [Bmim]Cl showed that the portion of the open-chain isomer increased while the furanose isomers decreased compared with fructose in D_2O, indicating that the ionic liquid solvent could promote the generation of the straight chain form of fructose compared with water. By contrast, the compositions of glucose isomers were similar in both [Bmim]Cl and D_2O. During the reaction, a 1,2-borate complex was detected in both ^{1}H and ^{13}C NMR spectra, and was proposed to be **2.42** (Scheme 2-14). Its resonance in the ^{11}B spectrum had a chemical shift of -7.90 ppm in D_2O, using $B(OH)_3$ as the external standard (δ = 0.00 ppm). This may not be a true intermediate in the mechanism but a side-product formed from **2.41** (Scheme 2-14, highlighted in green, R = OH). Complex **2.42** was quite stable under the reaction conditions explored since it was still seen in the NMR spectra of reaction mixtures after the full conversion of glucose and fructose, and this suggests that its conversion to 5-HMF is quite slow and therefore appears in a branch along the reaction pathway. However, there was no NMR identification of **2.41**, so conclusive evidence was lacking to prove that the detected **2.42** was truly a species different from **2.41**. The function of B_2O_3 in this study was to react with water, which could both facilitate the dehydration via Le Châtelier's principle and generate $B(OH)_3$ to promote the reaction. It is somewhat surprising given the widespread use of $B(OH)_3$ and related compounds in transformations of glucose and fructose that ^{11}B NMR spectroscopy has not been used more widely to identify reaction intermediates.

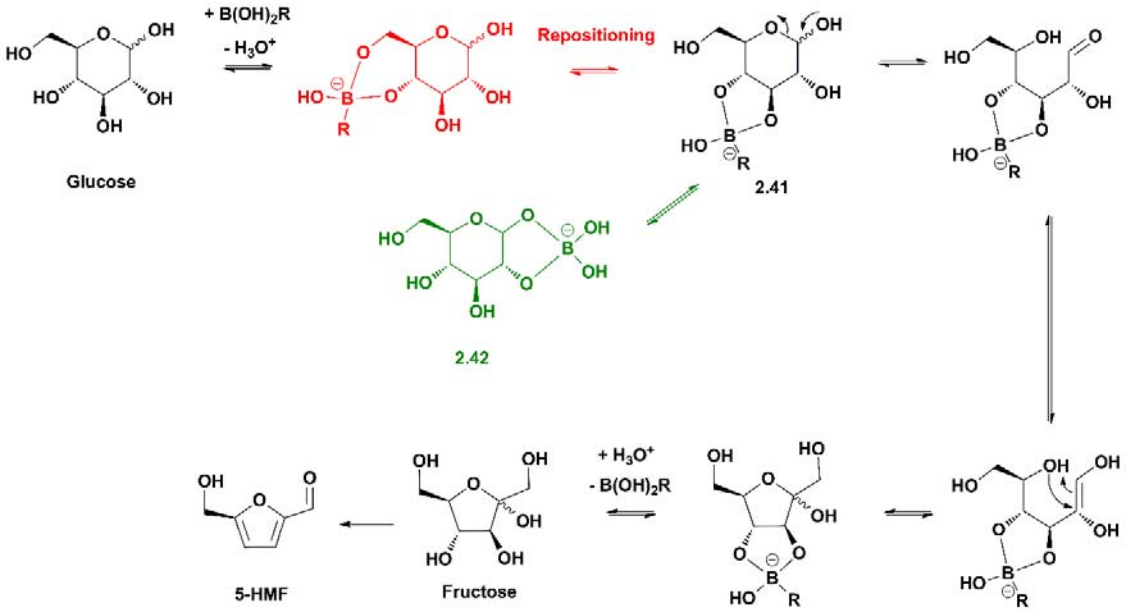

Scheme 2-14. The dehydration of glucose to 5-HMF catalyzed by boronic acid catalysts.[47, 53, 54, 64]

As can be seen from the discussion above, in most studies on glucose isomerisation the catalysts used were Lewis acids, mainly because of their excellent performance on the catalysis of glucose dehydration to get good 5-HMF yields. Nevertheless, there have been some studies reported using Brønsted acid catalysts. In 2014, Amarasekara and Razzaq implemented a NMR study of glucose dehydration catalyzed by a functionalized Brønsted acidic ionic liquid, 1-(1-propylsulfonic)-3-methylimidazolium chloride ([C_3SO_3Hmim]Cl), in DMSO-d_6.[42] [^{13}C-1] and [^{13}C-2] glucose were used as reactants and the reaction mixtures were analyzed using ^{13}C NMR spectroscopy. By t = 48 min, besides the C1 and C2 signals of α- and β-glucose isomers, the resonances of C1 and C2 of the open-chain fructose and 5-HMF were also observed. A 1,2-hydride shift mechanism involving the interaction

between the imidazolium cation and glucose was proposed (Scheme 2-15). The peaks at 74.15 and 72.58 ppm were assigned to C1 of the two isomers of **2.43**, and the peaks at 189.88 and 192.40 ppm were assigned to the C2 of the isomers. The resonances at 147.10 ppm and 136.30 ppm were assigned to C1 and C2 of **2.2** respectively. The authors claimed that the isomerisation proceeded along the 1,2-hydride shift pathway because no deuterium incorporation was detected. However, it needs to be noted that the solvent used in this study was DMSO-d_6, which does not release free deuterium into solution. Therefore, it would be more convincing if D_2O was used as the solvent for the deuterium detection experiments.

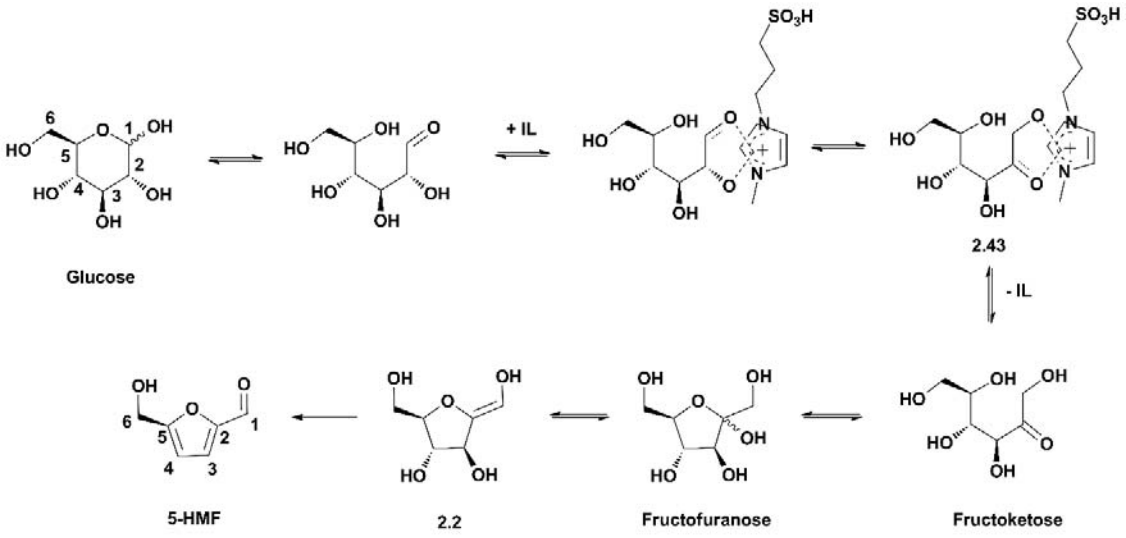

Scheme 2-15. The mechanism of Brønsted acid ionic liquid-catalyzed glucose transformation to 5-HMF proposed by Amarasekara et al.[42]

2.3.2 Computational Studies

Qian's group is the pioneer in the computational studies of glucose conversion. From 2005 to 2011, this group performed calculations about several transformations of glucose including dehydration, condensation, isomerisation and mutarotation, with a Brønsted acid (H^+) as the catalyst and water as the solvent.[68-71] In 2005, the group applied Car-Parrinello based ab initio molecular dynamics (CPMD) to simulate the reaction routes of glucose conversion to **2.2'** (Scheme 2-17, highlighted in red) both in vacuum and in water at 227 °C.[68, 69] As mentioned in Section **2.2.2**, compound **2.2** (or **2.2'**) was proposed to be an important intermediate in the dehydration of fructose to 5-HMF. Here it was also assumed to be significant in the direct dehydration of glucose to 5-HMF without the isomerisation to fructose. The pathways was initialized by the protonation at different hydroxyl groups or the O atom on the ring (O5) were simulated, and in both situations (with and without solvent) only protonation at O2H could lead to C2-O2 cleavage and the subsequent formation of **2.45** (the precursor of **2.2'**) via C1-O5 breaking and C2-O5 bonding. The protonation at O1H did not trigger the degradation of glucose under the applied conditions. The protonation at O3H and O4H led to the intermediates for polymerization. The proton at O6H transferred from O6 to O5 to form the O5 protonated glucopyranose, and no further conversion was observed. When the solvent was included, one glucose molecule was surrounded by 32 water molecules in a unit cell, and one proton was added into the system to simulate the acidic environment. It was found that the proton could transfer from the protonated hydroxyl groups of glucose to a nearby water molecule. Therefore, the

protonation of glucose might be the rate-limiting step, since the study in vacuum has showed the subsequent dehydration of the protonated glucose happened quickly. This proton transfer was attributed to the higher proton affinity of water compared with the hydroxyl groups of glucose. The NMR analysis from previous studies indicated that the downfield shifts of the hydroxyl groups after proton exchange with water decreased in the order O6H > O2H > O3H, O4H > O1H, corresponding to the decrease of their proton affinities.[72, 73] This further supports the calculation results that the O2H protonated glucose was the most likely starting point since O2H has a relatively high proton affinity. The simulation of the subsequent conversion was started from **2.44** to avoid the interruption of the proton transfer. **2.45** was generated on the same pathway as in vacuum. Since water has hydrogen bonding with O1H of **2.45**, the proton on O1H could be taken away and **2.2'** was produced. It can be seen that water as the solvent has a great influence in the simulation, mainly through its competition for protons with the hydroxyl groups of glucose. This again indicated the importance of the consideration of solvents in computational studies.

In 2011, Qian implemented a more comprehensive computational study about this cyclic mechanism of glucose direct dehydration.[70] A CPMD coupled with metadynamics (MTD) method was applied to simulate the reaction process and investigate the associated Gibbs energy surfaces (GESs). One advantage of this method is that the bond cleavage and formation can be concretely described through the coordination number of one atom to the other. For example, CV1 refers to the coordination number of C2 to O2. When CV1 ≈ 1, there is a single bond between C2 and O2; if CV1 ≈ 0, it means the C2-O2 bond is broken.

A simulation in the gas phase was performed first, with one H_3O^+ in the system to mimic the acidic environment. The changes of the coordination numbers of C2 to O2 (CV1), C2 to O5 (CV2) and O2 to the four protons from O1H and H_3O^+ (CV3) during the calculation were analyzed. Initially the proton transferred between O2H and the water molecule repeatedly. After around 80 MTD steps the C2-O2 bond was broken and the C2-O5 bond was formed to generate **2.45**, which was immediately transferred to **2.2'**. This process was reversible and repeated back and forward twice during the simulation (over 6500 MTD steps). The GESs of CV1 - CV3 and CV2 - CV3 were obtained and they reflected the proton affinities of the species formed during the process. The average proton affinities of various sites obtained was approximately 418.4 - 502.1 kJ/mol. This lower range compared with some previous results[74] was attributed to the surrounding water molecules, which formed hydrogen bonding with the reaction species and thus decreased their proton affinities. Afterwards, the simulation was performed in water by setting one glucose molecule surrounded by 76 water molecules. Initially the reversible protonation between O2H and water molecules were observed. The cleavage of C2-O2 bond and the formation of C2-O5 happened at around 230 MTD steps to generate **2.2'**, and no reverse reactionsappeared in the following calculation. The GES analysis showed that the overall reaction barrier was 125.5 - 146.4 kJ/mol, which was in good agreement with previous experimental results.[75] This barrier was mainly contributed by the protonation of O2H, the cleavage of C2-O2 bond and the formation of C2-O5 bond, and was influenced by the solvent through its proton affinity. The higher proton affinity the solvent has, the more difficult the protonation of O2H is, and hence the higher the barrier is.

In the work published in 2012, Qian also mentioned that the isomerisation of glucose to fructose could be realized through a 1,2-hydride shift of **2.45** (Scheme 2-16).[71] The hydride shifted from C2 to C1 to form a C2 carbocation (**2.4**), which reacted with water to produce fructose. The CPMD-MTD simulation results in the gas phase showed that the reaction barrier of the 1,2-hydride shift was as low as 20.9 - 29.3 kJ/mol because **2.4** was quite stable. Nevertheless, when the calculation was performed in water, **2.45** became less stable and the proton of O1H was easily removed by water to form **2.2'**.

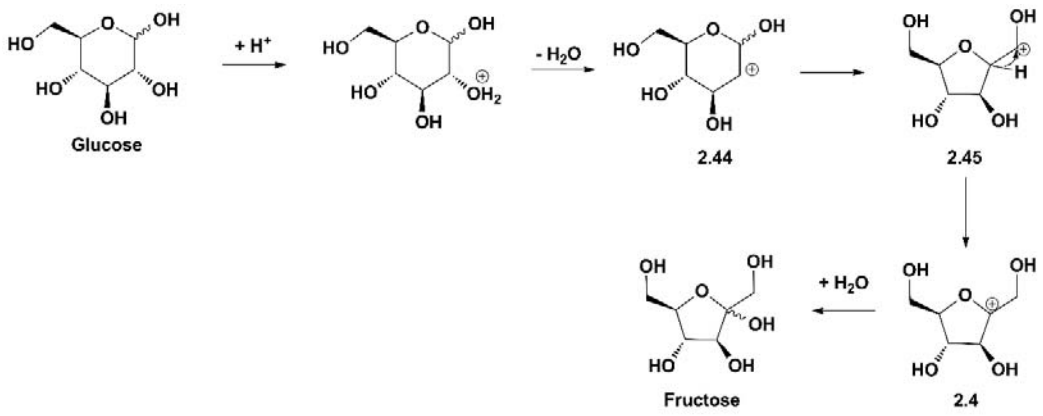

Scheme 2-16. The isomerisation of glucose to fructose through a 1,2-hydride shift proposed by Qian et al.[71]

In the study by Assary et al. in 2012, the mechanism for the Brønsted acid-catalyzed glucose dehydration in water was calculated for both the cyclic and acyclic routes without the isomerisation to fructose (Scheme 2-17).[25] The cyclic mechanism via **2.11** and **2.12** can be seen as a support to the work by Qian's group. In the acyclic route, O1 was protonated after the ring opening because of its higher proton affinity than other hydroxyl groups. **2.46** was produced and converted to an enediol (**2.47**). Similar to the fructose dehydration

process, water was believed to assist the conversion of **2.47** to **2.32** and **2.32** to **2.48** as a proton mediator. However, it should be noted that the protonation of O1H as the first step was rarely seen in computational studies of glucose dehydration.

In 2015, Yang et al. performed a DFT-based microkinetic model study of Brønsted acid-catalyzed transformations of glucose to 5-HMF, LA, FA and furfuryl alcohol.[76] The protonation of O2H was proposed as the first step. The geometry optimization and Gibbs energy calculations of all possible intermediates and transition states were carried out using Gaussian 09 program and B3LYP/6-31+G(d,p) basis set with two explicit water molecules included. Afterwards, a microkinetic model was built, which was composed of several reactions: the dehydration of glucose to 5-HMF via the isomerisation to fructose, the direct dehydration of glucose to 5-HMF via **2.11** and **2.12** (the cyclic route in the study by Assary et al.,[25] Scheme 2-17, highlighted in black), and some other conversions of glucose and 5-HMF. The analysis of reaction fluxes in the kinetic models was implemented and showed that the isomerisation of glucose to fructose contributed little in the overall rate of glucose consumption. The cyclic mechanism of glucose dehydration through **2.11** and **2.12** was claimed to be the main pathway.

Nevertheless, different mechanisms of Brønsted acid-catalyzed dehydration of glucose were proposed in several other studies. In the DFT study carried out by Pidko and co-workers in 2012, the Gaussian 09 program was applied with B3LYP/6-311+G(d,p) basis set.[26] The solvent effects were examined by performing test calculations, and it was claimed that the qualitative trends of the calculation results with and without a solvent were similar.

The protonation at all hydroxyl groups and O5 was calculated as the first step in the dehydration. The O1H protonated glucose was the most favorable because of its low Gibbs energy change (-23 kJ/mol). However, it led to side-reactions with no 5-HMF generation. Surprisingly, a total of 31 possible reaction routes initialized by the protonation of O2H were investigated and none of them produced 5-HMF, which was quite different from the results in Qian's study. The protonation of O5 led to the ring opening of glucose (**2.46**), and subsequently the protonated open-chain fructose (**2.49**) was obtained via a 1,2-hydride shift (Scheme 2-17). Similarly, in the DFT study by Daorattanachai et al. in 2012, the process was started from the O5 protonated glucose when a Brønsted acid was used as the catalyst.[77] The geometries were optimized and the frequencies were calculated in gas phase for all species involved using Gaussian 03 engine with the B3LYP/6-31G(d,p) basis set. Compared with the non-catalyst system, the protonation of O5 loosened the C1-O5 bond with an increase of the bond length from 1.43 Å to 1.60 Å. Consequently, the activation barrier of C1-O5 cleavage decreased from 184.1 kJ/mol to 30.4 kJ/mol. Afterwards **2.49** was isomerized to fructose through a 1,2-hydride shift with an overall activation barrier of 66.9 kJ/mol. Without any catalyst, the isomerisation of glucose to fructose was proposed to proceed via enolization and the overall activation energy barrier was 184.1 kJ/mol from the ring opening of glucose. In addition, the isomerisation catalyzed by a Brønsted base was also investigated by starting the process from the deprotonation of O1 of glucose (**2.50**). The cleavage of the C1-O5 bond was facilitated by the deprotonation of O1 with a low activation energy of 24.2 kJ/mol. The deprotonated open-chain glucose (**2.51**) was isomerized to the deprotonated fructose (**2.53**) through the deprotonated 1,2-enediol

intermediate (**2.52**) with an overall activation energy barrier of 173.7 kJ/mol (Scheme 2-17). The use of catalysts could clearly change the reaction routes and energies of the intermediates (thus the rate-limiting steps). However, it needs to be noted that this study was performed in gas phase and there was no explanation about their choice of the O5 protonated and O1 deprotonated glucose molecules as the starting points in the Brønsted acid and base calculations. Therefore, further study is needed for more accurate and reasonable results.

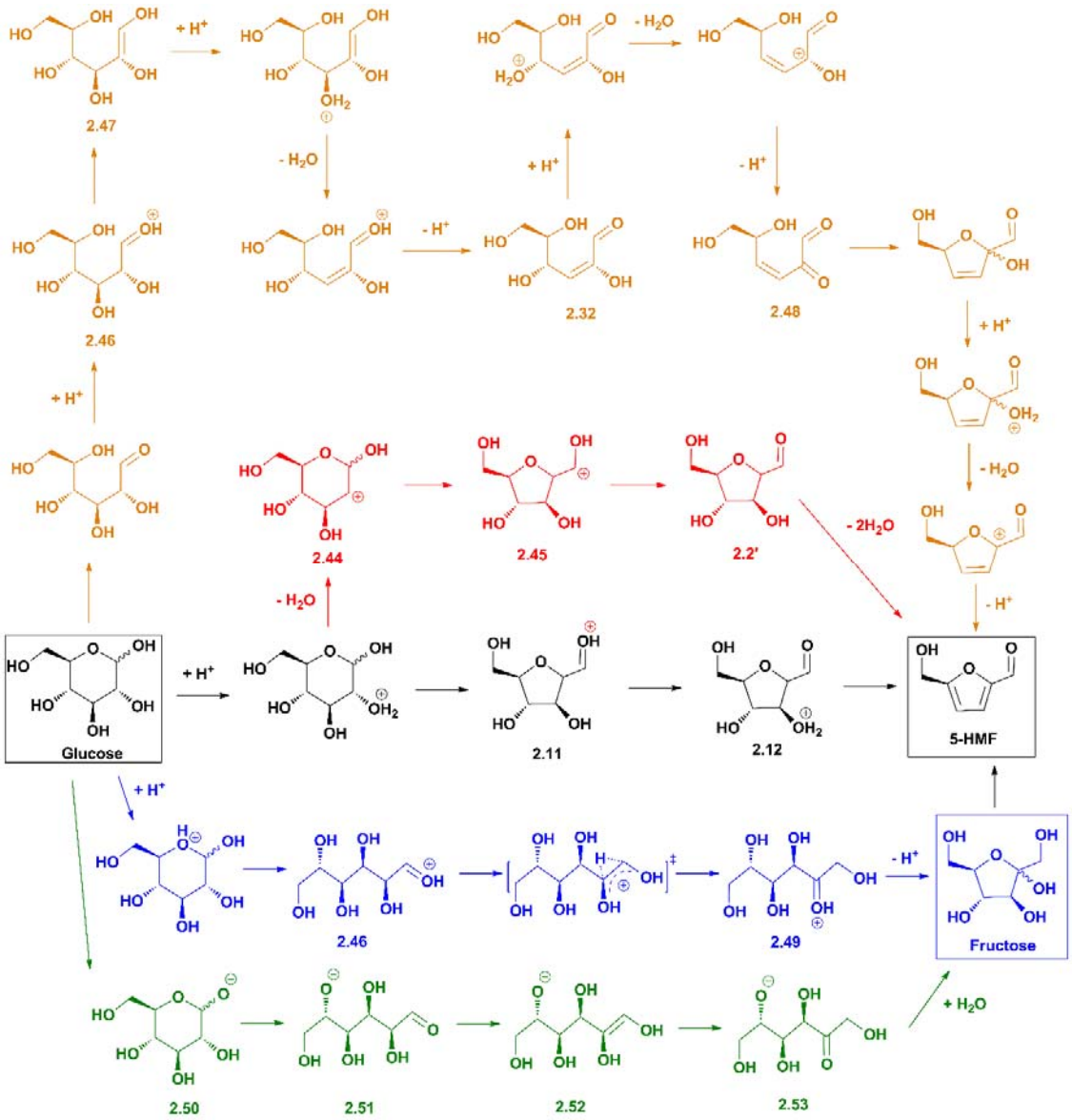

Scheme 2-17. The mechanisms of Brønsted acid/base-catalyzed glucose dehydration to 5-HMF proposed by Qian[68-71] (red), Assary[25] (black: cyclic route; orange: acyclic route), Pidko[26] (blue) and Daorattanachai[77] (blue: Brønsted acid; green: Brønsted base).

As was discussed in **2.3.1**, the direct dehydration of glucose through 3-DG (Scheme 2-9, route **A**) has been proposed as a potential pathway. In 2011, the Bols group combined lab experiments and a DFT study to investigate the role of 3-DG in the dehydration of glucose.[40] In an ion chromatogram, 3-DG has a broad peak at 8.2 min retention time, with glucose appearing at 3.6 min and fructose at 3.8 min. 5-HMF was synthesized from glucose with H_2SO_4 as the catalyst and DMA-LiCl as the solvent system. After 3 h of reaction, both 3-DG and fructose were observed in the ion chromatogram with a ratio of 2:1. The conversion of 3-DG to 5-HMF or its halogenated derivatives gave higher product yields and reaction rates than fructose did. Finally, the DFT calculations of glucose dehydration proceeding via 3-DG or fructose pathways were performed using Gaussian 03 program with the G3MP2 method. The Gibbs energies of all intermediates in the 3-DG route were lower than those in the fructose route, indicating the preference of the 3-DG route over the fructose one. Therefore, it was claimed that both reaction pathways (with and without the isomerisation of glucose) happened under the conditions applied, but the one through 3-DG was more favored (route **A**, Scheme 2-9).

In the quantum mechanical study using the RISM-SCF-SEDD method discussed in **2.2.2**, prior to the calculations on fructose dehydration to yield 5-HMF, both the cyclic and acyclic mechanisms of HCl-catalyzed glucose isomerisation were simulated in water and MmimCl (Scheme 2-18).[31] In the cyclic mechanism, after the transformation of glucose to **2.11**, a hydride shift from C2 to C1 led to the formation of an oxocarbenium cation (**2.4'**). Afterwards, a water molecule was attached to C2 and a proton left to generate fructose. In

the acyclic mechanism, the ring opening was initialized via the protonation of O5 and deprotonation of O1H. In MmimCl, the open-chain glucose interacted with HCl at O1 to form an intermediate (**2.54**), which was then converted to an enediol (**2.47**). The proton transfer from HCl to C1 and from O2H to Cl^- led to the formation of **2.56**. In water the acid-base pair from the catalyst and the solvent was H_3O^+-H_2O; while in MmimCl it was HCl-HCl_2^-. The cyclic mechanism was favored in water with an activation barrier of 99.6 kJ/mol, and the acyclic mechanism was favored in MmimCl with a barrier of 135.6 kJ/mol.

In DFT calculations reported by Li et al. concerning [$BmimSO_3H$]Cl-catalyzed dehydration of glucose discussed in **2.2.2**, two possible pathways were proposed after the generation of an enediol intermediate (**2.47**), and were simulated (Scheme 2-18).[32] Path **I** is through the isomerisation to fructose and Path **II** is the direct conversion of **2.47** to 5-HMF. During the conversion of glucose to **2.47**, the sulfonic acid group (-SO_3H) in the ionic liquid cation acted as a proton shuttle, which transferred protons to form the transition states (**2.57** and **2.58**). In path **I**, -SO_3H played the same role to promote the generation of fructose. The subsequent dehydration of fructose to 5-HMF has been discussed in detail in **2.2.2**. In path **II**, **2.32** was obtained through the interaction between **2.47** and -SO_3H at O1H and O3 (**2.59**). Afterwards, a diketone (**2.48**) was formed in a similar way through the interaction between **2.32** and -SO_3H at O2H and O4, and it lost one water molecule to achieve the ring-closed intermediate (**2.60**). The formation of an oxocarbenium intermediate (**2.61**) resulted from the interaction between O2H and the proton from -SO_3H. Finally, 5-HMF was produced through the interaction between **2.61**, -SO_3^- and a water

molecule. It was claimed that both pathways were accessible because they had similar activation barriers. The catalysis by [BmimSO_3H]Cl was achieved mainly through -SO_3H acting as a proton shuttle, and the intermediates and transition states were stabilized via hydrogen bonding with Cl^- anions.

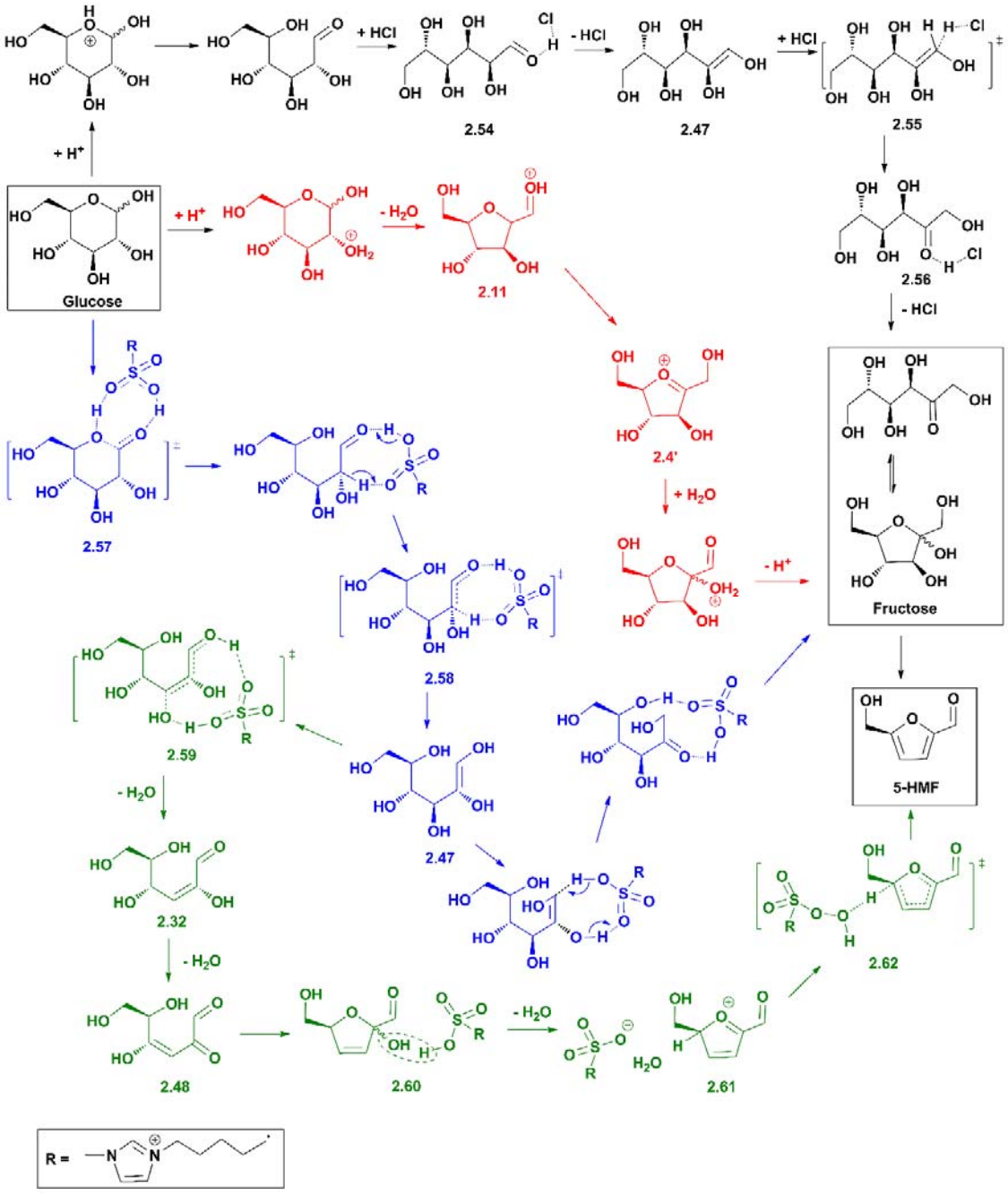

Scheme 2-18. The pathways of glucose conversion to 5-HMF in ionic liquids proposed by Arifin et al.[31] (black: acyclic; red: cyclic) and Li et al.[32] (blue: path I; green: path II)

It is a little surprising but understandable that the Brønsted acid-catalyzed glucose dehydration has been studied more extensively via computational calculations than in lab experiments. The main reason is the harsh conditions (e.g. high temperature, long reaction time) required and the limitation of 5-HMF yields in lab experiments. The differences in the conclusions obtained from these computational studies may be due to the different calculation methods used and the conditions set (e.g. temperature, gas-phase or solvent included).

During 2010 and 2011, the Hensen group implemented a series of studies of glucose complexation with chromium chlorides ($CrCl_2$ or $CrCl_3$) in ionic liquid solvents.[78-80] The DFT calculations were carried out using Gaussian 03 program with a basis set combination (6-31+G(d) for Cr, Cl and O atoms; 6-31G(d) for C, N and H atoms) for higher accuracy. At least two ionic liquid ion pairs per Cr atom were explicitly added in the system. The extended X-ray absorption fine structure (EXAFS) spectra at the Cr K edge were obtained during the reactions as supporting evidence to the computational results for the comprehensive analysis of the reaction process. In their first published work about $CrCl_2$ catalysis in EmimCl, the solvent effect was considered by applying PCM solvation model in the calculations.[78] When there was only $CrCl_2$ in EmimCl with no addition of glucose at 80 °C, both EXAFS spectra and DFT calculations showed that the Cr^{2+} coordinated with four Cl^- ions to form the square-planar $CrCl_4^{2-}$ species. After glucose was added and before the reaction started, the EXAFS spectra showed that the coordination number (CN) of Cr-Cl bond decreased from 3.9 to 2.9 and a new Cr-O bond appeared with a CN of 1.0 and a

coordination distance of 2.13 Å. This indicated that one Cl^- ligand was replaced by an O atom from a hydroxyl group of glucose (**2.63**). After being heated for 10 min at 100 °C, the fructose concentration reached the maximum. The EXAFS analysis showed that besides two Cr-Cl bonds (CN = 2.4) there were two Cr-O bonds (CN = 2.0) and one Cr-Cr interaction with a CN of 0.6 and a coordination distance of 3.45 Å. Considering the low CN and the long distance, this Cr-Cr interaction was assigned to a Cl- or O-bridged Cr dimer. At the end of the reaction by 180 min, this Cr-Cr interaction disappeared. The DFT calculations were carried out from the coordination of glucose to Cr^{2+} at O1, which triggered the ring opening and the subsequent 1,2-hydride shift to achieve the isomerisation to fructose. The Gibbs energies of intermediates and transition states during the isomerisation with mono- and binuclear Cr complex coordination were calculated at 100 °C. In the mononuclear route, the overall energy barrier was 120 kJ/mol, composed of 69 kJ/mol for the deprotonation of O2H and 51 kJ/mol for the subsequent transformation to the 1,2-hydride shift transition state. In the binuclear route, O1 bridged the two Cr centres after the deprotonation of O2H to generate **2.64**. The overall energy barrier of 63 kJ/mol was much lower than the mononuclear route. The deprotonation of O2H consumed 54 kJ/mol and only 9 kJ/mol was needed for the following hydride shift. After the hydride shift, the intermediate complexed with the Cr dimer was more stable (**2.65,** -25 kJ/mol) than the one complexed with one Cr centre (46 kJ/mol). Therefore, the binuclear route was more favored for the 1,2-hydride shift process (the rate-limiting step) (Scheme 2-19). The possible reason is that the coordination of O1 to two Lewis acidic Cr centres steadied the negative charge developed on O1 during the hydride shift, thus the transition state with the

highest energy was stabilized. Afterwards, the open-chain fructose in Cr dimer form (**2.66**, -3 kJ/mol) was slightly more favorable than in Cr monomer form (15 kJ/mol), but the final fructofuranose generated was more stable when coordinated with only one Cr centre (**2.67**, -23 kJ/mol) than with two (14 kJ/mol).

In the following year, the same group performed similar studies using Cr^{3+}.[80] The experimental results showed that the 5-HMF yield decreased in the order $CrCl_3 \cdot 6H_2O$ > $CrCl_3$ > $CrCl_2$ when they were used as catalysts. It was explained by 1) the higher rate of fructose dehydration with Cr^{3+} catalysis than Cr^{2+}; and 2) the higher solubility of $CrCl_3 \cdot 6H_2O$ than $CrCl_3$ in EmimCl. Therefore, the DFT study was carried out in the gas phase using $CrCl_3 \cdot 6H_2O$ as the catalyst. At 80 °C before glucose addition, the EXAFS spectra showed that the CN of Cr-Cl bond was 5.8, indicating that the six water ligands were replaced by six Cl^- to form an octahedral complex after the dissolution of $CrCl_3 \cdot 6H_2O$ in the ionic liquid. After glucose was added, two Cl ligands were replaced. The DFT optimization result showed that the new coordinating groups were O1 and O2 from the hydroxyl groups of glucose, with a Gibbs energy change of -12 kJ/mol (**2.68**). The two pathways with mono- and binuclear Cr complexes were simulated. During the initial ring opening of glucose, the mononuclear path was slightly more favored than the binuclear path. Nevertheless, during the following deprotonation of O2H and the 1,2-hydride shift the coordination with two Cr centres effectively decreased the energy barrier to 66 kJ/mol, compared with 90 kJ/mol for one Cr centre. Therefore, similar to Cr^{2+}, the binuclear Cr^{3+} complex (**2.69**) was preferred for the isomerisation of glucose via 1,2-hydride shift. It needs

to be noted that **2.69** was bridged through O1 as well as two Cl^- ligands, which was different from **2.64**. After the hydride shift, the intermediate was still more favored with the Cr dimer (**2.70**, -11 kJ/mol) than the monomer (-1 kJ/mol). However, the open-chain fructose finally obtained was quite unstable in the binuclear structure (64 kJ/mol; the mononuclear one **2.71**: -34 kJ/mol), caused by the repulsions between the bridging O1H and the Cl^- ligands around. In addition, the calculations of Cr^{2+} routes were also carried out and compared with Cr^{3+}. The activation barriers for Cr^{3+} were much lower than for Cr^{2+}, both in the mononuclear and binuclear paths. This was attributed to the higher Lewis acidity of Cr^{3+}, which led to the higher stability of the intermediates formed during the isomerisation.

In addition, $CuCl_2$ was also studied in terms of its complexation with glucose in ionic liquid solvents and was compared with $CrCl_2$.[79] Similar to $CrCl_2$, the main Cu^{2+} species in MmimCl before glucose addition was a four-coordinate complex ion ($CuCl_4^{2-}$), but in a distorted tetrahedral structure, as shown by the EXAFS spectra and DFT calculations. However, after glucose was added, there was no complexation of glucose with the Cu centre detected at 80 °C. The Gibbs energy calculations showed that this process was endothermic and thus was not favored.

In 2015, Wang and co-workers investigated the influence of organic solvents and Brønsted acid co-catalysts in the $CrCl_3$-catalyzed dehydration of glucose experimentally and computationally.[81] First, a series of experiments using different solvents were performed. The use of DMA led to the highest 5-HMF yield while DMSO resulted in the lowest one. Afterwards, the reaction was performed in DMA and co-catalyzed by several

ionic liquids and their corresponding Brønsted acids. The 5-HMF yield decreased when *N*-methyl-2-pyrrolidone hydrogen sulfate ([NMP]HSO_4) or H_2SO_4 was used. The reaction rate increased when *N*-methyl-2-pyrrolidone chloride ([NMP]Cl) or *N*-methyl-2-pyrrolidone bromide ([NMP]Br) was used but the 5-HMF yield was not improved. The use of hydrochloric acid (HCl) or hydrobromic acid (HBr) gave similar results. Without $CrCl_3$, the use of [NMP]Cl, [NMP]Br, HCl or HBr alone resulted in no production of 5-HMF from glucose but 5-HMF could be obtained directly from fructose. Therefore, it was claimed that these co-catalysts functionalized during the dehydration of fructose after the isomerisation of glucose happened. A DFT study using Gaussian 03 program with B3LYP level of theory was operated to probe the interactions among $CrCl_3$, glucose and the co-catalysts. The LanL2DZ basis set was used for Cr and Br elements while the 6-311 G(d,p) basis set was for others. The PCM solvent model at 120 °C was applied to consider the solvation effect. The energies of different Cr complexes that could form during the reaction were calculated (Figure 2-5). In the DMA-$CrCl_3$-glucose system, similar Gibbs energy changes for $CrCl_3$-DMA (-34.00 kJ/mol) and $CrCl_3$-glucose (-26.62 kJ/mol) coordination indicated that they were both favored and the reaction was catalyzed by both $CrCl_3$ and $CrCl_3$-DMA. In the DMSO-$CrCl_3$-glucose system, the extremely low Gibbs energy change of $CrCl_3$-3DMSO coordination (-114.56 kJ/mol) revealed the formation of a stable six-coordinated Cr complex, which inhibited the interaction of the Cr centre with glucose for further reaction. Similarly, $CrCl_3^-$-3HSO_4 coordination was also quite energetically favored (-78.61 kJ/mol) so the conversion of glucose was prevented because the hydrogen sulfate anions blocked sites at Cr where the glucose could coordinate. By contrast, for the halide systems, five-

coordinate Cr complexes ($CrCl_3$-$2Cl^-$ or $CrCl_3$-$2Br^-$) were generated, which had hemispheric structures so the Cr centre was exposed for the interaction with glucose. The isomerisation mechanism was proposed through a 1,2-hydride shift and the activation barriers were calculated. When the halides were involved, the generated $CrCl_3$-$2Cl^-$ or $CrCl_3$-$2Br^-$ could slightly decrease the activation barrier of the hydride shift process (the rate-limiting step) but the overall barriers were increased by approximately 20 kJ/mol. Therefore, the co-catalysts didn't effectively promote the isomerisation of glucose.

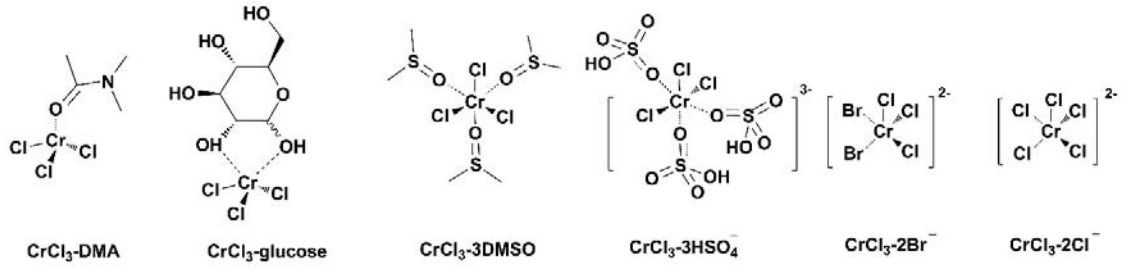

Figure 2-5. The Cr complexes formed between $CrCl_3$ and glucose, solvents (DMA, DMSO) or co-catalysts (H_2SO_4, HBr, HCl) proposed by Wang and co-workers.[81]

In the study by Guan et al. discussed in **2.2.2**, before the dehydration of fructose to 5-HMF they performed a DFT study of glucose isomerisation catalyzed by trivalent metal chlorides ($CrCl_3$, WCl_3, $MoCl_3$ and $FeCl_3$) in ionic liquids.[34] The ionic liquid cation ($[Bmim]^+$) was included as one ligand of the metal complexes and an isomerisation mechanism through enolization was proposed, which is different from Hensen's studies (Scheme 2-19). Before the complexation with glucose, the metal centre was proposed to coordinate to three Cl^- anions and one $[Bmim]^+$ cation. For the four metals studied, the overall activation barrier increased in the order WCl_3 (197.1 kJ/mol) < $MoCl_3$ (197.9 kJ/mol)

< $CrCl_3$ (219.7 kJ/mol) < $FeCl_3$ (243.1 kJ/mol). In natural bond orbital **(**NBO) calculations, it was shown that the net NBO charge of the W atom in the [Bmim]/WCl_3 moiety was the highest (0.971 a.u.), which led to stronger coordination with glucose and hence the activation barrier was decreased.

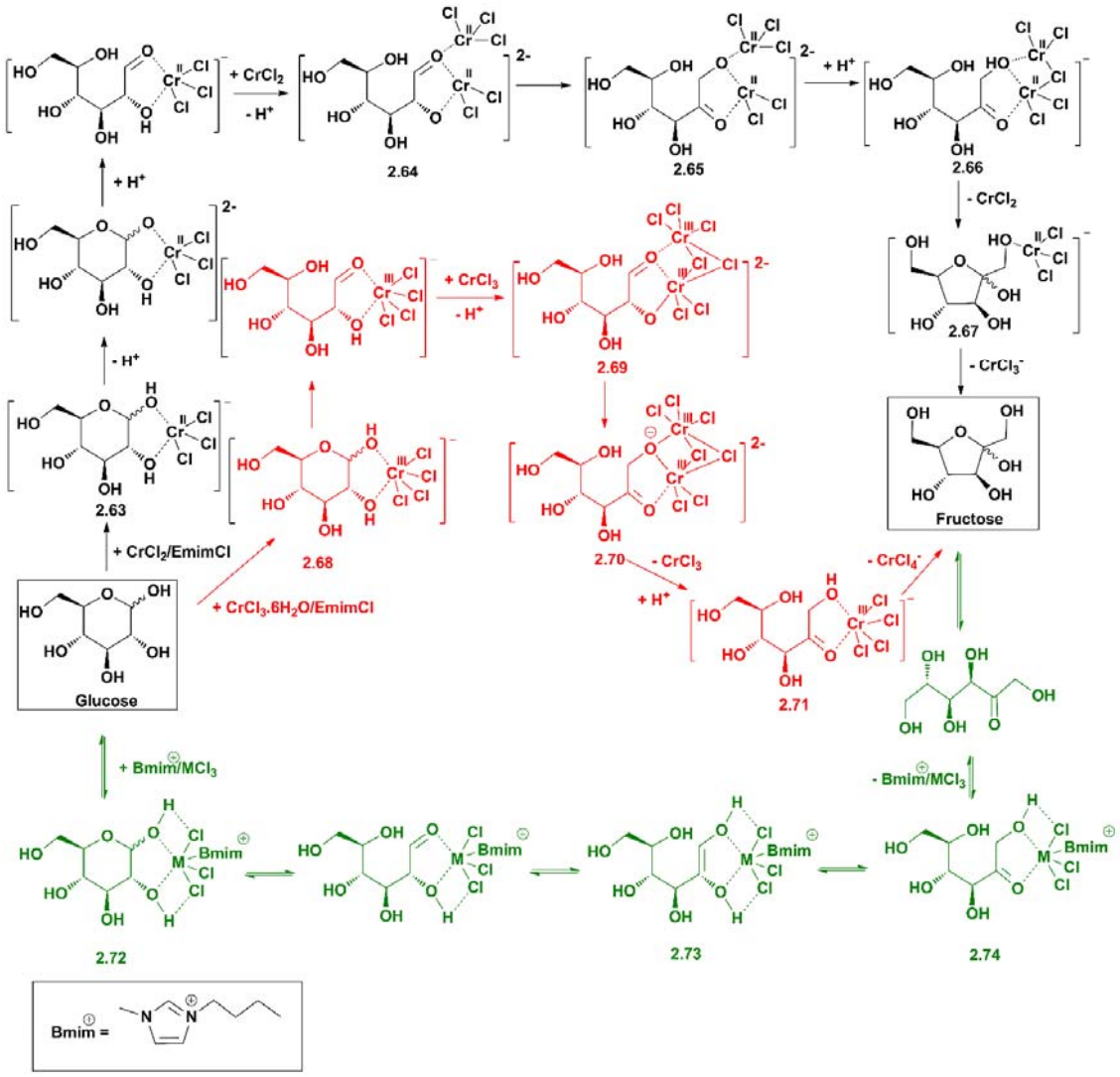

Scheme 2-19. The mechanisms of metal chloride-catalyzed glucose isomerisation proposed by the Hensen group[78-80] (black: Cr^{2+}; red: Cr^{3+}) and Guan et al.[34] (green)

In the study by the Rissager group in 2011, the isomerisation of glucose through two mechanisms (1,2-hydride shift and enolization) with and without $B(OH)_3$ catalysis in ionic liquid solvents were calculated and the results were compared (Scheme 2-20).[53] The DFT study was carried out using Jaguar 7.6 program with the B3LYP level of theory. The LACVP* basis set was used for B atom and the 6-31G* basis set was for the other elements. The solvation energies were calculated using the PB-SCRF solvation model (continuum). The reaction with no $B(OH)_3$ addition was calculated first. The enediol intermediate (**2.77**, 54 kJ/mol) was much more stable than the hydride shift transition state (**2.78**, 183 kJ/mol), so the enolization mechanism was favored. The generated open-chain fructose was stable with O1 deprotonated (**2.79**, 82 kJ/mol). The overall isomerisation process was endothermic by 10.4 kJ/mol. When $B(OH)_3$ was added, all possibilities of glucose complexation to $B(OH)_3$ were investigated and the 4,6-boroglucopyranose (Figure 2-6) was the most stable one (-60.5 kJ/mol). The following ring opening was energetically favored to produce a very stable 3,4-coordinated intermediate (**2.81**, -90 kJ/mol). Since the ring opening may be faster than the repositioning, the reaction route was modified to be initialized from the 3,4-boroglucopyranose (**2.80**). The extraordinary stability of **2.81** was attributed to the chelating effect of $B(OH)_3$. The protonation of **2.81** was easier with a lower energy increase (74 kJ/mol) compared with no $B(OH)_3$ addition (**2.75** → **2.76**, 121 kJ/mol), and was possibly promoted by the negative charge of the B centre. Again the 1,2-enediol (**2.82**, -29 kJ/mol) was preferred over the hydride shift transition state (**2.83**, 75 kJ/mol). The produced 3,4-borofructose was slightly more stable with O2 protonated (**2.84**, -2 kJ/mol). The final 3,4-borofructofuranose (**2.85**, 0 kJ/mol) could be rearranged to the more

stable 2,3-borofructofuranose (**2.86**, -74 kJ/mol) or 2,3,4,6-diborofructofuranose (**2.87**, -96 kJ/mol) (highlighted in green, Scheme 2-20). **2.87** is too stable to convert to 5-HMF, and this explains why the 5-HMF yield decreased when the ratio of $B(OH)_3$ to glucose was higher than 1:1. The overall $B(OH)_3$-catalyzed process was exothermic by -14 kJ/mol. Therefore, the use of $B(OH)_3$ increased not only the stability of the enediol intermediate but also the exothermicity of the isomerisation process. The comparison of the intermediates/transition states between two possible mechanisms made this study very convincing.

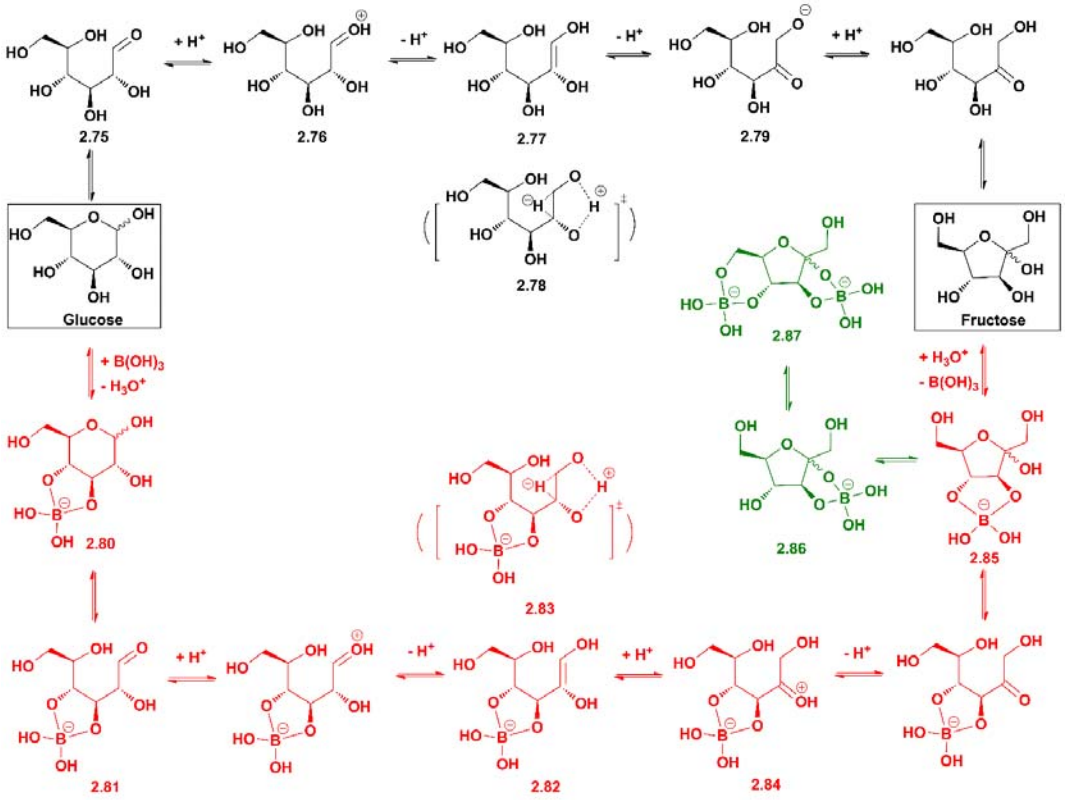

Scheme 2-20. The mechanisms of glucose isomerisation to fructose with (red) and without (black) $B(OH)_3$ proposed by the Riisager group.[53]

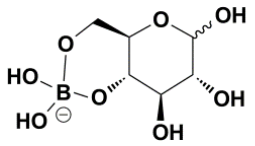

4,6-Boroglucopyranose

Figure 2-6. Structure of 4,6-boroglucopyranose from glucose complexation to $B(OH)_3$ proposed by the Riisager group.[53]

A poly-benzyl ammonium chloride resin (P-$BnNH_3Cl$) was used as the catalyst to build a metal-free system for the dehydration of glucose by the Zhang group in 2015.[82] A reasonable 5-HMF yield of 53% was achieved in a biphasic system composed of a mixture of aqueous NaCl and DMSO as the polar phase and methylisobutylketone (MIBK) as the non-polar organic phase. The isomerisation of glucose was proposed through an enolization pathway catalyzed by both the benzyl ammonium cation (P-NH_3^+) and the benzyl amine (P-NH_2) (Scheme 2-21). A DFT study using Gaussian 09 program with M062x density functional was performed to investigate the intermediates. The 6-31G(d) basis set was used for geometry optimization, and the 6-311++G(d,p) basis set was for energy calculations. The solvation effect was considered using IEFPCM model with water as the solvent. The whole isomerisation process was exothermic, possibly because the intermediates were stabilized through hydrogen bonding. In addition, the dehydration of glucose was performed in a DMSO/D_2O system and deuterium incorporation at C1 of the 5-HMF product was observed in the ^{13}C NMR spectra, hence the enolization path was verified.

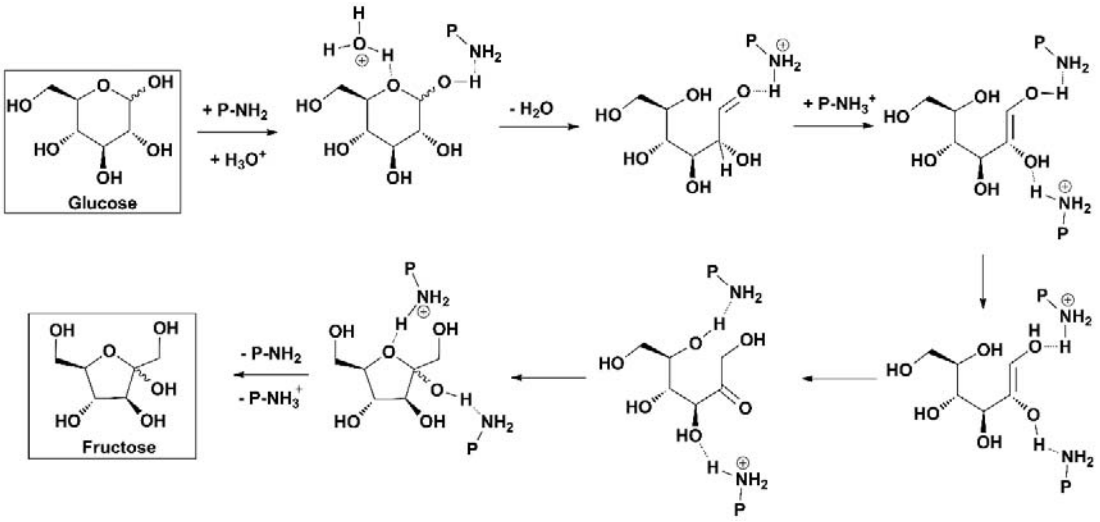

Scheme 2-21. Isomerisation of glucose catalyzed by P-BnNH3Cl proposed by the Zhang group.[82]

In 2016, Zhang et al. performed a DFT study of glucose transformation in supercritical water.[83] The simulations were carried out using Gaussian 09 program with B3LYP/aug-cc-pVDZ basis set at 400 °C and under 25 MPa. The influence of supercritical water was investigated through calculations with and without water molecules included. An acyclic mechanism without the isomerisation of glucose was proposed (Scheme 2-22). The addition of supercritical water effectively decreased the activation barrier for the ring opening of glucose through the interaction between the water molecule and glucose (**2.89**, Scheme 2-22, highlighted in red). The activation barriers for the removal of the first two water molecules were also decreased, but no interaction with the solvent was detected during the third dehydration, which was the rate-limiting step (260 kJ/mol). Therefore, the

dehydration of glucose to 5-HMF was extremely challenging with a high energy demand in supercritical water.

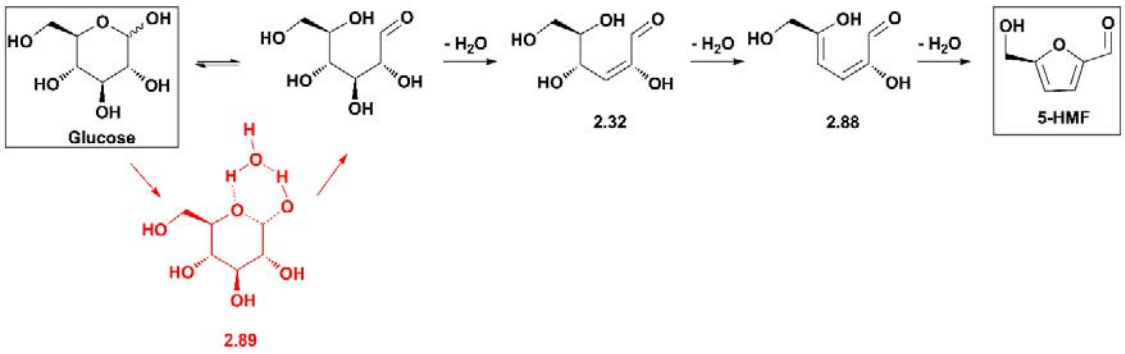

Scheme 2-22. The acyclic mechanism of glucose dehydration to 5-HMF in supercritical water proposed by Zhang et al.[83]

2.3.3 Other Methods

2.3.3.1 Ultraviolet (UV) Spectroscopy

In 1948, Wolfrom et al. applied UV-Vis spectroscopy to analyze the dehydration of glucose to 5-HMF in water catalyzed by HCl.[84] Initially the reaction was performed without HCl addition (pH = 6.5), and at t = 3.5 h a band at 228 nm (I) was observed in the UV region of the spectrum. With the reaction proceeding the optical density of band I increased, and at t = 8 h another band at 285 nm (II) appeared, which was assigned to the maximum absorption of 5-HMF. By t = 17 h, band I reached its maximum optical density value and band II kept increasing. At the end of the reaction (t = 23 h), a standard spectrum of 5-HMF was obtained. When HCl was added as the catalyst, the reactions were performed at pH = 4.3 and pH = 2.0 respectively. Similar trends in the spectra were observed, but band II

increased in intensity more rapidly with higher acidity, indicating the faster conversion of glucose to 5-HMF in a more acidic environment. Combined with the results from previous studies[85], band I was assigned to **2.32**. Two possible acyclic mechanisms were proposed for the transformation of glucose to 5-HMF, based on the previous studies by Hurd et al.[86] and Wolfrom et al.[87] (Scheme 2-23). One of them involved the generation of 3-DG from **2.32**, similar to the mechanism proposed by Bols group (Scheme 2-9, route A), but the subsequent steps are different. This study is an early one and its result is quite brief because of the limitations of lab conditions and the existing achievements in this field. However, it indeed shows that UV-vis spectroscopy can be used to observe the intermediates generated during the transformation process. In the study of glucose dehydration by the Rorrer group in 1993, a UV detector was used to monitor the column effluents after HPLC separation of the reaction mixture.[88]

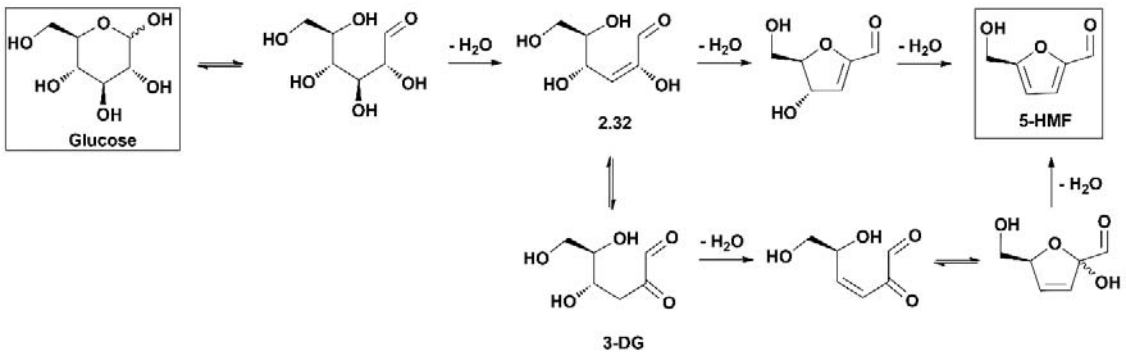

Scheme 2-23. The acyclic mechanisms proposed by Wolfrom et al.[84]

2.3.3.2 Radiochemical Studies

Scheme 2-24. The interconversion between fructose and glucose proposed by Harris and Feather.[89, 90]

In 1974 and 1975, Harris and Feather worked as pioneers to study the mechanism of the interconversion of glucose and fructose in aqueous H_2SO_4 solutions.[89, 90] Since the Lobry de Bruyn–van Ekenstein transformation can happen between ketoses and aldoses,[91] tritium labelled glucose (glucose-T) can be obtained from fructose with tritium at C-1 (fructose-T1) via acid treatment. The resulting glucose-T was allowed to react to release the tritium or hydrogen atoms at C-1 and C-2. The tritium content was determined via the measurement of the radiochemical activity of the water. The results indicated that 79% of the tritium was located on the C-2 of the glucose product. Upon isomerization, the tritium from glucose-T2 was found distributed almost evenly at the C-1 of (1*R*) and (1*S*)-fructose products. A 1,2-hydride shift was believed to have happened as a result of protonation of the carbonyl oxygen atom by the acid catalyst (Scheme 2-24). This study is a milestone since for the first time the 1,2-hydride shift was claimed to be an important step in the isomerisation between aldoses and ketoses.

2.3.3.3 Speciation Modeling

In the study of $CrCl_3$-catalyzed glucose dehydration in water by Vlachos and co-workers in 2013, it was found that the pH of the solution decreased from 2.9 to 1.6 during the process.[92] Therefore, it was assumed that the Lewis acid catalyst produced an intrinsic Brønsted acidity during its dissolution, solvation and further hydrolysis (Scheme 2-25) in the aqueous media, and the whole reaction was catalyzed by the combination of Lewis and Brønsted acidity.

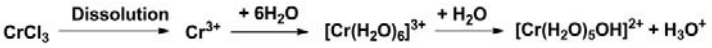

Scheme 2-25. Dissolution of $CrCl_3$ in water and the resulting generation of hydronium ions.

The speciation modeling of $CrCl_3$ aqueous solutions with various concentrations was carried out using OLI Systems' Stream Analyzer software. The pH values at 22 °C and 140 °C were calculated and were in good agreement with the data measured experimentally, both of which showed that the intrinsic Brønsted acidity increased with an increase in $CrCl_3$ concentration. The speciation analysis implied that the main species in the $CrCl_3$ aqueous solution were $[Cr(H_2O)_6]^{3+}$, $[Cr(H_2O)_5Cl]^{2+}$ and $[Cr(H_2O)_5OH]^{2+}$. Therefore, the process outlined in Scheme 2-25 was verified. When HCl was added into the speciation model, $[Cr(H_2O)_5OH]^{2+}$ was the only species whose concentration kept decreasing with the increase in HCl concentration. The kinetic experiments revealed that the rate of glucose consumption also decreased with HCl addition. In addition, the initial rate of glucose consumption had a linear relationship with the concentration of $[Cr(H_2O)_5OH]^{2+}$. All these

results indicated that $[Cr(H_2O)_5OH]^{2+}$ was the species which had a great influence on the isomerisation of glucose in aqueous $CrCl_3$. Afterwards, a 1,2-hydride shift mechanism was proposed and the coordination of glucose to the Cr complex was verified through EXAFS spectra analysis and CPMD simulations. When $CrCl_3$ was dissolved in water, the EXAFS spectra showed that the Cr centre was coordinated to six water molecules. As the EXAFS analysis could not determine the source of the O atoms (from glucose or water), the average Cr-O distance change was used to judge the coordination of glucose to the Cr centre. It was found that the Cr-O distance increased with the addition of glucose, suggesting the replacement of water ligands by glucose. In the CPMD simulations, initially two unhydrolyzed Cr^{3+} cations were created coordinated to a glucose molecule in water. After the calculation was started at 77 °C, only one Cr^{3+} kept the coordination with glucose at O1 and O2. Therefore, the subsequent simulations were performed with only one $[Cr(H_2O)_5OH]^{2+}$ group, which contrasts with the binuclear Cr complex mechanism proposed by Hensen's group[80] (see **2.3.2**). The coordination number of Cr was obtained from the number integral of RDF values. The Cr centre was coordinated with six O atoms in an octahedral structure, including one from OH^-, two from glucose and three from water (Figure 2-7). It was claimed that the coordination of glucose to the Cr complex promoted the ring opening of glucose for the Lewis acid-catalyzed isomerisation; while the intrinsic Brønsted acidity facilitated the subsequent dehydration of fructose to 5-HMF.

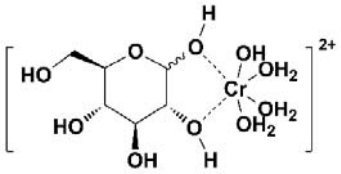

Figure 2-7. Complex formed upon coordination of glucose to $[Cr(H_2O)_5OH]^{2+}$ proposed by Vlachos and co-workers.[92]

2.3.3.4 Kinetic Studies

In 2015, Shanks and co-workers performed a kinetic study of glucose dehydration in water catalyzed by a series of Lewis acid catalysts.[93] When $AlCl_3$ was used, there was no significant difference in the rates of glucose conversion at pH = 2.5 and 3.5, but a much lower value was obtained at pH = 5.5. They proposed that in the lower pH environment, the main Al species in the aqueous media were hydrated forms of Al^{3+}, $AlCl^{2+}$ and $Al(OH)^{2+}$, which catalyzed the isomerisation of glucose. When the pH increased, they were converted to more complicated polycation species, which are less active in the catalysis. They proposed that $AlCl_3$ hydrolysis occurred in a similar fashion to $CrCl_3$ hydrolysis described by Vlachos and co-workers[92] (see section **2.3.3.3**). However, the trend of glucose conversion rate with pH increase was opposite to this previous work. The pH ranges of these two studies may be significant for the results, and the tendency of Al species to undergo polymerization at higher pH also has an influence. The small change of glucose conversion rates from pH = 2.5 to 3.5 and the significantly different results from different Lewis acid catalysts indicated that the dehydration rate of glucose was influenced by the Brønsted acidity but more significantly by the Lewis acidity. In addition, glucose-D2 was

used as the reactant, and a significant KIE was observed with k_H/k_D = 1.34 in glucose conversion, indicating once again that the 1,2-hydride shift was the rate-limiting step in such processes.

In 2015, Carraher et al. performed the Brønsted base-catalyzed isomerisation of glucose using aqueous triethylamine (TEA).[94] When both normal and labelled glucose (glucose-D2) were reacted at 100 °C in aqueous media at pH = 10.9, an obvious KIE was observed with k_H/k_D = 3.8, indicating that the deprotonation at C2 was the rate-limiting step. A mechanism involving proton transfer was proposed similar to the one given by Daorattanachai et al.[77] (Scheme 2-17) and are in agreement with the NMR observation of NaOH-catalyzed glucose-D2 reaction by the Davis group[52] (see **2.3.1**).

Significantly, a portion of the studies about Lewis acid-catalyzed glucose dehydration/isomerisation have been focused on the coordination of glucose to the metal complexes without details about the subsequent mechanism. Nevertheless, the results of several studies using glucose-D2 revealed that a 1,2-hydride shift is favored when metal Lewis acids are used as catalysts; while enolization is more dominant for $B(OH)_3$ and boronic acid catalysis. The Brønsted acid-catalyzed dehydration of glucose has been studied more computationally than experimentally, and a variety of mechanisms have been proposed including both cyclic and acyclic ones.

2.4 Sucrose and Cellulose

Sucrose is a disaccharide composed of fructose and glucose. Since both components can be converted to 5-HMF, the dehydration of sucrose has also been studied, and the

mechanism has been investigated. In 2008, Yaylayan and co-workers performed the transformation of labelled sucrose (^{13}C-1 labelled at the fructose moiety) through pyrolysis GC-MS.[95] If [^{13}C-1] 5-HMF is obtained from the [^{13}C-1] fructose portion, the mass spectrum should contain a parent ion at *m/z* 127 (M^+) and a fragment at *m/z* 126 ($(M-1)^+$) should also be observed. If 5-HMF is obtained from the glucose portion, the parent ion should be at *m/z* 126 and the fragment of $(M-1)^+$ should be at *m/z* 125. The percentages of ^{13}C-labelled and unlabelled 5-HMF can be used to calculate the contribution of fructose and glucose moieties to the production of 5-HMF. The pyrolysis reaction was performed at 250 °C and 90% of the generated 5-HMF was detected with a signal at *m/z* 127, indicating that 90% of the 5-HMF was produced from the ^{13}C labelled fructose portion and 10% was from the unlabelled glucose portion. The transformations of other oligosaccharides including raffinose, stachyose and lactose into 5-HMF were also studied. Raffinose and stachyose more readily produced 5-HMF than lactose indicating the importance of the glycosidically linked terminal fructose moieties in the production of 5-HMF. The pyrolysis reactions of sucrose, fructose, glucose and 3-DG were performed at 300 °C. The 5-HMF yield decreased in the order sucrose > fructose > 3-DG > glucose. The result that 3-DG was more efficient than glucose but less efficient than sucrose and fructose in 5-HMF formation implied that 3-DG was a main intermediate for the conversion of glucose but not for sucrose and fructose. The transformations of sucrose and fructose to 5-HMF were proposed to proceed through a fructofuranosyl cation (**2.4'**) as an important intermediate. In order to verify that sucrose was hydrolyzed to **2.4'** instead of fructose, the dehydration of [^{13}C-1] sucrose was performed catalyzed by *p*-toluenesulfonic acid in methanol. The yield of 5-

HMF was significantly decreased, because the **2.4'** generated reacted with methanol in situ to form methyl fructofuranoside.[35] Therefore, a mechanism of sucrose conversion was proposed (Scheme 2-26), which was initialized by the hydrolysis of sucrose to **2.4'** and glucose. Afterwards, 5-HMF was produced mainly from **2.4'** and only slightly from glucose via 3-DG. This mechanism was similar to the one suggested by Antal et al.[14] as was discussed in **2.2.3.1**.

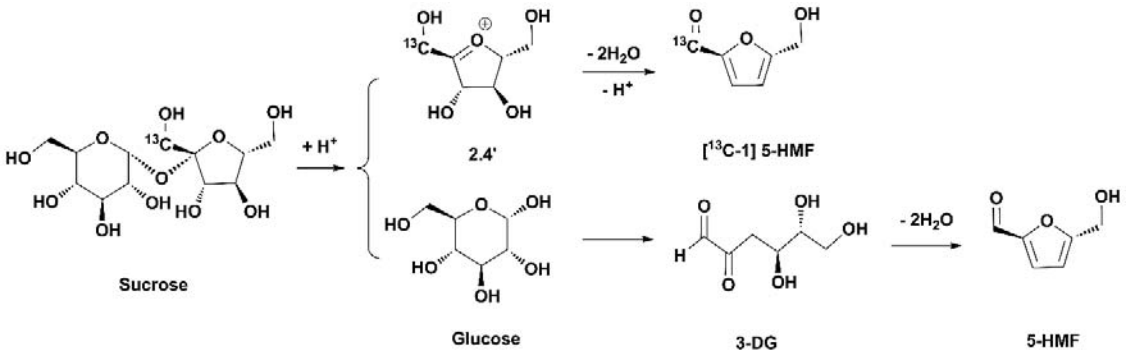

Scheme 2-26. The mechanism of sucrose (^{13}C-1 labelled at the fructose moiety) transformation to 5-HMF.[95]

Cellulose is the most abundant biopolymer on earth. It is a linear polysaccharide composed of hundreds to thousands of glucose units. The hydrolysis of cellulose to glucose and the subsequent production of 5-HMF is a hot area of research since this reactant is cheap and widely available. In 2011, the Ma group applied ^{13}C NMR spectroscopy to investigate the conversion of cellulose to glucose and 5-HMF.[96] The reaction was performed at 80 °C catalyzed by [BmimSO$_3$H]Cl in BmimCl. Samples of the reaction mixture were taken regularly during the whole process, and 10% DMSO-d$_6$ was added for

^{13}C NMR analysis. Initially only the characteristic resonance of cellulose at 101.8 ppm (C1) was observed. At t = 1 h, the characteristic signals of glucose at 96.6 ppm (C1, α-glucopyranose) and 91.9 ppm (C1, β-glucopyranose) appeared. With increasing time, the signals of cellulose decreased and the peaks of glucose increased in intensity. No other saccharides were detected indicating that glucose was the major product of cellulose hydrolysis under the applied conditions. By t = 1.5 h, a new peak at 109.3 ppm was detected and was assigned to 5-HMF. Afterwards, the signals of cellulose kept decreasing in intensity until they finally disappeared at approximately 3 h. The resonances of glucose increased up to t = 3.5 h and then started to decrease in intensity. The peaks of 5-HMF increased in intensity until the end of the reaction (t = 5 h). Based on these results, it can clearly be seen that the transformation of cellulose to 5-HMF is composed of two steps: 1) the hydrolysis of cellulose to glucose; and 2) the dehydration of glucose to 5-HMF (Scheme 2-27). It is assumed that the glucose yielded by cellulose dehydrates via similar pathways to those described above when glucose was used directly as the starting material. However, there is clearly scope to look at the mechanism of cellulose depolymerization in this field in more detail, as only ^{13}C NMR data is available at the present time to support this hypothesis.

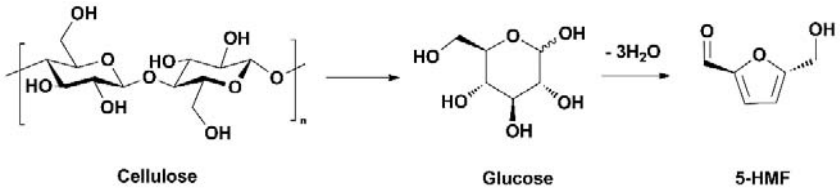

Scheme 2-27. The pathway of cellulose transformation to 5-HMF.[96]

2.5 Conclusions

The synthesis of 5-HMF from saccharides has been studied extensively in the area of biomass transformations. Fructose is used as the reactant most frequently because of the mild conditions needed for its dehydration and the high 5-HMF yield obtained. The conversion of glucose has also been adequately studied, but often limited by the harsh conditions required and the low product yields. The studies of glucose conversion are often focused on its isomerisation to fructose. A variety of achievements have been made in experiment design such as the use of ionic liquids as solvents or catalysts and the application of homogeneous and heterogeneous Lewis acid catalysts in glucose isomerisation. From the discussion above, it can be seen that the mechanisms of biomass transformations can be varied depending on the reaction conditions applied. Therefore, it is quite important for researchers to get an insight of the specific mechanisms of their own reaction processes. Most of the mechanistic studies on fructose described herein proceed via Brønsted acid-catalyzed dehydration. There have been two mechanisms proposed, and the cyclic route appears to be followed in most cases. In the transformations of glucose, most Lewis acid-catalyzed processes are proposed to go through the isomerisation to fructose, initialized by the coordination of glucose to the Lewis acid and via a 1,2-hydride shift or an enolization pathway. Fewer studies have been focused on Brønsted acid or base catalyzed transformations of glucose. 5-HMF is proposed to be produced either from glucose directly or through the isomerisation to fructose, and the mechanisms are closely related to the reaction environment, such as the solvent used.

NMR spectroscopy is a useful experimental tool to detect the intermediates formed during the transformations and analyze the fate of the protons and carbons of the reactants. In this regard, it is often important to use ^{13}C-labelled sugars. Computational studies can offer support to experimental results, especially when severe reaction conditions are required in lab work or the concentrations of the analytes are too low for convincible experimental analysis. In addition, calculations can simulate transition states during the processes while lab experiments cannot detect such species, and this helps researchers understand the mechanisms better. In such studies, although gas-phase calculations can be used as a starting point, it is important for solvents to be included in the model in some way. Besides these two main tools, other methods such as kinetic studies, IR and UV spectroscopy, and mass spectrometry can also be used to get a full picture of the reaction mechanisms. Hopefully through reading this tutorial a starter in this field can have a general idea about the transformations of these important saccharides and the mechanistic studies determining their reaction pathways for 5-HMF production. Using this review as a starting point, it might allow someone to design insightful experiments of their own in a shorter time and gain important data to understand their own transformations of such sugars.

2.6 References

1. K. Seri, Y. Inoue and H. Ishida, *Chem. Lett.*, 2000, **29**, 22-23.

2. A. Mukherjee, M.-J. Dumont and V. Raghavan, *Biomass Bioenergy*, 2015, **72**, 143-183.

3. T. Wang, M. W. Nolte and B. H. Shanks, *Green Chem.*, 2014, **16**, 548-572.

4. W. Deng, Q. Zhang and Y. Wang, *Sci. China: Chem.*, 2015, **58**, 29-46.

5. J. E. Holladay, J. J. Bozell, J. F. White and D. Johnson, *Top Value Added Chemicals from Biomass.* , U. S. DOE Report PNNL-16983, Pacific Northwest National Laboratory, the United States of America, 2007.

6. C. Moreau, M. N. Belgacem and A. Gandini, *Top. Catal.*, 2004, **27**, 11-30.

7. X. Tong, Y. Ma and Y. Li, *Appl. Catal., A*, 2010, **385**, 1-13.

8. S. Zhong, R. Daniel, H. Xu, J. Zhang, D. Turner, M. L. Wyszynski and P. Richards, *Energy Fuels*, 2010, **24**, 2891-2899.

9. R.-J. van Putten, J. C. van der Waal, E. De Jong, C. B. Rasrendra, H. J. Heeres and J. G. de Vries, *Chem. Rev.*, 2013, **113**, 1499-1597.

10. J. U. Nef, *Ann. Chem*, 1910, **376**, 1-119.

11. E. F. L. J. Anet, *J. Am. Chem. Soc.*, 1960, **82**, 1502.

12. E. F. L. J. Anet, *Aust. J. Chem.*, 1965, **18**, 240-248.

13. C. Moreau, R. Durand, S. Razigade, J. Duhamet, P. Faugeras, P. Rivalier, P. Ros and G. Avignon, *Appl. Catal., A*, 1996, **145**, 211-224.

14. M. J. Antal, W. S. Mok and G. N. Richards, *Carbohydr. Res.*, 1990, **199**, 91-109.

15. B. Cinlar, T. Wang and B. H. Shanks, *Appl. Catal., A*, 2013, **450**, 237-242.

16. A. S. Amarasekara, L. D. Williams and C. C. Ebede, *Carbohydr. Res.*, 2008, **343**, 3021-3024.

17. J. Zhang, A. Das, R. S. Assary, L. A. Curtiss and E. Weitz, *Appl. Catal., B*, 2016, **181**, 874-887.

18. G. R. Akien, L. Qi and I. T. Horváth, *Chem. Commun.*, 2012, **48**, 5850-5852.

19. J. Zhang and E. Weitz, *ACS Catal.*, 2012, **2**, 1211-1218.

20. H. Kimura, M. Nakahara and N. Matubayasi, *J. Phys. Chem. A*, 2013, **117**, 2102-2113.

21. S. H. Mushrif, S. Caratzoulas and D. G. Vlachos, *Phys. Chem. Chem. Phys.*, 2012, **14**, 2637-2644.

22. S. Caratzoulas and D. G. Vlachos, *Carbohydr. Res.*, 2011, **346**, 664-672.

23. N. Nikbin, S. Caratzoulas and D. G. Vlachos, *ChemCatChem*, 2012, **4**, 504-511.

24. R. S. Assary, P. C. Redfern, J. Greeley and L. A. Curtiss, *J. Phys. Chem. B*, 2011, **115**, 4341-4349.

25. R. S. Assary, T. Kim, J. J. Low, J. Greeley and L. A. Curtiss, *Phys. Chem. Chem. Phys.*, 2012, **14**, 16603-16611.

26. G. Yang, E. A. Pidko and E. J. M. Hensen, *J. Catal.*, 2012, **295**, 122-132.

27. F. S. Asghari and H. Yoshida, *Ind. Eng. Chem. Res.*, 2007, **46**, 7703-7710.

28. C. Moreau, A. Finiels and L. Vanoye, *J. Mol. Catal. A: Chem.*, 2006, **253**, 165-169.

29. Y. Li, X. Lu, L. Yuan and X. Liu, *Biomass Bioenergy*, 2009, **33**, 1182-1187.

30. C. Yao, Y. Shin, L.-Q. Wang, C. F. Windisch, W. D. Samuels, B. W. Arey, C. Wang, W. M. Risen and G. J. Exarhos, *J. Phys. Chem. C*, 2007, **111**, 15141-15145.

31. Arifin, M. Puripat, D. Yokogawa, V. Parasuk and S. Irle, *J. Comput. Chem.*, 2016, **37**, 327-335.

32. J. Li, J. Li, D. Zhang and C. Liu, *J. Phys. Chem. B*, 2015, **119**, 13398-13406.

33. Y.-N. Li, J.-Q. Wang, L.-N. He, Z.-Z. Yang, A.-H. Liu, B. Yu and C.-R. Luan, *Green Chem.*, 2012, **14**, 2752-2758.

34. J. Guan, Q. Cao, X. Guo and X. Mu, *Comput. Theor. Chem.*, 2011, **963**, 453-462.

35. W. Moody and G. N. Richards, *Carbohydr. Res.*, 1983, **124**, 201-213.

36. T. L. Mega and R. L. Van Etten, *J. Am. Chem. Soc.*, 1988, **110**, 6372-6376.

37. T. D. Swift, C. Bagia, V. Choudhary, G. Peklaris, V. Nikolakis and D. G. Vlachos, *ACS Catal.*, 2013, **4**, 259-267.

38. B. Siqueira, M. Silva and C. Moraes, *Brazilian Journal of Petroleum and Gas*, 2013, **7**, 71-82.

39. E. F. L. J. Anet, *Adv. Carbohydr. Chem.*, 1964, **19**, 181-218.

40. H. Jadhav, C. M. Pedersen, T. Sølling and M. Bols, *ChemSusChem*, 2011, **4**, 1049-1051.

41. H. Kimura, M. Nakahara and N. Matubayasi, *J. Phys. Chem. A*, 2011, **115**, 14013-14021.

42. A. S. Amarasekara and A. Razzaq, *Carbohydr. Res.*, 2014, **386**, 86-91.

43. R. Bermejo-Deval, R. S. Assary, E. Nikolla, M. Moliner, Y. Román-Leshkov, S.-J. Hwang, A. Palsdottir, D. Silverman, R. F. Lobo and L. A. Curtiss, *Proc. Nat. Acad. Sci. U.S.A.*, 2012, **109**, 9727-9732.

44. Z. Zhang, Q. Wang, H. Xie, W. Liu and Z. K. Zhao, *ChemSusChem*, 2011, **4**, 131-138.

45. R. Noma, K. Nakajima, K. Kamata, M. Kitano, S. Hayashi and M. Hara, *J. Phys. Chem. C*, 2015, **119**, 17117-17125.

46. S. Hu, Z. Zhang, J. Song, Y. Zhou and B. Han, *Green Chem.*, 2009, **11**, 1746-1749.

47. E. A. Khokhlova, V. V. Kachala and V. P. Ananikov, *ChemSusChem*, 2012, **5**, 783-789.

48. S. De, S. Dutta and B. Saha, *Green Chem.*, 2011, **13**, 2859-2868.

49. H. Zhao, J. E. Holladay, H. Brown and Z. C. Zhang, *Science*, 2007, **316**, 1597-1600.

50. Z. Zhang and Z. K. Zhao, *Bioresour. Technol.*, 2011, **102**, 3970-3972.

51. J. B. Binder, A. V. Cefali, J. J. Blank and R. T. Raines, *Energy Environ. Sci.*, 2010, **3**, 765-771.

52. Y. Román‐Leshkov, M. Moliner, J. A. Labinger and M. E. Davis, *Angew. Chem. Int. Ed.*, 2010, **49**, 8954-8957.

53. T. Ståhlberg, S. Rodriguez‐Rodriguez, P. Fristrup and A. Riisager, *Chem. Eur. J.*, 2011, **17**, 1456-1464.

54. B. R. Caes, M. J. Palte and R. T. Raines, *Chem. Sci.*, 2013, **4**, 196-199.

55. D. Neuhaus and M. P. Williamson, *The Nuclear Overhauser Effect in Structural and Conformational Analysis*, Wiley VCH, New York, 2nd edn., 1989.

56. V. Choudhary, A. B. Pinar, R. F. Lobo, D. G. Vlachos and S. I. Sandler, *ChemSusChem*, 2013, **6**, 2369-2376.

57. R. van den Berg, J. A. Peters and H. van Bekkum, *Carbohydr. Res.*, 1994, **253**, 1-12.

58. S. Arimori, M. D. Phillips and T. D. James, *Tetrahedron Lett.*, 2004, **45**, 1539-1542.

59. D. Stones, S. Manku, X. Lu and D. G. Hall, *Chem. Eur. J.*, 2004, **10**, 92-100.

60. M. Dowlut and D. G. Hall, *J. Am. Chem. Soc.*, 2006, **128**, 4226-4227.

61. M. Bielecki, H. Eggert and J. Norrild, *J. Chem. Soc., Perkin Trans. 2*, 1999, 449-456.

62. J. F. Mendicino, *J. Am. Chem. Soc.*, 1960, **82**, 4975-4979.

63. K. B. Hicks, E. V. Symanski and P. E. Pfeffer, *Carbohydr. Res.*, 1983, **112**, 37-50.

64. D. H. Lukamto, P. Wang and T. P. Loh, *Asian J. Org. Chem.*, 2013, **2**, 947-951.

65. D. S. Matteson and G. Y. Kim, *Org. Lett.*, 2002, **4**, 2153-2155.

66. P. R. Seidl, J. D. Yoneda and K. Z. Leal, *J. Phys. Org. Chem.*, 2005, **18**, 162-166.

67. V. P. Ananikov, *Chem. Rev.*, 2010, **111**, 418-454.

68. X. Qian, M. R. Nimlos, D. K. Johnson and M. E. Himmel, *Appl. Biochem. Biotechnol.*, 2005, 989-997.

69. X. Qian, M. R. Nimlos, M. Davis, D. K. Johnson and M. E. Himmel, *Carbohydr. Res.*, 2005, **340**, 2319-2327.

70. X. Qian, *J. Phys. Chem. A*, 2011, **115**, 11740-11748.

71. X. Qian, *Top. Catal.*, 2012, **55**, 218-226.

72. J. M. Harvey and M. C. R. Symons, *J. Solution Chem.*, 1978, **7**, 571-586.

73. J. M. Harvey, M. C. Symons and R. J. Naftalin, *Nature*, 1976, **261**, 435-436.

74. M. R. Nimlos, X. Qian, M. Davis, M. E. Himmel and D. K. Johnson, *J. Phys. Chem. A*, 2006, **110**, 11824-11838.

75. H. M. Pilath, M. R. Nimlos, A. Mittal, M. E. Himmel and D. K. Johnson, *J. Agric. Food. Chem.*, 2010, **58**, 6131-6140.

76. L. Yang, G. Tsilomelekis, S. Caratzoulas and D. G. Vlachos, *ChemSusChem*, 2015, **8**, 1334-1341.

77. P. Daorattanachai, S. Namuangruk, N. Viriya-empikul, N. Laosiripojana and K. Faungnawakij, *J. Ind. Eng. Chem.*, 2012, **18**, 1893-1901.

78. E. A. Pidko, V. Degirmenci, R. A. van Santen and E. J. Hensen, *Angew. Chem. Int. Ed.*, 2010, **49**, 2530-2534.

79. E. A. Pidko, V. Degirmenci, R. A. van Santen and E. J. Hensen, *Inorg. Chem.*, 2010, **49**, 10081-10091.

80. Y. Zhang, E. A. Pidko and E. J. Hensen, *Chem. Eur. J.*, 2011, **17**, 5281-5288.

81. Y. Yang, W. Liu, N. Wang, H. Wang, Z. Song and W. Li, *RSC Adv.*, 2015, **5**, 27805-27813.

82. X. Cao, S. P. Teong, D. Wu, G. Yi, H. Su and Y. Zhang, *Green Chem.*, 2015, **17**, 2348-2352.

83. Y. Zhang, C. Liu and X. Chen, *J. Anal. Appl. Pyrolysis*, 2016, **119**, 199-207.

84. M. Wolfrom, R. Schuetz and L. F. Cavalieri, *J. Am. Chem. Soc.*, 1948, **70**, 514-517.

85. L. Evans and A. Gillam, *J. Chem. Soc.*, 1943, 565-571.

86. C. D. Hurd and L. L. Isenhour, *J. Am. Chem. Soc.*, 1932, **54**, 317-330.

87. M. Wolfrom, E. Wallace and E. Metcalf, *J. Am. Chem. Soc.*, 1942, **64**, 265-269.

88. K. Lourvanij and G. L. Rorrer, *Ind. Eng. Chem. Res.*, 1993, **32**, 11-19.

89. D. W. Harris and M. S. Feather, *J. Org. Chem.*, 1974, **39**, 724-725.

90. D. W. Harris and M. S. Feather, *J. Am. Chem. Soc.*, 1975, **97**, 178-181.

91. S. J. Angyal, *The Lobry de Bruyn-Alberda van Ekenstein Transformation and Related Reactions* in *Glycoscience: Epimerisation, Isomerisation and Rearrangement Reactions of*

Carbohydrates, ed. A. E. Stütz, Springer Berlin Heidelberg, Berlin, Heidelberg, 2001, pp. 1-14.

92. V. Choudhary, S. H. Mushrif, C. Ho, A. Anderko, V. Nikolakis, N. S. Marinkovic, A. I. Frenkel, S. I. Sandler and D. G. Vlachos, *J. Am. Chem. Soc.*, 2013, **135**, 3997-4006.

93. T. Wang, J. A. Glasper and B. H. Shanks, *Appl. Catal., A*, 2015, **498**, 214-221.

94. J. M. Carraher, C. N. Fleitman and J.-P. Tessonnier, *ACS Catal.*, 2015, **5**, 3162-3173.

95. C. Perez Locas and V. A. Yaylayan, *J. Agric. Food. Chem.*, 2008, **56**, 6717-6723.

96. F. Jiang, Q. Zhu, D. Ma, X. Liu and X. Han, *J. Mol. Catal. A: Chem.*, 2011, **334**, 8-12.

Chapter 3

Synthesis of 3-Acetamido-5-acetylfuran from *N*-Acetyl-D-glucosamine in Ionic Liquids and Mechanistic Studies in a Range of Solvents

A part of this chapter (~15-20%) has been incorporated from the following published paper.

Xi Chen, Yi Liu, Francesca M. Kerton* and Ning Yan*

Conversion of Chitin and *N*-Acetyl-D-glucosamine into a *N*-Containing Furan Derivative in Ionic Liquids, *RSC Adv.*, 2015, **5**, 20073-20080.

Some modifications were made to the original part in the paper for inclusion as a chapter in this thesis (e.g. the supporting information was incorporated in this chapter). Also significant quantities of unpublished data are reported including: ILs from different sources, kinetic studies, mechanistic studies, IL reuse and use of seawater as reaction medium.

3.1 Introduction

The transformation of biomass into chemicals and fuels has been developed extensively during recent years.[1-3] This may be one way to relieve the current serious situation of high levels of CO_2 emission around the world, since the CO_2 produced during the conversion of biomass to new chemicals or materials can be balanced by the CO_2 consumed by the organisms during their lifetime.[4] Furthermore, the demand for products and energy derived from petroleum continues to grow because of an increased human population. As a replacement or in addition to petroleum, conversion of corn or sugarcane to bioethanol has been pursued extensively but this use of bio-feedstocks alone is far from enough in biomass utilization. Therefore, new processes using various lignocellulosic feeds are needed, such as the dehydration and/or hydrolysis of fructose, glucose and cellulose to 5-hydroxymethylfurfural (5-HMF, Figure 3-1).[5-7] 5-HMF is considered a platform chemical and can be used to produce a variety of chemicals and bio-fuels, such as levulinic acid, 2,5-diformylfuran and 2,5-dimethylfuran.

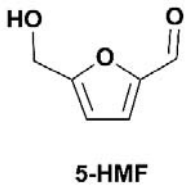

5-HMF

Figure 3-1. Structure of 5-hydroxymethylfurfural (5-HMF).

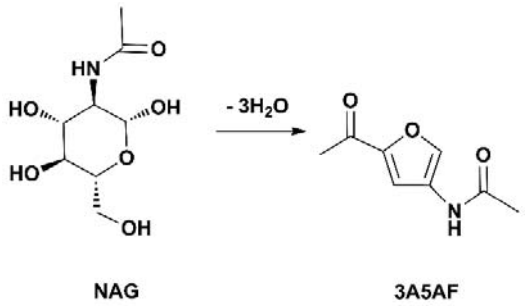

Scheme 3-1. Conversion of NAG to 3A5AF.

Similar to the synthesis of 5-HMF, the conversion of *N*-acetyl-D-glucosamine (NAG) to 3-acetamido-5-acetylfuran (3A5AF) is also an example of the synthesis of a platform chemical from a sugar (Scheme 3-1). NAG is an amino sugar and can be obtained from chitin, which is one of the components in the shells of crustaceans. Therefore, NAG could be obtained as a by-product from shellfish processing. 3A5AF is the first nitrogen-containing product obtained from the dehydration of a hexose in solution,[8] and it has the potential to be used to synthesize a further series of compounds. In 1984, the dehydration of NAG was performed via pyrolysis with a very low 3A5AF yield of around 2%.[9] In recent studies, the yield has been increased up to 60% by using dimethylacetamide (DMA) as the solvent and boric acid ($B(OH)_3$) and sodium chloride (NaCl) as additives under microwave irradiation.[10] Ionic liquids (ILs) were also used as solvents, and the yield of 3A5AF reached 60% by conventionally heating NAG in 1-butyl-3-methylimidazolium chloride ([Bmim]Cl) in the presence of $B(OH)_3$. By using other additives, the yields were also significantly improved.[8] The direct conversion of chitin to 3A5AF has also been studied. The best yield achieved was 7.5% in *N*-methyl-2-pyrrolidone as the solvent.[11] When [Bmim]Cl was used

together with $B(OH)_3$ and hydrochloric acid (HCl), a maximum 3A5AF yield of 6.2% was obtained.[12]

In the present research the synthesis of 3A5AF from NAG in ILs was optimized through the investigation of solvents, additives, in situ extraction and repeated heating of a single reaction mixture to maximize NAG conversion. Kinetic and mechanistic studies were performed to gain insight into the reaction mechanism. Finally, the reusability of [Bmim]Cl was investigated, as well as the use of seawater as the solvent.

3.2 Results and Discussion

3.2.1 Solvent Sreening

The dehydration of NAG was performed in different solvents including neutral ILs ([Bmim]Cl, [Emim]Cl, [Emim][OAc], PS[hmim]Cl), Brønsted acidic ILs ([Bmim][HSO_4], [Bmim-SO_3H][HSO_4], [Emim][HSO_4]), organic solvents (EG, PEG) and water (Figure 3-2). 100 mg (0.452 mmol) NAG was added to the desired amount of solvent, and 3 mL EtOAc was added as the extraction layer during the reaction. The starting materials were vortex-mixed for 2 min before heating by microwave irradiation. The use of EG, PEG or water did not lead to the generation of 3A5AF under these conditions. However, a previous research student in the Kerton group has developed a method for the synthesis of 3A5AF in water under hydrothermal conditions.[13]

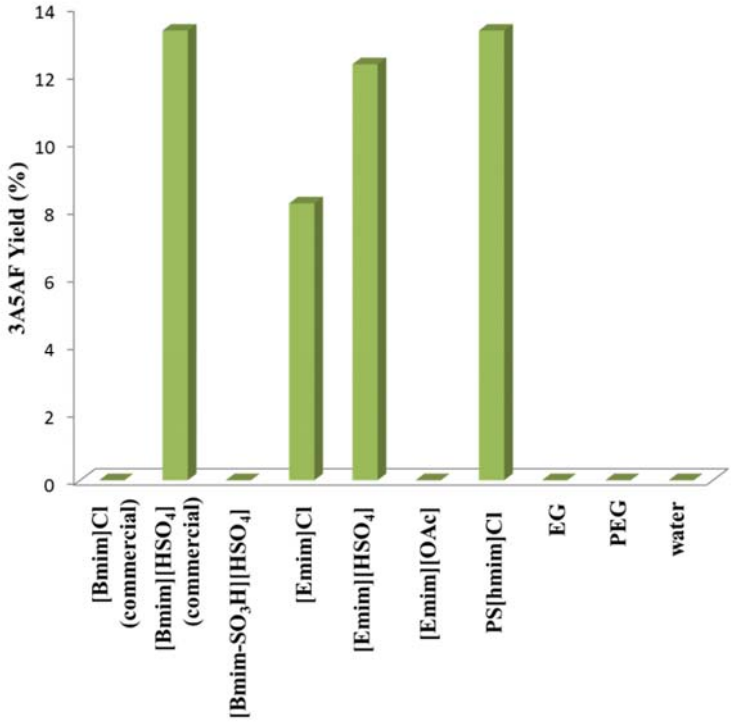

Figure 3-2. Production of 3A5AF in a range of solvents {1-butyl-3-methylimidazolium chloride ([Bmim]Cl), 1-butyl-3-methylimidazolium hydrogen sulfate ([Bmim][HSO_4]), 1-butyl sulfonic acid-3-methylimidazolium hydrogen sulfate ([Bmim-SO_3H][HSO_4]), 1-ethyl-3-methylimidazolium chloride ([Emim]Cl), 1-ethyl-3-methylimidazolium hydrogen sulfate ([Emim][HSO_4]), 1-ethyl-3-methylimidazolium acetate ([Emim][OAc]), polystyrene-supported 1-hexyl-3-methylimidazolium chloride (PS[hmim]Cl), ethylene glycol (EG), polyethylene glycol (PEG, Mn 600), and water}. Reaction conditions: 100 mg (0.452 mmol) NAG, 750 mg IL (or 2 mL other solvent applied), 3 mL ethyl acetate (EtOAc), MW, 180 °C, 3 min. 3A5AF yields were determined by GC-MS. Note: 55.87 mg $B(OH)_3$ was added in the reactions using PS[hmim]Cl.

When ILs were used, yields of 3A5AF were 13.3% from [Bmim][HSO_4], 12.3% from [Emim][HSO_4], 8.2% from [Emim]Cl and 0% from [Bmim-SO_3H][HSO_4], [Bmim]Cl and [Emim][OAc]. In the previous study by Drover et al., a 3A5AF yield of 20% was achieved in [Bmim]Cl.[8] This was attributed to the boron-containing impurity in the NAG used in their study, which acted as the catalyst for the reaction.[10] When the amount of [Bmim][HSO_4] was increased from 750 mg to 1.015 g, the 3A5AF yield decreased from 13.3% to 10.7%. For the reactions in acidic ILs ([Bmim][HSO_4] and [Bmim-SO_3H][HSO_4]), it was postulated that the acidic media might retain the product in the IL phase. Therefore, neutralization using bases (sodium bicarbonate or sodium carbonate) during the work-up was attempted, but no significant improvement in 3A5AF yield was observed.

In addition, a poly(ionic liquid), PS[hmim]Cl, was also tested, as it was thought that this would lead to an easily recyclable catalyst system. In the absence of an added solvent (i.e. an intimate mixture of the solid polymeric material and NAG) and with the presence of 2 molar equivalents of $B(OH)_3$, a 3A5AF yield of 13.3% was obtained via microwave irradiation for 3 min at 180 °C. In a larger scale reaction, the effect of an added solvent was assessed. 0.50 g (2.26 mmol) NAG, 1 molar equivalent of $B(OH)_3$ and NaCl were mixed with 0.2 molar equivalent of PS[hmim]Cl and 10 mL DMA (the solvent). The reaction was performed in an oil bath at 180 °C for 2 h, resulting in a 3A5AF yield of 16.0%. Finally, a control reaction in DMA/$B(OH)_3$/NaCl was performed where no PS[hmim]Cl was added to the reaction mixture and it gave a yield of 13.6%.

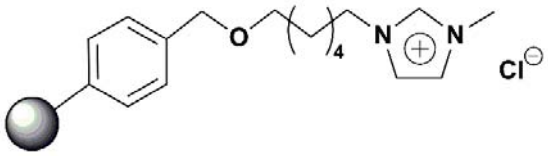

Figure 3-3. Structure of the poly(ionic liquid) (PS[hmim]Cl) used in the conversion of NAG to 3A5AF.

Table 3-1. Conversion of NAG to 3A5AF in the poly(ionic liquid) PS[hmim]Cl.

Entry	Additives and solvents	3A5AF yield (%)[a]
1	2 equiv. $B(OH)_3$	13.3[b]
2	1 equiv. $B(OH)_3$ + 1 equiv. NaCl, 10	16.0[c]
3	mL DMA	13.6[c, d]

a. Determined by GC-MS. b. 100 mg (0.452 mmol) NAG, 750 mg IL, 3 mL EtOAc, MW, 180 °C, 3 min. c. 0.50 g (2.26 mmol) NAG, 0.45 g (0.2 equiv.) IL, oil bath, 180 °C, 2 h. d. No PS[hmim]Cl added (control reaction).

In order to investigate the factors that influence the formation of 3A5AF in ILs, a simple NAG solubility test was performed. It was assumed that the best 3A5AF yields occurred in the reaction mixtures which were the most homogeneous (i.e. those in which NAG was completely dissolved). At 70 °C, the amount of NAG dissolved in 750 mg IL decreased in the order [Emim][OAc] (52.6 mg) > [Emim]Cl (51.2 mg) > [Bmim]Cl (46.4 mg) > [Emim][HSO_4] (20.1 mg) > [Bmim][HSO_4] (19.8 mg) > [Bmim-SO_3H][HSO_4] (9.8 mg). As reported in previous studies, the solubility of carbohydrates in an IL is related to

the intermolecular forces formed between the solute and the solvent.[14-21] Since the acetate and chloride anions can form strong hydrogen bonding interactions with NAG molecules, the solubility of NAG is higher in these ILs. For [Emim]Cl and [Bmim]Cl, since $[Emim]^+$ has a shorter alkyl chain than $[Bmim]^+$, the concentration of Cl^- is higher in the former. Therefore, the influence of hydrogen bonding is more significant in [Emim]Cl, resulting in the higher solubility of NAG. The low 3A5AF yield in $[Bmim\text{-}SO_3H][HSO_4]$ can be partially attributed to the low solubility of NAG in this IL. However, the extraordinary solubility of NAG in [Emim][OAc], [Emim]Cl and [Bmim]Cl did not lead to better 3A5AF yields than in $[Emim][HSO_4]$ and $[Bmim][HSO_4]$, implying that there should be some other factors affecting the dehydration of NAG.

The reaction using [Bmim]Cl alone gave a 3A5AF yield of 0% after the reaction mixture was heated at 180 °C for 3 min under microwave irradiation (Figure 3-2). Given the high solubility of NAG in [Bmim]Cl, it was thought that a mixture of the catalytically active (but more expensive) Brønsted acidic IL (i.e. $[Bmim][HSO_4]$ or $[Emim][HSO_4]$) with [Bmim]Cl might lead to a good conversion of NAG. Therefore, 100 mg $[Bmim][HSO_4]$ was added together with 750 mg [Bmim]Cl in the reaction, and a 3A5AF yield of 11.2% was obtained (the 3A5AF yield was 13.3% when $[Bmim][HSO_4]$ was used alone, Figure 3-2). This indicates that the acidity of the reaction system might have a significant influence on 3A5AF yield. Therefore, the relationship between the acidity of the ILs and 3A5AF yield was investigated (Figure 3-4). 0.1 mol/L aqueous solutions of ILs were prepared, and their pH values were measured. It was found that the maximum 3A5AF yield of 13.3%

corresponded to the use of [Bmim][HSO_4] with a pH of 1.4. [Emim][HSO_4] has a similar pH (1.4) to [Bmim][HSO_4], and its use gave a similar 3A5AF yield (12.3%). The most acidic IL studied, [Bmim-SO_3H][HSO_4] (pH = 1.0), did not afford any 3A5AF. In ILs with higher pH (less acidic), the 3A5AF yield decreased. Therefore, it is believed that the acidity of the IL impacts the production of 3A5AF from NAG and that there is a pH range in which 3A5AF generation is favored, whereas more or less acidic environments than this ideal range will lead to a decrease in yield. This is reasonable since in many studies concerned with the dehydration of saccharides the reactions can be promoted through appropriate acidic catalysis.[22-25] It needs to be noted that the [Emim]Cl used is quite acidic while a similar IL, [Bmim]Cl, is neutral. The strong acidity of [Emim]Cl is attributed to the acidic impurities it contains.

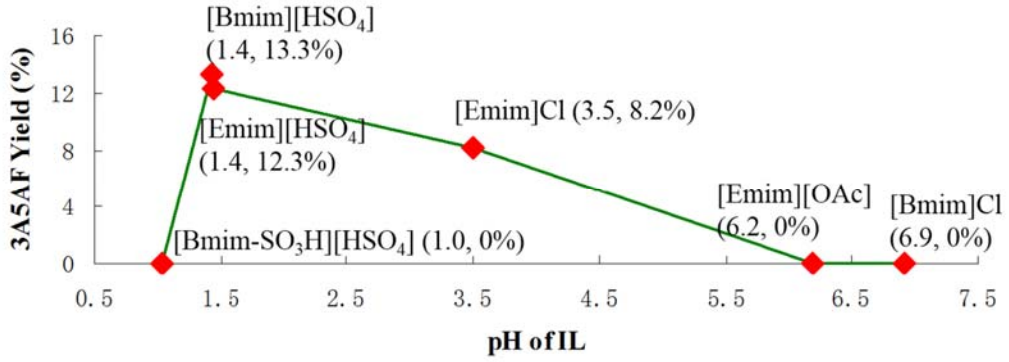

Figure 3-4. Effect of IL pH on 3A5AF production from 100 mg NAG in 750 mg IL and 3 mL EtOAc, heated by microwave irradiation at 180 °C for 3 min.

3.2.2 Additive Investigation

In previous studies it was found that the boron and chloride content of the reaction mixture had an important influence on 3A5AF production,[8, 10] hence experiments were designed to study the effect of $B(OH)_3$ and NaCl as well as some other additives in more detail (Table 3-2). The investigation was mainly focused on the reactions in [Bmim]Cl and [Bmim][HSO_4]. Since [Bmim-SO_3H][HSO_4] did not produce any 3A5AF in previous work (see **3.2.1**) and is expensive, it was not studied further.

Table 3-2. Effect of additives on 3A5AF production from NAG.[a]

Entry	IL	Additives	3A5AF yield (%)[b]
1	[Bmim]Cl (commercial)	-	0
2		1 equiv. $B(OH)_3$	19.1
3		2 equiv. $B(OH)_3$	32.9
4			40.4[d]
5			53.5[e]
6		4 equiv. $B(OH)_3$	48.0[e]
7		2 equiv. $B(OH)_3$ + 2 equiv. NaCl	62.3[f]
8		1 equiv. $B(OH)_3$ + 4 equiv. NaCl	61.8[f]
9		2 equiv. metaboric acid + 2 equiv. NaCl	56.5[f]
11		2 equiv. $B(OH)_3$ + molecular sieves (4 Å)	36.6
12		2 equiv. $FeCl_3$	10.0[g]
13		2 equiv. $CrCl_3$	25.6[g]
14	[Bmim]Cl (self-made)	2 equiv. $B(OH)_3$	50.2
15	[Emim]Cl	2 equiv. $B(OH)_3$	24.8
16	$[B(OH)_2hmim]Br$ + [Hmim]Br	-	13.5
17	[Hmim]Br	2 equiv. $B(OH)_3$	15.0
18		2 equiv. $B(OH)_3$ + 2 equiv. NaCl	22.0
19	$[Emim][HSO_4]$	2 equiv. $CrCl_3$	8.4[g]
20	$[Bmim][HSO_4]$[c] (commercial)	-	10.7
21		2 equiv. $B(OH)_3$	6.3[h]
22			9.8
23		1 equiv. NaCl	15.4[g]
25		1 equiv. Na_2SO_4	14.2[g]
26		1 equiv. $NaNO_3$	5.0[g]
27	$[Bmim][HSO_4]$[c] (self-made)	-	19.8
28			17.8[i]
29		1 equiv. $B(OH)_3$	20.2
30		2 equiv. $B(OH)_3$	6.4[j]
31			19.7
32			9.2[k]
33		1 equiv. NaCl	18.3[g]
34		2 equiv. NaCl	19.8[g]
35			0.8[l]
36		100 μL water	19.7

a. Reaction conditions: 100 mg (0.452 mmol) NAG, 750 mg IL, 3 mL EtOAc, MW, 180 °C, 3 min. b. Determined by GC-MS. Reactions were performed multiple times with a standard deviation of ±0.2%.c. 1.015 g (4.294 mmol) $[Bmim][HSO_4]$. d. 3 mL EtOAc; two runs. e. 9 mL EtOAc, 9 min; two runs. f. 9 mL EtOAc, 100, 120, 140, 160, 180 °C, each for 3 min; two runs. g. 100, 120, 140, 160, 180 °C, each for 1 min. h. 170 °C, 6 min. i. 180 °C, 15 min. j. 120 °C, 3 min. k. 10 mL EtOAc, oil bath, 70 °C, 45 h. l. Oil bath, 180 °C, 1 h.

3.2.2.1 Boron-containing species

As can be seen from Table 3-2, the addition of 1 molar equivalent or 2 molar equivalents of $B(OH)_3$ gave a 3A5AF yield in [Bmim]Cl of 19.1% (entry 2) and 32.9% (entry 3) respectively (cf. 0% using [Bmim]Cl alone, Figure 3-2). Under the same reaction conditions, increasing the amount of $B(OH)_3$ to 4 molar equivalents resulted in a decrease in yield (48.0%, entry 6) compared with 53.5% (entry 5). In [Emim]Cl, the 3A5AF yield was 24.8% (entry 15) in the presence of 2 molar equivalents of $B(OH)_3$ (cf. 8.2% using [Emim]Cl alone, Figure 3-2).

When heated at 80 - 100 °C, $B(OH)_3$ can be dehydrated to metaboric acid and water (Scheme 3-2). Since the experiments in this study were all carried out above 100 °C, it was suspected that during the reaction $B(OH)_3$ dehydrated and metaboric acid was the actual effective catalytic component in the reaction. Therefore, a reaction with the addition of 2 molar equivalents of metaboric acid and NaCl was performed and the result was compared with the one using $B(OH)_3$ and NaCl. The 3A5AF yield using metaboric acid (56.5%, entry 9) was not better than the reaction using $B(OH)_3$ (62.3%, entry 7), indicating that either boron species might be present during the reaction process and promote the generation of 3A5AF. It should be noted that under the reaction conditions, the presence of other materials (e.g. IL, NAG) will affect the amount of these boron species present in the dehydration equilibrium between $B(OH)_3$ and metaboric acid.

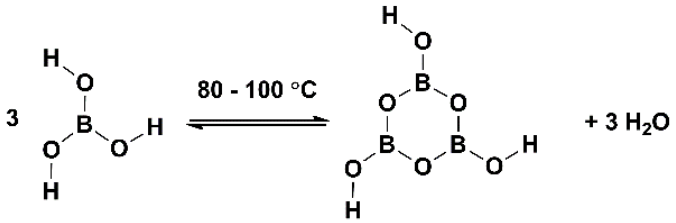

Scheme 3-2. Dehydration of $B(OH)_3$ at high temperatures (80 - 100 °C).

Also, an IL containing a boronic acid group, 3-(6-boronohexyl)-1-methylimidazolium bromide ([$B(OH)_2$hmim]Br, Figure 3-5), was prepared because it might allow easy recycling of the boron component in the reaction mixture. Two molar equivalents of this IL was used as the replacement for $B(OH)_3$, and [Hmim]Br was added as the co-solvent. The 3A5AF yield obtained was 13.5% (entry 16), which was similar to the result in [Hmim]Br with $B(OH)_3$ addition (15.0%, entry 17).

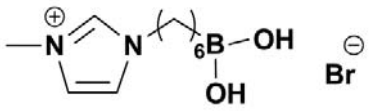

Figure 3-5. Structure of the boronic acid-containing IL used in the conversion of 100 mg NAG heated by microwave irradiation (180 °C, 3 min, 3 mL EtOAc as the in situ extraction layer).

Since pH of ILs was shown to have a significant effect on 3A5AF formation in the absence of additives (see **3.2.1** and Figure 3-4), pH studies on additive containing systems were undertaken. The pH values of 0.1 mol/L aqueous solutions of [Bmim]Cl and [Emim]Cl in the presence of $B(OH)_3$ (13.0 mg and 10.9 mg respectively) were measured. Surprisingly, these two systems have pH values of 6.3 and 3.4 respectively. These pH

values should have led to much lower yields of 3A5AF if based on the trend in Figure 3-4 (actual yields: 32.9% in [Bmim]Cl, entry 3; 24.8% in [Emim]Cl, entry 15). Therefore, it was assumed that the function of $B(OH)_3$ in the reaction was not only its Brønsted acidity. $B(OH)_3$ is also a Lewis acid and can also act as a chelating group with sugars.[26] Therefore, two other Lewis acids, iron (III) chloride ($FeCl_3$) and chromium (III) chloride ($CrCl_3$) were used as additives to the reactions in [Bmim]Cl and afforded 3A5AF yields of 10.0% (entry 12) and 25.6% (entry 13) respectively (cf. 0% using [Bmim]Cl alone, Figure 3-2). However, the use of $CrCl_3$ in the reaction in [Emim][HSO_4] did not improve the yield (8.4%, entry 19; cf. 12.3% with no additives, Figure 3-2), indicating that the influence of Lewis acidity on 3A5AF production was not positive in a strongly Brønsted acidic system. This was confirmed by the reactions using $B(OH)_3$ in [Bmim][HSO_4]. For commercial [Bmim][HSO_4], the yield of 3A5AF was 9.8% (entry 22) when 2 molar equivalents of $B(OH)_3$ was added. For self-made [Bmim][HSO_4], the use of 1 molar equivalent or 2 molar equivalents of $B(OH)_3$ led to 3A5AF yields of 20.2% (entry 29) and 19.7% (entry 31) respectively. (The differences between the commercial and self-made [Bmim][HSO_4] will be discussed in more detail in **3.2.5**). These results were all similar to those in the absence of $B(OH)_3$ (10.7%, entry 20; 19.8%, entry 27). Therefore, it appears that $B(OH)_3$ has little influence on 3A5AF yield in a strongly Brønsted acidic IL ([Bmim][HSO_4]), but it has a very significant effect on reactions in a neutral IL ([Bmim]Cl). In conclusion, it is believed that both the Brønsted and Lewis acidities of $B(OH)_3$ affect the conversion of NAG to 3A5AF, while the Brønsted acidity is a more significant factor than the Lewis acidity. It has been reported that the combination of mineral acids and $B(OH)_3$ increased the 3A5AF

yield when prepared directly from chitin,[12] but this kind of synergistic effect was not observed when NAG was the reactant in the current study.

3.2.2.2 Effect of Chloride Ions

In the previous work by the Kerton group, it was found that different 3A5AF yields were obtained when using NAG from different suppliers.[10] The study showed that the NAG containing higher Cl content had the higher yield of 3A5AF. Therefore, Cl concentration was believed to be quite important in the conversion of NAG to 3A5AF. In Table 3-2, the Br containing ILs generally gave lower 3A5AF yields than [Bmim]Cl ([Hmim]Br with $B(OH)_3$: 15.0%, entry 17; [$B(OH)_2$hmim]Br: 13.5%, entry 16; [Bmim]Cl with $B(OH)_3$: 32.9%, entry 3). Therefore, Cl ions cannot be replaced by ions of another halide species. When 2 molar equivalents of NaCl was added to the [Hmim]Br and $B(OH)_3$ system, the 3A5AF yield was increased to 22.0% (entry 18). In [Bmim]Cl, when 2 molar equivalents of NaCl was added besides 2 molar equivalents of $B(OH)_3$, the 3A5AF yield was effectively increased to 62.3% (entry 7) compared with using $B(OH)_3$ alone (53.5%, entry 5), but more NaCl (4 molar equivalents) failed to further promote 3A5AF generation (61.8%, entry 8). In [Bmim][HSO_4] (commercial), the addition of 1 molar equivalent of NaCl increased the 3A5AF yield to 15.4% (entry 23) from 10.7% (entry 20). It was thought that the chloride ions may play a role in 'salting-out' 3A5AF into the EtOAc in situ extraction phase. Therefore, the effect of non-chloride containing salts on the yield of 3A5AF was studied. The use of 1 molar equivalent of sodium sulfate (Na_2SO_4) or sodium nitrate ($NaNO_3$) gave lower yields (14.2%, entry 25; 5.0%, entry 26) compared with the reaction using NaCl

(15.4%, entry 23). The Cl content in these two salts was measured using inductively coupled plasma-mass spectrometry (ICP-MS), and was 6558 ppb and 1703 ppb respectively. These ICP-MS data correlate with the yields of 3A5AF obtained, i.e. the system containing the higher concentration of Cl had a higher 3A5AF yield. This lends further evidence about the significant role of Cl ions in the dehydration of NAG, which involves some complicated mechanism not clearly understood yet. It should be noted that for reactions with salt addition (NaCl, Na_2SO_4, $NaNO_3$), the microwave temperature had to be ramped (e.g. for NaCl reactions, 3 min at 100 °C, 3 min at 120 °C, 3 min at 140 °C, 3 min at 160 °C, 3 min at 180 °C) to prevent overheating and temperature spikes, which are caused by the increased ion concentrations and the consequent increased conduction of microwave heating. Temperature spikes could lead to rapid increases in vapor pressure within the microwave vial, thus resulting in the rupture of the vial.

In some studies on the synthesis of 5-HMF the addition of a certain amount of water has been shown to improve the product yield.[27-29] Similar experiments were performed in the conversion of NAG to 3A5AF in [Bmim]Cl (entry 10) and [Bmim][HSO_4] (entry 36), and no improvement in 3A5AF yield was observed. Considering that water is the other product in the dehydration reaction and its existence may inhibit the reaction going towards the generation of 3A5AF, molecular sieves were added in the microwave vial above the starting materials in order to absorb the water vapor generated during the reaction. The sieves were suspended above the reaction mixture (Figure 3-6) to prevent them from being crushed by the stir bar during the reaction. Furthermore, after reactions are performed,

water can be seen condensed on the top portion of the vial and therefore, this seems like a suitable place to put the sieves. The obtained 3A5AF yield of 36.6% (entry 11) was slightly higher than that without molecular sieves (32.9%, entry 3).

Figure 3-6. The set-up used to suspend molecular sieves above the reaction mixture, in order to have molecular sieves absorb the water produced during the microwave reactions of NAG conversion and not be crushed by the stir bar.

3.2.3 In situ Extraction Solvent Screening

A reaction in [Bmim][HSO_4] (self-made) was performed without the EtOAc extraction layer, and a 3A5AF yield of 7.8% was obtained (entry 1, Table 3-3), which was much lower than the one with the EtOAc extraction layer (19.8%, entry 27, Table 3-2). This indicates that the presence of EtOAc during the reaction can effectively extract the product in situ and thus leads to an increase in the 3A5AF yield by overcoming product inhibition, according to Le Chatelier's principle.

Besides EtOAc, some other organic solvents which have been useful in the extraction of 5-HMF in biorefinery-related processes[28, 30] were also employed as the extraction layer,

including 2, 5-dimethyltetrahydrofuran (2, 5-Me THF), 1-butanol, 1-hexanol and methyl isobutyl ketone (MIBK) (Table 3-3). The use of 1-hexanol and MIBK in [Bmim]Cl afforded similar 3A5AF yields to the one using EtOAc (32.9%, entry 3, Table 3-2). Considering its low boiling point, price and relatively environmentally-benign nature,[31] EtOAc was selected as the most suitable solvent.

Table 3-3. Conversion of NAG to 3A5AF using different in situ extraction solvents.[a]

Entry	IL	Extraction solvent	3A5AF yield (%)[b]
1	[Bmim][HSO_4]	-	7.8[c]
2	(self-made)	3 ml MIBK	15.7[c]
3		3 mL 2, 5-Me THF	9.9
4	[Bmim]Cl	10 mL 1-butanol	14.6[d]
5	(commercial)	10 mL 1-hexanol	34.6[e]
6		3 mL MIBK	30.2

a. Reaction conditions: 100 mg (0.452 mmol) NAG, 2 equiv. $B(OH)_3$, 4.294 mmol IL, MW, 180 °C , 3 min. b. Determined by GC-MS. c. No $B(OH)_3$ addition. d. Oil bath, 110 °C, 23 h. e. Oil bath, 160 °C, 3 h.

In the reactions described previously in this section, microwave heating was employed. A similar reaction in [Bmim][HSO_4] (self-made) without an EtOAc layer was performed using conventional heating in an oil bath at 180 °C for 1 h. This afforded a 3A5AF yield of 6.6%. Compared with the result in entry 1 (Table 3-3), the shorter reaction time with a higher product yield from the microwave-assisted reaction indicated the superiority of microwave irradiation over conventional heating in reaction efficiency.

3.2.4 Optimization of Reaction Procedure

In the current study, the dehydration of NAG was usually performed for 3 min under microwave irradiation. With the assumption that NAG might not have full conversion during the short reaction time, another 3 mL fresh EtOAc was added into the microwave vial after the completion of the original reaction and the removal of the extraction layer. The reaction was performed for the second time (the second run), and the total yield of 3A5AF was increased to 40.4% (entry 2, Table 3-4). Inspired by this improvement, the reaction procedure was optimized through the adjustment of the times the reaction was performed for a single reaction mixture (number of runs) and extractions between the runs, in order to achieve higher 3A5AF yields (Table 3-4).

Table 3-4. Influence of number of runs and extractions on 3A5AF production from a single reaction mixture.[a]

Entry	Number of runs	3A5AF yield (%)[b]
Runs with extractions between[c]		
1	1	32.9
2	2	40.4
3	3	48.8
4	5	50.0
5	7	48.0
Runs without extractions between[d]		
6	3	41.7
7	4	42.7
8	5	44.8
9	6	47.5
Runs with increased extraction volume[e]		
10	2	53.5
11	3	55.6

a. Reaction conditions: 100 mg (0.452 mmol) NAG, 2 equiv. $B(OH)_3$, 750 mg (4.29 mmol) [Bmim]Cl, 3 mL EtOAc, MW, 180 °C, 3 min. b. Determined by GC-MS. c. 3 × 5 mL EtOAc extractions of the reaction mixture between runs. d. No extractions between runs. e. 9 mL EtOAc, MW, 180 °C, 9 min.

For entries 1 - 5, 3 × 5 mL EtOAc extractions were performed on the reaction mixture between runs. For entries 6 - 9, no extractions were performed between runs. When the reaction was performed three times, the yield of 3A5AF with EtOAc extractions between runs (48.8%, entry 3) was higher than that without extractions (41.7%, entry 6), indicating that these extractions were necessary to improve the 3A5AF yield. This was further confirmed when the reaction was run five times (with extraction: 50.0%, entry 4; without extraction: 44.8%, entry 8). Increasing the number of runs from five to seven led to a decrease in 3A5AF yield from 50.0% (entry 4) to 48.0% (entry 5), probably because that NAG has been fully consumed and side reactions of 3A5AF can then dominate, such as deamination. Deamination at long reaction times and high temperatures has been observed by a previous graduate student in the Kerton group.[13] Importantly, an increase in the volume of EtOAc from 3 mL to 9 mL and the reaction time from 3 min to 9 min resulted in an increased overall yield of 55.6% within 3 runs (entry 11).

The influence of reaction temperature and time was briefly investigated for reactions in [Bmim]Cl (Table 3-5) under microwave irradiation. When the reaction temperature was decreased to 120 °C and the reaction time was correspondingly increased to 3 h 12 min based on the Arrhenius equation, a yield of 33.7% (entry 2) was obtained, which was similar to 32.9% in entry 1 (180 °C, 3 min). Decreasing the reaction time to 30 min gave a lower yield of 19.5%. Furthermore, a large-scale reaction was performed using 500 mg (2.26 mmol) NAG in 1.50 g (8.59 mmol) [Bmim]Cl and 9 mL EtOAc. When 0.8 molar equivalent of $B(OH)_3$ was added and the mixture was heated at 180 °C for 15 min, a 35.1% yield was

obtained after two runs (entry 4), compared with 53.5% (entry 10, Table 3-4) from a normal-scale reaction (100 mg NAG, 750 mg [Bmim]Cl, 2 equiv. $B(OH)_3$, 9 mL EtOAc, 180 °C, 9 min). If 0.8 molar equivalent of NaCl was also added, the yield had a further increase to 41.3% (entry 5), but it is still much lower than the normal-scale one. Therefore, no further study was undertaken for large-scale reactions.

Table 3-5. Effect of reaction temperature and time on 3A5AF production from NAG.[a]

Entry	T (°C)	t	3A5AF yield (%)[b]
1	180	3 min	32.9
2	120	3 h 12 min	33.7
3	120	30 min	19.5
4	180	15 min	35.1[c]
5	100, 120, 140, 160, 180 °C, each for 5 min		41.3[c, d]

a. Reaction conditions: 100 mg (0.452 mmol) NAG, 2 equiv. $B(OH)_3$, 750 mg (4.29 mmol) [Bmim]Cl, 3 mL EtOAc, MW. b. Determined by GC-MS. c. 500 mg (2.26 mmol) NAG, 0.8 equiv. $B(OH)_3$, 1.50 g (8.59 mmol) [Bmim]Cl, 9 mL EtOAc, MW, 2 runs. d. 0.8 equiv. NaCl.

3.2.5 ILs From Different Sources

The 3A5AF yields obtained from the use of commercial and self-made [Bmim]Cl or [Bmim][HSO_4] have non-ignorable differences under the same reaction conditions (entries 3 and 14, 20 and 27, 22 and 31, 23 and 33, Table 3-2), leading us to think about the influence of the source of the ILs. The impurity levels in [Bmim][HSO_4] were studied using ICP-MS, and it was found that the self-made [Bmim][HSO_4] had a Cl content of 4% while the commercial one only had ≤ 1% (Table 3-6). The water content determined through Karl-

Fisher titration was 0.6% for the self-made [Bmim][HSO_4] and 0.2% for the commercial one. Therefore, it is believed that the Cl impurity in the self-made IL was the main cause of higher 3A5AF yields, thus confirming the important role of Cl in the synthesis of 3A5AF from NAG.

Table 3-6. Impurities in [Bmim][HSO_4] from different sources.

Impurity	Commercial	Self-made
Cl[a]	⩽1%	4%
water[b]	0.2%	0.6%

a. Determined by ICP-MS. b. Determined by Karl-Fisher titration.

3.2.6 Kinetic Studies

Kinetic studies were performed to calculate the activation energy and pre-exponential factor associated with the dehydration of NAG in [Bmim]Cl in the presence of $B(OH)_3$ (Figure 3-8, a). In a typical experiment, 424 mg (1.92 mmol) NAG and 2 molar equivalents of $B(OH)_3$ were added into 1.000 g (5.725 mmol) [BMim]Cl. The starting materials were heated in an oil bath at a given temperature and an aliquot (20 - 60 mg) was taken at the desired time. 10 μL acetophenone was added to the sample as the internal standard. The mixture was weighed and dissolved in 600 μL dimethyl sulfoxide-d_6 (DMSO-d_6). The sample was analyzed by ^{1}H NMR spectroscopy, and the concentration of NAG was calculated through the integration ratio of acetophenone to NAG. The reactions were performed at 110, 120, 130 and 140 °C, and the data obtained were fitted to first-order rate

plots with linear correlation coefficients (R^2) close to unity. Through a plot of ln(k_{obs}) as a function of 1/T, the activation energy and pre-exponential factor were determined to be 106.7 kJ/mol and 1.31×10^{12} min^{-1} respectively. Drover et al. reported that the conversion of NAG to 3A5AF in the absence of an additive had an activation energy of 82.8 kJ/mol and a pre-exponential factor of 1.34×10^{8} min^{-1}.[8] The pre-exponential factor of the reaction using $B(OH)_3$ is four orders of magnitude higher than that of the reaction without $B(OH)_3$, indicating that the addition of $B(OH)_3$ increased the number of effective collisions among reactant molecules and hence increased the reaction rate.

N-Acetylgalactosamine (NAGal) and *N*-acetylmannosamine (NAMan) are two isomers of NAG (Figure 3-7). Kinetic studies of their dehydration with $B(OH)_3$ addition were also performed (Figure 3-8, b and c). The activation energies and pre-exponential factors were 120.6 kJ/mol and 1.05×10^{14} min^{-1} for NAGal conversion, and 106.3 kJ/mol and 1.53×10^{12} min^{-1} for NAMan. These values are close to those determined for NAG conversion.

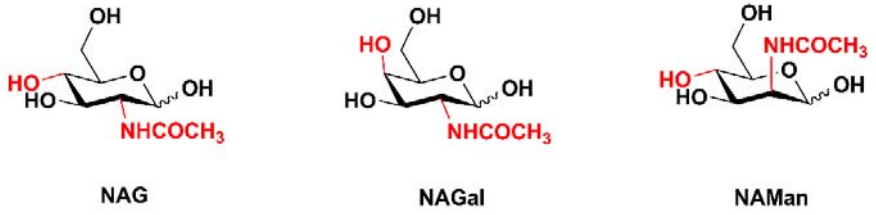

Figure 3-7. Structures of NAG and its two isomers (NAGal and NAMan).

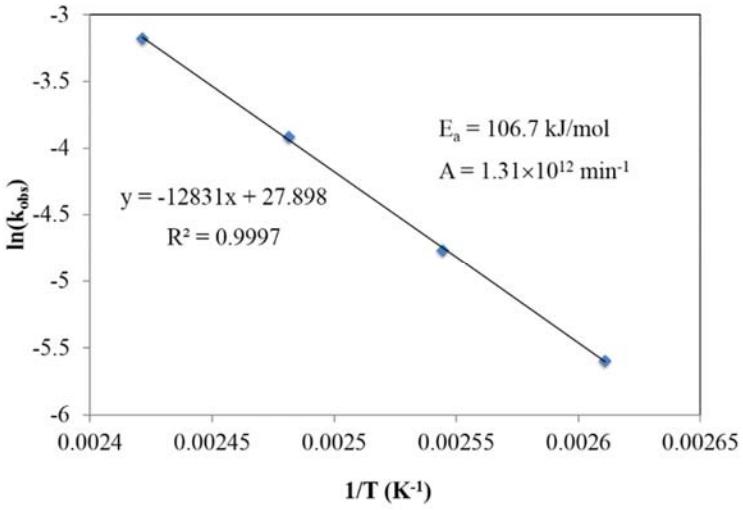
-3
-3.5
-4
-4.5
-5
-5.5
-6
0.0024
0.00245
0.0025
0.00255
0.0026
0.00265
ln(k_obs)
1/T (K-1)
Ea = 106.7 kJ/mol
A = 1.31×10^12 min-1
y = -12831x + 27.898
R² = 0.9997

(a)

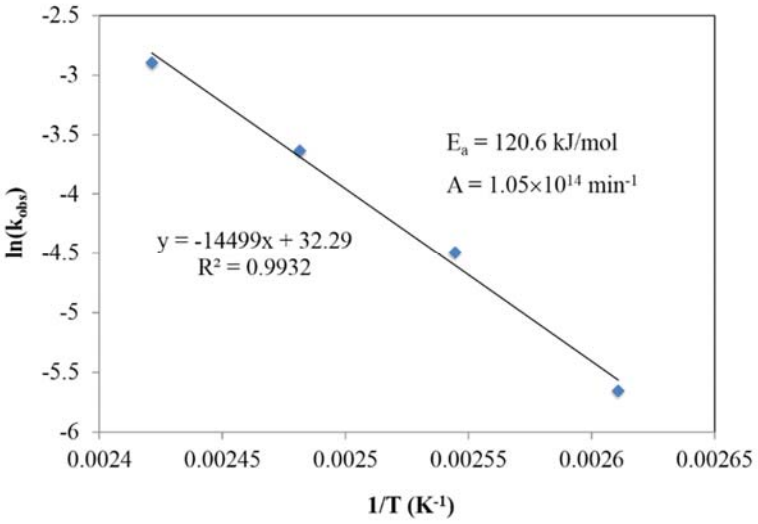
-2.5
-3
-3.5
-4
-4.5
-5
-5.5
-6
0.0024
0.00245
0.0025
0.00255
0.0026
0.00265
ln(k_obs)
1/T (K-1)
Ea = 120.6 kJ/mol
A = 1.05×10^14 min-1
y = -14499x + 32.29
R² = 0.9932

(b)

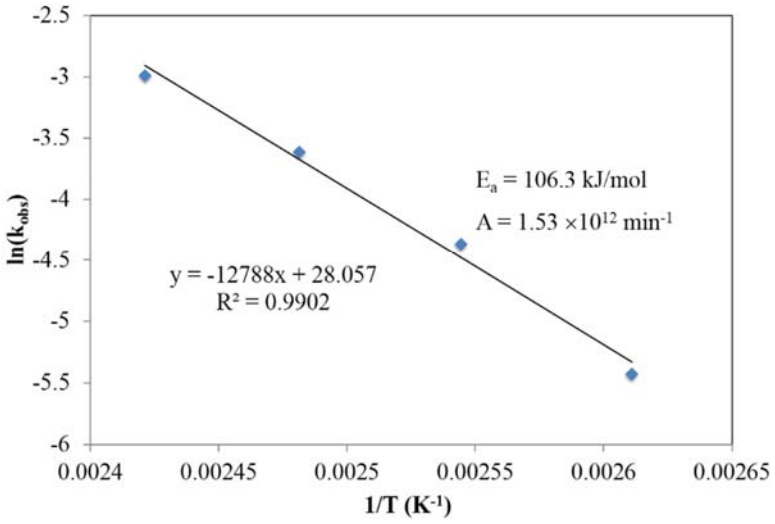

(c)

Figure 3-8. Arrhenius plots for the conversion of NAG (a), NAGal (b) and NAMan (c) to 3A5AF in [BMim]Cl with 2 equiv. $B(OH)_3$ addition.

The dehydration of 100 mg (0.452 mmol) NAG or NAGal was performed in 3 mL water with the addition of 1.5 molar equivalents of $B(OH)_3$ and NaCl. The 3A5AF yields obtained from these two reactions were similar (2.1% for NAG and 2.0% for NAGal) in addition to the similar activation energies determined above. As the product from the reactions using NAGal and NAMan are identical to the product from NAG (i.e. 3A5AF), the intermediates prior to product formation must be identical (i.e. Chromogen I and III, Scheme 3-4). A mechanism of NAG conversion to 3A5AF through ring opening of NAG was proposed (Scheme 3-4), and it is believed that the same process occurs in the conversion of NAGal and NAMan to 3A5AF. Based on literature data, the rate constants of ring opening of glucose and galactose from their pyranose to open chain forms have non-

ignorable differences (Scheme 3-3).[32, 33] Similarly, it is assumed that for NAG and NAGal, the rate constants of their ring opening (i.e. the first step in their conversions to 3A5AF in the mechanism proposed) are also different. Therefore, this ring opening step is not the rate-limiting step of their conversions to 3A5AF, since otherwise the activation energies for conversion of NAG and NAGal would be quite different. No literature data about the ring opening of NAMan or mannose was found, but it can be assumed that NAMan would also have a different rate for the initial ring opening step.

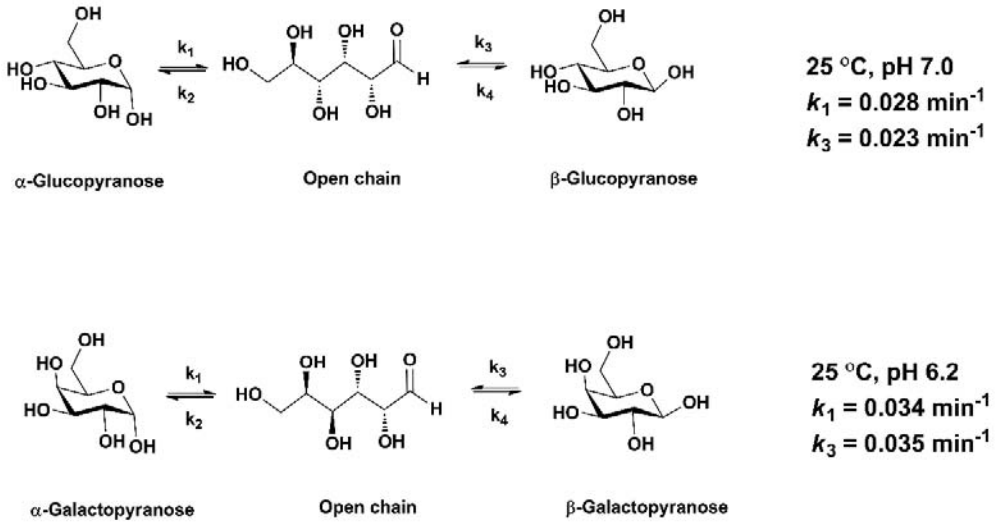

Scheme 3-3. Interconversion of glucose and galactose between pyranose and open chain forms.[32, 33]

3.2.7 Mechanistic Studies

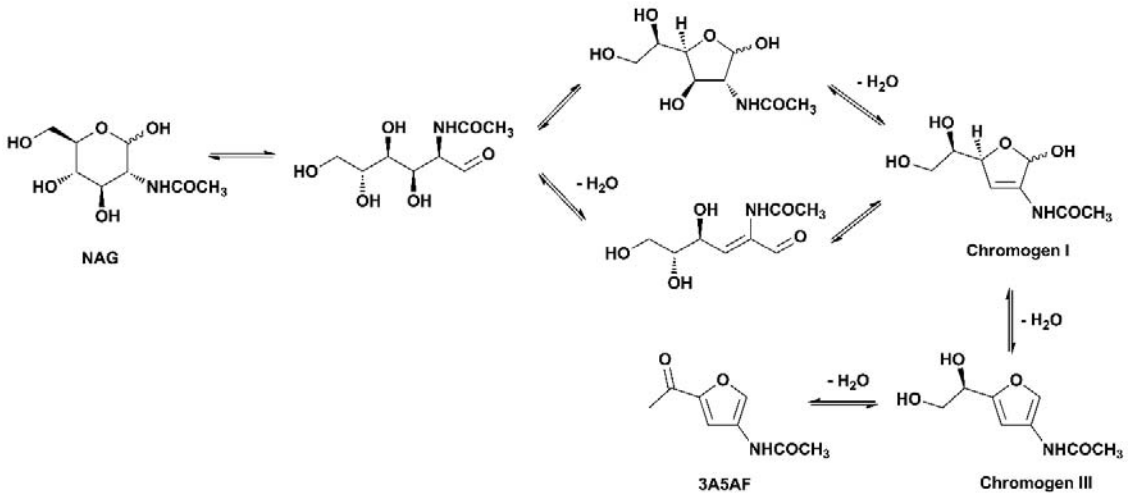

Scheme 3-4. Proposed mechanism for the conversion of NAG to 3A5AF.

Chromogen I and III have been reported as products of NAG dehydration in aqueous solutions in several studies,[34-39] one of which involved the reaction in borate solution (pH 7.0) at 100 °C.[36] The most recent study was performed in high-temperature water (120 - 220 °C) and did not require the addition of any catalyst.[37] Therefore, a mechanism of NAG conversion to 3A5AF in water in the presence of $B(OH)_3$ at high temperatures was proposed with Chromogen I and III as intermediates (Scheme 3-4). In order to observe these intermediates, reactions were performed in D_2O. 2.10 g (9.49 mmol) NAG, 2 molar equivalents of $B(OH)_3$ and 1 molar equivalent of NaCl were dissolved in 28 mL deuterium oxide (D_2O). The solution was divided into seven equal samples (4 mL each), which were heated by microwave irradiation at 180 °C for 0, 1, 2, 4, 6, 8 and 10 min respectively and analyzed by ^1H NMR spectroscopy (Figure 3-9). Compared with the reference data,[37] the

resonances at 6.04 ppm and 5.96 ppm were assigned to the characteristic peaks of α- and β-Chromogen I, which appeared at 1 min and then decreased in intensity until they disappeared by 6 min. The peak at 7.75 ppm at 2 min was assigned to Chromogen III and similarly to Chromogen I, this peak disappeared by 6 min. A similar study was performed for the reactions in [Bmim]Cl, and samples of the reaction mixture in both DMSO-d_6 and D_2O were taken for ^1H NMR analysis (Figure 3-26). For the samples of the [Bmim]Cl reaction mixture dissolved in DMSO-d_6, the signal at 6.26 ppm during 1 - 2 min was assigned to Chromogen III, according to the NMR data for Chromogen III in DMSO-d_6 reported previously.[40] For the samples of the [Bmim]Cl reaction mixture dissolved in D_2O, peaks were also assigned based on literature data.[36, 37, 41] The signal at 6.16 ppm was assigned to Chromogen I, which appeared at 1 min and disappeared by 4 min; and the resonance at 2.06 ppm at 2 min was assigned to Chromogen III. These results lend credence to the putative route in Scheme 3-4, which is different from the mechanism previously proposed in the study by Drover et al.[8] Furthermore, the peaks of Chromogen I and III appeared at an early stage during the reaction, and the signals of 3A5AF were not observed until the intermediate peaks disappeared. Therefore, it is assumed that the final step from Chromogen III to 3A5AF might be rate-limiting.

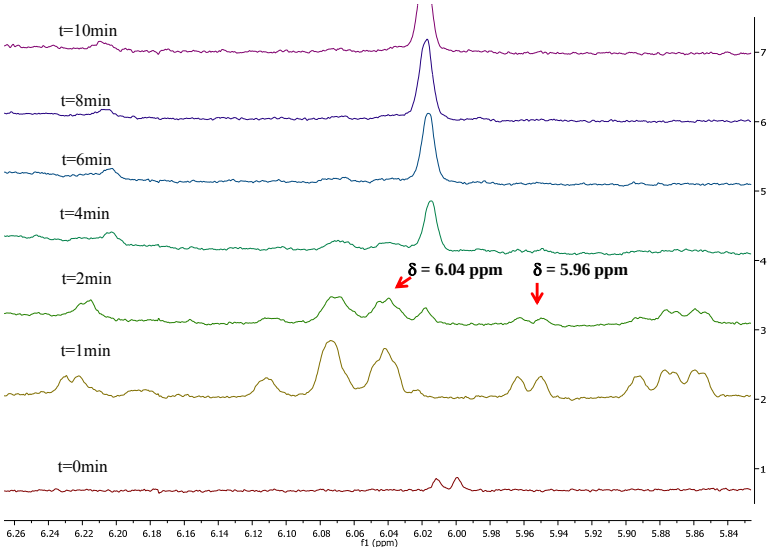

(a)

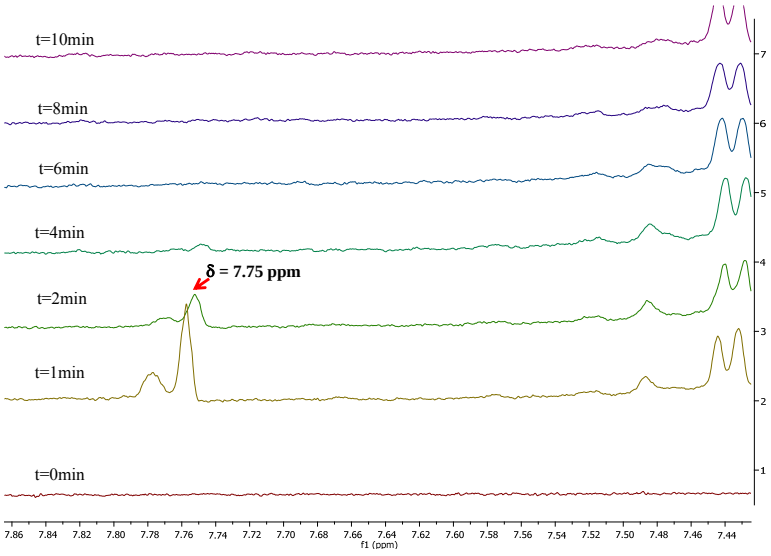

(b)

Figure 3-9. Detection of Chromogen I (a) and III (b) in ^{1}H NMR spectra of NAG conversion in D_2O with 2 equiv. $B(OH)_3$ and 1 equiv. NaCl addition, heated by microwave irradiation at 180 °C.

Since $B(OH)_3$ is important to promote the production of 3A5AF, ^{11}B NMR spectroscopy was used to analyze the boron species during the reaction process. A sample of 300 mg (1.36 mmol) NAG, 2 molar equivalents of $B(OH)_3$ and 1 molar equivalent of NaCl in 5 mL D_2O had a pH of 4.1. Another three samples were prepared in the same way, and the pH values were adjusted to be 7.8, 9.5 and 13.2 respectively by adding sodium deuteroxide (NaOD) solutions (0.036 and 0.060 mol/L). The ^{11}B NMR spectra showed that there was one significant peak in each sample whose chemical shift decreased with the increase in pH (a - d, Figure 3-10). Another sample of 0.23 mol/L NAG and 1 molar equivalent of $B(OH)_3$ with a pH of 13.0 (adjusted by a 0.060 mol/L NaOD solution) was also analyzed by ^{11}B NMR spectroscopy (e, Figure 3-10). The comparison among a, b, d and e indicated that the chemical shift of this boron peak was not determined by the concentration of NAG or $B(OH)_3$ but significantly influenced by the pH of the solution.

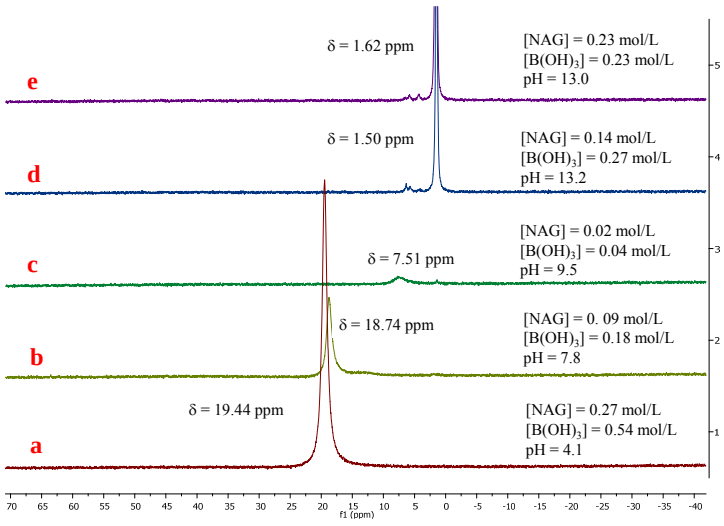

Figure 3-10. Influence of pH of D_2O solutions of NAG/$B(OH)_3$/NaCl on δ_B in ^{11}B NMR spectroscopy.

In order to investigate whether other kinds of boron species with different ^{11}B resonances were produced during the conversion of NAG, microwave heating of the acidic, neutral and basic D_2O solutions (pH = 4.1, 7.8 and 9.5) at 180 °C for 10 min were performed. After heating, reaction mixtures exhibited decreased pH values (3.7, 4.3 and 7.8) and a downfield shift of the previously detected boron peaks was observed (Table 3-7 and Figure 3-11), but no additional boron peaks were observed.

Table 3-7. Changes of pH and δ_B in ^{11}B NMR spectroscopy before and after microwave reactions in acidic (a), neutral (b) and basic (c) environment.[a]

NAG/$B(OH)_3$/NaCl solution	Acidic	Neutral	Basic
Before microwave reactions			
pH	4.1	7.8	9.5
δ_B (ppm)	19.4	18.7	7.6
After microwave reactions[b]			
pH	3.7	4.3	7.8
δ_B (ppm)	19.5	19.5	18.2

a. The neutral and basic solutions were prepared by adding NaOD solutions (0.036 and 0.060 mol/L) to the aqueous NAG/$B(OH)_3$/NaCl solutions. b. Microwave reaction conditions: 5 mL D_2O solution of NAG, 2 equiv. $B(OH)_3$ and 1 equiv. NaCl, 180 °C, 10 min.

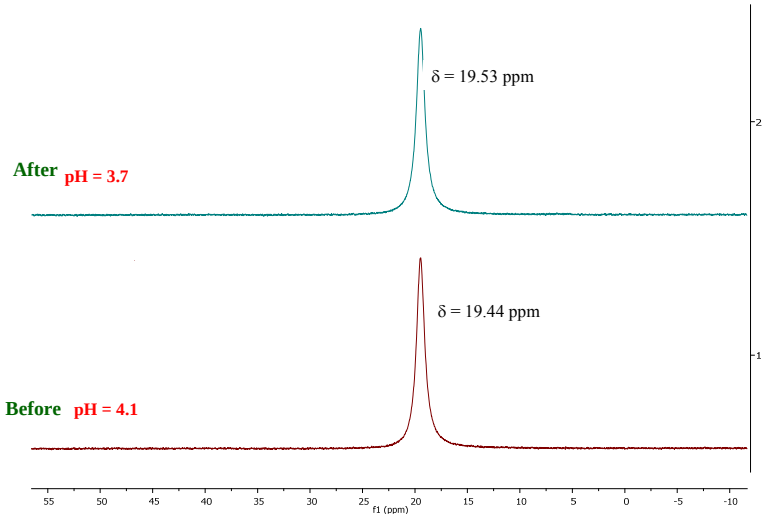
δ = 19.53 ppm
After pH = 3.7
δ = 19.44 ppm
Before pH = 4.1
f1 (ppm)

(a)

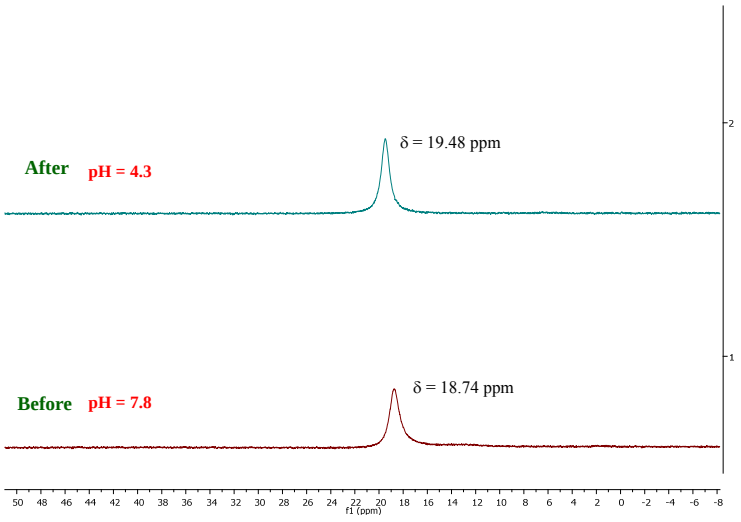
δ = 19.48 ppm
After pH = 4.3
δ = 18.74 ppm
Before pH = 7.8
f1 (ppm)

(b)

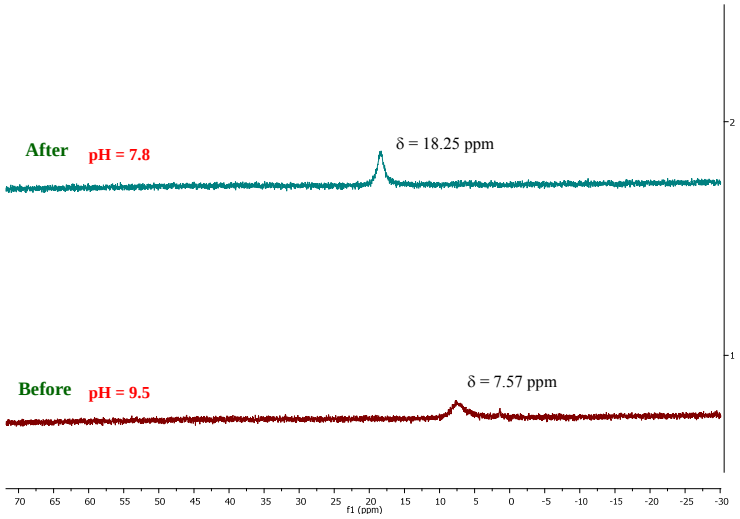

(c)

Figure 3-11. Changes of pH and δ_B in ^{11}B NMR spectroscopy before and after microwave reactions (180 °C, 10 min) of NAG in 5 mL D_2O with 2 equiv. $B(OH)_3$ and 1 equiv. NaCl addition in acidic (a), neutral (b) and basic (c) environment (the neutral and basic solutions were prepared by adding NaOD solutions (0.036 and 0.060 mol/L) to the aqueous NAG/$B(OH)_3$/NaCl solutions).

In some previous studies of borate complexes formed between $B(OH)_3$ and sugars or diols (Figure 3-12),[42-44] $B(OH)_3$ was used as the external standard (0 ppm) in ^{11}B NMR spectroscopy. δ_B for complexes formed between $B(OH)_3$ and one equivalent of a sugar (BL^-) was in a range of -12 ~ -18 ppm, which corresponds to 2 - 8 ppm on the ^{11}B NMR scale used in this thesis ($BF_3.OEt_2$ as the external standard, δ_B for $B(OH)_3$ is 19.8 ppm, Table 3-8). For complexes formed between $B(OH)_3$ and two equivalents of a sugar (BL_2^-) in previous studies, δ_B was in a range of -8 ~ -10 ppm, corresponding to 10 - 12 ppm on the

^{11}B NMR scale used in this thesis. Besides the peaks of the borate-sugar complexes, there is often one additional signal observed for the equilibrium between $B(OH)_3$ and $B(OH)_4^-$ and its position is pH dependent.[44] In some studies of glucose dehydration catalyzed by $B(OH)_3$ or its derivatives, it was proposed that a 5 or 6-membered borate-hexose complex was formed between the boron species and one equivalent of glucose (Scheme 3-5).[26, 45, 46] This complex facilitated the ring opening of the sugar and hence promoted the dehydration of glucose. In the ^{11}B NMR spectra obtained within this thesis, the signal of $B(OH)_3$ was at 19.8 ppm with $BF_3.OEt_2$ as the external standard. The only boron peak observed in the D_2O solution of NAG/$B(OH)_3$ was at around 1.5 ppm when the environment was basic (pH ca.13), and was at around 20 ppm (similar to $B(OH)_3$) when the environment was acidic or neutral, which is similar to the actual reaction environment in the current study. (The pH of the actual reaction environment was measured through a reaction in water using the same NAG:$B(OH)_3$ ratio (1:2) as used in the IL reactions performed within this thesis and/or the near-critical water reactions performed by a previous member in the Kerton group[13], and the pH was 4.1 and 3.7 before and after the reaction respectively (Figure 3-11, a).) Therefore, it is suspected that the only boron peak observed during NMR studies of relevance to the actual reaction conditions (i.e. pH 7 or lower) at δ_B 18 - 19 ppm in the current study was from $B(OH)_3/B(OH)_4^-$ equilibrium. Under the reaction conditions for NAG conversion within this thesis, $B(OH)_3$ did not form a borate-hexose chelate complex with NAG as is proposed in related glucose dehydrations, or this complex was formed in such a low concentration (below the limit of detection) that it is not a significant or long-lived intermediate in the conversion of NAG. If a borate-hexose complex had formed in the

reactions mixture, a separate signal should be observed at approximately 2 - 8 ppm in the ^{11}B NMR spectra. (Indeed, at basic pH, signals are observed at 7.5 and 1.5 ppm (pH 9.5 and pH 13.2 respectively).) Instead, it is possible that $B(OH)_3$ coordinated with Chromogen III to promote the generation of 3A5AF in later steps.

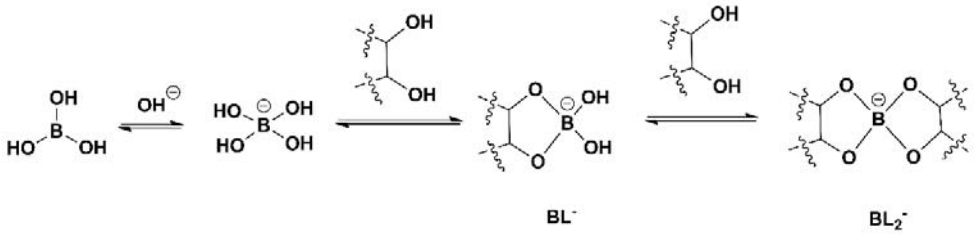

Figure 3-12. Complexes formed between $B(OH)_3$ and one or two equivalents of a sugar or diol.

Table 3-8. Literature data of δ_B of boron species in sugar/$B(OH)_3$ solutions and the corresponding data on ^{11}B NMR scale in this thesis.

δ_B (ppm)	Literature data	Corresponding data on ^{11}B NMR scale in this thesis
External standard (0 ppm)	$B(OH)_3$	$BF_3.OEt_2$
$B(OH)_3$	0	19.8[a]
$B(OH)_4^-$	-17.6	2.2
$B(OH)_3/B(OH)_4^-$ Equilibrium[b]	0 ~ -17.6	2- 20
BL^-	-12 ~ - 18	2 - 8
BL_2^-	-8 ~ - 10	10 - 12

a. Determined by ^{11}B NMR spectroscopy. b. pH 3 - 14.

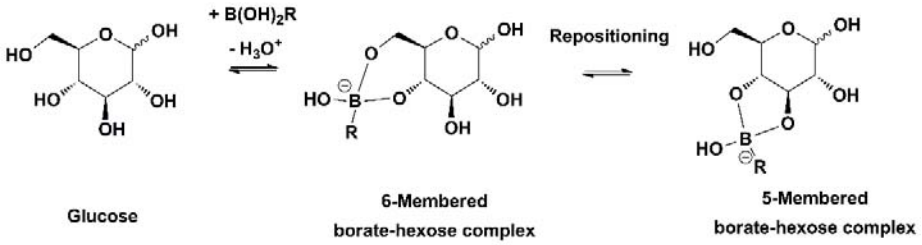

Scheme 3-5. 5 or 6-Membered borate-hexose complexes formed in the dehydration of glucose catalyzed by $B(OH)_3$ or its derivatives.

In order to determine whether it was realistic or not to see the formation of a borate-hexose complex under the concentration regime of the reactions in this thesis, the limit of detection of ^{11}B NMR spectroscopy was investigated using D_2O solutions of NAG/$B(OH)_3$ with an original pH of 4.6 (Figure 3-13). When the concentrations of NAG and $B(OH)_3$ in D_2O were decreased to 2.76×10^{-4} mol/L and 5.44×10^{-4} mol/L from the original concentrations of 0.276 mol/L and 0.544 mol/L, the boron resonance could no longer be detected. This indicated that if the 5 or 6-membered borate-hexose complex from the coordination of NAG with $B(OH)_3$ did exist, its concentration was lower than the magnitude of 2×10^{-3} mol/L. The boron concentration in an actual reaction has the magnitude of 10^{-1} mol/L, so this means that if the borate-hexose complex exists it is less than 1% than the total boron content in the reaction mixture, which suggests that if present the boron complexes are not long-lived intermediates. The same procedure was performed using D_2O solutions of NAG/$B(OH)_3$/NaCl, and the ^{11}B NMR spectra obtained indicated that NaCl had no influence on determination of the limit of detection (Figure 3-27).

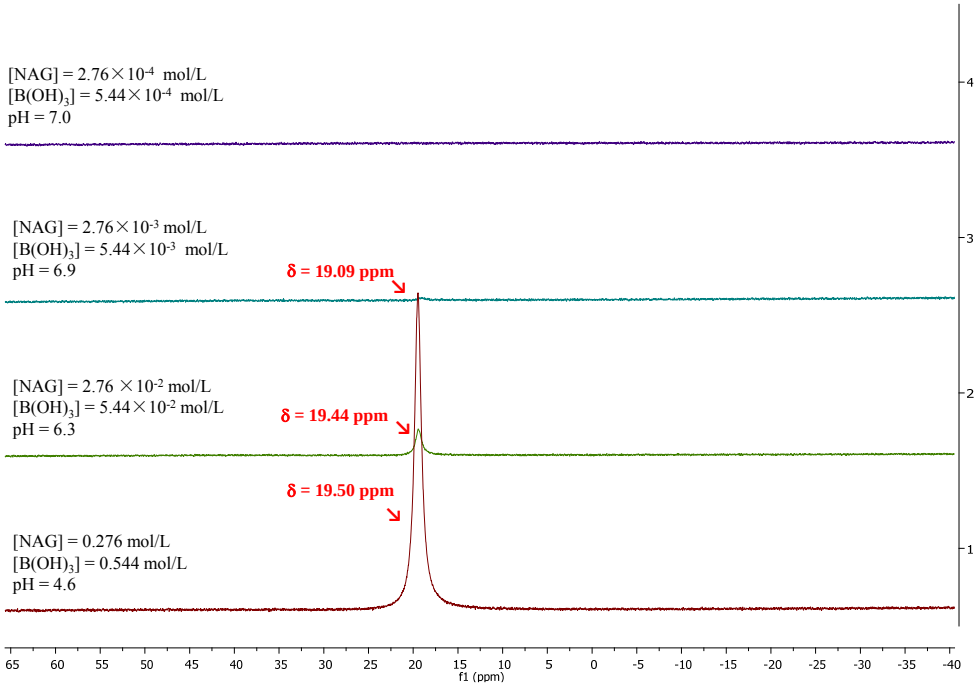

Figure 3-13. Limit of detection of ^{11}B NMR spectroscopy for D_2O solutions of NAG/$B(OH)_3$ (acidic environment).

Poisoning studies (or competition studies) have been performed in the dehydration of sugars to determine the moiety in the sugar that reacted with the catalyst or to investigate the structure of the intermediate formed.[11, 46-49] In the study by the Yan group of the $B(OH)_3$-catalyzed conversion of chitin/NAG to 3A5AF, ethanol, EG or 1,3-propanediol were added into the starting materials for the reaction.[11] For both chitin and NAG conversions, the yield of 3A5AF had a larger decrease with EG addition and a smaller decrease with 1,3-propanediol addition, but had no change with ethanol addition. This indicated that chitin/NAG forms 5- or 6-membered ring borate-hexose complexes instead of acyclic borate-hexose complexes with $B(OH)_3$ during the conversion, and the 6-

membered ring borate-hexose complexes are probably more significant (since the 3A5AF yield had a more obvious decrease with 1,3-propanediol addition) (Scheme 3-6). However, it cannot be determined whether it is NAG or another intermediate (e.g. Chromogen III) during the reaction that forms complexes with $B(OH)_3$ via the poisoning study, so no poisoning studies were performed for the mechanistic studies of $B(OH)_3$-catalyzed reactions within this thesis.

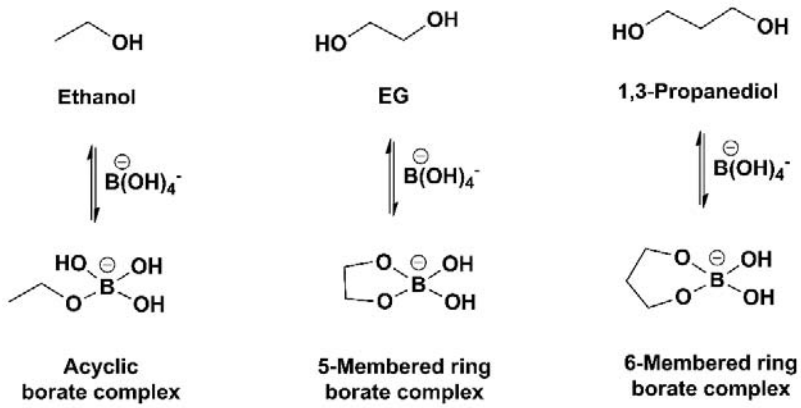

Scheme 3-6. Borate complexes formed from ethanol, EG and 1,3-propanediol with $B(OH)_3$.

3.2.8 IL Reuse

The reusability of [Bmim]Cl was studied by adding fresh NAG and EtOAc into the reaction mixture after every two runs. In a typical experiment, 100 mg (0.452 mmol) NAG, 2 molar equivalents of $B(OH)_3$, 750 mg (4.29 mmol) [Bmim]Cl and 9 mL EtOAc were added into the microwave vial and the mixture was heated at 180 °C for 9 min. The EtOAc layer was decanted and extraction of the reaction mixture was conducted using an additional 3 × 5 mL EtOAc. Then another 9 mL EtOAc was added to the [Bmim]Cl, which

still contained some unreacted reagents or intermediates, and the mixture was heated in the microwave for a second time (i.e. the second run). The EtOAc layer was collected and three extractions were performed as described above for the first heating of the mixture. Then, 100 mg fresh NAG and 9 mL EtOAc were added to the [Bmim]Cl and another reaction was performed. At no point in this series of experiments on reusability was more $B(OH)_3$ acid added.

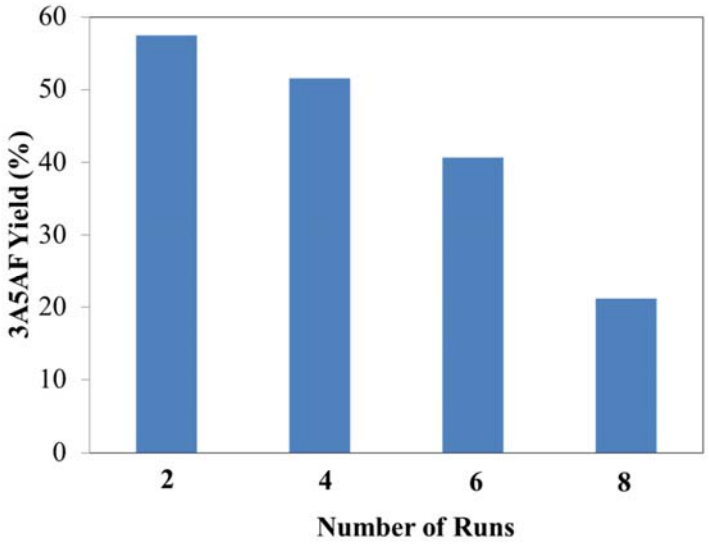

Figure 3-14. Reuse of [Bmim]Cl in the conversion of NAG with 2 equiv. $B(OH)_3$ addition in 750 mg [Bmim]Cl and 9 mL EtOAc, heated by microwave irradiation at 180 °C for 9 min.

The yield of 3A5AF decreased significantly between runs 6 and 8 from 40.68% to 21.17% (Figure 3-14). However, for runs 1 to 6, the yields were all in excess of 40%. The cause of the decrease in yield could be due to many factors including a build up of water and/or humin-like insoluble substances in the [Bmim]Cl phase, decomposition of the ionic

liquid or leaching of the required $B(OH)_3$ additive. It has been reported that [Bmim]Cl is not stable at high temperatures and 1-butylimidazole has been observed as one decomposition product.[50, 51] In order to investigate whether [Bmim]Cl decomposed in reactions performed in the current study, aliquots of both the EtOAc layer and the reaction mixture were taken and dissolved in chloroform-d for NMR analysis after two, four, six and eight runs. The ^{1}H and ^{13}C NMR spectra obtained were compared with those of pure NAG, 3A5AF, $B(OH)_3$, [Bmim]Cl and EtOAc. The spectra of 1-methylimidazole, 1-butylimidazole and chlorobutane were also obtained and used for comparison as they are possible decomposition products from [Bmim]Cl. In the ^{1}H NMR spectrum of the EtOAc layer after six runs, the resonances at 7.55 ppm, 7.06 ppm, 6.92 ppm and 3.93 - 3.97 ppm were assigned to 1-butylimidazole and 1-methylimidazole (Figure 3-28). This suggests that one of the reasons for the poor reusability of [Bmim]Cl in the conversion of NAG under the applied conditions was its ease of decomposition.

3.2.9 Seawater as the Replacement for NaCl and Water

Although ILs have many advantages as alternative solvents, water is more environmentally and economically friendly for use.[52] The Kerton group has endeavored to perform the conversion of NAG to 3A5AF in subcritical water (180 - 220 °C, 250 - 450 psi) using a Parr reactor.[13] The highest 3A5AF molar yield achieved was 75.4% with a selectivity of 90.6% from a reaction at 220 °C for 10 min. Besides $B(OH)_3$, NaCl was also used as an additive, leading me to consider whether seawater can be employed to replace the use of NaCl and water. Two reactions were performed, one of which was in 3 mL water

with 1 molar equivalent of NaCl and the other one was in 3 mL seawater. Both reactions were heated under microwave irradiation at 180 °C for 10 min. The 3A5AF yields obtained were 1.9% and 2.1%, indicating the feasibility of using seawater as the replacement. These yields are lower than those from the Parr reactor reactions described above, as the maximum operable temperature of the microwave reactor used in this thesis is 180 °C and not 220 °C as was used in the other study using the Parr reactor. The use of seawater is promising and advantageous since it is cheap and easily available, especially in Newfoundland. It should be noted that besides NaCl there are other kinds of minerals in seawater, which may promote NAG dehydration or side-reactions. Further studies should be carried out to design routes for NAG conversion in seawater with higher 3A5AF yield obtained. Reactions performed in a Parr reactor at 220 °C should give similar yields to those studied previously by Curtis.[13]

3.3 Conclusions

The conversion of NAG into 3A5AF was optimized with the maximum 3A5AF yield of 62.3% achieved after two runs under microwave irradiation (100 - 180 °C) in [Bmim]Cl. Two molar equivalents of $B(OH)_3$ and NaCl were added, and 9 mL EtOAc was used as the extraction layer. The 3A5AF yield was found to be closely related to the Brønsted acidity of the system. The importance of $B(OH)_3$ and NaCl in increasing the 3A5AF yield was confirmed during a study of additives, but the detailed mechanism especially with regards to the role of chloride ions needs to be further investigated. EtOAc was chosen as the ideal solvent for 3A5AF extraction because of its environmentally benign nature compared with

other VOCs and the high 3A5AF yield obtained. The yield of 3A5AF could be significantly improved by increasing the number of runs and use of multiple EtOAc extraction layers. The higher 3A5AF yields from the use of self-made ILs ([Bmim]Cl and [Bmim][HSO_4]) were attributed to the high Cl content, confirming that chloride ions promote 3A5AF formation. The activation energies and pre-exponential factors of the conversion of NAG and its two isomers (NAGal and NAMan) in the presence of $B(OH)_3$ were calculated. The mechanism of NAG conversion and the role of $B(OH)_3$ were briefly investigated through ^1H and ^{11}B NMR spectroscopy. Chromogen I and III were proposed as important intermediates for 3A5AF generation, and $B(OH)_3$ was assumed to coordinate with Chromogen III to promote the formation of 3A5AF. The reusability of [Bmim]Cl was studied and the 3A5AF yield had a significant decrease after six runs, presumably due to the decomposition of the IL. Finally, the potential of seawater as the replacement for water and NaCl was investigated and it is a promising solvent for use in future studies.

Further studies are needed to design better routes for the synthesis of 3A5AF from NAG (the improvement of 3A5AF yield, and the use of more environmentally friendly solvents) and to investigate the mechanism in more detail. It is also intended to study the reactivity of 3A5AF, including being a platform chemical of renewable amines (see **Chapter 5**) and a precursor to proximicins.[53, 54]

3.4 Experimental

3.4.1 Materials and Instruments

NAG was purchased in 98% purity from AK Scientific. $B(OH)_3$ was purchased in 99.5% purity from Sigma Aldrich. NaCl was purchased in 99.0% purity from Anachemia. [Bmim]Cl, [Bmim][HSO_4], [Bmim-SO_3H][HSO_4], [Emim]Cl, [Emim][HSO_4], [Emim][OAc], PS[hmim]Cl, [$B(OH)_2$hmim]Br and HmimBr were synthesized according to literature procedures[28, 55-59] or purchased from Alfa Aesar, Sigma Aldrich and IoLiTec. EtOAc (ACS grade, 99.5%) was purchased from Caledon. Other chemicals including $FeCl_3$, $CrCl_3$, metaboric acid, $NaNO_3$, $NaSO_4$, benzamide, acetophenone and sodium hydroxide were purchased from Strem, Alfa Aesar, Fisher Scientific, Sigma Aldrich and BDH. Molecular sieves (4 Å) were purchased from Sigma Aldrich. Solvents including EG, PEG (Mn 600), 2, 5-Me THF, 1-hexanol, 1-butanol, MIBK and methanol were purchased from Sigma Aldrich, Alfa Aesar, Fisher Scientific and ACP. Deionized water was obtained from distilled water processed by a Nanopure II system (manufactured by Barnstead/Thermolyne, USA). All NMR solvents were purchased in 99.8% or 99.9% purity from Cambridge Isotope Laboratories. All chemicals and solvents were used as received.

Microwave reactions were performed using a Biotage Initiator 2.5 microwave reactor. 2 - 5 mL or 10 - 20 mL reaction volume vials were used. The “very high” absorption level was applied in each reaction to control the power delivered to heat the reaction mixture. Vortex-mixing of the reaction mixture was carried out using a Thermo Scientific Vortex Maxi Mix II. Centrifugation was performed using an Eppendorf centrifuge 5430.

Evaporation of solvents was achieved using a Buchi Rotavap. Gas chromatography-mass spectrometry (GC-MS) was performed on an Agilent 7890A GC system coupled with an Agilent 5975C MS detector. ^{1}H (300 MHz), ^{13}C (75 MHz) and ^{11}B (96 MHz) NMR analysis was accomplished on a Bruker 300 MHz spectrometer. Tetramethylsilane (Me_4Si, $\delta = 0$ ppm) was used as the internal reference for ^{1}H and ^{13} C NMR spectroscopy, and boron trifluoride diethyl etherate ($BF_3.OEt_2$, $\delta = 0$ ppm) is used as the external reference for ^{11}B NMR spectroscopy. For ^{11}B NMR experiments, Quartz NMR tubes were used in order to eliminate the interference from the boron contained in glass. Infrared (IR) spectra were recorded using a Bruker Alpha FTIR spectrometer (4 cm^{-1} resolution) with a diamond ATR single reflectance module (24 scans). Aqueous pH measurements were conducted using a VWR sympHony B10P Meter. ICP-MS analysis was performed using a Perkin Elmer Sciex ElAN DRC II instrument. Karl-Fisher titration was carried out on a Mettler Toledo C30 Coulometric KF Titrator.

3.4.2 Synthesis of ILs

[Bmim]Cl: 23.51 g (0.2863 mol) 1-methylimidazole and 26.51 g (0.2863 mol) chlorobutane were placed in a 250 mL round bottom flask. The mixture was stirred under reflux at 70 °C for 24 h. The top layer was removed. The bottom layer was washed using 3 × 10 mL EtOAc, and dried under vacuum using a Schlenk line at 70 °C overnight to give a colorless viscous liquid product. The product sometimes solidified upon storage at room temperature. ^{1}H NMR δ_H (298 K, 300 MHz; DMSO-d_6; Me_4Si) 0.89 (t, 3H), 1.19 - 1.31 (m, 2H), 1.71 - 1.81 (m, 2H), 3.86 (s, 3H), 4.18 (t, 2H), 7.76 (t, 1H), 7.83 (t, 1H), 9.38 (s, 1H);

^{13}C NMR δ_C (298 K, 75 MHz; DMSO-d_6) 13.17, 18.67, 31.24, 35.65, 48.56, 122.13, 123.45, 136.14. The NMR data are in agreement with those reported in the literature.[60]

[Bmim][HSO$_4$]: 4.36 g (0.0250 mol) [Bmim]Cl was dissolved in 10 mL methanol, to which 3.45 g (0.0250 mol) sodium hydrogen sulfate monohydrate was added. The mixture was stirred under reflux at 40 °C for 24 h and then filtered. The filtrate was dried under vacuum using a Schlenk line at room temperature overnight, affording a pale yellow viscous liquid product. ^{1}H NMR δ_H (298 K, 300 MHz; DMSO-d_6; Me_4Si) 0.89 (t, 3H), 1.19 - 1.31 (m, 2H), 1.71 - 1.81 (m, 2H), 3.85 (s, 3H), 4.17 (t, 2H), 7.73 (t, 1H), 7.79 (t, 1H), 9.23 (s, 1H); ^{13}C NMR δ_C (298 K, 75 MHz; DMSO-d_6) 13.18, 18.67, 31.24, 35.65, 48.57, 122.13, 123.46, 136.14. The NMR data are in agreement with those reported in the literature.[61]

[Bmim-SO$_3$H][HSO$_4$]: 8.21 g (0.100 mol) 1-methylimidazole and 13.62 g (0.100 mol) 1,4-butane sultone were placed in a 100 mL round bottom flask and stirred at 60 °C for 10 h. After filtration, the white solid obtained was washed using 3 × 5 mL diethyl ether, and dried under vacuum in a 100 mL round bottom flask using a Schlenk line at room temperature overnight. To the round bottom flask 10.01 g (0.100 mol) 98% sulfuric acid was added dropwise. The mixture was stirred at 80 °C for 6 h. The obtained liquid was washed using 4 × 5 mL diethyl ether and dried under vacuum using a Schlenk line at room temperature overnight, affording a pale yellow viscous liquid product. ^{1}H NMR δ_H (298 K, 300 MHz; DMSO-d_6; Me_4Si) 1.49 - 1.59 (m, 2H), 1.82 - 1.92 (m, 2H), 2.55 (t, 2H), 4.17 (t, 2H), 7.40 (s, 1H), 7.71 (t, 1H), 7.77 (t, 1H), 9.00 (s, 3H), 9.16 (s, 1H); ^{13}C NMR δ_C (298 K,

75 MHz; DMSO-d_6) 21.61, 28.59, 35.81, 48.53, 50.50, 122.40, 123.70, 136.71. The NMR data are in agreement with those reported in the literature.[62]

PS[hmim]Cl: 1.44 g (60.0 mmol) sodium hydride was weighed into a 150 mL Schlenk flask in a glove box. The Schlenk flask was removed from the glove box and connected to a Schlenk line. Under N_2 flow, dry tetrahydrofuran (THF, ca. 80 mL) was added into the flask. The flask was cooled in an ice bath and 8.20 g (60.0 mmol) 6-chloro-1-hexanol was added slowly. The mixture was stirred for 30 min. Afterwards, 5.00 g (7.50 mmol) Merrifield peptide resin was added into the flask, followed by the addition of 2.77 g (7.50 mmol) tetra-*n*-butylammonium iodide. The mixture was stirred at room temperature for 2 days and then filtered. The white powdery solid (resin 1) was washed using THF, water, acetone, water, methanol and dichloromethane (ca. 10 mL each time) and dried under vacuum using a Schlenk line at room temperature overnight. 3.25 g (5.20 mmol) of resin 1 was weighed into a 150 mL round bottom flask, to which 75 mL 1-methylimidazole (excess) was added. The mixture was stirred at 90 °C for 3 days. After being cooled to room temperature, the mixture was filtered. The pale yellow powdery solid was washed using dichloromethane, methanol, acetone-water (1:1), water, methanol, acetone and diethyl ether (ca. 10 mL each time) and dried under vacuum using a Schlenk line at room temperature overnight. $^{13}C\{^1H\}$ CP-MAS solid state NMR δ_C (20 kHz) 26.52, 30.42, 40.54, 45.64, 71.91, 125.73, 126.90, 128.53, 137.00, 145.75. The NMR data are in agreement with those reported in the literature.[59]

[Hmim]Br: 8.21 g (0.100 mol) 1-methylimidazole and 16.51 g (0.100 mol) bromohexane were placed in a 100 mL round bottom flask. The mixture was stirred at 80 °C for 2 days. The top layer was removed. The bottom layer was washed using 3 × 10 mL EtOAc and dried under vacuum using a Schlenk line at room temperature overnight, giving a colorless viscous liquid. ^{1}H NMR δ_H (298 K, 300 MHz; DMSO-d_6; Me_4Si) 0.85 (t, 3H), 1.25 (s, 6H), 1.72 - 1.82 (m, 2H), 3.86 (s, 3H), 4.17 (t, 2H), 7.75 (t, 1H), 7.82 (t, 1H), 9.26 (s, 1H); ^{13}C NMR δ_C (298 K, 75 MHz; DMSO-d_6) 13.82, 21.85, 25.11, 29.34, 30.53, 35.76, 48.71, 122.24, 123.56, 136.50. The NMR data are in agreement with those reported in the literature.[63]

[B(OH)$_2$hmim]Br: 0.50 g (2.4 mmol) (6-bromohexyl)boronic acid was dissolved in 25 mL dry toluene in a 100 mL Schlenk flask in a glove box. The flask was removed from the glove box and connected to a Schlenk line. Under N_2 flow, 0.28 g (4.5 mmol) EG was added dropwise to the solution. The mixture was stirred under N_2 at room temperature for 24 h. The solvent was removed under vacuum using a Schlenk line, and a colorless viscous liquid was obtained. The liquid was dissolved in 5 mL EtOAc, which was added dropwise to a 5 mL EtOAc solution of 0.24 g (2.9 mmol) 1-methylimidazole. The mixture was stirred at room temperature for 24 h. Afterwards, 10 mL methanol was added and the mixture was stirred at room temperature for 20 min. The solution was added to 50 mL THF, and the precipitated white solid was collected via filtration. The solid product was washed using 3 × 5 mL THF, and dried under vacuum using a Schlenk line at 30 °C overnight. ^{1}H NMR δ_H (298 K, 300 MHz; DMSO-d_6; Me_4Si) 0.72 (t, 2H), 1.23 - 1.38 (m, 6H), 1.72 - 1.81 (m, 2H),

3.85 (s, 3H), 4.14 (t, 2H), 7.35 (s, 2H), 7.71 (t, 1H), 7.77 (t, 1H), 9.13 (s, 1H); ^{13}C NMR δ_C (298 K, 75 MHz; DMSO-d_6) 23.88, 25.26, 29.29, 30.96, 35.74, 48.76, 122.25, 123.23, 123.59, 136.48. The NMR data are in agreement with those reported in the literature.[58]

3.4.3 Solubility Test

In a typical test, a small amount of NAG (< 10 mg) was added to a vial containing 750 mg of the IL, followed by stirring for at least 10 min to allow for equilibration (i.e. until no change in appearance was apparent or all solid had dissolved). This procedure was repeated until the solid added no longer dissolved.

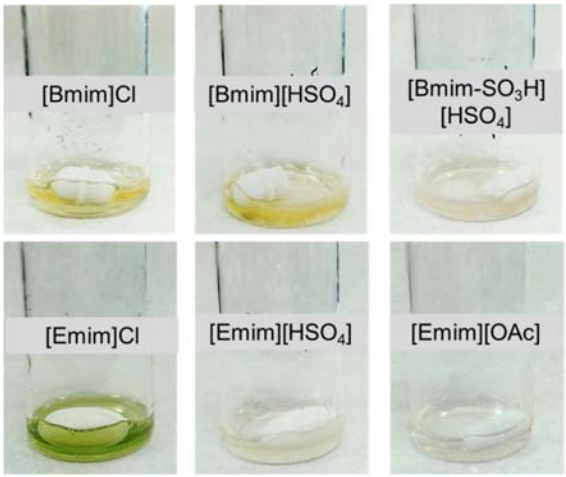

Figure 3-15. Solubility test of NAG in 750 mg IL at room temperature.

3.4.4 pH Measurement of Aqueous IL Solutions

In a typical experiment, a 0.1 mol/L aqueous solution of the IL was prepared by dissolving 0.5 mmol IL in 5 mL water. After calibration, the pH meter was used to measure the pH of the solution in triplicate, and an average pH value was obtained as the final result.

3.4.5 General Procedure for NAG Conversion to 3A5AF

In a typical reaction, 100 mg (0.452 mmol) NAG, known amounts of the solvent, additives and the in situ extraction layer were placed in a microwave vial. The mixture was heated to the desired temperature under microwave irradiation or in an oil bath for a specific period of time. Afterwards, the reaction mixture was cooled to room temperature and vortex-mixed at high speed for 1 min to maximize the amount of material extracted. Then the mixture underwent centrifugation at 4500 rpm for 5 min in order to facilitate the separation of the IL and the in situ extraction layers, and the in situ extraction layer on the top was collected. For multiple runs, extraction of the reaction mixture was performed using 3 × 5 mL EtOAc and the EtOAc layers were combined. Another known amount of fresh in situ extraction layer was added to the reaction mixture and the reaction procedure was repeated as described above. For each type of reaction conditions applied, reactions were performed multiple times. Yields reported have a standard deviation of ± 0.2%.

3.4.6 3A5AF Quantification

Extraction part: the in situ extraction layers and the combined EtOAc extracts were concentrated using a Buchi Rotavap (180 mbar, 40 °C), and then diluted with 3 mL EtOAc. For each solution, an aliquot (300 μL) was taken and 100 μL of 2 mg benzamide/mL EtOAc solution (GC internal standard) was added. The mixture was analyzed via GC-MS and the 3A5AF content in this extraction part was calculated using the calibration curve (Figure 3-16, a).

Reaction mixture: an aliquot (15 - 30 mg) of the reaction mixture was taken. 100 µL of 2 mg benzamide/mL EtOAc solution, 1 mL deionized water and 3 mL EtOAc were added. After vortex-mixing at high speed for 1 min, the mixture was centrifuged at 4500 rpm for 5 min, and the EtOAc layer was collected. Two further extractions using 3 mL EtOAc were performed. The obtained extract was concentrated on a Buchi Rotavap (180 mbar, 40 °C) yielding a yellow solid, which was dissolved in 800 µL EtOAc and analyzed via GC-MS for quantification using the calibration curves (Figure 3-16, b).

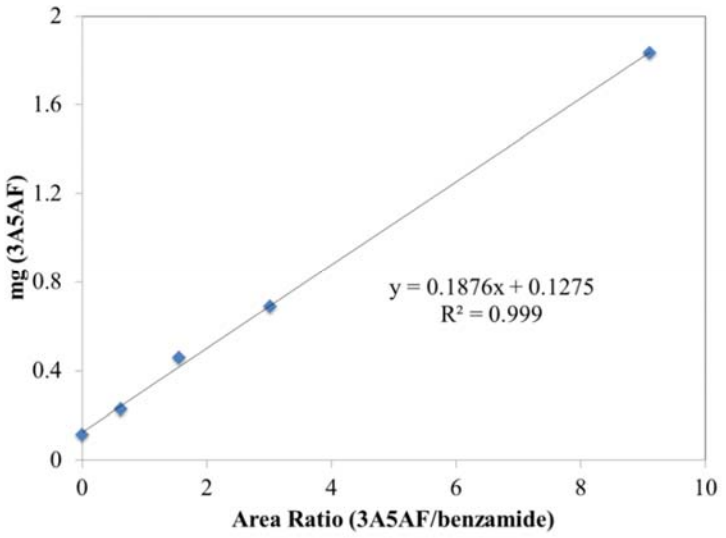

(a)

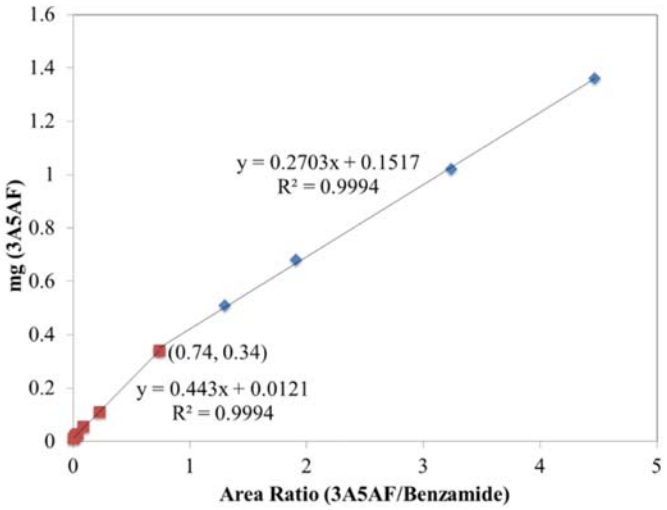

(b)

Figure 3-16. Calibration curves of 3A5AF in the extraction part (a) and reaction mixture (b).

3.4.7 3A5AF Identification

^{1}H NMR δ_H (298 K, 300 MHz; DMSO-d_6; Me_4Si) 2.02 (s, 3H), 2.40 (s, 3H), 7.18 (d, 1H), 8.17 (d, 1H), 10.21 (s, 1H)

^{13}C NMR δ_C (298 K, 75 MHz; DMSO-d_6) 22.76, 25.81, 110.99, 127.00, 135.24, 149.74, 167.71, 186.05

MS *m/z* (% ion) 167 (40), 125 (60), 110 (100), 96 (13), 83 (20), 69 (6), 54 (13)

Selected IR data (cm^{-1}) solid 3340.64 (s) (N-H stretch), 1657.85 (s) (C=O stretch in amide and ketone), 1556.89 (s) (N-H bending); solution (in diethyl ether) 1668.68 (s) (C=O stretch in amide and ketone)

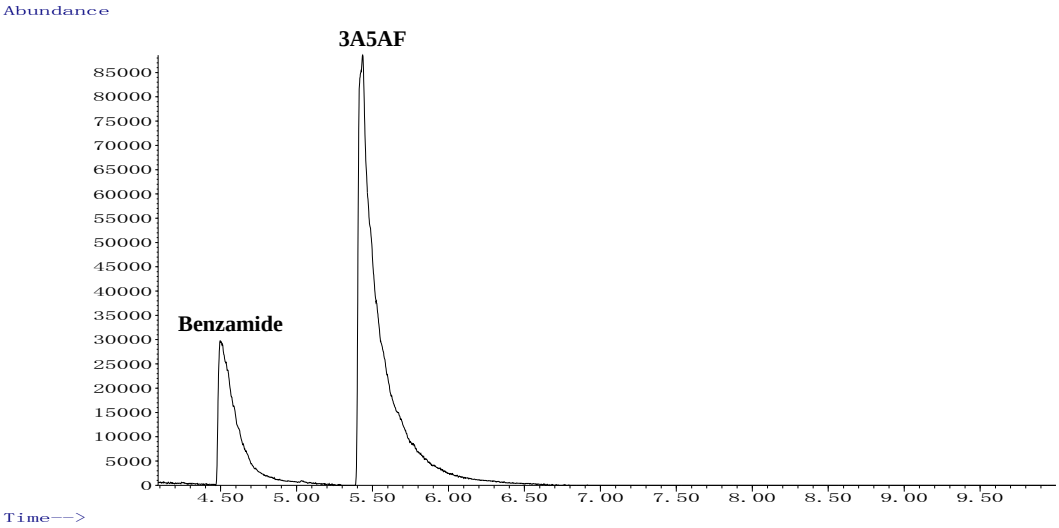

Figure 3-17. Gas chromatogram of 3A5AF.

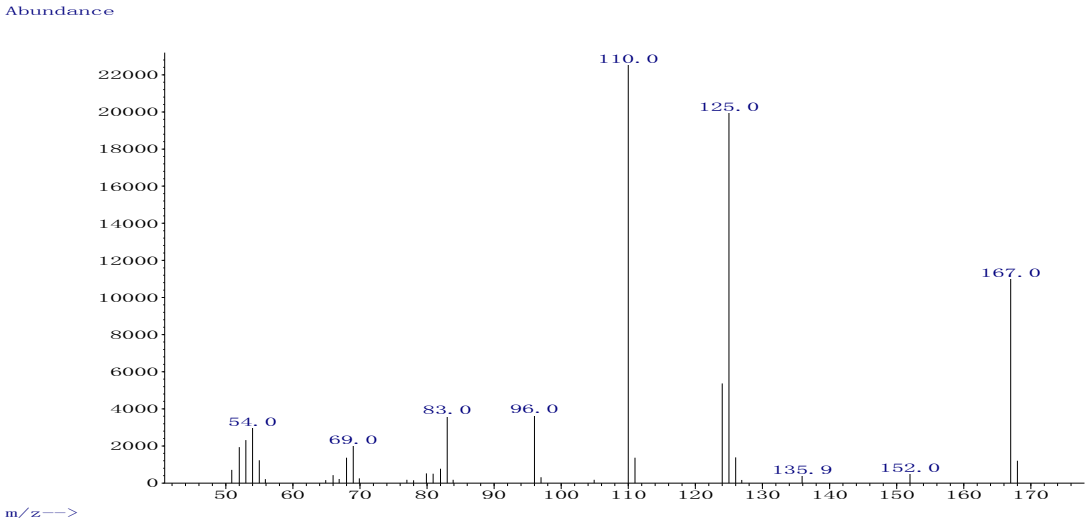

Figure 3-18. Mass spectrum of 3A5AF.

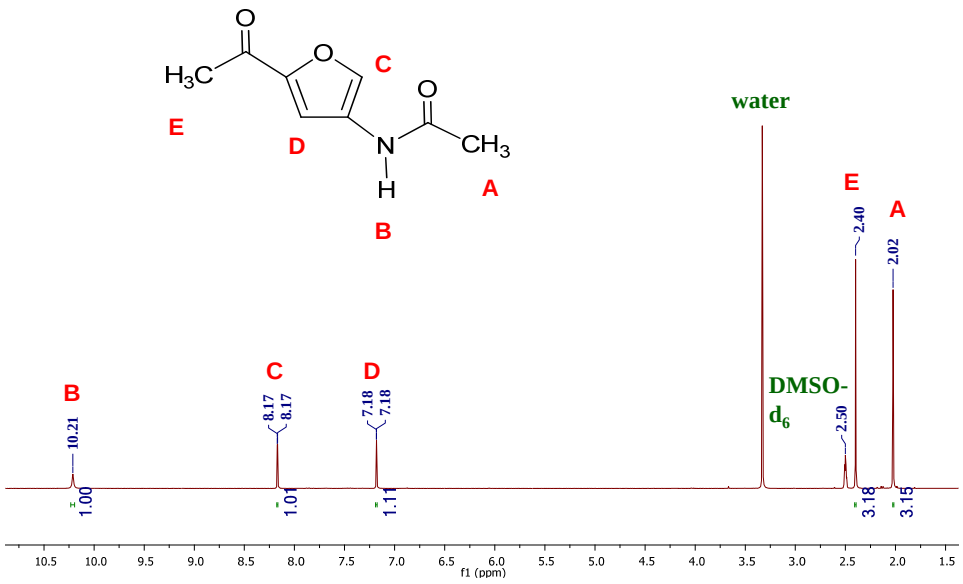

Figure 3-19. ^{1}H NMR spectrum of 3A5AF.

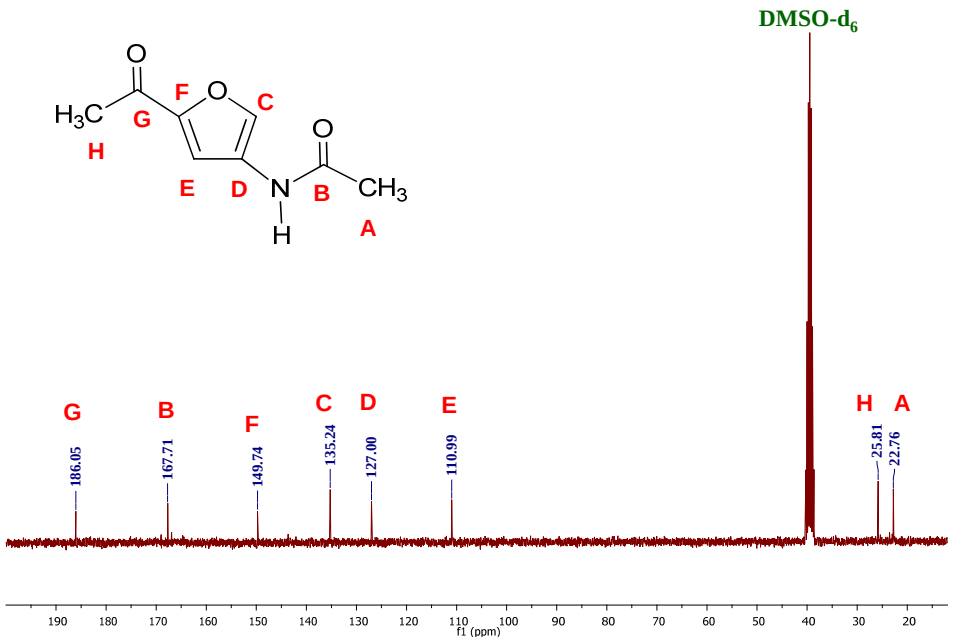

Figure 3-20. ^{13}C NMR spectrum of 3A5AF.

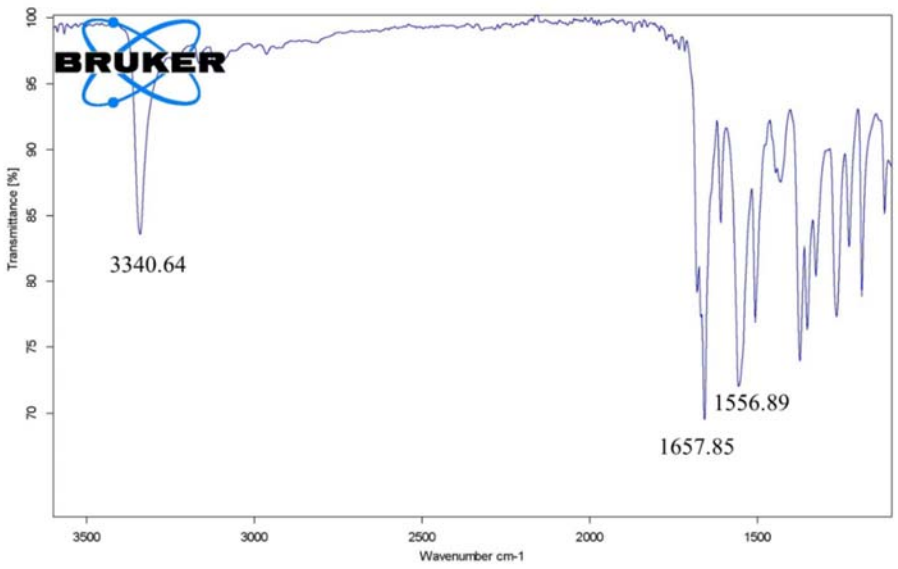

Figure 3-21．IR spectrum of solid 3A5AF.

3.4.8 General Procedure for Kinetic Studies

In a typical experiment, 424 mg (1.92 mmol) sugar (NAG, NAGal or NAMan) and 2 molar equivalents of $B(OH)_3$ were added into 1.000 g (5.725 mmol) [BMim]Cl. The mixture was heated in an oil bath at a given temperature. An aliquot (20 - 60 mg) was taken at the desired time into a small vial and weighed, to which 10 μL acetophenone was added as the internal standard. The mixture was weighed and dissolved in 600 μL DMSO-d_6 for NMR analysis. Combining the accurate amount of acetophenone with the integration ratio of the methyl group of the sugar to that of acetophenone, the sugar amount in the sample was calculated and the first-order rate plots were obtained.

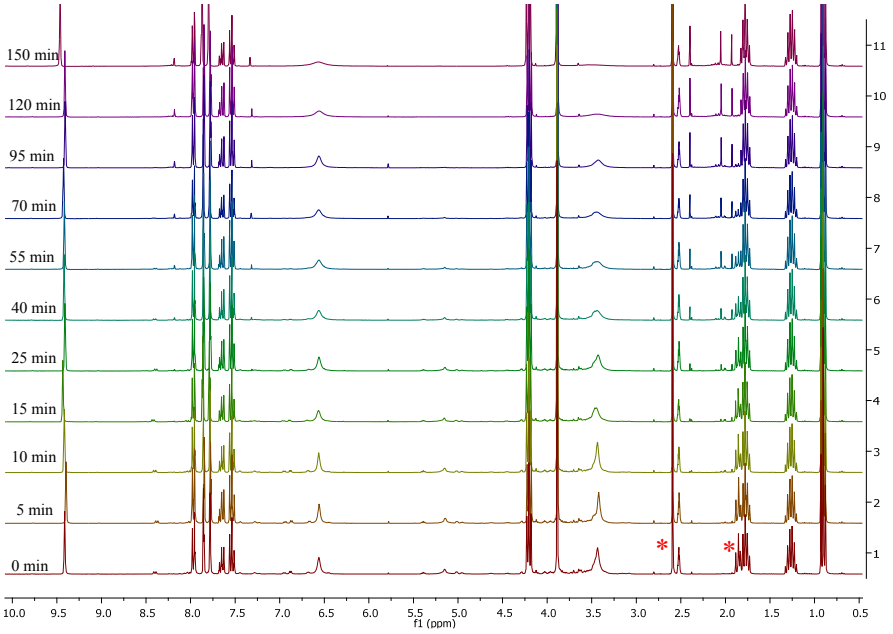

Figure 3-22. Stacked ^{1}H NMR spectra of the samples taken during 424 mg NAG conversion with 2 equiv. $B(OH)_3$ in 1.000 g [Bmim]Cl, heated by microwave irradiation at 130 °C (starred peaks are the methyl groups of acetophenone at 2.58 ppm and NAG at 1.88 ppm).

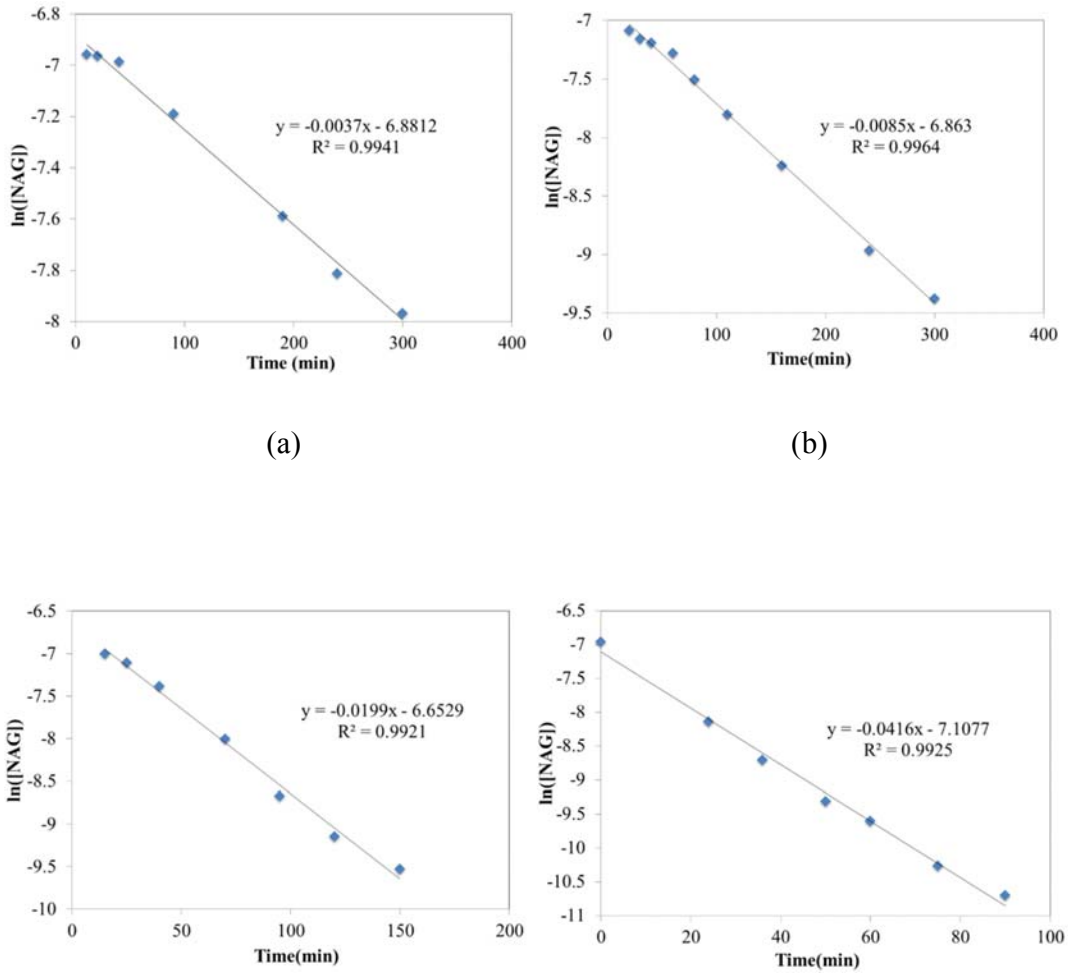

Figure 3-23. First-order rate plots of 424 mg NAG conversion with 2 equiv. $B(OH)_3$ addition in 1.000 g [Bmim]Cl heated by microwave irradiation at 110 (a), 120 (b), 130 (c) and 140 °C (d).

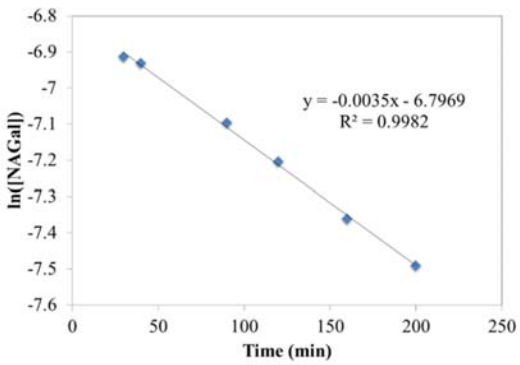

(a)

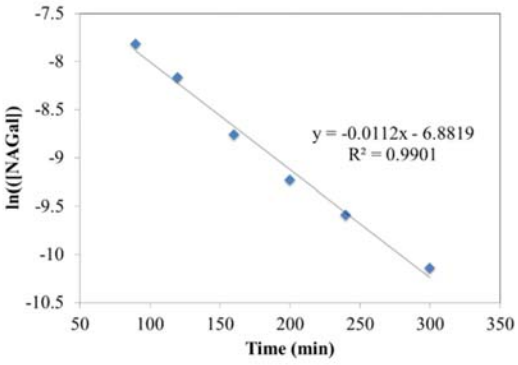

(b)

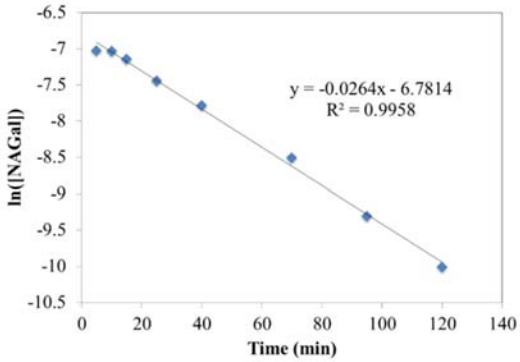

(c)

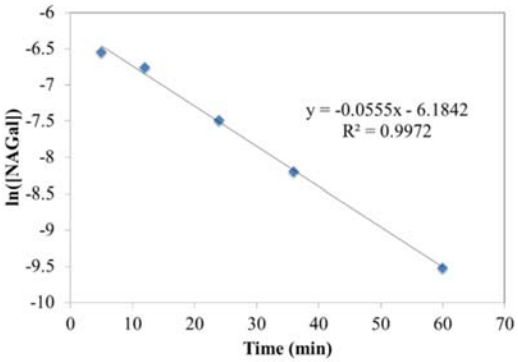

(d)

Figure 3-24. First-order rate plots of 424 mg NAGal conversion with 2 equiv. $B(OH)_3$ addition in 1.000 g [Bmim]Cl heated by microwave irradiation at 110 (a), 120 (b), 130 (c) and 140 °C (d).

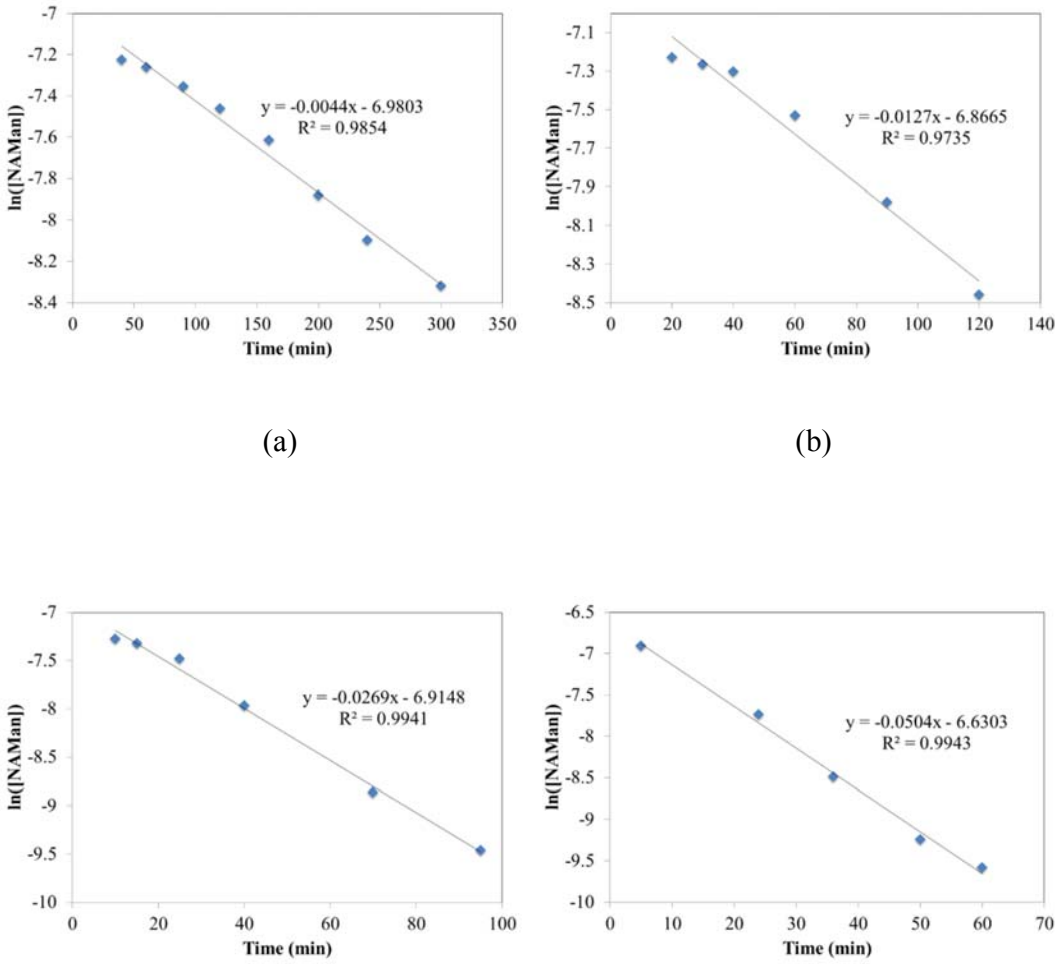

Figure 3-25. First-order rate plots of 424 mg NAMan conversion with 2 equiv. $B(OH)_3$ addition in 1.000 g [Bmim]Cl heated by microwave irradiation at 110 (a), 120 (b), 130 (c) and 140 °C (d).

Table 3-9. Kinetic data for the Arrhenius plot of NAG conversion.

Temperature (°C)	Temperature (K)	1/T (K^{-1})	k_{obs}	ln(k_{obs})
110	383	0.00261	0.0037	-5.5994
120	393	0.00254	0.0085	-4.7677
130	403	0.00248	0.0199	-3.9170
140	413	0.00242	0.0416	-3.1797

Table 3-10. Kinetic data for the Arrhenius plot of NAGal conversion.

Temperature (°C)	Temperature (K)	1/T (K^{-1})	k_{obs}	ln(k_{obs})
110	383	0.00261	0.0035	-5.6550
120	393	0.00254	0.0112	-4.4918
130	403	0.00248	0.0264	-3.6344
140	413	0.00242	0.0555	-2.8914

Table 3-11. Kinetic data for the Arrhenius plot of NAMan conversion.

Temperature (°C)	Temperature (K)	1/T (K^{-1})	k_{obs}	ln(k_{obs})
110	383	0.00261	0.0044	-5.4261
120	393	0.00254	0.0127	-4.3662
130	403	0.00248	0.0269	-3.6156
140	413	0.00242	0.0504	-2.9878

3.4.9 General Procedure for Detection of Chromogen I and III

Reactions in water: 2.10 g (9.49 mmol) NAG, 2 molar equivalents of $B(OH)_3$ and 1 molar equivalent of NaCl were dissolved in 28 mL D_2O. The solution was divided into seven equal samples (4 mL each), which were heated under microwave irradiation at 180 °C for 0, 1, 2, 4, 6, 8 and 10 min respectively. Afterwards, 1 mL of each sample was taken and analyzed by ^1H NMR spectroscopy.

Reactions in [Bmim]Cl: 100 mg (0.452 mmol) NAG, 2 molar equivalents of $B(OH)_3$, 750 mg (4.29 mmol) [Bmim]Cl and 3 mL EtOAc were placed in a 2 - 5 mL microwave vial. This procedure was repeated another six times to obtain a total of seven samples, which were heated under microwave irradiation at 180 °C for 0, 1, 2, 4, 6, 8 and 10 min respectively. Two aliquots were taken from each reaction mixture and dissolved in 1 mL DMSO-d_6 and 1 mL D_2O respectively for ^1H NMR analysis.

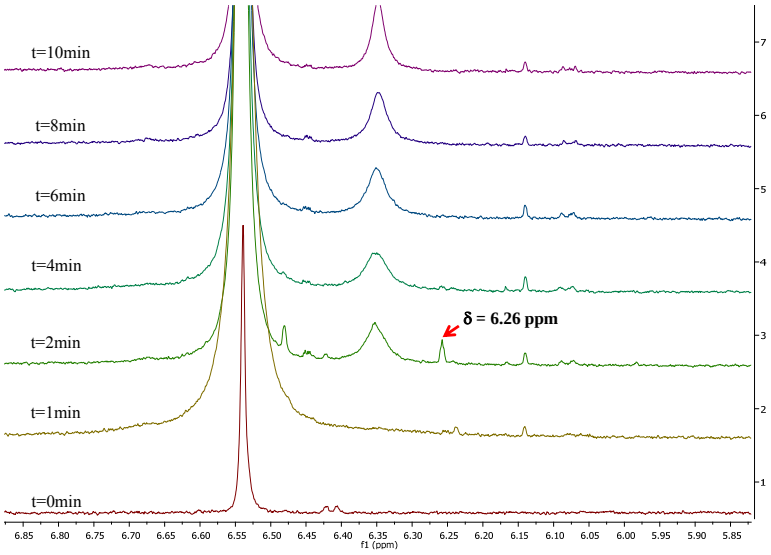

(a)

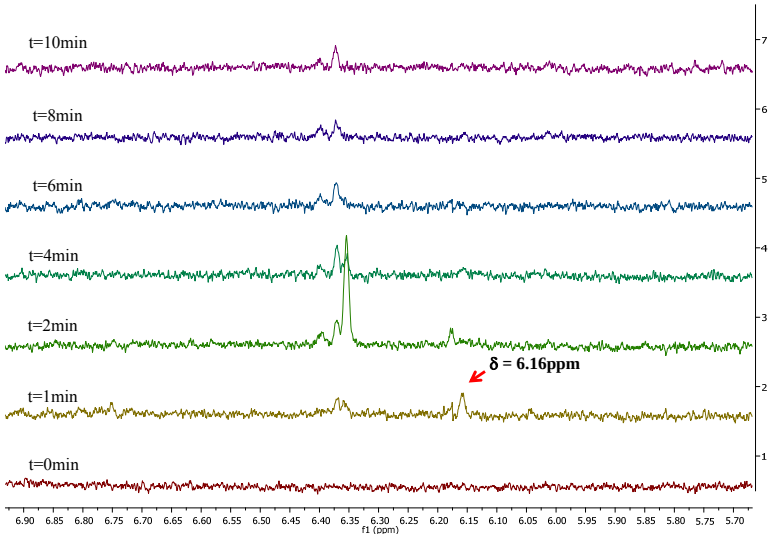

(b)

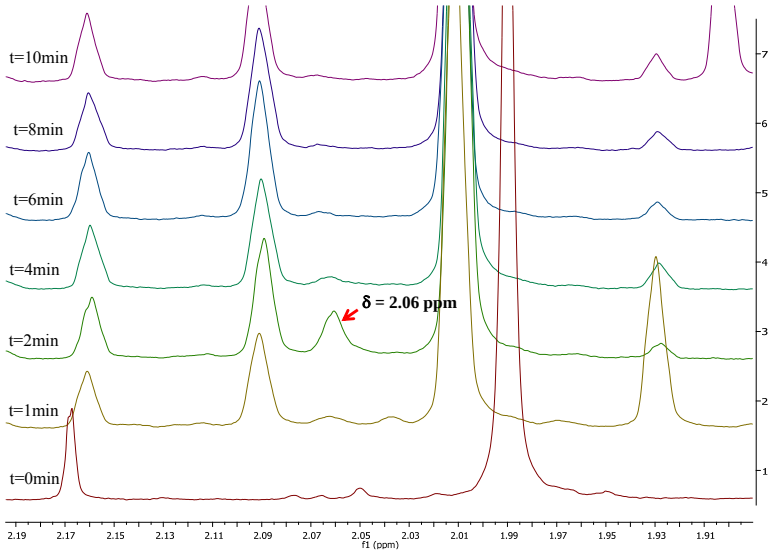

(c)

Figure 3-26. Detection of Chromogen III in DMSO-d_6 (a), Chromogen I (b) and Chromogen III (c) in D_2O in ^1H NMR spectra of NAG conversion with 2 equiv. $B(OH)_3$ in 750 mg [Bmim]Cl and 3 mL EtOAc, heated by microwave irradiation at 180 °C.

3.4.10 ^{11}B NMR Spectroscopy

Detection of boron signals in solutions with different pH: 300 mg (1.36 mmol) NAG, 2 molar equivalents of $B(OH)_3$ and 1 molar equivalent of NaCl were dissolved in 5 mL D_2O. Another four aqueous NAG solutions were prepared in a similar way, and NaOD solutions (0.036 and 0.060 mol/L) were added for pH adjustment. After equilibration for 12 h, the pH values of these five solutions were measured, followed by their analysis via ^{11}B NMR spectroscopy.

pH change and ^{11}B shift before and after reactions: three aqueous NAG solution samples, which were acidic (pH = 4.1), neutral (pH = 7.8) and basic (pH = 9.5), were prepared for microwave reactions at 180 °C for 10 min. The pH values were measured when the reactions were completed and the samples were analyzed using ^{11}B NMR spectroscopy.

Limit of detection: 300 mg (1.36 mmol) NAG and 2 molar equivalents of $B(OH)_3$ were dissolved in 5 mL D_2O. After equilibration for 12 h, the pH was measured and ^{11}B NMR spectroscopy was performed. Then 0.5 mL of the solution was taken and diluted by adding 4.5 mL D_2O. The pH of this new solution was measured and the ^{11}B NMR spectrum was taken. The dilution procedure was repeated and every new solution obtained was analyzed using ^{11}B NMR spectroscopy after pH measurement, until there was no signal detected in the ^{11}B NMR spectrum. In the experiment with NaCl addition, 1 molar equivalent of NaCl was added together with 300 mg (1.36 mmol) NAG and 2 molar equivalents of $B(OH)_3$ in 5 mL D_2O, and the same procedure was followed.

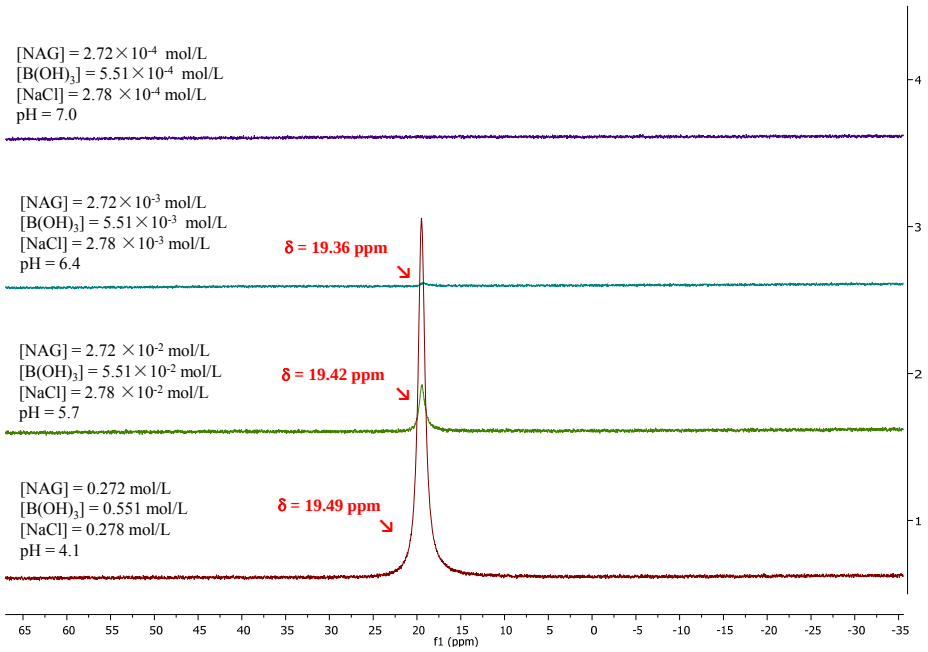

Figure 3-27. Limit of detection of ^{11}B NMR spectroscopy for D_2O solutions of NAG/$B(OH)_3$/ NaCl (acidic environment).

3.4.11 IL Reuse

100 mg (0.452 mmol) NAG, 2 molar equivalents of $B(OH)_3$, 750 mg (4.29 mmol) [Bmim]Cl and 9 mL EtOAc were added into a 10 - 20 mL microwave vial and the mixture was heated at 180 °C for 9 min. The EtOAc layer was collected after the reaction was completed. Extractions of the reaction mixture were performed using 3 × 5 mL EtOAc. The [Bmim]Cl phase was isolated and 9 mL EtOAc was added and heated again (180 °C, 9 min), the EtOAc layer was collected and another three extractions were performed. Aliquots of the extraction part and the reaction mixture (10 - 20 mg) were taken for

quantification and NMR analysis. Afterwards, 100 mg fresh NAG and 9 mL EtOAc were added to the reaction mixture for the new run.

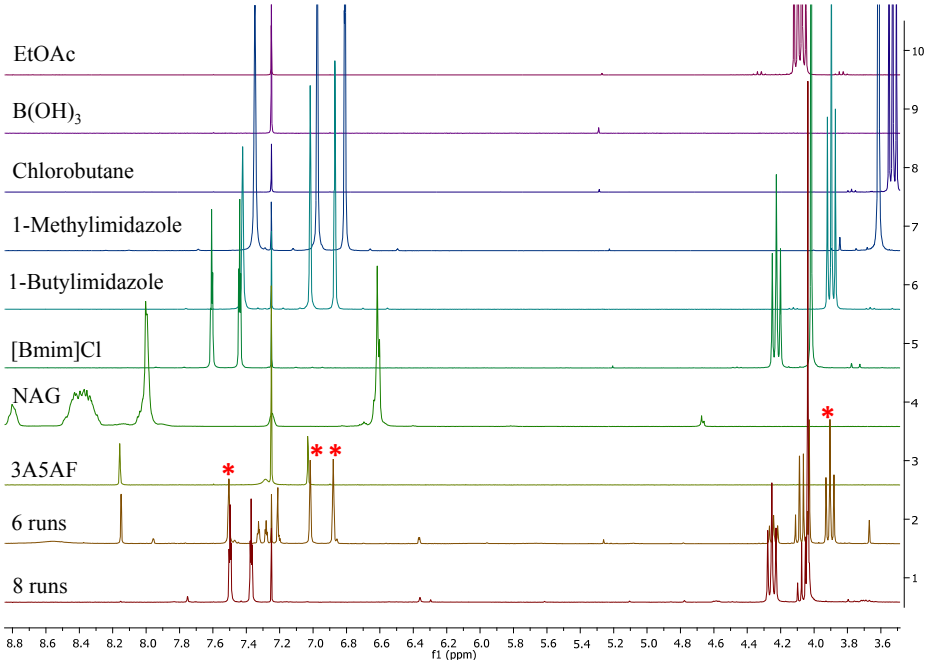

Figure 3-28. Decomposition of [Bmim]Cl in the conversion of NAG with 2 equiv. $B(OH)_3$ in 750 mg [Bmim]Cl and 9 mL EtOAc, heated by microwave irradiation at 180 °C (starred peaks are from possible decomposition products).

3.5 References

1. B. M. Upton and A. M. Kasko, *Chem. Rev.*, 2015, **116**, 2275-2306.

2. U. Addepally and C. Thulluri, *Fuel*, 2015, **159**, 935-942.

3. B. R. Caes, R. E. Teixeira, K. G. Knapp and R. T. Raines, *ACS Sustainable Chem. Eng.*, 2015, **3**, 2591-2605.

4. J. N. Chheda, G. W. Huber and J. A. Dumesic, *Angew. Chem. Int. Ed.*, 2007, **46**, 7164-7183.

5. P. Zhou and Z. Zhang, *Catal. Sci. Technol*, 2016, **6**, 3694-3712.

6. A. Chinnappan, C. Baskar and H. Kim, *RSC Adv.*, 2016, **6**, 63991-64002.

7. Z. Xue, M.-G. Ma, Z. Li and T. Mu, *RSC Adv.*, 2016, **6**, 98874-98892.

8. M. W. Drover, K. W. Omari, J. N. Murphy and F. M. Kerton, *RSC Adv.*, 2012, **2**, 4642-4644.

9. R. A. Franich, S. J. Goodin and A. L. Wilkins, *J. Anal. Appl. Pyrolysis*, 1984, **7**, 91-100.

10. K. W. Omari, L. Dodot and F. M. Kerton, *ChemSusChem*, 2012, **5**, 1767-1772.

11. X. Chen, S. L. Chew, F. M. Kerton and N. Yan, *Green Chem.*, 2014, **16**, 2204-2212.

12. X. Chen, Y. Liu, F. M. Kerton and N. Yan, *RSC Adv.*, 2015, **5**, 20073-20080.

13. G. C. T. Curtis, MSc Research, Memorial University of Newfoundland, 2014.

14. M. E. Zakrzewska, E. Bogel-Łukasik and R. Bogel-Łukasik, *Energy Fuels*, 2010, **24**, 737-745.

15. R. C. Remsing, R. P. Swatloski, R. D. Rogers and G. Moyna, *Chem. Commun.*, 2006, 1271-1273.

16. Y. Fukaya, A. Sugimoto and H. Ohno, *Biomacromolecules*, 2006, **7**, 3295-3297.

17. P. Mäki-Arvela, I. Anugwom, P. Virtanen, R. Sjöholm and J.-P. Mikkola, *Ind. Crops Prod.*, 2010, **32**, 175-201.

18. R. P. Swatloski, S. K. Spear, J. D. Holbrey and R. D. Rogers, *J. Am. Chem. Soc.*, 2002, **124**, 4974-4975.

19. A. A. Rosatella, L. C. Branco and C. A. Afonso, *Green Chem.*, 2009, **11**, 1406-1413.

20. J. S. Moulthrop, R. P. Swatloski, G. Moyna and R. D. Rogers, *Chem. Commun.*, 2005, 1557-1559.

21. A. Xu, J. Wang and H. Wang, *Green Chem.*, 2010, **12**, 268-275.

22. A. Morone, M. Apte and R. Pandey, *Renewable Sustainable Energy Rev.*, 2015, **51**, 548-565.

23. M. B. Fusaro, V. Chagnault and D. Postel, *Carbohydr. Res.*, 2015, **409**, 9-19.

24. T. Wang, M. W. Nolte and B. H. Shanks, *Green Chem.*, 2014, **16**, 548-572.

25. R.-J. van Putten, J. C. van der Waal, E. De Jong, C. B. Rasrendra, H. J. Heeres and J. G. de Vries, *Chem. Rev.*, 2013, **113**, 1499-1597.

26. T. Ståhlberg, S. Rodriguez‐Rodriguez, P. Fristrup and A. Riisager, *Chem. Eur. J.*, 2011, **17**, 1456-1464.

27. Z. Ding, J. Shi, J. Xiao, W. Gu, C. Zheng and H. Wang, *Carbohydr. Polym.*, 2012, **90**, 792-798.

28. F. Tao, H. Song and L. Chou, *RSC Adv.*, 2011, **1**, 672-676.

29. T. Okano, K. Qiao, Q. Bao, D. Tomida, H. Hagiwara and C. Yokoyama, *Appl. Catal., A*, 2013, **451**, 1-5.

30. Y. Roman-Leshkov, C. J. Barrett, Z. Y. Liu and J. A. Dumesic, *Nature*, 2007, **447**, 982-985.

31. D. Prat, J. Hayler and A. Wells, *Green Chem.*, 2014, **16**, 4546-4551.

32. C. E. Grimshaw, *Carbohydr. Res.*, 1986, **148**, 345-348.

33. P. W. Wertz, J. C. Garver and L. Anderson, *J. Am. Chem. Soc.*, 1981, **103**, 3916-3922.

34. W. T. J. Morgan and L. A. Elson, *Biochem. J*, 1934, **28**, 988-995.

35. R. Kuhn and G. Krüger, *Chem. Ber.*, 1956, **89**, 1473-1486.

36. M. Ogata, T. Hattori, R. Takeuchi and T. Usui, *Carbohydr. Res.*, 2010, **345**, 230-234.

37. M. Osada, K. Kikuta, K. Yoshida, K. Totani, M. Ogata and T. Usui, *Green Chem.*, 2013, **15**, 2960-2966.

38. R. Kuhn and G. Krüger, *Chem. Ber.*, 1957, **90**, 264-277.

39. V. Derevitskaya, L. Likhosherstov, V. Schennikov and N. Kochetkov, *Carbohydr. Res.*, 1971, **20**, 285-291.

40. N. Pravdic and H. G. Fletcher Jr, *J. Org. Chem.*, 1967, **32**, 1806-1810.

41. K. Chiku, M. Nishimoto and M. Kitaoka, *Carbohydr. Res.*, 2010, **345**, 1901-1908.

42. R. van den Berg, J. A. Peters and H. van Bekkum, *Carbohydr. Res.*, 1994, **253**, 1-12.

43. S. Chapelle and J.-F. Verchere, *Tetrahedron*, 1988, **44**, 4469-4482.

44. M. Makkee, A. Kieboom and H. Van Bekkum, *Recl. Trav. Chim. Pays-Bas*, 1985, **104**, 230-235.

45. B. R. Caes, M. J. Palte and R. T. Raines, *Chem. Sci.*, 2013, **4**, 196-199.

46. D. H. Lukamto, P. Wang and T. P. Loh, *Asian J. Org. Chem.*, 2013, **2**, 947-951.

47. H. Zhao, J. E. Holladay, H. Brown and Z. C. Zhang, *Science*, 2007, **316**, 1597-1600.

48. S. Hu, Z. Zhang, J. Song, Y. Zhou and B. Han, *Green Chem.*, 2009, **11**, 1746-1749.

49. J. Tang, X. Guo, L. Zhu and C. Hu, *ACS Catal.*, 2015, **5**, 5097-5103.

50. B. Chan, N. Chang and M. Grimmett, *Aust. J. Chem.*, 1977, **30**, 2005-2013.

51. Z. Zhang, W. Liu, H. Xie and Z. K. Zhao, *Molecules*, 2011, **16**, 8463-8474.

52. J. H. Clark and S. J. Tavener, *Org. Process Res. Dev.*, 2007, **11**, 149-155.

53. F. E. Wolter, K. Schneider, B. P. Davies, E. R. Socher, G. Nicholson, O. Seitz and R. D. Süssmuth, *Org. Lett.*, 2009, **11**, 2804-2807.

54. K. Schneider, S. Keller, F. E. Wolter, L. Röglin, W. Beil, O. Seitz, G. Nicholson, C. Bruntner, J. Riedlinger and H. P. Fiedler, *Angew. Chem. Int. Ed.*, 2008, **47**, 3258-3261.

55. S. A. Dharaskar, M. N. Varma, D. Z. Shende, C. K. Yoo and K. L. Wasewar, *The Scientific World Journal*, 2013, **2013**.

56. X. Wang, W. Wu, G. Tu and K. Jiang, *Zhongshan Daxue Xuebao, Ziran Kexueban*, 2009, **48**, 69-72.

57. H. Shekaari, Y. Mansoori and R. Sadeghi, *J. Chem. Thermodyn.*, 2008, **40**, 852-859.

58. M. Yoshizawa-Fujita, T. Kinoshita, Y. Ono, Y. Takeoka and M. Rikukawa, *Chem. Lett.*, 2013, **42**, 1185-1187.

59. D. W. Kim, D. J. Hong, K. S. Jang and D. Y. Chi, *Adv. Synth. Catal.*, 2006, **348**, 1719-1727.

60. E. Priede, S. Brica, N. Udris and A. Zicmanis, *ARKIVOC*, 2015, **7**, 243-252.

61. A. Brandt, M. J. Ray, T. Q. To, D. J. Leak, R. J. Murphy and T. Welton, *Green Chem.*, 2011, **13**, 2489-2499.

62. J. Gui, X. Cong, D. Liu, X. Zhang, Z. Hu and Z. Sun, *Catal. Commun.*, 2004, **5**, 473-477.

63. J. M. Obliosca, S. D. Arco and M. H. Huang, *J. Fluoresc.*, 2007, **17**, 613-618.

Chapter 4

Combined Experimental and Computational Studies on the Physical and Chemical Properties of the Renewable Amide, 3-Acetamido-5-acetylfuran

A version of this chapter has been published.

Yi Liu, Christopher N. Rowley* and Francesca M. Kerton*

Combined Experimental and Computational Studies on the Physical and Chemical Properties of the Renewable Amide, 3-Acetamido-5-acetylfuran, *ChemPhysChem*, 2014, **15**, 4087-4094.

Some modifications were made to the original paper for inclusion as a chapter in this thesis. For example, the supporting information was incorporated in this chapter.

4.1 Introduction

Nowadays chemicals generated from biomass are being studied extensively because of the potential crisis surrounding the depletion of fossil fuels. Biomass can be derived from plants or animals, including lignocellulosic biomass. To date, the products obtained from biomass mainly contain C, H and O atoms.[1-7] The use of biomass-feedstocks containing other elements and functional groups would broaden the range of chemicals that can be derived from biomass. Therefore, the synthesis of renewable compounds containing heteroatoms is of considerable interest but remains relatively underexplored.[8, 9] Chitin is an abundant biopolymer and can be obtained from the shells of crustaceans (i.e. fishery/food industry waste).[10, 11] NAG is the monomer of chitin, and can be converted to a *N*-containing product, 3A5AF, through dehydration (Scheme 4-1). As far as the Kerton group is aware, 3A5AF is the first reported nitrogen-containing product that can be obtained from the dehydration of a hexose in solution,[12] and it is hoped to be a building block for a range of renewable amines and polymers in the future. Previously, 3A5AF was obtained from NAG using pyrolysis methods, but the yields were very low (2% and 0.04%).[13, 14] In recent research, the yield of 3A5AF from NAG was increased up to 60% by the use of DMA as the solvent, with $B(OH)_3$ and NaCl as additives under microwave irradiation.[12] Very soon after that, another study on the dehydration of NAG in ILs achieved a similar yield of 3A5AF.[15] More recently, 3A5AF has been prepared directly from chitin, albeit in lower yields, due to the incalcitrant nature of the biopolymer.[16] NAG has also been partially dehydrated in superheated water under autocatalytic conditions to yield Chromogen I and

Chromogen III in yields of 23%.[17] As an alternative to dehydrative approaches to using this renewable aminosugar, the aerobic oxidation of NAG has been performed in water using gold nanoparticle catalysts to give *N*-acetylglucosaminic acid.[18]

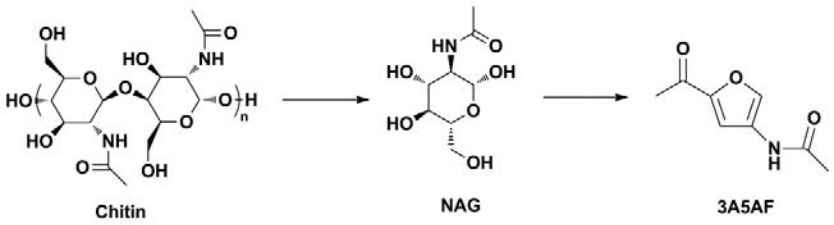

Scheme 4-1. Conversion of chitin to NAG and the dehydration of NAG to 3A5AF.

To date, no studies on the chemistry of 3A5AF beyond its preparation have been reported, so this compound is awaiting further exploration in terms of its physical and chemical properties. In this study some important properties of 3A5AF are described, including its pK_a value, intermolecular interactions and electronic structure. These properties are of interest because they are fundamental to understanding the chemistry of this renewable molecule and will allow chemists to design better routes towards its isolation. For example, could $scCO_2$ be used to extract this product in an environmentally friendly way from reaction mixtures, or could acidification/basification approaches be used to separate this amide from non-*N*-containing by-products (e.g. LA, 5-HMF) in a biorefinery using shellfish waste as a feedstock? The pK_a of 3A5AF will be important in determining its reactivity in this regard. Furthermore, these data could help predict other possible reactions and optimizations to obtain desirable products.

Computational chemistry has become very effective in predicting properties of compounds and explaining their behaviour.[19-21] In this way, computational work can be thought of as a complement to experimental research. In this study, we used computational calculations to predict the pK_a value and possible reaction sites within 3A5AF, and to explain the solubility performance of 3A5AF in the non-polar "green" solvent $scCO_2$.

4.2 Results and Discussion

4.2.1 pK_a Calculation and Measurement

In this study, DMSO was chosen as the solvent because it permits a wide range of pK_a values from 0 to 30 to be determined and also allows easy comparison with other values in the scientific literature.[22, 23] Computational investigations were performed before UV-Vis titrations, so that an indicator with an appropriate pK_a range could be selected.

4.2.1.1 Computational Studies

The pK_a of a molecule is related to the standard Gibbs energy of deprotonation in solution (ΔG^o_{soln}) by the relation $pK_a = \Delta G^o_{soln}/(RTln10)$. The thermodynamic cycle in Scheme 4-2 was used, following the computational procedure of Sadlej-Sosnowska.[24-27] The Gibbs energy change in solution (ΔG^o_{soln}) is the sum of the Gibbs energy change in the gas-phase (ΔG^o_g) and the change in the solvation energy (ΔG^o_s).

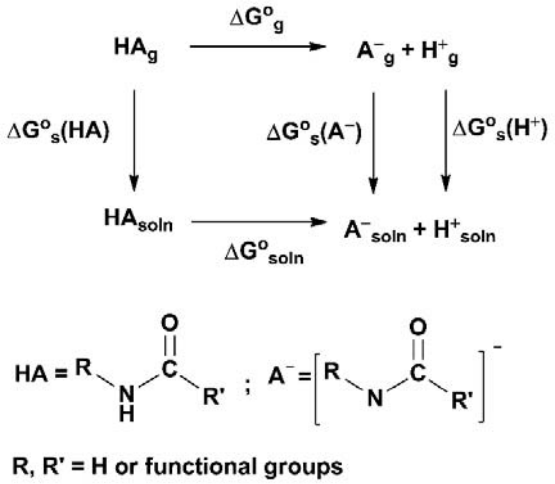

Scheme 4-2. A thermodynamic cycle of an amide HA.

From Scheme 4-2, Equations 4-1, 4-2 and 4-3 are obtained as follows (HA is the molecule of interest):

$$\Delta G^{o}_{soln} = \Delta G^{o}_{g} + \Delta G^{o}_{s}$$

Equation 4-1

$$\Delta G^{o}_{g} = G^{o}(A^{-}_{g}) + G^{o}(H^{+}_{g}) - G^{o}(HA_{g})$$

Equation 4-2

$$\Delta G^{o}_{s} = \Delta G^{o}_{s}(A^{-}) + \Delta G^{o}_{s}(H^{+}) - \Delta G^{o}_{s}(HA)$$

Equation 4-3

Although some studies have attempted to calculate the absolute pK_a from computational data,[28-31] there are limitations to the accuracy of these methods, due to the sensitivity of the pK_a to small errors in the calculation of ΔG^{o}_{soln} and uncertainty in the

solvation energy of a proton.[26, 32, 33] Instead, in the current study the pK_a of 3A5AF is calculated relative to amides with known pK_a values. As pK_a = ΔG^o_{soln}/(RTln10), for two compounds the relationship pK_{a1} - pK_{a2} = (ΔG^o_{soln1} - ΔG^o_{soln2})/(RTln10) will exist. The advantage of this method is that uncertainty associated with the solvation energy of a proton is eliminated. For this method, another acid with a known pK_a value is needed. Ideally, acids with similar structures and acidities are used. During the model establishment for species in solution, the solvent effect was considered. The solvation energy is calculated from the difference between the standard Gibbs energy in solution and the standard Gibbs energy in the gas-phase. The pK_a values of a series of aromatic amides were used as references, thus several pK_a values of 3A5AF were calculated and found to be in the range of 18.5 - 21.5 (Table 4-1). These pK_a values are similar to those of most amides,[22, 23] indicating that 3A5AF has a weak Brønsted acidity. The importance of solvation to the relative acidities of amides is apparent when the pK_a values calculated for solution are compared to those calculated for the gas phase. For example, with solvation taken into account, a pK_a of 18.5 was obtained using phenylacetamide as a reference, but a significantly more acidic value of 14.8 was predicted based on gas-phase calculations.

Table 4-1. pK_a(DMSO) of 3A5AF estimated computationally using the pK_a(DMSO) of amides as references and measured experimentally using UV-Vis titration.[a]

	Reference Compounds[b]	ΔG^o_g[c] (kJ/mol)	ΔG^o_s[c] (kJ/mol)	pK_a of 3A5AF[d]
Computational estimates	Phenylacetamide (21.4)	1463.48	-188.55	18.5
	Benzamide (23.4)	1499.89	-226.76	20.7
	Isonicotinamide (21.5)	1450.79	-192.23	21.4
	2-Thiophenecarboxamide (22.3)	1484.24	-222.19	21.5
	Phenoxyacetamide (23.0)	1465.85	-193.47	20.5
Experimental measurement	–	–	–	20.7 ± 0.1

a. The Gibbs energy changes in the gas phase were calculated using G3MP2.[36] The solvation energy changes were calculated using the PCM-B3LYP/6-311+G(2d,p) method.[37-40] b. The reference pK_a values were obtained from experimental data.[22, 23] c. Gas-phase energy changes and solvation energy changes of the compounds with known pK_a values. d. ΔG^o_g(3A5AF) = 1424.17 kJ/mol; ΔG^o_s(3A5AF) = -166.31 kJ/mol.

4.2.1.2 Experimental Measurement via UV-Vis Titration

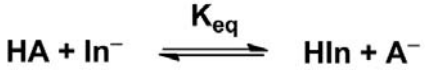

Scheme 4-3. Equilibrium between the indicator (HIn) and the compound of interest (HA) in solution.

In order to measure the pK_a of 3A5AF experimentally, an overlapping indicator method was used.[34, 35] An acid (HIn) with a known pK_a value is used as the indicator and its conjugate anion (In^-) must give rise to a strong absorption in the UV-Vis region. The

solution of the unknown acid is then added to the indicator solution, and an equilibrium will form as shown in Scheme 4-3.

The pK_a value of HA can be calculated using Equation 4-4, which relates this to the pK_a value of the indicator:

$$pK_a(HA) = pK_a(HIn) - \log K_{eq} = pK_a(HIn) - \log\{([HIn][A^-])/([HA][In^-])\}$$

Equation 4-4

In the UV-Vis spectra, a wavelength is chosen at which only the absorption of one species in the equilibrium is observed and the intensity of absorption at this wavelength is monitored as concentrations change. By recording these changes during the titration, the concentration of the species can be determined using Beer's law, and the concentrations of the other three species present can be calculated by using the reaction equation.

Fluorene (pK_a = 22.6) was selected as the indicator on the basis of its similar pK_a to those determined computationally for 3A5AF (Table 4-1). The average pK_a value of 3A5AF was 20.7 ± 0.1, after obtaining titration data in triplicate. This value is within the range of the computational calculations, and is closest to the computational result obtained using benzamide as the reference, 20.7 (Table 4-1). This indicates that pK_a estimates provided by computation are reasonable. This value is slightly lower than the values of most amides reported in the literature,[22, 23] but overall 3A5AF is still a very weak acid. The fact that benzamide (a primary amide) rather than phenylacetamide (a secondary amide) gave the closest computational result to the experimental data is a little surprising. It was assumed that phenylacetamide, which has the most similar structure to 3A5AF compared

with other amides employed, would give the best agreement between experiment and theory. A systematic determination of amide pK_a values by using a consistent experimental method could resolve some of these discrepancies.

4.2.2 Solubility Measurement

4.2.2.1 Determination of Solubility of 3A5AF in Supercritical Carbon Dioxide Using a Phase Monitor

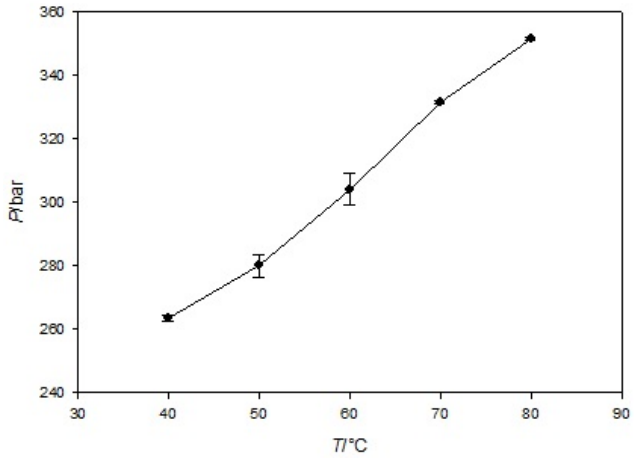

Figure 4-1. Temperature-pressure phase diagram for 3A5AF in $scCO_2$/methanol. Error bars: pressure ± 0.3 to 5.1 bar.

The phase behavior of 3A5AF in $scCO_2$ was studied by use of a phase monitor. A small amount of solid 3A5AF (17.5 mg) was placed in the cell and then liquid CO_2 (30 mL) was added. In neat $scCO_2$, at 60 °C and pressures up to 462 bar, the mixture in the cell was cloudy indicating incomplete dissolution. Therefore, methanol was used as a co-solvent. 3A5AF was dissolved in methanol first and the solution was injected into the cell. The

mixture could be readily dissolved at all temperatures tested by increasing the pressure to certain values. The mole fraction solubility was determined to be 3.23×10^{-4}. Cloud points were observed at the following pressures (in bar) at all five temperatures: 40 °C, 263.5 ± 0.9; 50 °C, 280.1 ± 3.7; 60 °C, 304.2 ± 5.1; 70 °C, 331.8 ± 0.5; 80 °C, 351.7 ± 0.3 (Figure 4-1). Compared with the solubilities of several other biosourced molecules in $scCO_2$/methanol also determined by the Kerton group,[41] from 45 to 80 °C, 3A5AF is more soluble than tartaric acid, less soluble than 2,5-furandicarboxylic acid, fumaric acid, oxalacetic acid and malic acid, and has a similar solubility to succinic acid. However, it is significantly less soluble than 5-HMF, which is the product of fructose and glucose dehydration reactions and is prepared in a similar way to 3A5AF. 5-HMF is soluble in neat $scCO_2$ and does not need a hydrogen-bonding co-solvent to dissolve in this medium. This likely indicates that the intermolecular forces between molecules of 3A5AF (solute-solute interactions) are significantly stronger in comparison to 5-HMF. For sugars and their amide derivatives, Potluri et al. showed that acetylation increased the solubilities of these compounds in $scCO_2$ because hydrogen bonding between solute molecules was reduced.[42] As $scCO_2$ is a nonpolar solvent and has a relatively low density,[43] only substances with weak solute-solute interactions will dissolve readily in it without an additional co-solvent. Computational studies were undertaken in order to get a more detailed understanding of the differences in strength of solute-solute interactions between 5-HMF and 3A5AF.

4.2.2.2 Calculation of Dimerization Energy

In order to investigate the factors influencing the solubility of 3A5AF and 5-HMF in $scCO_2$, we modeled the intermolecular interactions for these compounds. These calculations are based on the Gibbs energy of mixing.

$$\Delta G_{mix} = \Delta H_{mix} - T\Delta S_{mix}$$

Equation 4-5

From the experimental studies, for a binary mixture of $scCO_2$ and these furans, ΔG_{mix}(5-HMF) < ΔG_{mix}(3A5AF). As experimentally, the temperature range and mole ratios of solute to solvent were similar, one can assume that $T\Delta S_{mix}$(5-HMF) ≈ $T\Delta S_{mix}$(3A5AF). The differences in ΔG_{mix} (Equation 4-5) for these two systems must arise from enthalpic contributions i.e. their intermolecular interactions. These intermolecular interactions favor the separation of the solute into a separate phase. Beyond the common central furan-ring motif, these molecules contain different functional groups and therefore, stronger interactions such as hydrogen bonding will play a significant role in the different values of ΔG_{mix} between the two systems.

In order to examine this hypothesis, the Gibbs energies of dimerization (ΔG_{dimer}) of 5-HMF and 3A5AF molecules were calculated. 5-HMF, which dimerizes through an O–H ⋯ O=C hydrogen bond, has a ΔG_{dimer} of −10.7 kJ/mol (Figure 4-2). For 3A5AF, intermolecular hydrogen bonds can be formed between the amide N–H bond and the

carbonyl of either the amide or acetyl groups (Figure 4-3, model 1 and model 2). Dimerization energies were calculated to be –30.7 kJ/mol and –24.1 kJ/mol, respectively.

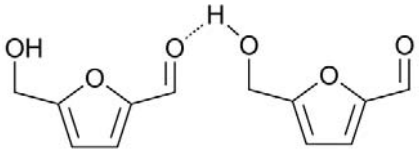

Figure 4-2. Schematic of the hydrogen bonded 5-HNMF dimer.

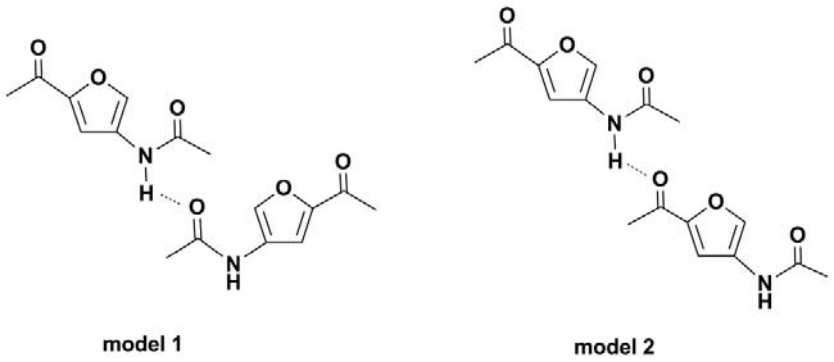

Figure 4-3. Schematics of the two putative hydrogen bonded 3A5AF dimers. (Dimerization energies: model 1: –24.1 kJ/mol; model 2: –30.7 kJ/mol).

The greater hydrogen bonding abilities of amides, such as 3A5AF, in comparison with alcohols, such as 5-HMF, is apparent in the dimerization energies. Comparing ΔG_{dimer} values, 3A5AF forms dimers more readily than 5-HMF, indicating that stronger solute-solute interactions will exist within a bulk sample of 3A5AF, and thus that is less readily dissolved in $scCO_2$. It should be noted that the enthalpic contribution from such hydrogen-bonding processes is not the exclusive reason for the observed differences in solubility, but these data clearly show the presence of stronger hydrogen bonding within 3A5AF than 5-

HMF. These results indicate that useful solvent systems for future reactions of 3A5AF will require alcohols (and other "green" hydrogen-bonding solvents) or combinations of such solvents with $scCO_2$ to overcome the hydrogen bonding-tendency of the amide moiety.

4.2.2.3 IR and NMR Detection of H-bonding in 3A5AF Molecules

In order to better prove the existence of hydrogen bonding between 3A5AF molecules, IR spectra were obtained for both a solid sample of 3A5AF and a dilute solution (Et_2O as the solvent) (Figure 4-4). The carbonyl stretching frequency ($\nu_{C=O}$) for 3A5AF was 1652.68 cm^{-1} in the solid sample and 1668.68 cm^{-1} in solution. This is a difference of 16 cm^{-1}. As the bands for $\nu_{C=O}$ of secondary amide and ketone functional groups appear in the same region, it is not possible to use IR spectroscopy to distinguish between the modes of intermolecular hydrogen bonding. However, one might assume that as 3A5AF molecules are closer together in the solid state more hydrogen bonding will occur and this might cause a shift of $\nu_{C=O}$ towards a lower frequency. In the diluted sample, interactions between 3A5AF molecules will be reduced and hydrogen bonding between the amide proton and the ethereal oxygen atom will also decrease. For 5-HMF the $\nu_{C=O}$ is 1656.65 cm^{-1} in the solid state and 1685.47 cm^{-1} in the solution (Et_2O as the solvent) (Figure 4-5). The difference is 28.8 cm^{-1}, which is larger than for 3A5AF samples. To some extent, this supports the hypothesis that stronger hydrogen bonding exists in samples of 3A5AF than in 5-HMF, as the difference between $\nu_{C=O}$ values for neat samples to diluted solutions is less for 3A5AF.

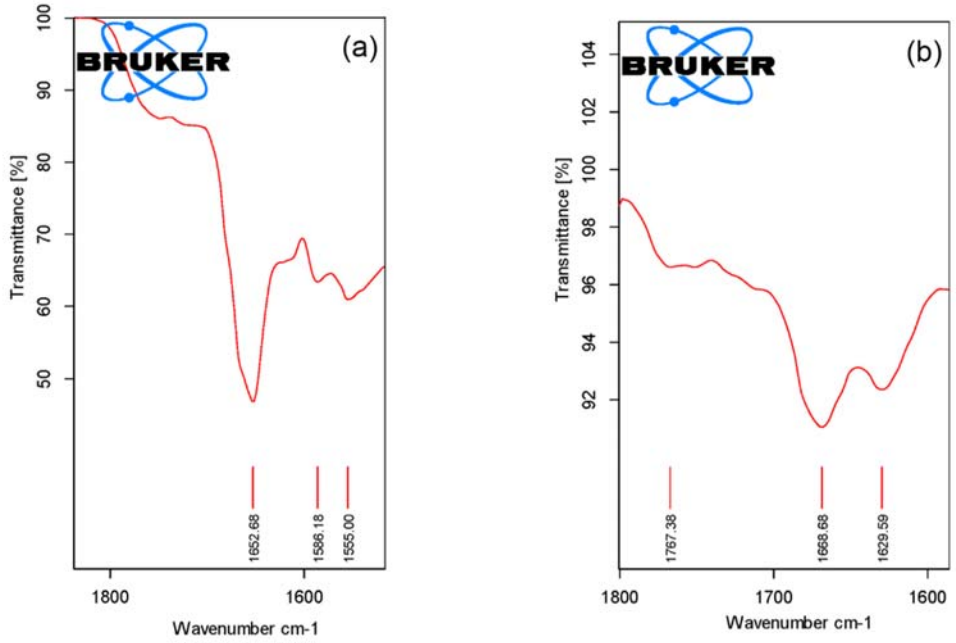

Figure 4-4. Portions of IR spectra of 3A5AF solid (a) and solution (b).

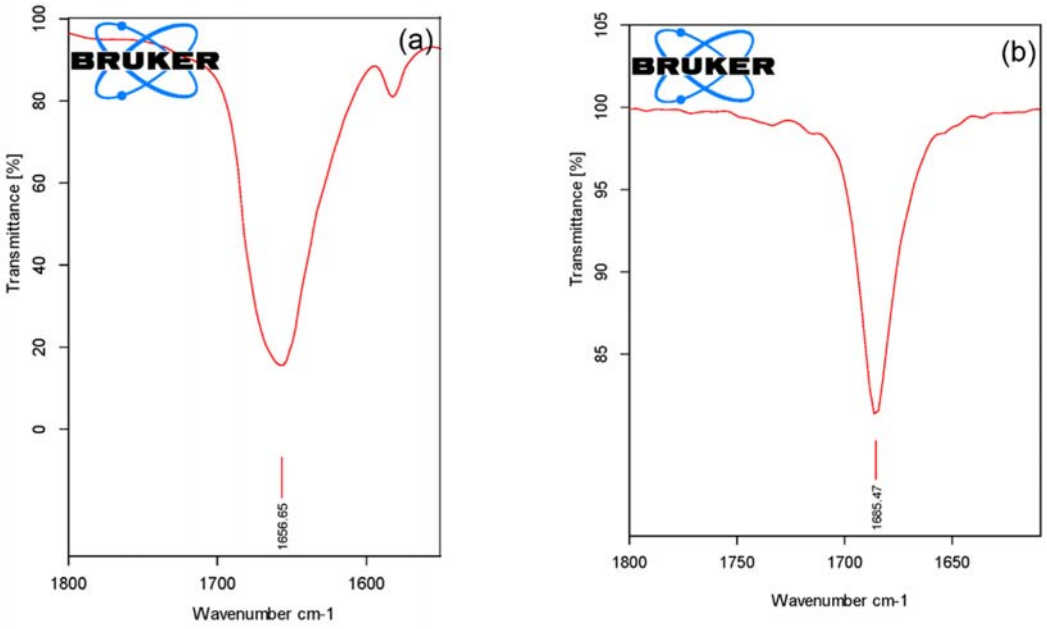

Figure 4-5. Portions of IR spectra of 5-HMF solid (a) and solution (b).

NMR spectroscopy was also used to detect the hydrogen bonding. Three NMR samples of 3A5AF with different concentrations were prepared (Figure 4-6). At 298 K, as the concentration of 3A5AF in chloroform-d ($CDCl_3$) was increased from 1.23 mg/mL to 7.35 mg/mL, δ(NH) shifted downfield from 7.18 ppm to 7.67 ppm, which is indicative of increased hydrogen bonding within the sample.[44] Spectra were also obtained at a higher temperature (323 K), and δ(NH) shifted to a lower frequency, as hydrogen bonding was disrupted by the increase in temperature (Figure 4-7). Compared with the spectra obtained at 298 K, the concentrated (7.35 mg/mL) sample exhibited a smaller temperature-dependent shift ($\delta = 0.06$ ppm), than the dilute (1.23 mg/mL) sample ($\delta = 0.13$ ppm). The more concentrated sample contains more extensive hydrogen bonding between the 3A5AF molecules, so the chemical shift varies less with changes in temperature. Finally, deuterium oxide (D_2O) was added to the samples so that deuterium exchange would occur (Figure 4-8). Qualitatively, the rate of deuterium incorporation into 3A5AF for the more concentrated samples occurred more slowly than for the dilute samples. This might also illustrate that the hydrogen bonding is stronger in the more concentrated sample, which would inhibit the rate of deuterium exchange.

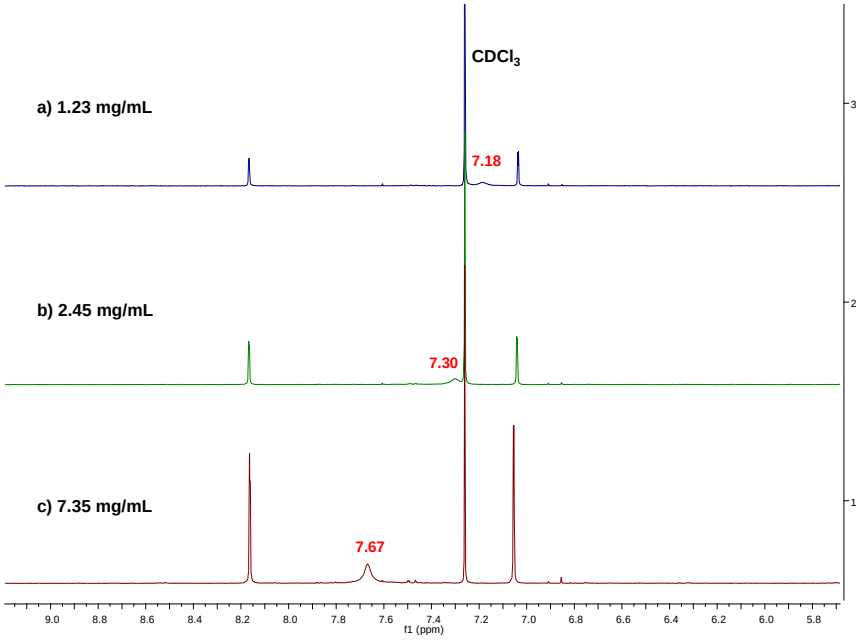

Figure 4-6. δ(NH) of 3A5AF in $CDCl_3$ solutions with different concentrations.

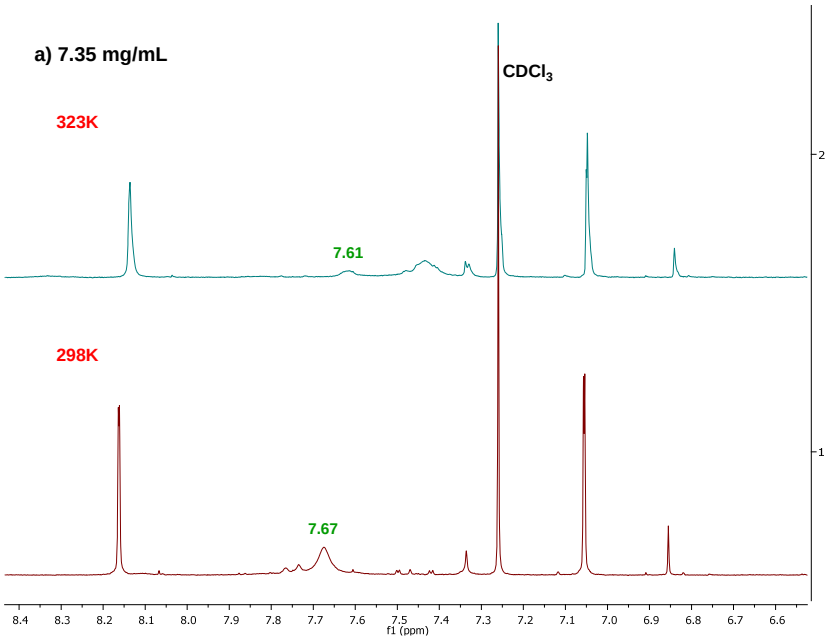

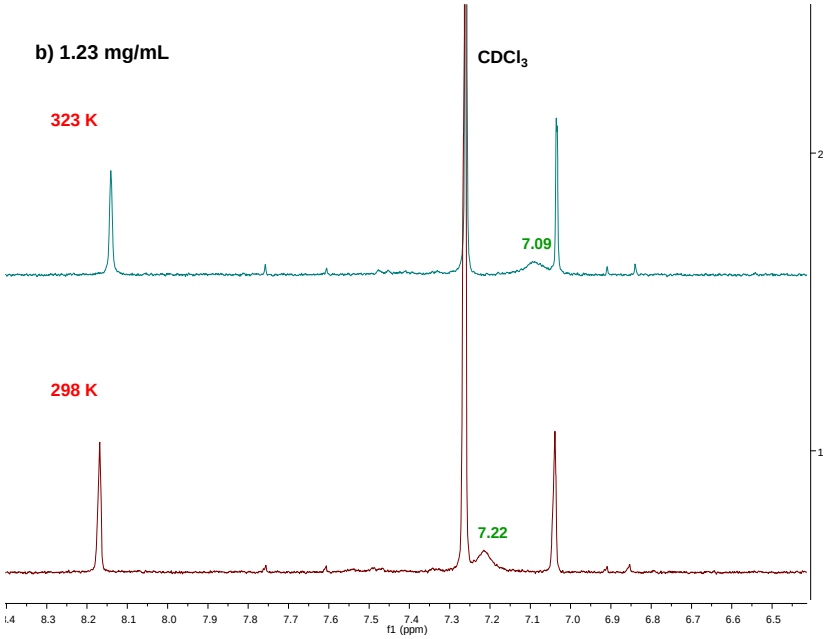

Figure 4-7. Temperature dependence of δ(NH) of 3A5AF in $CDCl_3$ solutions.

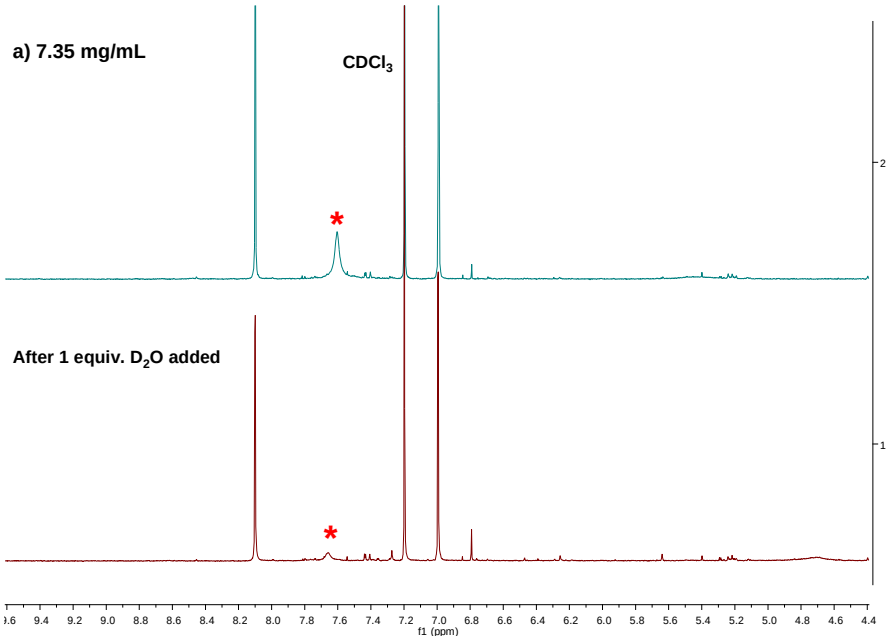

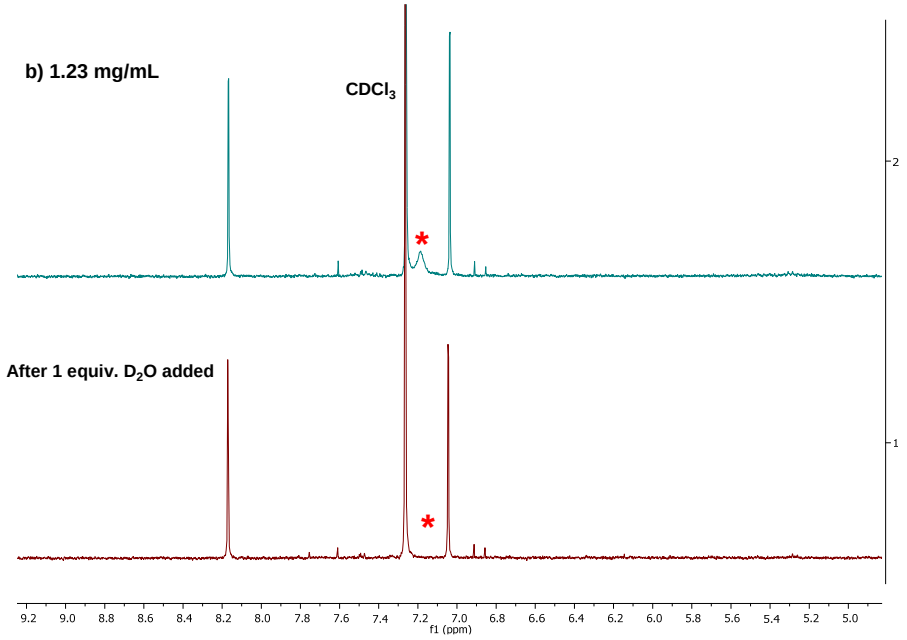

Figure 4-8. Deuterium exchange between H in the amide group of 3A5AF and D in D_2O.

4.2.3 Chemical Properties of 3A5AF

4.2.3.1 Computational Deduction

Firstly, the energies of frontier orbitals for the geometry-optimized structure of 3A5AF were calculated using a TD-DFT study. The excitation energy (ΔE) obtained was 4.278 eV, which corresponds to a wavelength of 289.83 nm. The primary component of this excitation is a π- π^* highest occupied molecular orbital (HOMO) to lowest unoccupied molecular orbital (LUMO) transition. This is in acceptable agreement with experimental data for 3A5AF, as the UV-Vis spectrum exhibits a π- π^* transition at 266.8 nm (4.650 eV). Figure 4-9 shows the isosurfaces of the frontier orbitals.

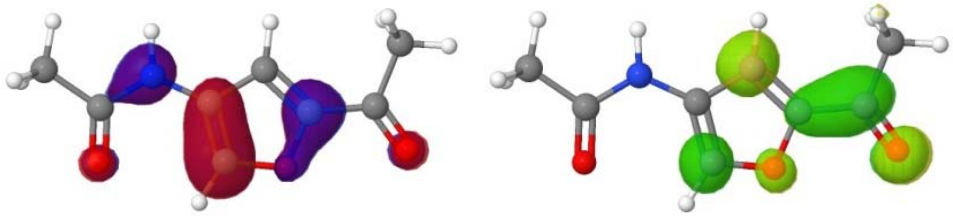

Figure 4-9. Isosurfaces of the HOMO (left) and LUMO (right) of 3A5AF.

These data were used to visualize the electrostatic potential of 3A5AF. This is affected by the electronegativity of atoms, the dipole moment and partial charges.[45] At points around the molecule, the electrostatic potential, *V(r)*, is defined as the energy required to remove a unit point charge from a point, *r*, at the molecular surface.[46, 47] Sections of the surface with a more positive electrostatic potential surface, corresponding to a net positive charge, are rendered in blue. Sections with more negative values of the electrostatic potential, corresponding to a net negative charge, are rendered in red. The colors of neutral regions range from green to yellow. The electrostatic potential map of 3A5AF is shown in Figure 4-10 (left). The surface near the carbonyl oxygens is strongly negatively charged, while the amide proton shows a blue positive charge. This is consistent with the amide-amide hydrogen-bonding interactions examined in **4.2.2.2**. The surface near the hydrogen on the 4 position of the furan ring also has a significantly positive electrostatic potential, indicating that this hydrogen is protic. In contrast, the electrostatic potential surface of 5-HMF (Figure 4-10, right) shows the molecule to be largely non-polar, consistent with the weaker dimerization energy of 5-HMF.

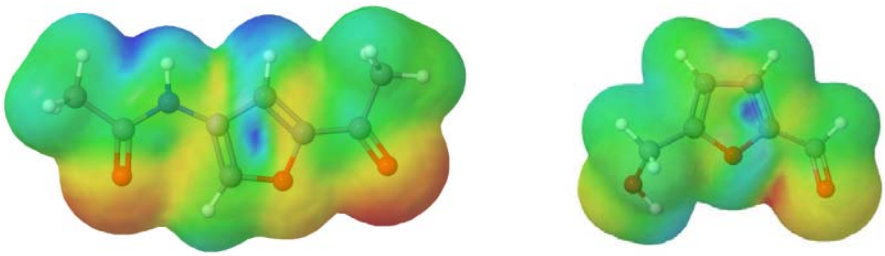

Figure 4-10. Electrostatic potential maps of 3A5AF (left) and 5-HMF (right).

In addition, the electrostatic potential (ESP) atomic partial charges of 3A5AF were calculated (Table 4-2). Surprisingly, the ESP charge of O15 (amide group) is more negative than that of O18 (acetyl group). This means that the amide of one 3A5AF molecule should form a strong hydrogen-bond with a neighbouring molecule. This contradicts conclusions based on the dimerization energies described in **4.2.2.2**. Therefore, it is believed that the steric interactions are more favorable between two 3A5AF molecules via amide-acetyl hydrogen bonding compared with amide-amide hydrogen bonding.

Table 4-2. ESP charges of several atoms in 3A5AF.[a]

3A5AF structure	Code	Atom	ESP charge (e)
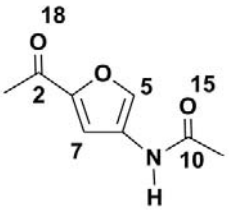	2	C	0.532
	5	C	-0.153
	7	C	-0.415
	10	C	0.791
	15	O	-0.601
	18	O	-0.511

a. The ESP charges were calculated using B3LYP/6-311+G(2d,p) method.

4.2.3.2 Reaction of 3A5AF with a Methyl Grignard Reagent

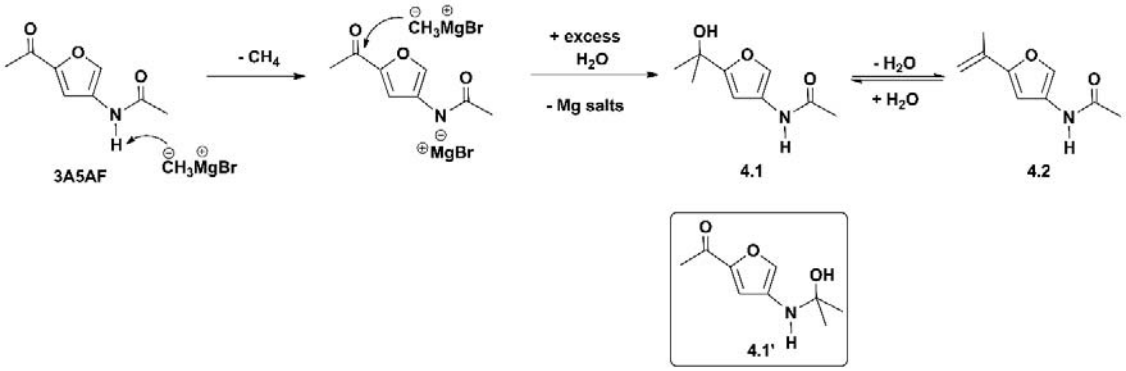

Scheme 4-4. Reaction of 3A5AF and CH_3MgBr to yield amido-alcohol (**4.1**) and alkene (**4.2**) products. Alternative product (**4.1'**), an isomer of **4.1**, is shown in the box. Reaction conditions: 51.4 mg 3A5AF, 2 equiv. CH_3MgBr solution (3.0 mol/L in Et_2O), 8 mL THF, stirred under N_2 at room temperature for 1h.

The data in Table 4-2 suggest that C10 will react more readily with a nucleophile (e.g. Grignard reagent) than C2 due to its more positive atomic charge. However, these calculations were performed on a neutral molecule and as many nucleophiles are basic, the first equivalent of such reagents will act to deprotonate the amide group. In this study, 3A5AF was mixed with two equivalents of methylmagnesium bromide (CH_3MgBr) under N_2 at room temperature for 1 h. The conditions for the reaction were chosen based on reactivity studies performed on commercially available aromatic compounds e.g. acetophenone. Upon addition of CH_3MgBr to 3A5AF, bubbles could be seen indicating the formation of methane gas as a result of deprotonation of the amide by the Grignard reagent (Scheme 4-4). After quenching using excess water and extraction, the reaction mixture was

analyzed by GC-MS, IR spectroscopy, ^{1}H and ^{13}C NMR spectroscopy. As there was approximately 26% (as indicated by ^{1}H NMR data) unreacted 3A5AF in the mixture, the reactivity of 3A5AF towards nucleophiles is relatively low compared with the analogous reaction of acetophenone where 100% conversion was achieved under identical conditions. **4.1** and **4.1'** are possible products of the Grignard reaction with 3A5AF. Unfortunately, due to the residual 3A5AF present in the mixture, the unequivocal identification of the products was challenging. GC-MS analysis showed that two products, in addition to 3A5AF, were present with retention times of 4.876 min (*m/z* 165.1 g/mol; the major product) and 5.086 min (*m/z* 183.1 g/mol) (Figure 4-11, Figure 4-12 and Figure 4-13). The latter could be assigned to product **4.1** or **4.1'** based on their mass and the former to **4.2** as proposed in Scheme 4-4 (or an imine that would form via dehydration of **4.1'**). Dehydration would be favoured in these reactions as it results in the formation of a multiple bond conjugated with the furan ring. As **4.1** and **4.1'** are isomers, the reaction work-up was varied in order to determine which products had formed. In the presence of acid, the peak assigned to **4.1** at retention time 5.086 min disappeared and the peak for **4.2** at 4.876 min grew in intensity - indicating that an acid-catalyzed dehydration had occurred (Figure 4-14). However, upon further aqueous work up in the presence of sodium bicarbonate to quench excess acid, the peak for **4.2** disappeared and a single product peak for **4.1** was observed in the GC trace. It should be noted that in a Grignard reaction of another acetyl-substituted aromatic secondary amide, *N*-(4-acetyl-3-methoxyphenyl)-acetamide, either the tertiary alcohol or hemiaminol product could be isolated depending on the exact nature of the reaction conditions employed.[48]

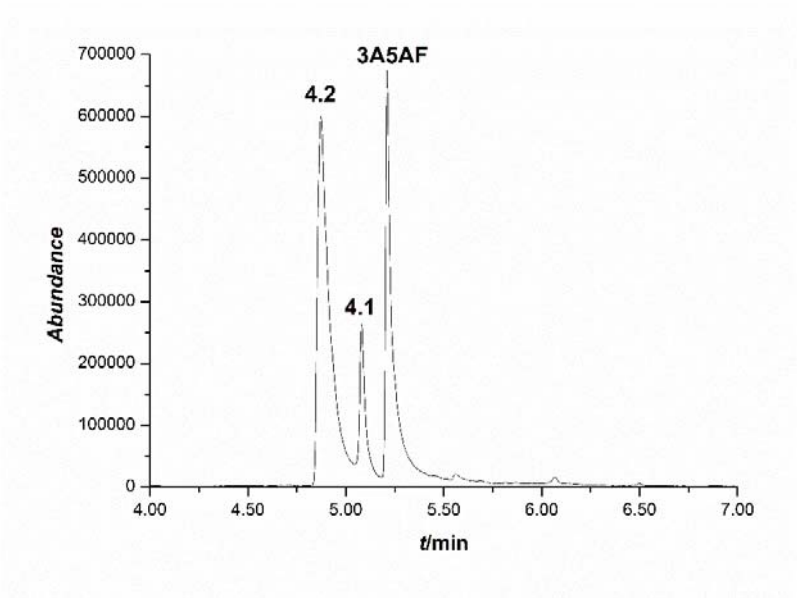

Figure 4-11. Gas chromatogram of the Grignard reaction mixture.

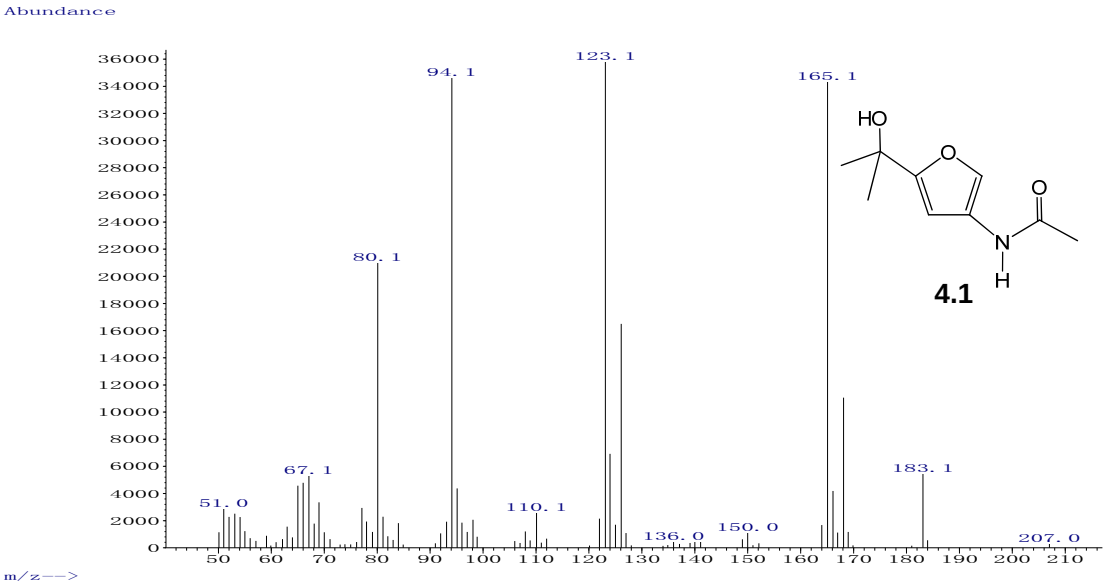

Figure 4-12. Mass spectrum of **4.1**.

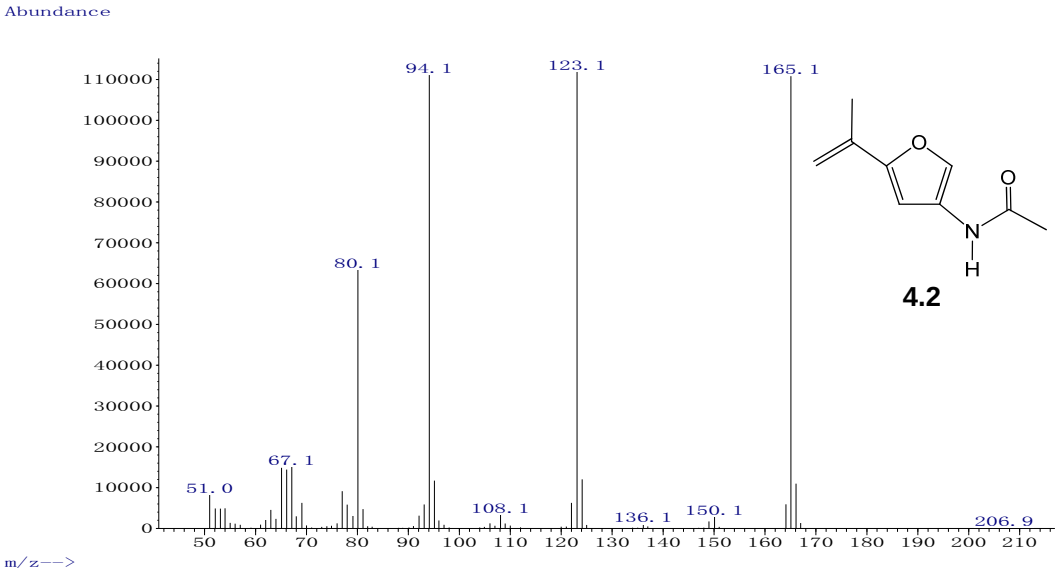

Figure 4-13. Mass spectrum of **4.2**.

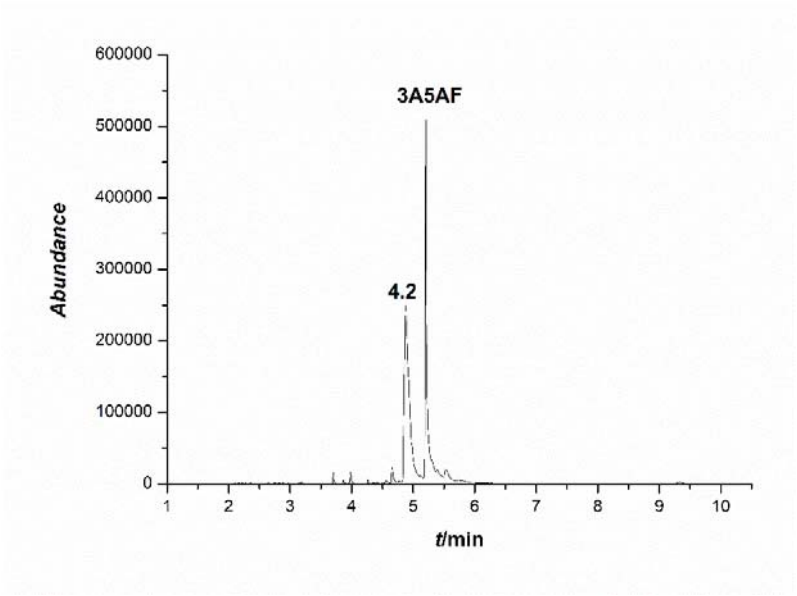

Figure 4-14. Gas chromatogram of the Grignard reaction mixture after treatment using dilute hydrochloric acid.

The IR spectrum of the reaction mixture was compared with that of pure 3A5AF (Figure 4-15). As there was still some unreacted 3A5AF in the mixture, conclusions regarding changes of $\nu_{C=O}$ could not be made. Furthermore, the generation of the alkenyl C=C bond in **4.2** could not be confirmed because the range of $\nu_{C=C}$ would overlap with the aromatic $\nu_{C=C}$ of the furan ring. However, the IR ν_{C-H} bands of the methyl groups increased in intensity for the reaction mixture (2920 - 2978 cm^{-1}), confirming the addition of a methyl group.

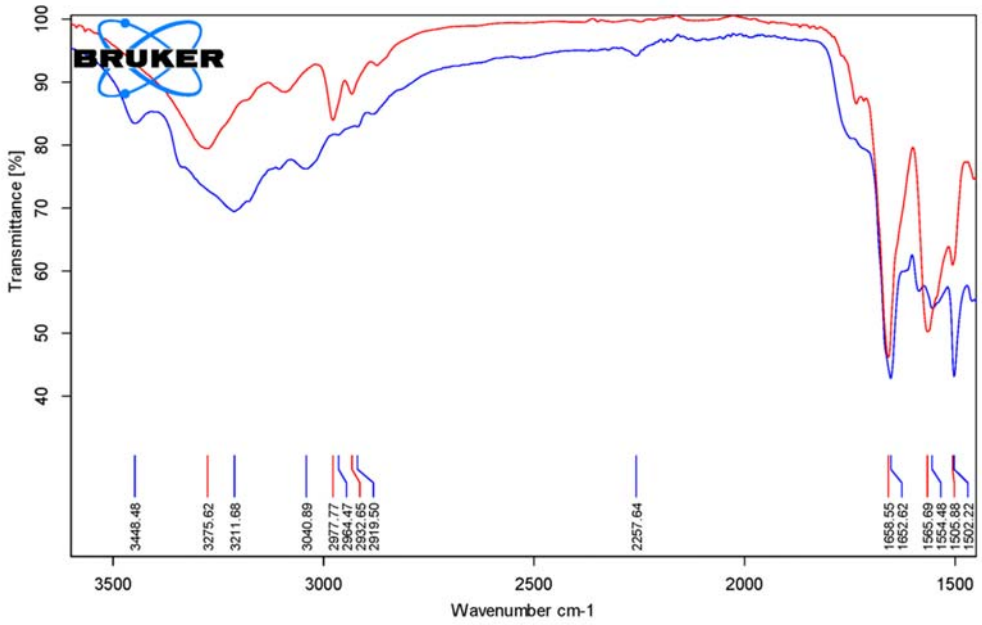

Figure 4-15. IR spectral comparison of the Grignard reaction mixture (red) and pure 3A5AF (blue).

In addition to IR and mass spectrometric analysis, NMR spectra of possible products were predicted computationally, and were compared with the experimental results. In the

experimental ^{13}C NMR spectrum (Figure 4-16), a peak at 167.4 ppm was assigned to δ(CO) in the product **4.1**. The predicted δ(CO) occurs at a higher frequency (176.0 ppm, Figure 4-17) but was acceptably in accordance with the experimental data. The alcoholic quaternary C atom in **4.1** has a predicted chemical shift of 74.9 ppm (cf. 67.8 ppm experimentally) and is located in a unique position within the ^{13}C NMR spectrum compared with the predicted spectra of **4.1**' (Figure 4-18). This strongly suggests that the product of the Grignard reaction is a tertiary alcohol. Although, ^{13}C NMR spectroscopy, both experimental and computational, has aided in identifying **4.1** - it cannot be relied on alone to unequivocally identify the reaction products.

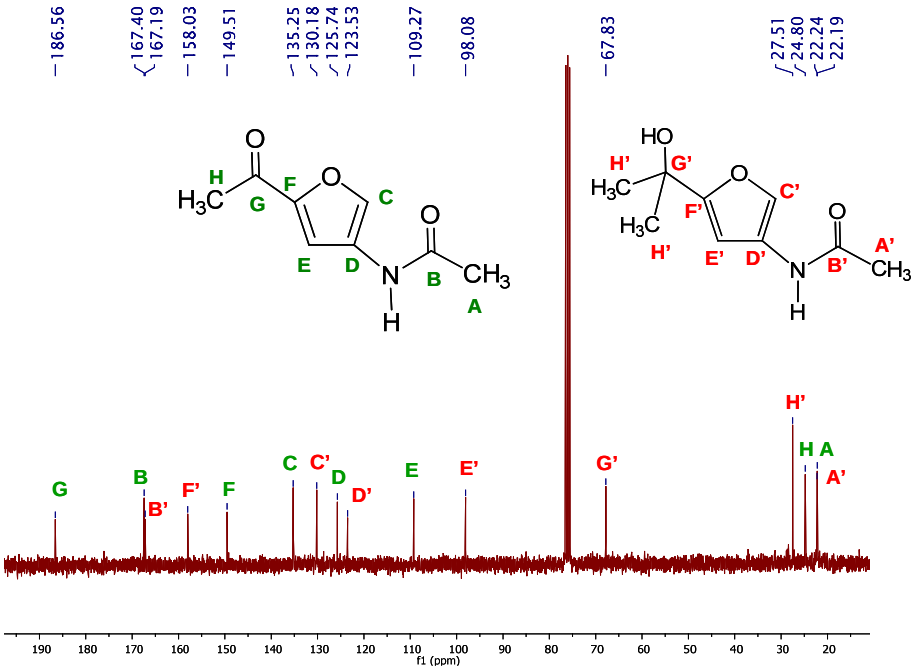

Figure 4-16. ^{13}C NMR spectrum of the Grignard reaction mixture. (Separation of 3A5AF and the product **4.1** was not possible.)

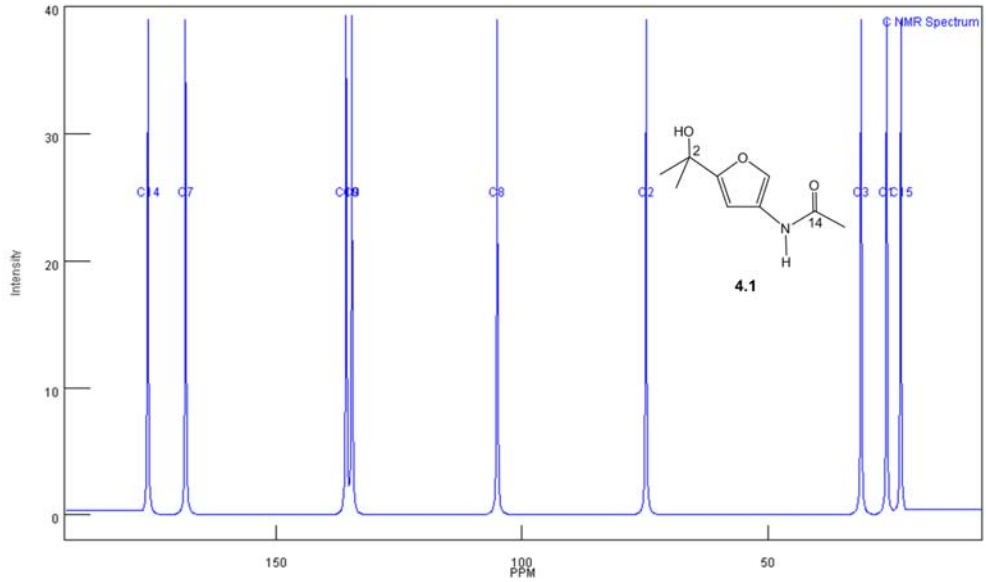

Figure 4-17. Predicted ^{13}C NMR spectrum of **4.1**.

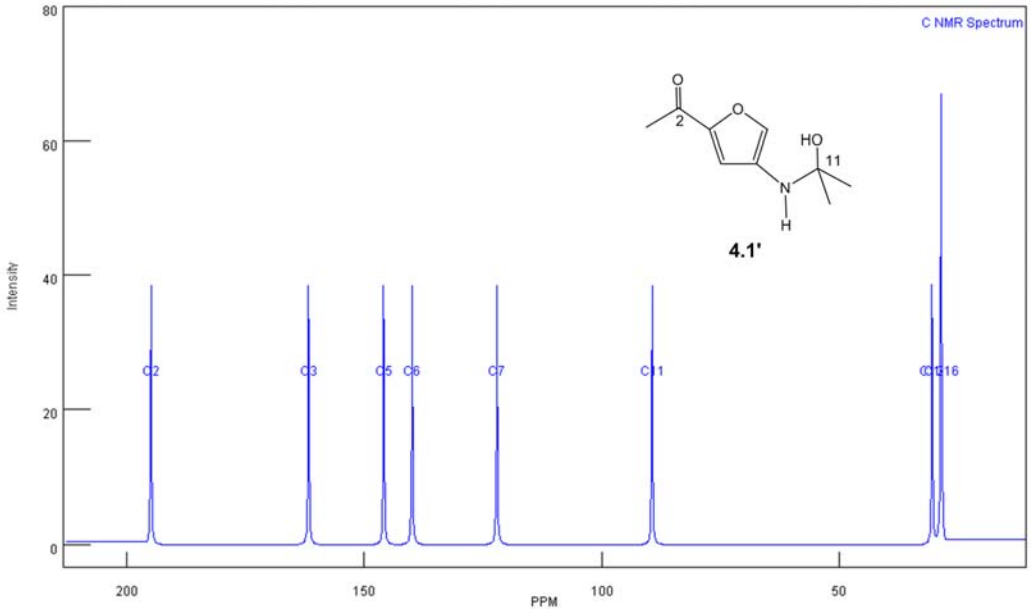

Figure 4-18. Predicted ^{13}C NMR spectrum of **4.1'**.

4.3 Conclusions

3-Acetamido-5-acetylfuran is a recently developed renewable compound that can be obtained from *N*-acetyl-D-glucosamine, the monomer of chitin. Several physical and chemical properties of 3A5AF were studied by both computational and experimental work. The experimental pK_a value of 3A5AF was obtained as 20.7 ± 0.1 through UV-Vis titration, which was consistent with the theoretical prediction of a pK_a in the range 18.5 - 21.5. 3A5AF is soluble in $scCO_2$ with methanol as a co-solvent, but could not dissolve directly in neat $scCO_2$ within the temperature and pressure ranges tested. Compared with some other chemicals from biomass such as 5-HMF, the solubility of 3A5AF in $scCO_2$ is low. A possible reason is that stronger solute-solute interactions exist between 3A5AF molecules such as intermolecular hydrogen bonding between the acetyl and amide groups. The computed dimerization energies provided further evidence that 3A5AF can form dimers more easily than 5-HMF. The frequency of the C=O stretching band for 3A5AF neat was lower than that in solution, indicating stronger intermolecular forces (hydrogen bonding) exist in the solid state. In ^{1}H NMR spectra, samples with higher concentrations exhibited less temperature dependent variation in δ(NH). These results show that hydrogen bonding exists between 3A5AF molecules in solution, and is stronger in higher concentration samples. Furthermore, the rate of deuterium exchange in more concentrated samples was slower than in dilute samples. The frontier orbitals and ESP charges of 3A5AF were determined. A Grignard reaction of 3A5AF with CH_3MgBr was performed. 3A5AF was found to be less reactive than acetophenone under similar conditions and a tertiary alcohol

product (**4.1**) that was susceptible to acid-catalyzed dehydration was formed. As 3A5AF is still a relatively new compound, which has not been studied extensively, these studies will be helpful in designing future reactions and processes involving this molecule.

4.4 Experimental

4.4.1 Computational Details

All calculations were carried out using Gaussian 09.[48] Each structure was first optimized using the B3LYP functional and the 6-311+G(2d,p) basis set.[37-40] For the calculation of the pK_a, the gas-phase Gibbs energies were calculated using the G3MP2[36] method to obtain greater accuracy. The solvation energies were calculated using the Polarizable Continuum Model (PCM)[49, 50] for DMSO and B3LYP/6-311+G(2d,p) method. In the dimerization energy calculations, molecular energies were calculated for 3A5AF and 5-HMF molecules using the B3LYP/6-311+G(2d,p) method. A counterpoise correction was performed in the interaction energy calculation.[51] The TD-DFT excitation energies, ESP charges, electrostatic potential surfaces, and molecular orbitals were calculated using B3LYP/6-311+G(2d,p). The predicted NMR spectra were calculated using the PCM for chloroform as the solvent and B3LYP/6-311+G(2d,p) method.

4.4.2 pK_a Measurement

DMSO was dried with calcium hydride and distilled prior to use. All glassware was oven-dried. The potassium dimsyl solution was prepared in a glovebox by adding potassium hydride (ca. 40 mg) to 10.00 mL DMSO slowly with stirring. The solution obtained was pale yellow, and turned pink after the addition of one drop of

triphenylmethane solution (1.3 mg dissolved in several drops of DMSO) to stabilize the solution. The accurate concentration of the potassium dimsyl solution was measured internally in the first stage of the titration (Figure 4-19). 103.7 mg fluorene was added to 12.00 mL DMSO to form a 51.99 mmol/L indicator solution. 3A5AF was synthesized using a literature procedure,[12] extracted from the reaction mixture using EtOAc (ACS grade), purified using flash chromatography, and dried overnight under vacuum using a Schlenk line. 48.9 mg 3A5AF was dissolved in 6.00 mL DMSO to form a 48.8 mmol/L solution.

The titration process followed the work of Bordwell and co-workers,[35] using an Ocean Optics USB4000-UV-Vis spectrometer. As part of the absorption band of the fluorenide anion (400 - 600 nm) overlaps with sections of the absorption bands of the 3A5AF molecule and its anion (300 - 700 nm), a wavelength for the calculation outside of this region was used. In a DMSO solution of 3A5AF (Figure 4-20), the extinction coefficient of 3A5AF molecule, ε_1, was calculated using Beer's law at wavelength λ_1. In the ionized 3A5AF solution in potassium dimsyl (Figure 4-21), the concentration of 3A5AF molecules could be calculated from the absorbance at λ_1, thus allowing the concentration of 3A5AF anions to be calculated. λ_2 in the region of the 3A5AF anion absorption was chosen so it did not overlap with the region of the 3A5AF molecular absorption, allowing the extinction coefficient for the 3A5AF anion, ε_2, to be obtained. Therefore, in the titration process, the changes in absorption intensity at λ_2 could be recorded and used for calculating the 3A5AF anion concentration (Figure 4-22).

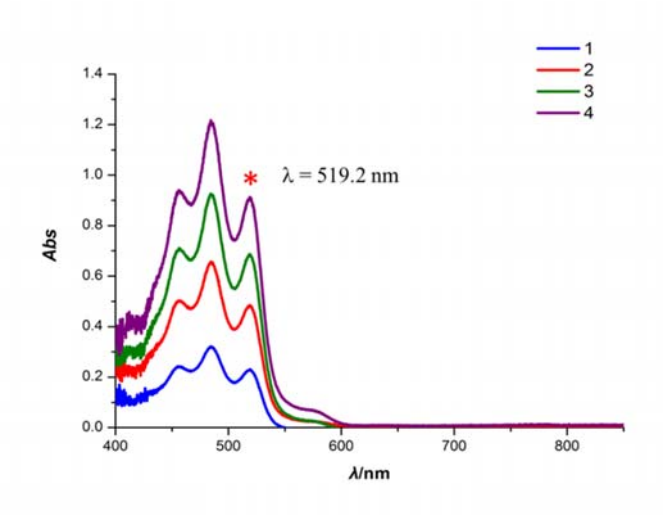

Figure 4-19. UV-Vis spectra of fluorenide ion for different amount of fluorene solution added to the potassium dimsyl solution in the internal titration.

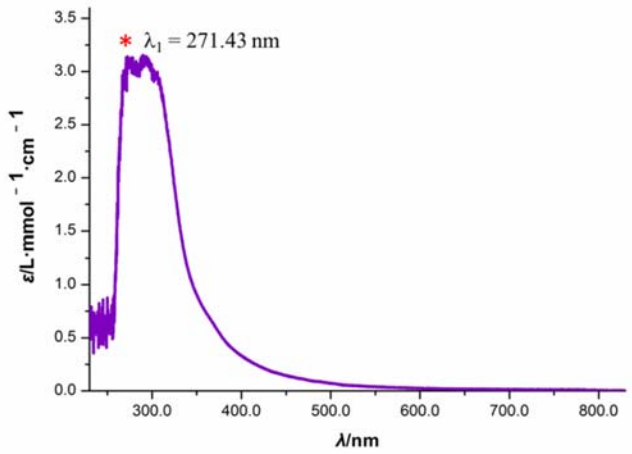

Figure 4-20. Molar absorption of 3A5AF in DMSO.

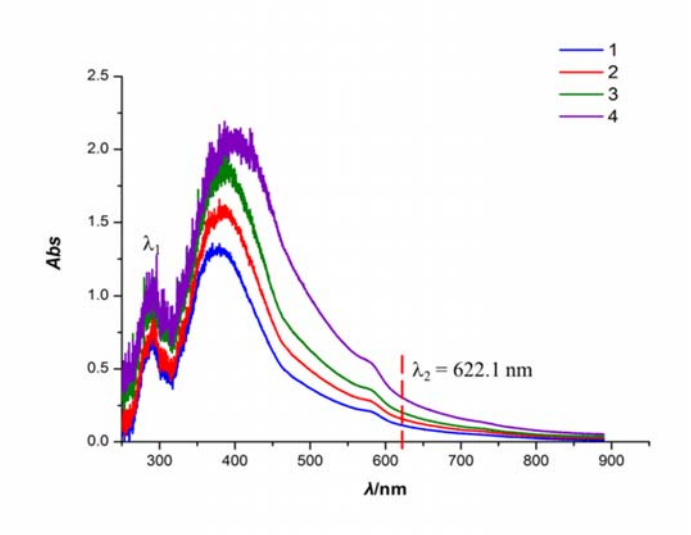

Figure 4-21. UV-Vis spectra of 3A5AF for different amount of 3A5AF solution added to the potassium dimsyl solution.

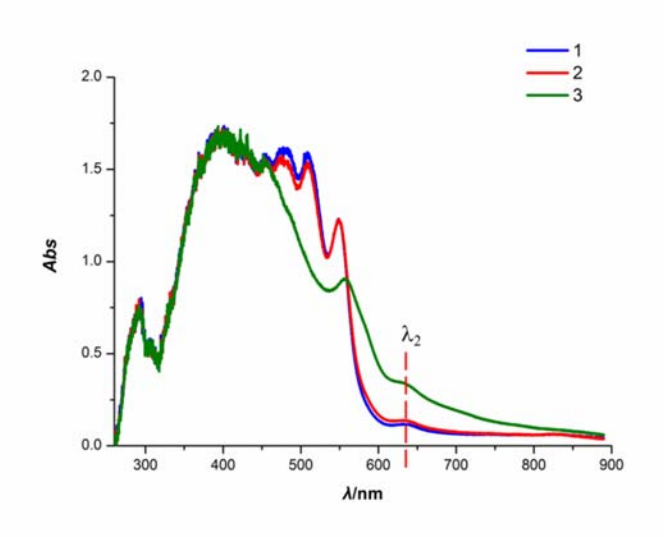

Figure 4-22. UV-Vis spectra of the titration process for various amount of 3A5AF solution added to the fluorenide ion solution.

4.4.3 Solubility in $scCO_2$

A SFT-Phase Monitor II instrument (Supercritical Fluid Technologies Inc.) was used to adjust temperatures and pressures, and record cloud points for mixtures. The view cell was 30 mL in volume. In the first test, solubility in neat $scCO_2$, 17.5 mg solid 3A5AF was placed directly into the cell. In the second test, 13.0 mg 3A5AF was dissolved in 3.00 mL methanol (HPLC grade), then the solution was injected into the cell. Cloud point data were obtained using a previously reported experimental procedure (including pressurization and equilibration steps).[41] A video of a phase change for 3A5AF in $scCO_2$/methanol at 50 °C is available at https://youtu.be/5mXZ-MGa9EI and in the Supporting Information of the published version of this chapter.

4.4.4 Infrared Measurement

A Bruker Alpha FT-IR spectrometer was used. 3A5AF and 5-HMF solid, a 4.88 mmol/L 3A5AF in Et_2O solution and a 5.15 mmol/L 5-HMF in Et_2O solution were measured.

4.4.5 NMR Measurement for the Hydrogen-bonding Experiments

29.4 mg 3A5AF was dissolved in 4.00 mL $CDCl_3$ to give a 7.35 mg/mL solution. 1.00 mL was withdrawn and diluted with 2.00 mL $CDCl_3$, from which 1.00 mL was taken and mixed with 2.00 mL $CDCl_3$. Thus the 2.45 mg/mL and 1.23 mg/mL solutions were prepared. On a Bruker AVANCE III NMR 300, ^1H NMR spectra were obtained for the three samples at 298 K and 323 K. Then approximately one equivalent of D_2O was added to the three

solutions. After being shaken and left for 10 minutes, the samples were run again to observe the exchange of the proton in the amide group with the deuterium in D_2O.

4.4.6 Reaction of 3A5AF with CH_3MgBr

3A5AF (51.4 mg, 0.307 mmol) was dissolved in dry tetrahydrofuran (THF) and transferred to a Schlenk flask. The solvent was evaporated under vacuum. Under N_2 flow, dry THF (ca. 8 mL) was added to the Schlenk flask to dissolve the solid. The flask was cooled in an ice bath and 0.26 mL (0.78 mmol) CH_3MgBr solution (3.0 M, in Et_2O) was added with stirring. The ice bath was removed and the mixture was stirred under N_2 at room temperature for 1 h. Deionized water (ca. 10 mL) was added to the brown cloudy mixture. The mixture was stirred for 30 min. THF was removed under vacuum, and EtOAc (5 × ca. 3 mL) was added to extract the products. An aliquot of the combined EtOAc extracts was injected into GC-MS for analysis. EtOAc was removed under vacuum from the combined extracts and the resulting solid was dissolved in $CDCl_3$ for ^1H and ^{13}C NMR analysis. This reaction was repeated with both (i) acidic work-up (a few drops of $HCl_{(aq)}$ were added during the reaction quenching step) and (ii) acidic/basic work-up (same as (i) but aqueous sodium bicarbonate was added prior to extraction with EtOAc).

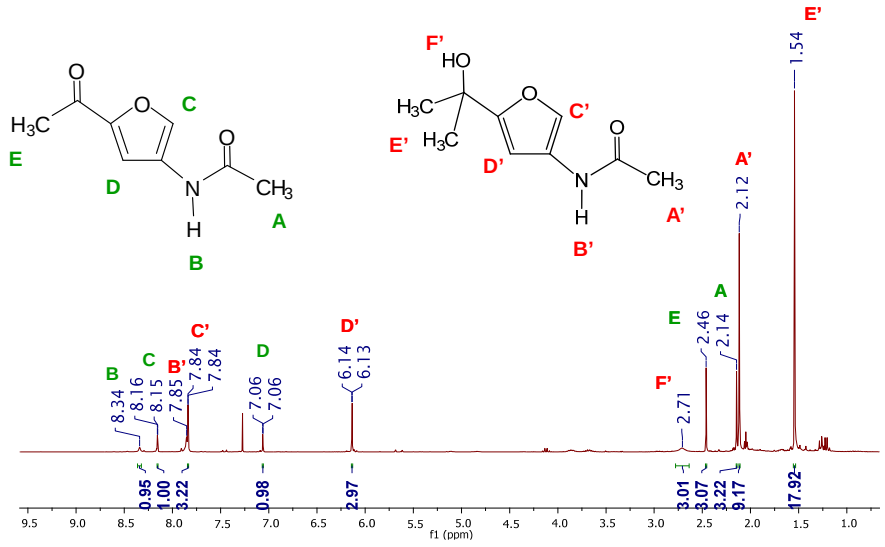

Figure 4-23. ^{1}H NMR spectrum of the Grignard reaction mixture. (Separation of 3A5AF and the product **4.1** was not possible.)

4.5 References

1. D. M. Alonso, J. Q. Bond and J. A. Dumesic, *Green Chem.*, 2010, **12**, 1493-1513.

2. J. J. Bozell and G. R. Petersen, *Green Chem.*, 2010, **12**, 539-554.

3. P. Gallezot, *Chem. Soc. Rev.*, 2012, **41**, 1538-1558.

4. H. Kobayashi and A. Fukuoka, *Green Chem.*, 2013, **15**, 1740-1763.

5. L. E. Manzer, *Top. Catal.*, 2010, **53**, 1193-1196.

6. R. A. Sheldon, *Green Chem.*, 2014, **16**, 950-963.

7. J.-L. Wertz, *Lignocellulosic Biorefineries*, EFPL Press, Lausanne, 2013.

8. T. Buntara, S. Noel, P. H. Phua, I. Melian-Cabrera, J. G. de Vries and H. J. Heeres, *Angew. Chem. Int. Ed.*, 2011, **50**, 7083-7087.

9. T. M. Lammens, M. C. R. Franssen, E. L. Scott and J. P. M. Sanders, *Green Chem.*, 2010, **12**, 1430-1436.

10. M. Rinaudo, *Prog. Polym. Sci.*, 2006, **31**, 603-632.

11. F. M. Kerton, Y. Liu, K. W. Omari and K. Hawboldt, *Green Chem.*, 2013, **15**, 860-871.

12. K. W. Omari, L. Dodot and F. M. Kerton, *ChemSusChem*, 2012, **5**, 1767-1772.

13. R. A. Franich, S. J. Goodin and A. L. Wilkins, *J. Anal. Appl. Pyrolysis*, 1984, **7**, 91-100.

14. J. Chen, M. Wang and C.-T. Ho, *J. Agric. Food. Chem.*, 1998, **46**, 3207-3209.

15. M. W. Drover, K. W. Omari, J. N. Murphy and F. M. Kerton, *RSC Adv.*, 2012, **2**, 4642-4644.

16. X. Chen, S. L. Chew, F. M. Kerton and N. Yan, *Green Chem.*, 2014, **16**, 2204-2212.

17. M. Osada, K. Kikuta, K. Yoshida, K. Totani, M. Ogata and T. Usui, *Green Chem.*, 2013, **15**, 2960-2966.

18. Y. Ohmi, S. Nishimura and K. Ebitani, *ChemSusChem*, 2013, **6**, 2259-2262.

19. K. Jackson, S. K. Jaffar and R. S. Paton, *Annu. Rep. Prog. Chem., Sect. B: Org. Chem.*, 2013, **109**, 235-255.

20. D. J. Tantillo, *Nat. Prod. Rep.*, 2013, **30**, 1079-1086.

21. J. P. Bardhan, *Comput. Sci. Discovery.*, 2012, **5**, 013001.

22. F. G. Bordwell, *Acc. Chem. Res.*, 1988, **21**, 456-463.

23. K. Iutsu, *Acid-base Dissociation Constants in Dipolar Aprotic Solvents*, Blackwell Scientific Publications, Oxford, 1990.

24. D. Gao, P. Svoronos, P. K. Wong, D. Maddalena, J. Hwang and H. Walker, *J. Phys. Chem. A*, 2005, **109**, 10776-10785.

25. J. H. Jensen, H. Li, A. D. Robertson and P. A. Molina, *J. Phys. Chem. A*, 2005, **109**, 6634-6643.

26. S. Gangarapu, A. T. Marcelis and H. Zuilhof, *ChemPhysChem*, 2013, **14**, 990-995.

27. N. Sadlej-Sosnowska, *Theor. Chem. Acc.*, 2007, **118**, 281-293.

28. V. S. Bryantsev, M. S. Diallo and W. A. Goddard, *J. Phys. Chem. A*, 2007, **111**, 4422-4430.

29. T. Matsui, T. Baba, K. Kamiya and Y. Shigeta, *Phys. Chem. Chem. Phys.*, 2012, **14**, 4181-4187.

30. Z. X. Wong and H. H. Abdallah, *Acta Chim. Slov.*, 2012, **59**.

31. J. Ho and M. L. Coote, *J. Chem. Theory Comput.*, 2009, **5**, 295-306.

32. C. Lim, D. Bashford and M. Karplus, *J. Phys. Chem.*, 1991, **95**, 5610-5620.

33. M. D. Liptak and G. C. Shields, *J. Am. Chem. Soc.*, 2001, **123**, 7314-7319.

34. Y. Chu, H. Deng and J.-P. Cheng, *J. Org. Chem.*, 2007, **72**, 7790-7793.

35. W. S. Matthews, J. E. Bares, J. E. Bartmess, F. Bordwell, F. J. Cornforth, G. E. Drucker, Z. Margolin, R. J. McCallum, G. J. McCollum and N. R. Vanier, *J. Am. Chem. Soc.*, 1975, **97**, 7006-7014.

36. L. A. Curtiss, P. C. Redfern, K. Raghavachari, V. Rassolov and J. A. Pople, *J. Chem. Phys.*, 1999, **110**, 4703-4709.

37. K. Raghavachari and G. W. Trucks, *J. Chem. Phys.*, 1989, **91**, 1062-1065.

38. A. D. Becke, *Phys. Rev. A*, 1988, **38**, 3098-3100.

39. C. Lee, W. Yang and R. G. Parr, *Phys. Rev. B*, 1988, **37**, 785-789.

40. S. H. Vosko, L. Wilk and M. Nusair, *Can. J. Phys.*, 1980, **58**, 1200-1211.

41. S. M. Payne and F. M. Kerton, *Green Chem.*, 2010, **12**, 1648-1653.

42. V. K. Potluri, J. Xu, R. Enick, E. Beckman and A. D. Hamilton, *Org. Lett.*, 2002, **4**, 2333-2335.

43. F. M. Kerton, in *Alternative Solvents for Green Chemistry*, RSC Publishing, Cambridge, UK, 2013, ch. 5, pp. 115-148.

44. B. Hakkarainen, K. Fujita, S. Immel, L. Kenne and C. Sandström, *Carbohydr. Res.*, 2005, **340**, 1539-1545.

45. C. J. Cramer, *Essentials of Computational Chemistry: Theories and Models*, John Wiley & Sons, West Sussex, England, 2nd edn., 2013.

46. P. Politzer and J. S. Murray, *Fluid Phase Equilib.*, 2001, **185**, 129-137.

47. J. S. Murray and P. Politzer, *J. Mol. Struct.: THEOCHEM*, 1998, **425**, 107-114.

48. C. Broka, D. Carter, M. Dillon, R. Hawley, A. Jahangir, C. Lin and D. Parish, *Preparation of Diaminopyrimidines as P2X3 and P2X2/3 Antagonists*, US20050209260A1, 2005.

49. M. J. Frisch, G. W. Trucks, H. B. Schlegel, G. E. Scuseria, M. A. Robb, J. R. Cheeseman, G. Scalmani, V. Barone, B. Mennucci, G. A. Petersson, H. Nakatsuji, M. Caricato, X. Li, H. P. Hratchian, A. F. Izmaylov, J. Bloino, G. Zheng, J. L. Sonnenberg, M. Hada, M. Ehara, K. Toyota, R. Fukuda, J. Hasegawa, M. Ishida, T. Nakajima, Y. Honda, O. Kitao, H. Nakai, T. Vreven, J. A. Montgomery, J. E. P. Jr., F. Ogliaro, M. Bearpark, J. J. Heyd, E. Brothers, K. N. Kudin, V. N. Staroverov, R. Kobayashi, J. Normand, K. Raghavachari, A. Rendell, J. C. Burant, S. S. Iyengar, J. Tomasi, M. Cossi, N. Rega, J. M.

Millam, M. Klene, J. E. Knox, J. B. Cross, V. Bakken, C. Adamo, J. Jaramillo, R. Gomperts, R. E. Stratmann, O. Yazyev, A. J. Austin, R. Cammi, C. Pomelli, J. W. Ochterski, R. L. Martin, K. Morokuma, V. G. Zakrzewski, G. A. Voth, P. Salvador, J. J. Dannenberg, S. Dapprich, A. D. Daniels, Ö. Farkas, J. B. Foresman, J. V. Ortiz, J. Cioslowski and D. J. Fox, Gaussian 09, Revision D.01, Gaussian, Inc., Wallingford, CT, 2009.

50. J. Tomasi, B. Mennucci and R. Cammi, *Chem. Rev.*, 2005, **105**, 2999-3094.

51. M. Cossi, N. Rega, G. Scalmani and V. Barone, *J. Comput. Chem.*, 2003, **24**, 669-681.

52. S. F. Boys and F. Bernardi, *Mol. Phys.*, 1970, **19**, 553-566.

Chapter 5

Formation of a Renewable Amine and an Alcohol via Transformations of 3-Acetamido-5-acetylfuran

A version of this chapter has been submitted for publication.

Yi Liu, Cosima Stähler, Jennifer N. Murphy, Brandon J. Furlong and Francesca M. Kerton*

Formation of a Renewable Amine and an Alcohol via Transformations of 3-Acetamido-5-acetylfuran, *ACS Sustainable Chemistry and Engineering*, 2017, **5**, 4916-4922.

Some modifications were made to the original paper for inclusion as a chapter in this thesis. For example, antimicrobial screening results and the supporting information were incorporated in this chapter.

5.1 Introduction

In recent years, the use of renewable feedstocks to produce chemicals and biofuels has become a significant research area,[1-5] due to the depletion of fossil fuels and climate change. So far, most studies about biomass transformations are limited to carbohydrates containing only C, H and O atoms, and there is a lack of research on heteroatom-containing carbohydrates.[6-7] Chitin is the second most abundant biopolymer after cellulose on earth. *N*-Acetyl-D-glucosamine (NAG) is the monomer of chitin, and has been successfully converted to a nitrogen-containing product, 3-acetamido-5-acetylfuran (3A5AF) (Scheme 5-1). 3A5AF was first obtained from NAG using pyrolysis methods with quite low yields of 2% and 0.04%.[8-9] In recent research by Omari et al., the yield of 3A5AF was increased to 60% through microwave irradiation with dimethylacetamide as the solvent and sodium chloride and boric acid as additives.[10] In the study by Drover et al., ionic liquids were used as solvents in the conversion of NAG and the highest 3A5AF yield achieved was also 60%.[11] In 2014, Chen et al. performed the direct conversion of chitin to 3A5AF in *N*-methyl-2-pyrrolidone, and the best yield obtained was 7.5%.[12] In 2015, the same group switched to ionic liquids as solvents in the dehydration of chitin to 3A5AF.[13] The use of 1-butyl-3-methylimidazolium chloride together with boric acid and hydrochloric acid led to a maximum 3A5AF yield of 6.2%.

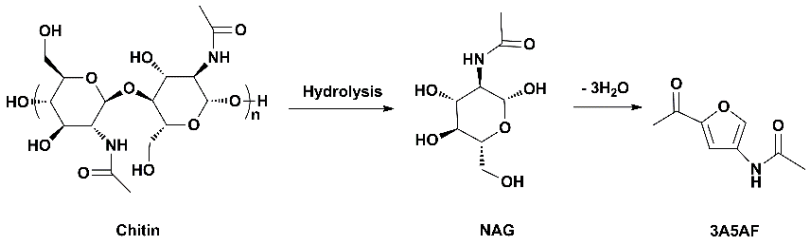

Scheme 5-1. Conversion of chitin and NAG to yield an amido-furan (3A5AF).

To date, besides its preparation there is little information on the properties of 3A5AF,[14] including its reactivity and conversion into other chemicals. As a promising platform chemical for a variety of useful compounds (Scheme 5-2), reactions of 3A5AF should be investigated. The current study reports the formation of a renewable amine product, 2-acetyl-4-aminofuran (**5.1,** Scheme 5-3), from the hydrolysis of 3A5AF. Also, the reduction of 3A5AF was performed using sodium borohydride ($NaBH_4$) or via transfer hydrogenation, and an alcohol was obtained (**5.2**, Scheme 5-4). In addition, the potential of 3A5AF and **5.1** in CO_2 capture and their antimicrobial ability were investigated.

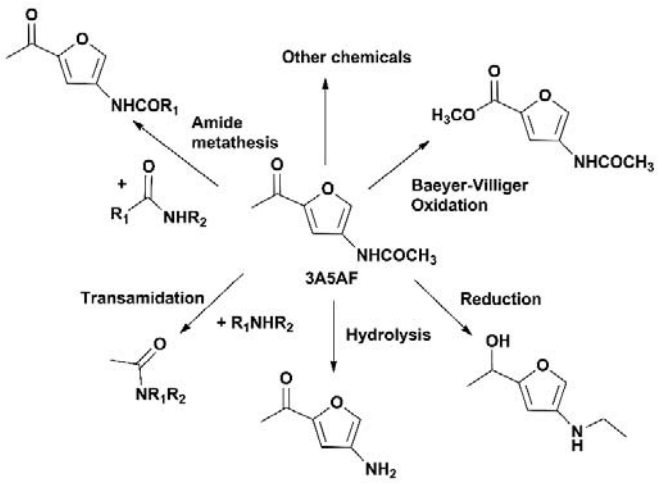

Scheme 5-2. Proposed reactions of 3A5AF.

5.2 Results and Discussion

5.2.1 3A5AF Hydrolysis - 2^3 Factorial Design.

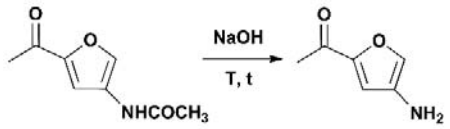

3A5AF 5.1

Scheme 5-3. 3A5AF hydrolysis catalyzed by NaOH.

Table 5-1. Hydrolysis of 3A5AF catalyzed by NaOH.

Factors:	**A**	**B**	**C**		
Entry	NaOH concentration (mol/L)	T (°C)	t (h)	Conversion of 3A5AF (%)[a]	Yield of **5.1** (%)[a]
1	5	80	1	5.2	0
2	6	80	1	67.3	9.4
3	7	60	1	16.6	1.8
4	7	60	2	64.4	8.3
5	7	80	1	72.1	26.7
6	7	80	2	100	0
7	9	60	1	45.5	8.5
8	9	60	2	78.8	24.9
9	9	80	1	96.6	57.1
10	9	80	2	100	0
11	8	70	1.5	84.1	28.7
12[b]	9	100	0.25	> 99	34.7

a. Determined by ^{1}H NMR spectroscopy. b. Performed in a microwave reactor.

As a relatively simple reaction, the hydrolysis of 3A5AF was studied first. An initial screening was performed using a number of mineral acids and bases. From the initial test reactions, it became clear that sodium hydroxide (NaOH) gave superior reactivity in this reaction and so was studied in more detail.

The hydrolysis of 3A5AF was performed in aqueous media catalyzed by NaOH (Table 5-1) and a Design of Experiments approach was used. In this way, it was hoped that the most important variables in this reaction and any potential interactions between them could be more readily ascertained, which may be overlooked using a traditional one variable (factor) at a time approach. A 2^3 factorial design with one center point was used to study the effects of concentration of NaOH (A), temperature (B), and time (C). The incorporation of NaOH concentration as a factor for study was because in initial experiments an increase in NaOH concentration led to an increase in the yield of **5.1** (Table 5-1, entries 1, 2, 5 and 9), possibly because the increase in concentration of OH^- could more effectively promote the hydrolysis. Each factor (A-C) was studied at a high (+1) and low (-1) value. The concentration of NaOH was investigated at 7 and 9 mol/L; the temperature was investigated at 60 and 80 °C; the time was investigated at 1 and 2 h. The yield of **5.1** was analyzed as the response. The total number of experiments for the factorial design was 9 including one center point (Table 5-1, entry 11). In a 2-level factorial design the resulting model can only be linear. Testing a center point where all factors are at the 0 level, allows us to see if the model has curvature (i.e. has a higher order).

In a typical reaction, 15 mg (0.090 mmol) 3A5AF was dissolved in 1 mL methanol. After 3 mL of the aqueous NaOH solution was added, the reaction mixture was heated in an oil bath under reflux at the desired temperature for a fixed time. After work-up, a golden solid was obtained, which was analyzed by GC-MS, and ^{1}H and ^{13}C NMR spectroscopy. The highest yield of **5.1** obtained was 57.1% (6.02 mg), when the reaction was catalyzed by the 9 mol/L NaOH solution and was heated at 80 °C for 1 h (Table 5-1, entry 9).

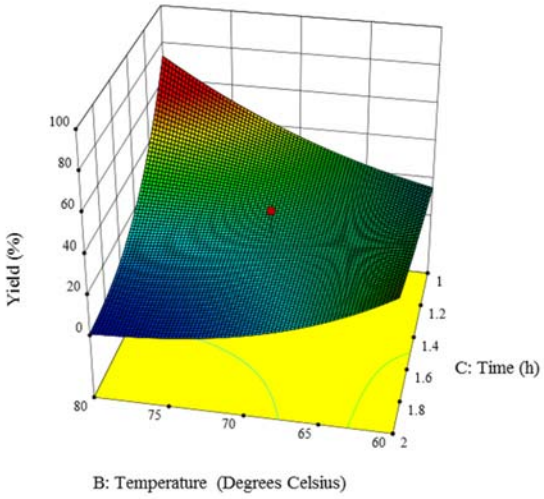

Figure 5-1. The response surface plot of yield of **5.1** based on the factors temperature (B) and time (C) in the NaOH-catalyzed hydrolysis of 3A5AF.

The results were analyzed using Design Expert ®. Analysis of variance (ANOVA) of the model with 5% significance showed that curvature was significant as well as the two-factor interaction between temperature and time (BC). When both the temperature and time are low, the yield of **5.1** is low. When the temperature is high, the yield is high only when the reaction time is low. This is illustrated in Figure 5-1, and the response surface for the

model shows that a yield of around 75% is predicted at a temperature of 80 °C and 1 h reaction time. Surprisingly, the concentration of NaOH (A) was not as significant a factor as was expected based on the initial trial reactions. This further illustrates that using a factorial design for consideration of factor combinations is valuable in designing and optimizing chemical processes.

The reaction in entry 12 was heated through microwave irradiation and the result was compared with that of entry 9 (Table 5-1). In the ^{1}H NMR spectrum of the reaction mixture from entry 12, only a trace amount of 3A5AF was present indicating the conversion of 3A5AF reached almost 100%. However, the yield of **5.1** (34.7%) was lower than that from entry 9 (57.1%). Among the conventionally heated reactions, when the temperature was high (80 °C) and the reaction time was long (2 h), **5.1** could not be obtained despite full conversion of 3A5AF (entry 6 and 10). These results indicate that the selectivity of 3A5AF hydrolysis towards **5.1** was not 100%, and is affected by the reaction conditions. The low yield of **5.1** is possibly due to the occurrence of side reactions of 3A5AF or **5.1** at the high temperatures. For example, the amine group in **5.1** could react with the carbonyl group to produce an imine compound. However, no identifiable signals from possible side-products were observed in GC-MS and NMR analyses, so no definite conclusions could be made. It is also noted that no insoluble by-products were observed during reaction work-up. In terms of sustainability, further research is needed in order to maximize yields and this should be pursued using a heterogeneous base catalyst, which would allow catalyst reuse.

5.2.2 Characterization of 5.1.

The yield of **5.1** was the highest (57.1%) from the experiment in entry 9 (Table 5-1), and the portion of **5.1** in the solid obtained reached 92.6 wt% (determined by ^{1}H NMR spectroscopy). Therefore, this sample was analyzed for the characterization of **5.1**. In the ^{1}H NMR spectrum of the sample (Figure 5-9), impurities were present at negligible levels, and there was only approximately 5.7 mol% unreacted 3A5AF. Therefore, this sample reached 94.3 mol% purity of **5.1**. It is surprising to find that the amine group of **5.1** had two separate signals at 8.39 ppm and 11.43 ppm. In order to verify this, 10 μL deuterium oxide (D_2O) was added to the NMR sample. After being shaken and equilibrated for 1 h, the sample was analyzed via ^{1}H NMR spectroscopy (Figure 5-12). Both peaks at 8.39 ppm and 11.43 ppm disappeared because of deuterium exchange, indicating that they are both exchangeable protons and potentially both from the amine group. It is assumed that the presence of two proton environments in this region is due to them having different strengths of intermolecular hydrogen bonding with another molecule of **5.1**, which results in their different chemical shifts in the ^{1}H NMR spectra. It has been seen previously that significant hydrogen bonding can happen in samples of 3A5AF,[14] and therefore it is not surprising that **5.1** would also be affected by such phenomena. A further study should be carried out in the future to gain more insight. The tertiary and quaternary carbon atoms (C3, C4, C5, C6) on the furan ring of **5.1** gave rise to very weak resonances in the ^{13}C NMR spectrum (Figure 5-10). Computational calculations were performed for NMR prediction of **5.1**. The predicted ^{13}C NMR spectrum (Figure 5-11) is in acceptable agreement with the

experimental one, and it confirms the assignment of C3 - C6 peaks in the experimental spectrum.

The GC-MS analysis of the sample (Figure 5-13) showed that besides a small amount of unreacted 3A5AF at 5.314 min (*m/z* 167.0), the main component was the amine product **5.1** at 4.348 min with *m/z* 125.0. In the HRMS spectrum, the peak of (**5.1**+H)$^+$ (*m/z* 126.0550) had an overwhelming abundance. The molecular ion of **5.1** appeared at *m/z* 125.0478, which has only 0.84 ppm difference from the theoretical value (125.0477), thus supporting the identification of **5.1**.

The IR spectrum was obtained for a solid sample of **5.1** and compared with that of pure 3A5AF (Figure 5-15). **5.1** exhibits amine stretching bands (ν_{N-H}, stretch) at 3139.2 cm^{-1} and 3046.3 cm^{-1}, and an amine bending band (ν_{N-H}, bending) at 1570.9 cm^{-1}. The peak at 1618.9 cm^{-1} in **5.1** was assigned to the carbonyl stretching frequency ($\nu_{C=O}$). In 3A5AF, the band at 1657.9 cm^{-1} is attributed to the combination of the $\nu_{C=O}$ of the secondary amide and ketone functional groups. The shift of ν_{N-H} and $\nu_{C=O}$ in **5.1** compared with 3A5AF towards lower frequencies may be the result of intermolecular hydrogen bonding.

5.2.3 3A5AF Reduction

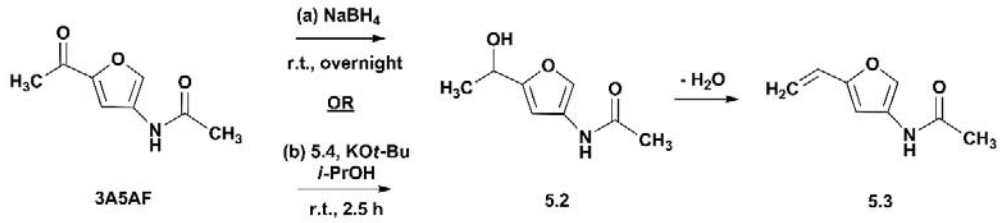

Scheme 5-4. Synthesis of furyl-alcohol **5.2** via (a) reduction of 3A5AF with $NaBH_4$ or (b) transfer hydrogenation of 3A5AF.

The reduction of 3A5AF was performed with the aim of obtaining a *N*-containing compound with hydroxyl groups instead of carbonyl groups. A mixture of 3A5AF and $NaBH_4$ was stirred overnight under N_2 flow at room temperature (Scheme 5-4, a). After work-up, a yellow oil was obtained and analyzed by GC-MS, HRMS, and ^{1}H and ^{13}C NMR spectroscopy. The use of $NaBH_4$ led to the reduction of the carbonyl in the acetyl group to a hydroxyl. The compound obtained, 3-acetamido-5-(1-hydroxylethyl)furan (**5.2**), was previously observed in a study by Kuhn et al. in 1958.[15] In the GC-MS and NMR analyses no 3A5AF was detected, indicating its 100% conversion. However, the amide functional group remained in tact. Another product **5.3** (*m/z* 151.0) was observed besides product **5.2** (*m/z* 169.1) in GC-MS analysis, which resulted from the dehydration of **5.2**. This dehydration happened in a similar way as was observed previously in the reaction of 3A5AF with a Grignard reagent.[14] **5.3** could not be seen in the NMR spectra possibly because its amount was too small or it was formed in situ within the inlet of the GC-MS instrument. In the ^{1}H NMR spectrum of **5.2** (Figure 5-16), a broad peak at 2.75 ppm was

assigned to δ(OH). In the ^{13}C NMR spectrum (Figure 5-17), the reduced carbon atom had a chemical shift of 63.54 ppm.

The reducing ability of $NaBH_4$ is not sufficient to reduce the amide functional group. Therefore, lithium aluminum hydride ($LiAlH_4$), a stronger reducing agent, was studied. The products obtained were analyzed by ^{1}H and ^{13}C NMR spectroscopy. The ^{13}C NMR spectrum showed that all significant signals were in the range of 10 - 70 ppm, indicating that the furan ring had opened to yield linear acyclic products. Unfortunately, a single product from the reaction mixture could not be isolated and characterized. However, it can be concluded that in the reaction using $LiAlH_4$, instead of the generation of functional (amino-alcohol) furan products as expected, the furan ring in 3A5AF was also reduced and ring-opened.

Ir-catalyzed transfer hydrogenation of 3A5AF was also studied as a more efficient route to **5.2**. As 3A5AF is not commercially available, the reaction was initially performed using 5-hydroxymethylfurfural (5-HMF) and then the same conditions employed for 3A5AF. The iridium complex $IrH_2Cl[(^{i}Pr_2PC_2H_4)_2NH]$ (**5.4**) has been reported as an exceptionally active catalyst in the presence of base for the transfer hydrogenation of acetophenone to phenylethanol.[16] The reaction conditions were mild (room temperature, 2 h) and a conversion of acetophenone over 99% and a phenylethanol yield of 98% were obtained. The catalytic reduction of 5-HMF to bis(2,5-hydroxymethyl)furan (BHMF) has previously been performed using metal (Ru, Pt, Zr) catalysts and H_2 as the reducing agent.[17-19] Transfer hydrogenation of 5-HMF has also been achieved with ethanol or formic

acid as the hydrogen donor catalyzed by metal (Zr, Ni-Co) catalysts.[20-21] Herein, reactions were performed using the combination of **5.4** and potassium *tert*-butoxide (KO*t*-Bu) in dry isopropyl alcohol (*i*-PrOH) at room temperature (Scheme 5-5) and aliquots were taken for monitoring via ^{1}H NMR spectroscopy. After 2.5 h, the peak corresponding to the aldehyde moiety in 5-HMF had disappeared and so it was assumed complete conversion was achieved. Filtration of the reaction solution through a plug of silica and removal of the solvent under vacuum allowed the isolation of BHMF in 95% yield. Similarly, using a 3A5AF:Ir 100:1, **5.2** could be obtained in 80% yield (Scheme 5-4, b). Given the exceptional reactivity of **5.4** towards ketone reduction, it may be possible to use a lower catalyst loading, but in this study the aim was to perform the reaction at room temperature in a minimal amount of time so a relative high catalyst loading of 1 mol% was used. A moderately lower yield of **5.2** (80%) compared with BHMF (95%) may be due to a number of factors, e.g. catalyst inhibition by the amide functional group, reduction of a ketone rather than an aldehyde, but further studies would be needed to confirm such hypotheses.

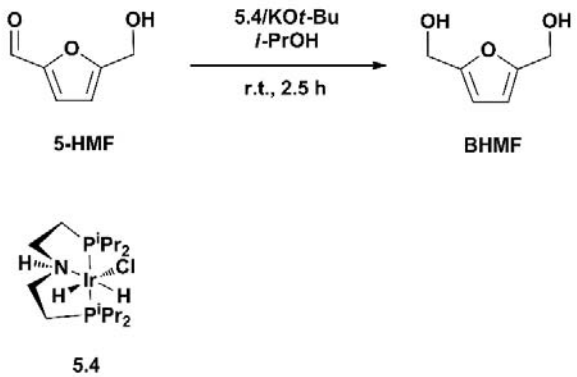

Scheme 5-5. Ir-catalyzed transfer hydrogenation of 5-HMF to BMHF.

5.2.4 Carbon Dioxide (CO_2) Capture Investigation.

Emissions of CO_2 and its subsequent influence on the climate have become serious problems that can no longer be neglected. CO_2 capture is an important solution to alleviate this situation. As a solvent-based approach to CO_2 capture, amine-scrubbing technology has been used for many years in the oil and chemical industries for removal of CO_2 and hydrogen sulfide (H_2S) from gas streams.[22-24] Monoethanolamine (MEA) is a widely used amine for CO_2 and H_2S capture. Aqueous 30% (w/v) MEA solution (pK_a = 9.50[25]) was optimized by Moser et al. as a benchmark solvent with a CO_2 removal rate up to 90%.[26] However, there are still concerns about MEA application in CO_2 capture. Amine solvents are volatile, so during the process part of the amine will evaporate to the atmosphere and produce some environmentally hazardous compounds.[27] MEA is vulnerable to thermal and oxidative degradation in the presence of O_2, CO_2, SO_x and NO_x.[28] This will have negative influence on its CO_2 capture capacity, and the compounds generated cause equipment corrosion, solvent contamination, viscosity increases, and both environmental and human health hazards.[29-30] In addition, a great amount of energy is needed for the regeneration of the amine.[31] Therefore, researches about improved methods and alternative materials for CO_2 capture are being constantly carried out.[32-34]

As 3A5AF contains an amide group and **5.1** has an amine group in their structures, they were expected to capture CO_2 via reactions between the functional groups and CO_2. In a typical experiment, 50 mg dry solid was dissolved in 1 mL dry methanol-d_4 (CD_3OD) (for 3A5AF) or dry dimethyl sulfoxide-d_6 (for **5.1**), and the solution was degassed under

vacuum using a Schlenk line. The test was performed for both a dry solution and a solution with 30 μL deionized water added. In each situation, the solution was stirred under CO_2 flow at room temperature and at 40 °C, each for 1 h. After each test, the solution was analyzed by ^1H and ^{13}C NMR spectroscopy. Unfortunately, neither 3A5AF nor **5.1** showed the ability to capture CO_2. The aqueous pK_a values of 3A5AF and **5.1** were calculated computationally, using an approach that have been used previously,[14] in order to provide an reasonable explanation for their negative performance. When acetanilide (pK_a = 13.0) was used as the reference, the calculated pK_a value of 3A5AF was 6.0. The pK_a value of **5.1** was 7.1 with aniline (pK_a = 9.4) as the reference. Aqueous carbon dioxide (CO_2 dissolved in water) has a pK_a of 6.36. Therefore, 3A5AF and **5.1** are not sufficiently basic in water and this makes it a challenge for them to react with CO_2. The weak basicity of 3A5AF and **5.1** is attributed to resonance effects and the delocalization of the lone pair on the N atom (Scheme 5-6).

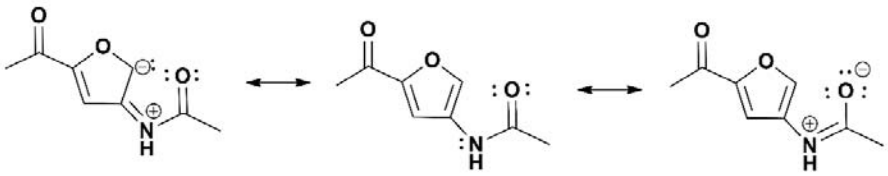

Scheme 5-6. Resonance structures leading to delocalization of the lone pair on the N atom of 3A5AF.

One unexpected finding during the current studies of 3A5AF was the ability of the protons of the methyl group in the acetyl moiety to undergo deuterium exchange. In the ^1H NMR spectrum of 3A5AF in CD_3OD after it was mixed with CO_2, the signal of δ(CH_3) of

the acetyl methyl group disappeared (Figure 5-2, see the full spectrum in **5.4.10**). At first it was thought that 3A5AF had undergone hydrolysis catalyzed by the in situ formed carbonic acid. The solvent (CD_3OD) in this NMR sample was removed using a Rotavap, and the solid obtained was dissolved in methanol, CH_3OH, with the aim of performing H-D exchange on the mixture. When this solution was injected into the GC-MS system, it showed only one component, which was 3A5AF (*m/z* 167.0). The methanol was removed using a Rotavap and re-dissolved in chloroform-d for NMR analysis. In the ^1H NMR spectrum, the expected signals for 3A5AF were all present. These results implied that the acetyl protons had undergone exchange with the deuterium in CD_3OD, which is rare since usually the protons in a methyl group do not exchange. This can be explained by the fact that 3A5AF undergoes keto-enol tautomerism in solution (Scheme 5-7). All protons in the methyl group will be replaced by deuterium during this process, thus resulting in the disappearance of the signal in the ^1H NMR spectrum. In addition, the carbonyl group is strongly electron withdrawing, which activates the protons in its neighbouring methyl group. As a consequence, the protons become acidic and more readily undergo deuterium exchange. In the corresponding ^{13}C NMR spectrum of 3A5AF in CD_3OD after deuterium exchange, the peak of the carbon atom of this methyl group is split into a multiplet caused by C-D coupling (Figure 5-3).

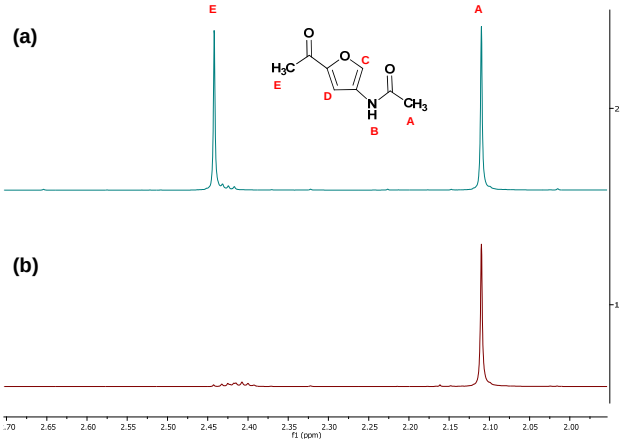

Figure 5-2. Selected regions of the ^{1}H NMR spectra of 3A5AF in CD_3OD (a) initially (t = 0 min) before and (b) after deuterium exchange.

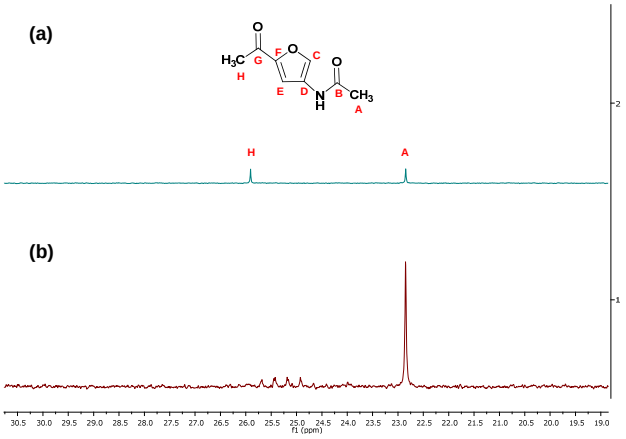

Figure 5-3. Selected regions of the ^{13}C NMR spectra of 3A5AF in CD_3OD (a) initially (t = 0 min) before and (b) after deuterium exchange.

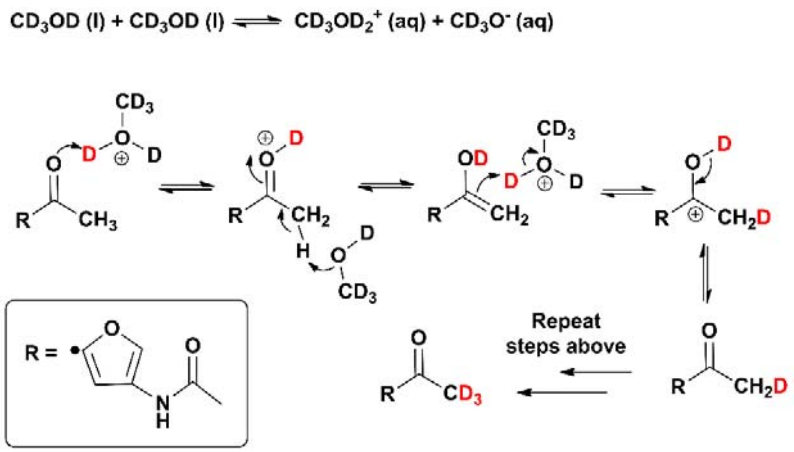

Scheme 5-7. Deuterium exchange of the methyl group in 3A5AF with CD_3OD (the deuterium exchange of the amide group is not shown for clarity).

5.2.5 Antimicrobial Screening

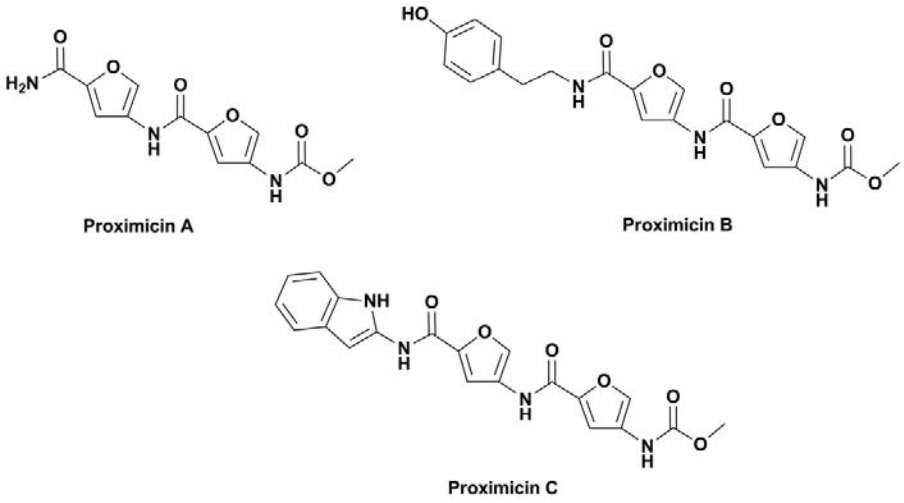

Figure 5-4. Structures of proximicin A, B and C.

Proximicin A, B and C (Figure 5-4) are a family of peptide metabolites that can be extracted from marine actinomycetes.[35-36] They have been studied as antitumor and

antibiotic drugs.[37-40] 3A5AF has some structural similarity to the proximicins as they all contain furan rings and acetamido functional groups. An antimicrobial screening was performed for 3A5AF to see whether it has any ability to kill microorganisms or inhibit their growth. 1.5 mg 3A5AF solid was weighed in a 1.5 mL Eppendorf tube and sent to The University of Queensland for test. There were five bacteria (*Escherichia coli*, *Klebsiella pneumoniae, Acinetobacter baumannii, Pseudomonas aeruginosa* and *Staphylococcus aureus*) and two yeasts (*Candida albicans* and *Cryptococcus neoformans*) used in the test. The result showed no inhibitory activity of 3A5AF for these bacteria and yeasts. The same screening was performed for amine **5.1**, and it also has no influence on the growth of the bacteria and yeasts tested.

5.3 Conclusions

An amine product, 2-acetyl-4-aminofuran (**5.1**), was successfully synthesized via the hydrolysis of 3A5AF catalyzed by NaOH. The highest yield of **5.1** obtained was 57.12% with 94.3 mol% purity, when the reaction was performed at 80 °C for 1 h. The golden solid was characterized using GC-MS, HRMS, NMR and IR spectroscopies. The reduction of 3A5AF was performed using $NaBH_4$. A secondary alcohol, 3-acetamido-5-(1-hydroxylethyl)furan (**5.2**), was obtained and an alkene (**5.3**) was observed from the subsequent dehydration of **5.2** during GC-MS analysis. **5.2** can also be obtained through Ir-catalyzed transfer hydrogenation of 3A5AF. The ability of 3A5AF and **5.1** in CO_2 capture was investigated, but they are not effective absorbents due to their weak basicity.

It is hoped that these initial reactions can be a good starting point for the development of 3A5AF as a platform chemical to yield products containing naturally fixed nitrogen. Further studies on the applications of both 3A5AF and the obtained products are needed to make full use of these biomass-derived compounds.

5.4 Experimental

5.4.1 Materials and Instruments.

N-Acetyl-D-glucosamine (NAG) was purchased in 98% purity from AK Scientific. Boric acid ($B(OH)_3$) was purchased in 99.5% purity from Sigma Aldrich. Sodium chloride (NaCl) was purchased in 99.0% purity from Anachemia. 1-Butyl-3-methyl imidazolium chloride ([Bmim]Cl) was purchased in 96% purity from Alfa Aesar. Sodium borohydride ($NaBH_4$, 98.5%) was purchased from Sigma Aldrich. Lithium aluminum hydride ($LiAlH_4$, 95%) was purchased from Alfa Aesar. $IrH_2Cl[(^iPr_2PC_2H_4)_2NH]$ (**5.4**) was purchased from Strem Chemicals. Potassium *tert*-butoxide (KO*t*-Bu, 97%) was purchased from Alfa Aesar. Ethyl acetate (EtOAc) and isopropyl alcohol (both ACS grade, 99.5%) were purchased from Caledon. Isopropyl alcohol (*i*-PrOH) was dried over calcium oxide and distilled under nitrogen. Methanol (99.8%) and was purchased from ACP Chemicals. Deionized water was obtained from distilled water processed by a Nanopure II system (manufactured by Barnstead/Thermolyne, USA). Compressed carbon dioxide (CO_2, chromatographic grade) and compressed nitrogen (N_2, 90%) were purchased from Praxair. All NMR solvents were purchased in 99.8% or 99.9% purity from Cambridge Isotope Laboratories. All chemicals and solvents were used as received.

Microwave reactions were performed using a Biotage Initiator 2.5 microwave reactor. 2 - 5 mL or 10 - 20 mL reaction volume vials were used. The "very high" absorption level was applied in each reaction to control the power to heat the reaction mixture. Vortex-mixing of the reaction mixture was carried out on a Thermo Scientific Vortex Maxi Mix II. Centrifugation was performed on an Eppendorf centrifuge 5430. Evaporation of solvents was achieved using a Buchi Rotavap or a Radleys Greenhouse Blowdown Evaporator. Gas chromatography-mass spectrometry (GC-MS) was performed on an Agilent 7890A GC system coupled with an Agilent 5975C MS detector. High resolution mass spectroscopy (HRMS) was performed on an Agilent 1260 Infinity HPLC-chip/MS system combined with the 6230 TOF LC/MS system. ^{1}H and ^{13}C Nuclear Magnetic Resonance (NMR) analyses were accomplished on a Bruker 300 MHz spectrometer. Infrared (IR) spectra were recorded using a Bruker Alpha FTIR spectrometer (4 cm^{-1} resolution) with a diamond ATR single reflectance module (24 scans).

5.4.2 Computational Details.

All calculations were carried out using Gaussian 09 program.[35] Each structure was first optimized using the B3LYP functional and the 6-311+G(2d,p) basis set.[36-39] For the calculation of pK_a, the gas-phase Gibbs energies were calculated using the G3MP2[40] method to obtain greater accuracy. The solvation energies were calculated using the Polarizable Continuum Model (PCM)[41-42] for water and the B3LYP/6-311+G(2d,p) method. The pK_a calculations were performed based on the literature procedure.[14] The predicted

NMR spectra were calculated using the PCM for dimethyl sulfoxide-d_6 as the solvent and the B3LYP/6-311+G(2d,p) method.

5.4.3 3A5AF Synthesis and Identification.

The preparation of 3-acetamido-5-acetylfuran (3A5AF) was based on a literature procedure with modifications.[13] 500.0 mg (2.260 mmol) NAG, 111.7 mg (1.807 mmol) $B(OH)_3$, 105.6 mg (1.807 mmol) NaCl, 1.5 g (8.6 mmol) [Bmim]Cl, and 9 mL EtOAc were placed in a 10 - 20 mL Biotage microwave vial and sealed. The mixture was heated under microwave irradiation at 100, 120, 140, 160 and 180 °C for 5 min each. The reaction mixture was cooled to room temperature and vortex-mixed at high speed for 1 min. After centrifugation at 4500 rpm for 5 min, the top EtOAc layer was collected. Extraction of 3A5AF from the reaction mixture was performed using 3 × 10 mL EtOAc, and the extraction layers were combined. Then another 9 mL EtOAc was added to the residual reaction mixture for a second run of the reaction.

After the second run of the reaction, the EtOAc layer was decanted and combined with the previously collected one. A saturated NaCl solution and a 30% NaOH solution were added to the bottom layer. The use of the saturated NaCl solution is to maximize the transfer of 3A5AF into the organic layer during extractions; while the use of the NaOH solution is to neutralize the $B(OH)_3$ residual in the reaction mixture. The mixture was distributed into several vials, and EtOAc was added to each vial for extraction. After vortex-mixing at high speed for 1 min, the mixture was centrifuged at 4500 rpm for 5 min. The collected EtOAc layers were combined in a 1000 mL round bottom flask and concentrated under reduced

pressure using a Rotavap (180 mbar, 40 °C) to yield a condensed orange solution. The solution was transferred to vials and dried at 50 °C under N_2 flow using a Blowdown Evaporator, aiming to get rid of the acetic acid left in the 3A5AF solid, which came from the slight hydrolysis of 3A5AF. Two aliquots were taken and dissolved in 500 μL EtOAc and 800 μL chloroform-d ($CDCl_3$) respectively for GC-MS and NMR analyses. The quantification was performed based on the method developed by Omari et al.[10], and the yield of 3A5AF from this two-run procedure reached 41.3%. As indicated in the ^{1}H NMR spectrum (Figure 5-5), besides a water peak at 1.56 ppm, there are no significant impurities.

^{1}H NMR δ_H (298 K, 300 MHz; $CDCl_3$; Me_4Si) 2.17 (s, 3H), 2.46 (s, 3H), 7.04 (d, 1H), 7.40 (s, 1H), 8.16 (d, 1H)

^{13}C NMR δ_C (298 K, 75 MHz; $CDCl_3$) 23.34, 25.85, 109.95, 126.50, 136.23, 150.68, 168.11, 187.51

MS *m/z* (% ion) 167 (40), 125 (60), 110 (100), 96 (13), 83 (20), 69 (6), 54 (13)

Selected IR data (cm^{-1}) 3340.64 (s) (N-H stretch), 1657.85 (s) (C=O stretch in amide and ketone), 1556.89 (s) (N-H bending)

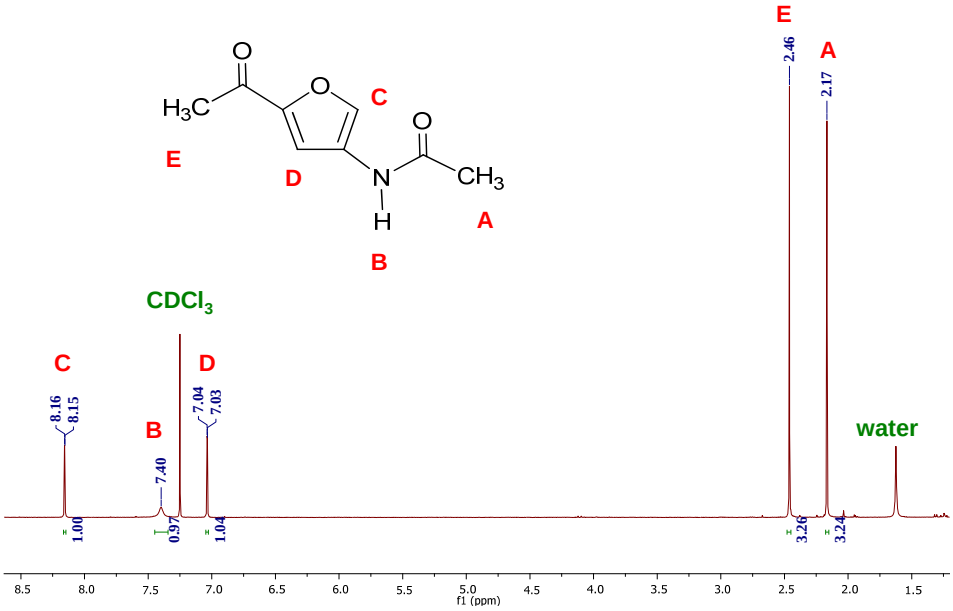

Figure 5-5. ^{1}H NMR spectrum of 3A5AF.

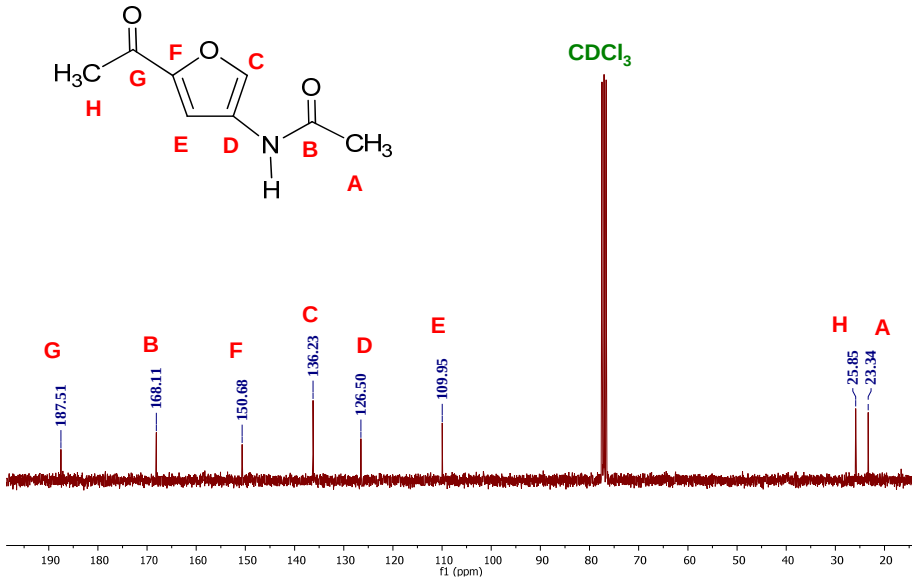

Figure 5-6. ^{13}C NMR spectrum of 3A5AF.

5.4.4 Synthesis of 2-Acetyl-4-aminofuran (5.1)

15.0 mg (0.0900 mmol) 3A5AF was dissolved in 1 mL methanol, and 3 mL NaOH solution (concentrations as per Table 5-1) was added. The starting materials were heated at the desired temperature in an oil bath under reflux for a fixed time. After the reaction was complete, 37% aqueous HCl was added dropwise to the reaction mixture until the solution was slightly acidic. Following this, 28% aqueous NH_3 (aq) was added to neutralize the solution. The solvent was evaporated on a Blowdown Evaporator at 55 °C. The obtained orange solid was re-dissolved in methanol and filtered. The orange filtrate was concentrated on a Rotavap at 300 mbar, 40 °C. The obtained orange solid was re-dissolved using EtOAc and filtered. The golden solution was concentrated on a Rotavap at 180 mbar, 40 °C until a golden solid was obtained. After being weighed, the solid was analyzed by GC-MS and ^{1}H and ^{13}C NMR spectroscopy. In the reaction under microwave irradiation, the starting materials were place in a 2 - 5 mL vial and heated in the microwave reactor at 100 °C for 15 min.

In ^{1}H NMR spectra, the methyl groups of the acetyl moieties in the unreacted 3A5AF and **5.1** were integrated. The integration ratio is equal to the molar ratio of unreacted 3A5AF to **5.1** in the final golden solid obtained. Since there were no significant peaks of other impurities observed, it was assumed that the final solid was composed of only **5.1** and unreacted 3A5AF. Using this molar ratio in combination with the weight of the solid, the mass of **5.1** and unreacted 3A5AF (to calculate the conversion of 3A5AF) in the final product could be calculated.

5.4.5 2^3 Factorial Design Results

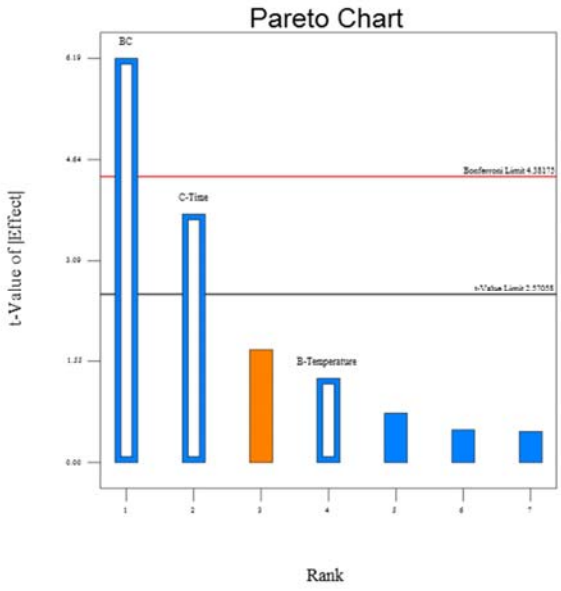

Figure 5-7. Pareto chart of the effects for the 2^3 FD.

(a)

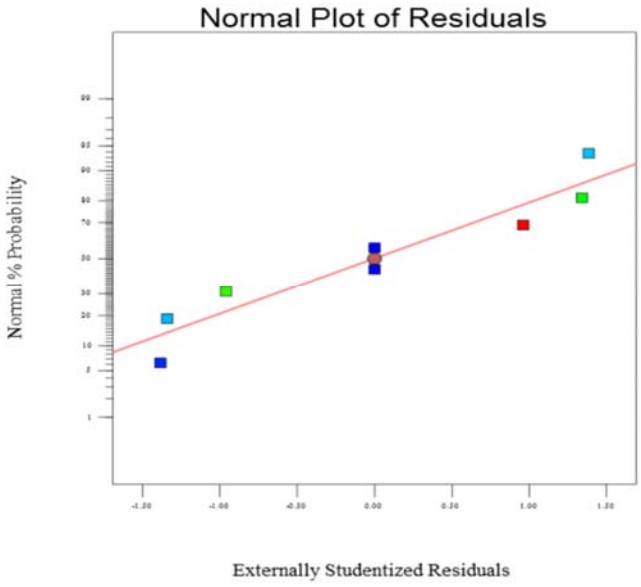

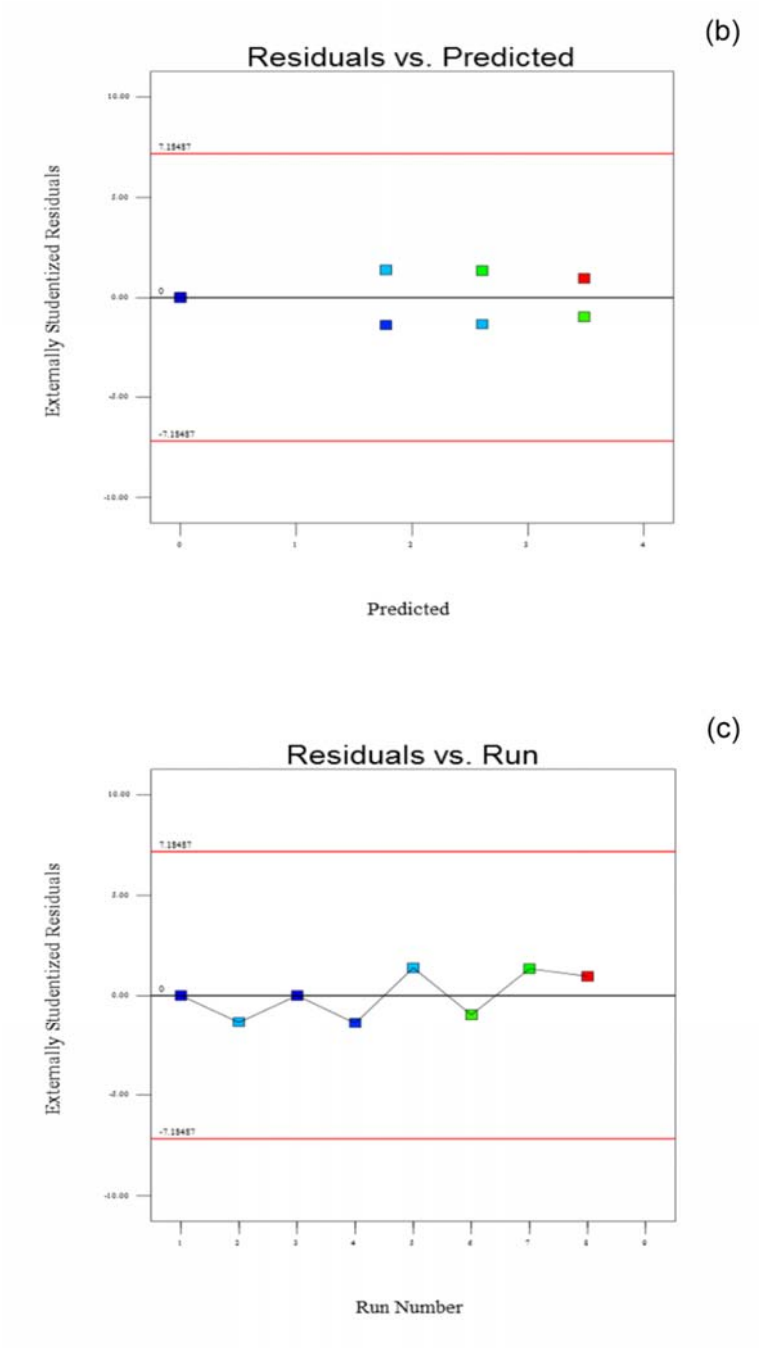

Figure 5-8. The residual diagnostics for the 2^3 FD. (a: normal plot of residuals; b: residual versus predicted plot; c: residual diagnostics versus run plot.)

5.4.6 Characterization of 5.1

^{1}H NMR δ_H (298 K, 300 MHz; DMSO-d_6; Me_4Si) 2.09 (s, 3H), 6.33 (s, 1H), 8.39 (s, 1H), 9.11 (s, 1H), 11.43 (s, 1H)

^{13}C NMR δ_C (298 K, 75 MHz; DMSO-d_6) 9.65, 123.58, 126.51, 142.23, 149.94, 176.48

MS *m/z* (% ion) 125 (100), 124 (72), 96 (31), 78 (4), 69 (6), 55 (12)

HRMS calculated exact mass for **5.1** ($C_6H_7NO_2$) = 125.0477, found = 125.0478, difference = 0.84 ppm

Selected IR data (cm^{-1}) solid 3139.15, 3046.29 (N-H stretch), 1618.88 (C=O stretch), 1570.92 (N-H bending)

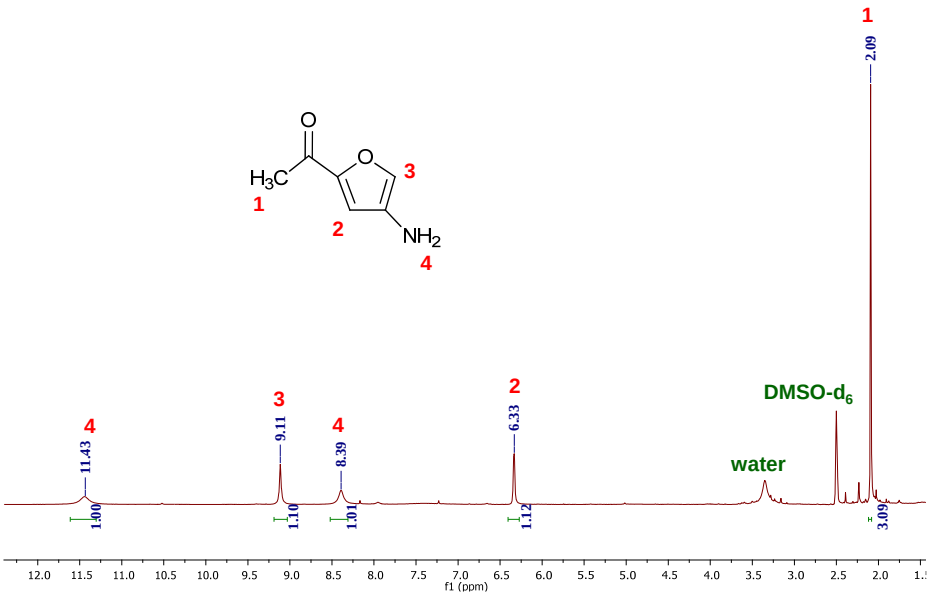

Figure 5-9. ^{1}H NMR spectrum of **5.1**.

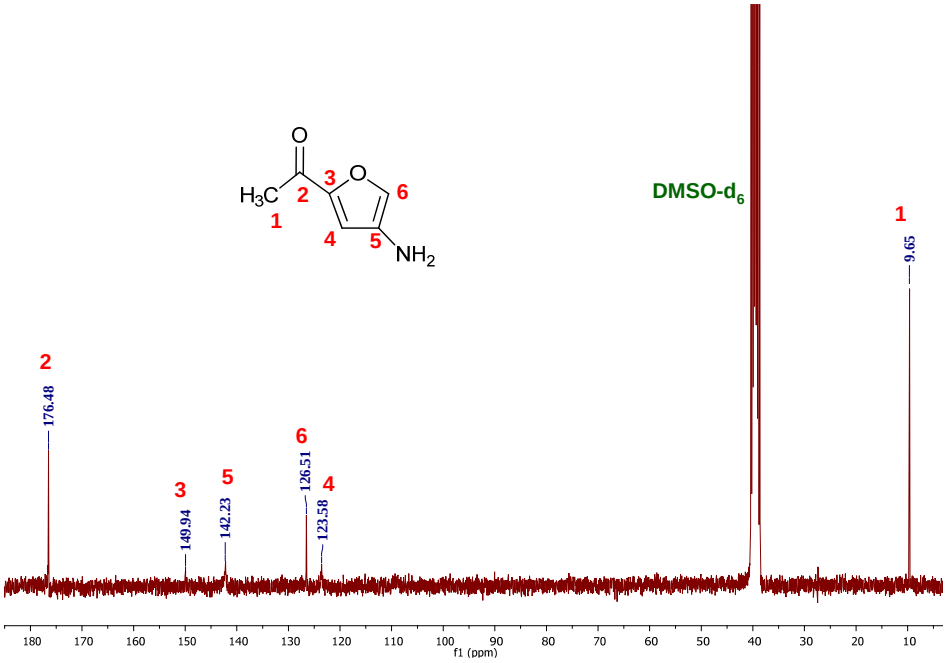

Figure 5-10. ^{13}C NMR spectrum of **5.1**.

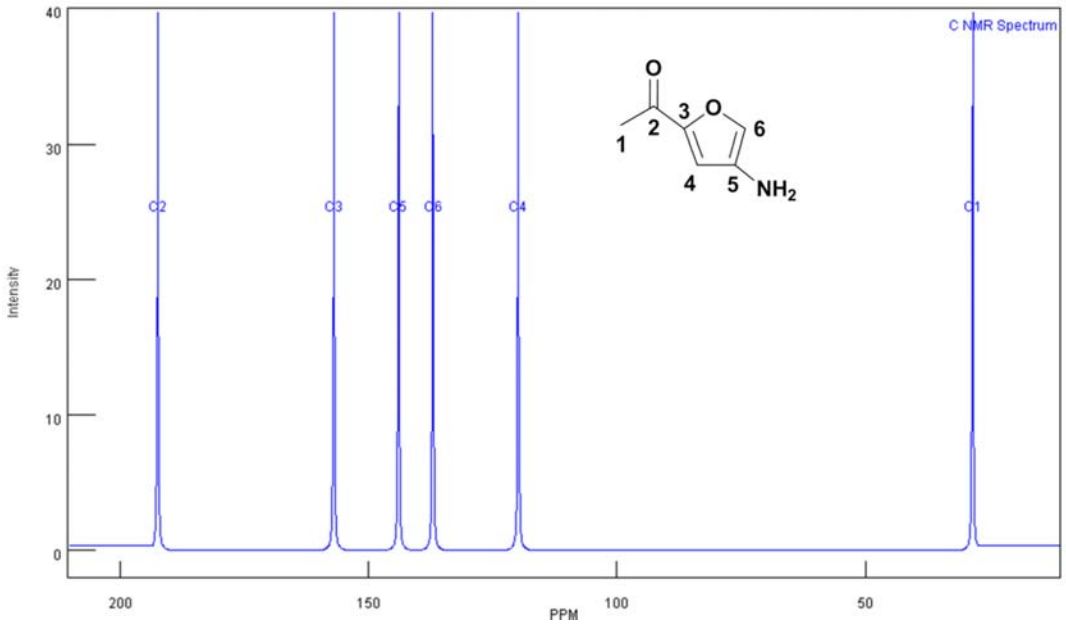

Figure 5-11.^{13}C NMR prediction of **5.1**.

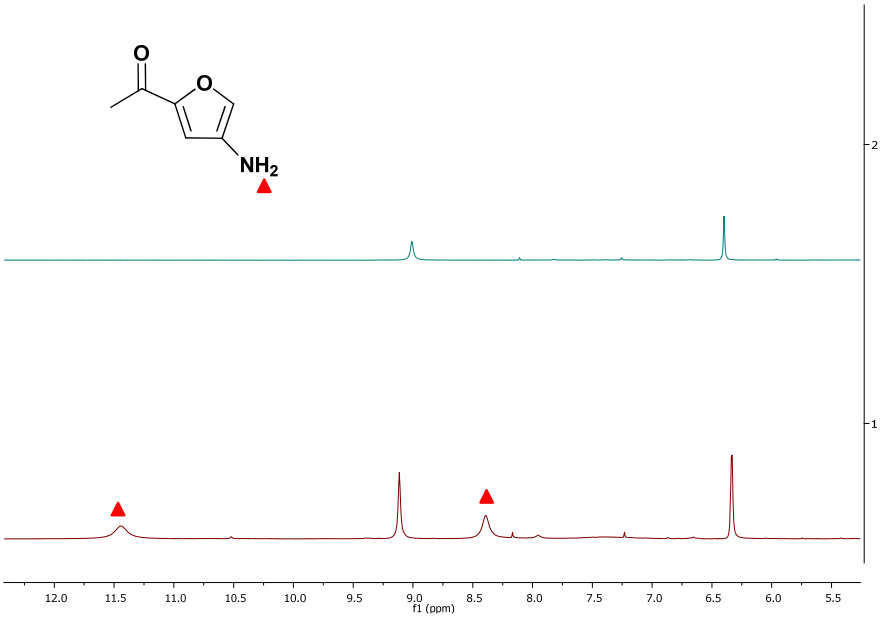

Figure 5-12. ^{1}H NMR spectrum of **5.1** before (bottom) and after (top) the addition of 10 µL D_2O.

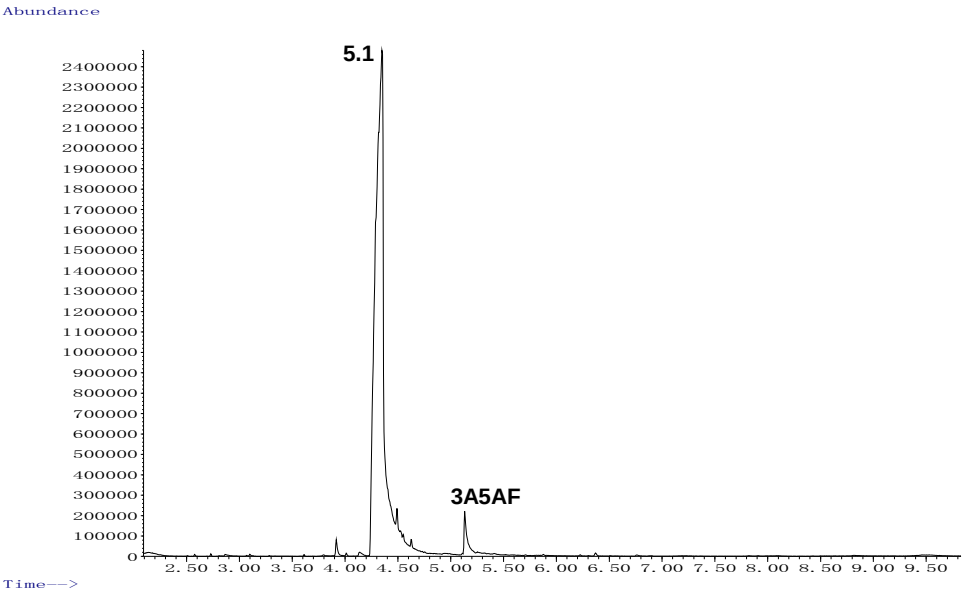

Figure 5-13. Gas chromatography of the reaction mixture of 3A5AF hydrolysis.

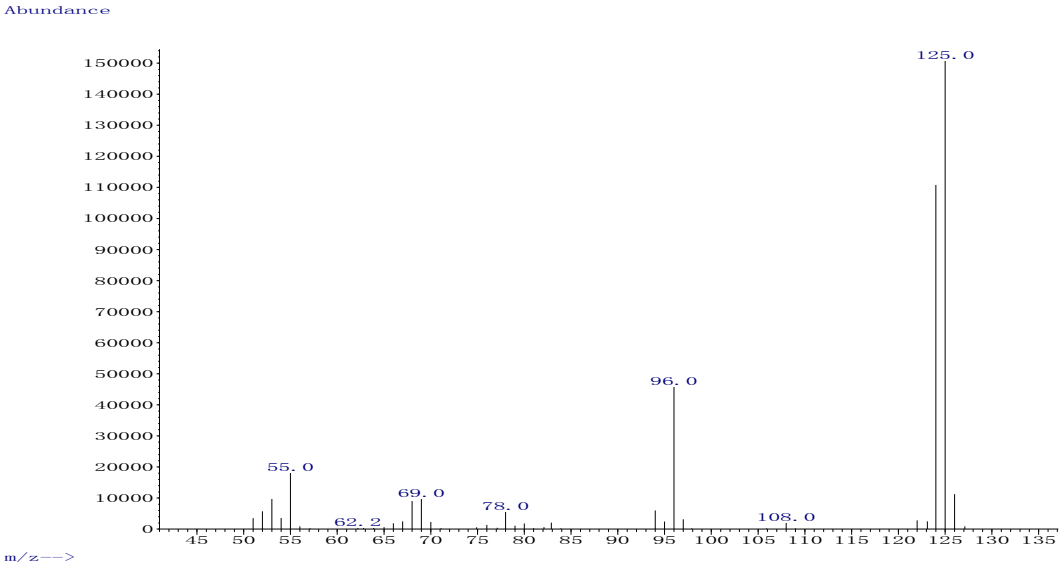

Figure 5-14. Mass spectrum of **5.1** (4.348 min).

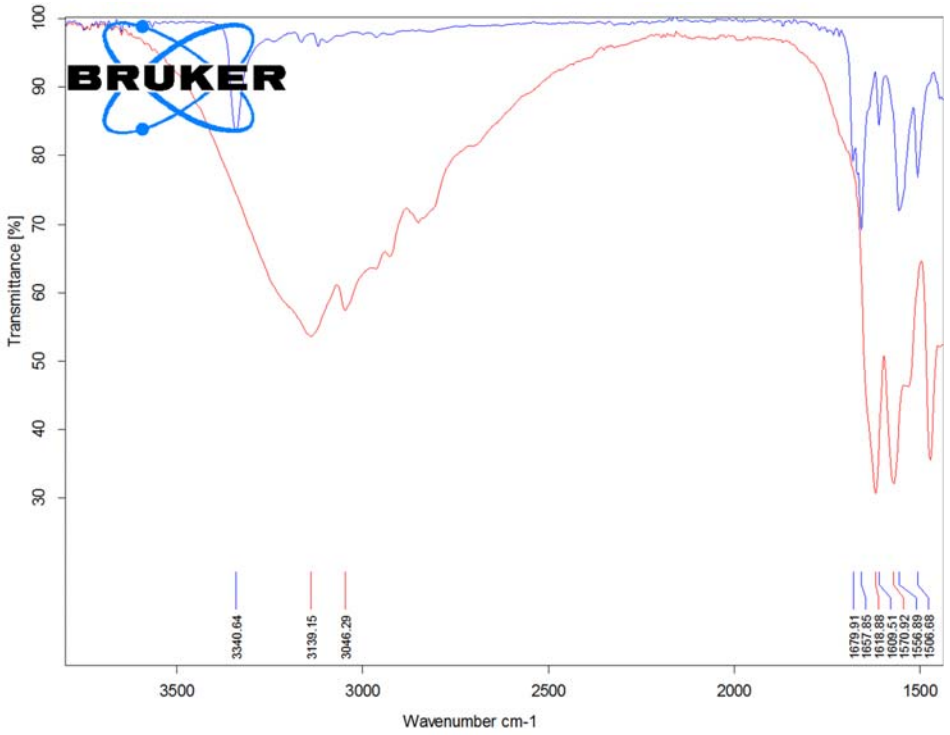

Figure 5-15. IR spectra of 3A5AF (blue) and **5.1** (red).

5.4.7 3A5AF Reduction Using $NaBH_4$

31.5 mg (0.188 mmol) 3A5AF was dissolved in 5 mL dry ethanol in a Schlenk tube. 21.2 mg (0.560 mmol) $NaBH_4$ was weighed in a Schlenk tube in a glovebox. After being transferred out of the glovebox, the $NaBH_4$ solid was dissolved in dry ethanol under N_2 flow. With N_2 flow and stirring going, the $NaBH_4$ solution was added dropwise to the 3A5AF solution at 0 °C in an ice bath. Afterwards, the ice bath was removed and the starting materials were stirred at room temperature overnight under N_2 flow. After the reaction, the mixture was filtered, and the filtrate was concentrated on a Rotavap at 130 mbar, 40 °C. A yellow oily liquid was obtained. Two aliquots were taken and dissolved in 500 μL EtOAc and 800 μL $CDCl_3$ respectively for GC-MS and NMR analyses. For the GC analysis, 1 μL of the sample was injected through a 7683B Series Injector using a split mode of 50%. The GC separation was done using a DB5 column at a flow rate of 1 mL/min He 99.999%. The oven temperature was programmed as follows: 50 °C (hold 1 min), 65 °C/min to 215 °C, 2.5 °C/min to 225 °C, and 20 °C/min to 250 °C for 1.2 min. (The total run time was 10 min). Products were detected at *m/z* 50 - 250 scan range. Under these conditions, the retention times of **5.2** and **5.3** were 5.252 and 4.689 min respectively.

5.4.8 Ir-catalyzed Reduction of 5-HMF and 3A5AF

The reactions were performed using standard glovebox techniques (with circulation turned off during manipulation of the alcohol). 5-HMF or 3A5AF (10 - 200 mg) were weighed into a vial and dissolved in isopropyl alcohol. Solutions of **5.4** (100 mg in 25 mL isopropyl alcohol) and KO*t*-Bu (300 mg in 25 mL isopropyl alcohol) were prepared. The

active catalyst was prepared by mixing these two solutions together in a vial in a mole ratio 1:15 Ir:KO*t*-Bu. The solution containing 5-HMF or 3A5AF was added dropwise to the vial containing **5.4**/ KO*t*-Bu, at a substrate:Ir ratio of 100:1. The reaction mixture was stirred for 2.5 h at room temperature. After which time, it was removed from the glovebox, filtered through a short plug of silica, rinsed with EtOAc and the solvents were removed under vacuum. In the case of 2,5-bis(hydroxymethyl)furan (BHMF), the resulting pale yellow solid was isolated in 95% yield and analytical data were consistent with the literature.[43] In the case of **5.2**, a yellow oil was isolated (80% yield) with ^{1}H and ^{13}C NMR spectra identical to those obtained via $NaBH_4$ reduction described herein.

5.4.9 Characterization of 5.2

^{1}H NMR δ_H (298 K, 300 MHz; $CDCl_3$; Me_4Si) 1.44 (d, 3H), 2.05 (s, 3H), 2.75 (s, 1H), 4.71 - 4.78 (q, 1H), 6.12 (s, 1H), 7.82 (s, 1H), 7.99 (s, 1H)

^{13}C NMR δ_C (298 K, 75 MHz; $CDCl_3$) 21.24, 23.14, 63.54, 100.28, 124.72, 131.43, 156.35, 168.14

MS *m/z* (% ion) 169 (20), 151 (64), 127 (16), 109 (71), 97 (13), 80 (100), 68 (9), 53 (24)

HRMS calculated exact mass for **5.2** ($C_8H_{11}NO_3$) = 169.0739, found = 169.0746, difference = 0.7 ppm

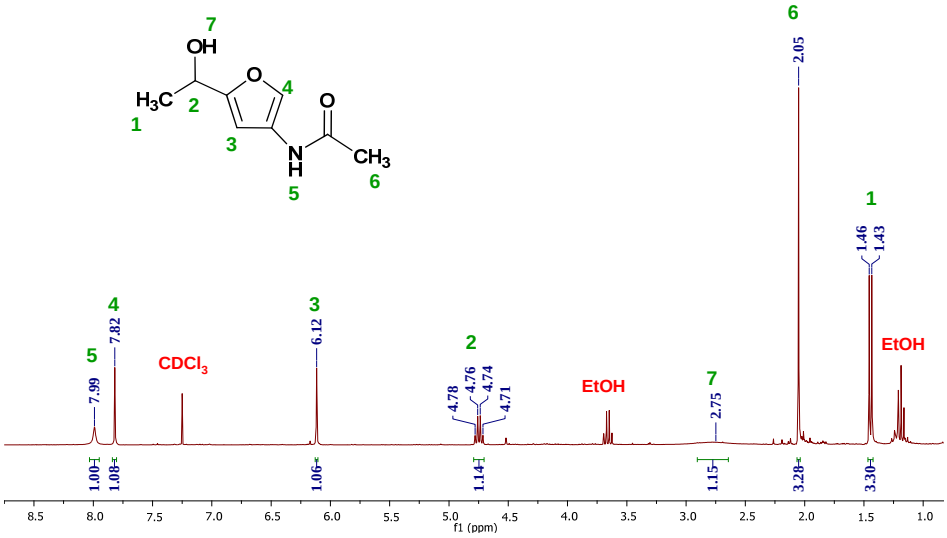

Figure 5-16. ^{1}H NMR spectrum of **5.2**.

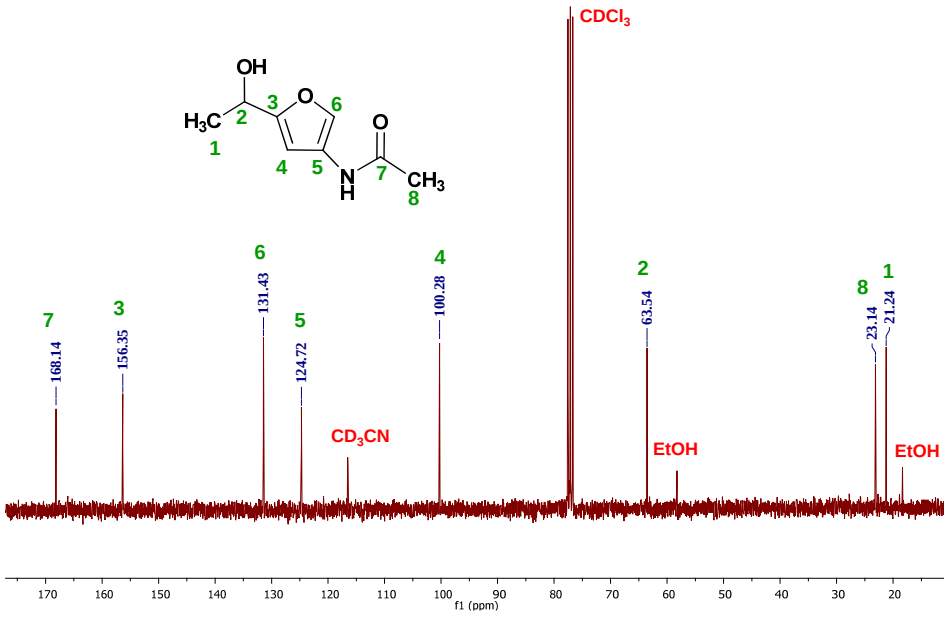

Figure 5-17. ^{13}C NMR spectrum of **5.2**.

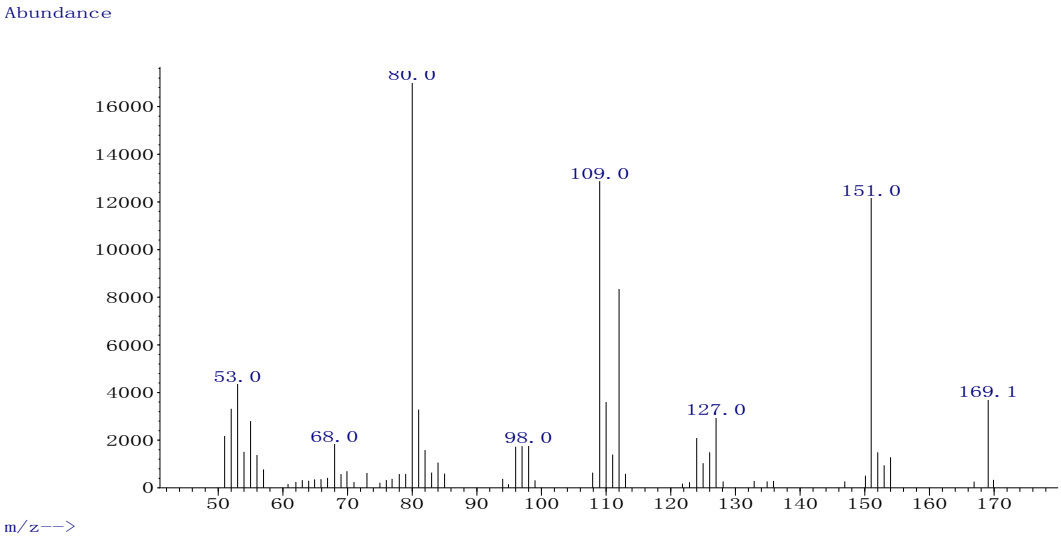

Figure 5-18. Mass spectrum of **5.2** (5.252 min).

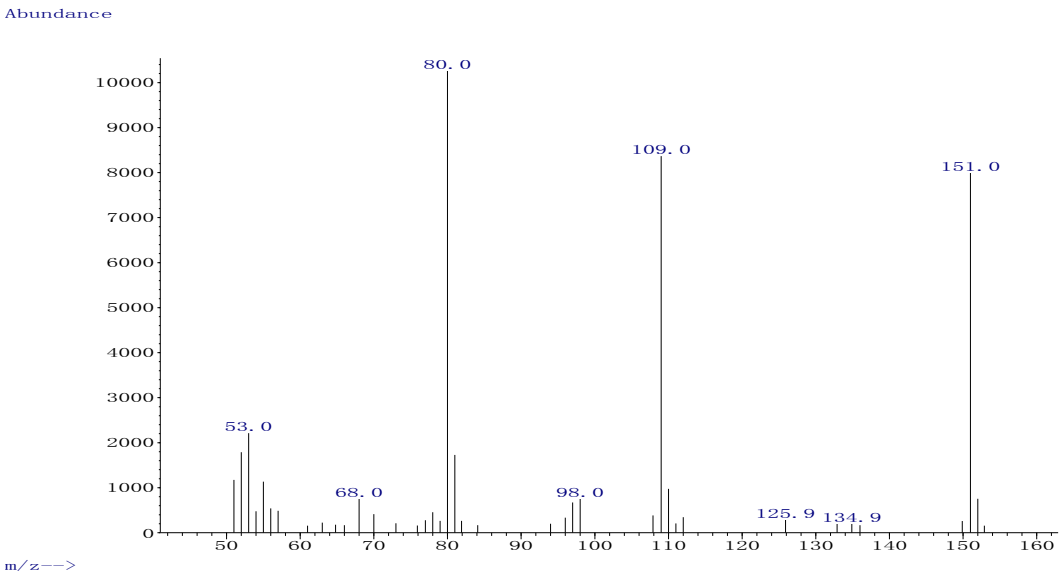

Figure 5-19. Mass spectrum of **5.3** (4.689 min).

5.4.10 Attempted CO_2 Capture Experiments

50.0 mg dry 3A5AF (or **5.1**) solid was dissolved in 1 mL dry methanol-d_4 (CD_3OD) and analyzed by ^1H and ^{13}C NMR spectroscopy. Afterwards, the sample was transferred to a Schlenk flask. The flask was freeze-pump-thawed three times to degas. In the first experiment, the solution was stirred at room temperature under CO_2 flow for 1 h. The second test was performed at 40 °C in an oil bath for 1 h. Subsequently, 30 μL deionized water was added into the solution. The mixture was stirred at room temperature and at 40 °C under CO_2 flow, each for 1 h. After each experiment the solution was analyzed by NMR spectroscopy and the results were compared with the original NMR spectra of 3A5AF or **5.1**.

In order to further study the deuterium exchange within 3A5AF, the CD_3OD was removed from the NMR sample using a Rotavap and the solid obtained was dissolved in 5 mL methanol. The solution was stirred overnight to allow the deuterium in 3A5AF to have sufficient exchange with protons in methanol. Then the solvent was evacuated using a Rotavap, and the solid obtained was dissolved in 500 μL EtOAc for GC-MS and 750 μL $CDCl_3$ for NMR analyses.

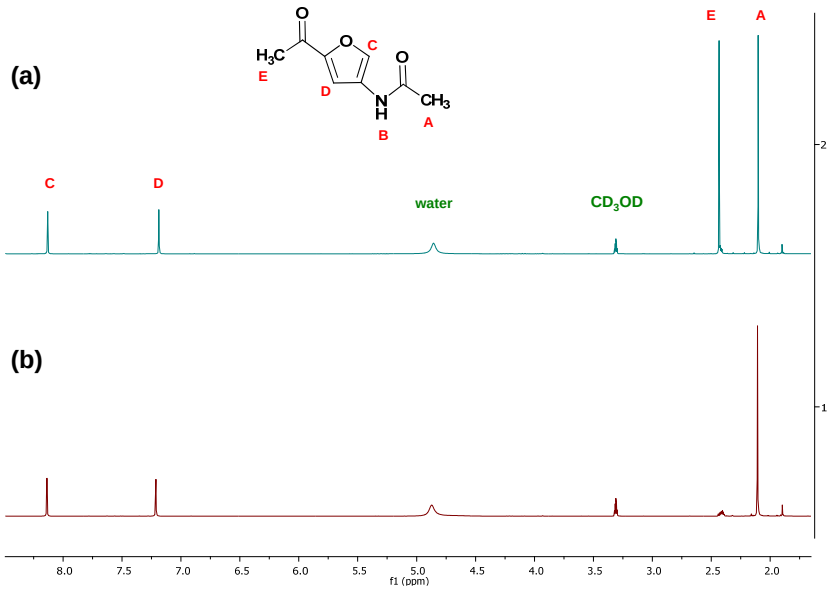

Figure 5-20. ^{1}H NMR spectra of 3A5AF in CD_3OD (a) initially (t = 0 min) before and (b) after deuterium exchange.

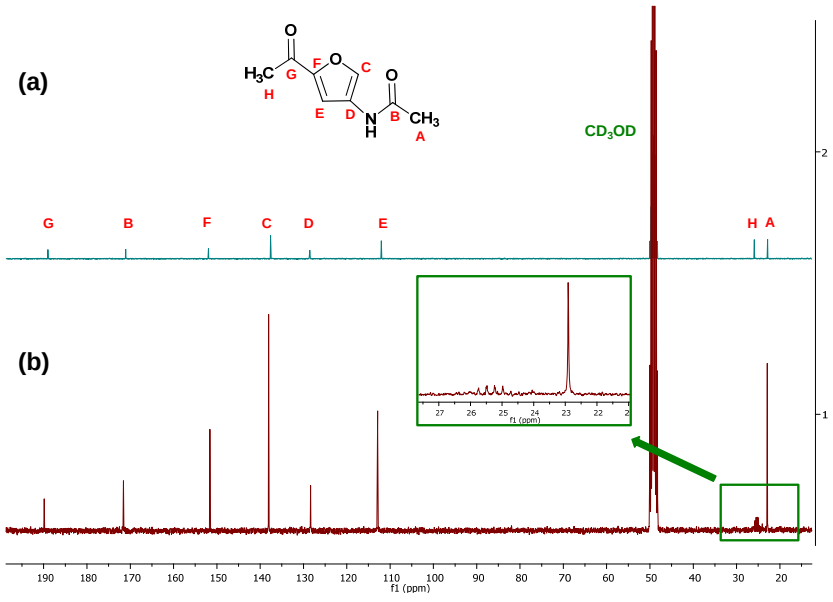

Figure 5-21. ^{13}C NMR spectra of 3A5AF in CD_3OD (a) initially (t = 0 min) before and (b) after deuterium exchange.

5.5 References

1. G. Fiorentino, M. Ripa and S. Ulgiati, *Biofuels, Bioprod. Biorefin.*, 2017, **11**, 195-214.

2. X. Zhang, H. Lei, S. Chen and J. Wu, *Green Chem.*, 2016, **18**, 4145-4169.

3. B. M. Upton and A. M. Kasko, *Chem. Rev.*, 2015, **116**, 2275-2306.

4. S. Chatterjee and T. Saito, *ChemSusChem*, 2015, **8**, 3941-3958.

5. X. Chen, B. Zhang, Y. Wang and N. Yan, *CHIMIA*, 2015, **69**, 120-124.

6. N. C. Yan, Xi, *Nature*, 2015, **524**, 155-157.

7. X. Chen, H. Yang and N. Yan, *Chem. Eur. J.*, 2016, **22**, 13402-13421.

8. R. A. Franich, S. J. Goodin and A. L. Wilkins, *J. Anal. Appl. Pyrolysis*, 1984, **7**, 91-100.

9. J. Chen, M. Wang and C.-T. Ho, *J. Agric. Food. Chem.*, 1998, **46**, 3207-3209.

10. K. W. Omari, L. Dodot and F. M. Kerton, *ChemSusChem*, 2012, **5**, 1767-1772.

11. M. W. Drover, K. W. Omari, J. N. Murphy and F. M. Kerton, *RSC Adv.*, 2012, **2**, 4642-4644.

12. X. Chen, S. L. Chew, F. M. Kerton and N. Yan, *Green Chem.*, 2014, **16**, 2204-2212.

13. X. Chen, Y. Liu, F. M. Kerton and N. Yan, *RSC Adv.*, 2015, **5**, 20073-20080.

14. Y. Liu, C. N. Rowley and F. M. Kerton, *ChemPhysChem*, 2014, **15**, 4087-4094.

15. R. Kuhn, W. Bister and W. Dafeldecker, *Justus Liebigs Ann. Chem.*, 1958, **617**, 115-128.

16. Z. E. Clarke, P. T. Maragh, T. P. Dasgupta, D. G. Gusev, A. J. Lough and K. Abdur-Rashid, *Organometallics*, 2006, **25**, 4113-4117.

17. T. Pasini, G. Solinas, V. Zanotti, S. Albonetti, F. Cavani, A. Vaccari, A. Mazzanti, S. Ranieri and R. Mazzoni, *Dalton Trans.*, 2014, **43**, 10224-10234.

18. M. Chatterjee, T. Ishizaka and H. Kawanami, *Green Chem.*, 2014, **16**, 4734-4739.

19. J. Han, Y.-H. Kim, H.-S. Jang, S.-Y. Hwang, J. Jegal, J. W. Kim and Y.-S. Lee, *RSC Adv.*, 2016, **6**, 93394-93397.

20. W. Hao, W. Li, X. Tang, X. Zeng, Y. Sun, S. Liu and L. Lin, *Green Chem.*, 2016, **18**, 1080-1088.

21. P. Yang, Q. Xia, X. Liu and Y. Wang, *Fuel*, 2017, **187**, 159-166.

22. CCP, CO_2 Capture Project, http://www.co2captureproject.org, (accessed January 24th, 2017).

23. N. MacDowell, N. Florin, A. Buchard, J. Hallett, A. Galindo, G. Jackson, C. S. Adjiman, C. K. Williams, N. Shah and P. Fennell, *Energy Environ. Sci.*, 2010, **3**, 1645-1669.

24. B. Dutcher, M. Fan and A. G. Russell, *ACS Appl. Mat. Interfaces*, 2015, **7**, 2137-2148.

25. H. Hall Jr, *J. Am. Chem. Soc.*, 1957, **79**, 5441-5444.

26. P. Moser, S. Schmidt, G. Sieder, H. Garcia, T. Stoffregen and V. Stamatov, *Energy Procedia*, 2011, **4**, 1310-1316.

27. T. Nguyen, M. Hilliard and G. Rochelle, *Energy Procedia*, 2011, **4**, 1624-1630.

28. S. A. Mazari, B. S. Ali, B. M. Jan, I. M. Saeed and S. Nizamuddin, *Int. J. Greenhouse Gas Control*, 2015, **34**, 129-140.

29. K.-S. Zoannou, D. J. Sapsford and A. J. Griffiths, *Int. J. Greenhouse Gas Control*, 2013, **17**, 423-430.

30. F. Vega, A. Sanna, B. Navarrete, M. M. Maroto-Valer and V. J. Cortés, *Greenhouse Gases: Sci. Technol.*, 2014, **4**, 707-733.

31. X. Wu, Y. Yu, Z. Qin and Z. Zhang, *Energy Procedia*, 2014, **63**, 1339-1346.

32. W. H. Chan, M. N. Mazlee, Z. A. Ahmad, M. A. M. Ishak and J. B. Shamsul, *J. Mater. Cycles Waste Manage.*, 2017, **19**, 1-14.

33. K. A. Mumford, Y. Wu, K. H. Smith and G. W. Stevens, *Front. Chem. Sci. Eng.*, 2015, **9**, 125-141.

34. J. E. Bara, D. E. Camper, D. L. Gin and R. D. Noble, *Acc. Chem. Res.*, 2009, **43**, 152-159.

35. K. Schneider, S. Keller, F. E. Wolter, L. Röglin, W. Beil, O. Seitz, G. Nicholson, C. Bruntner, J. Riedlinger and H.-P. Fiedler, *Angew. Chem. Int. Ed.*, 2008, **47**, 3258-3261.

36. H.-P. Fiedler, C. Bruntner, J. Riedlinger, A. T. Bull, G. Knutsen, M. Goodfellow, A. Jones, L. Maldonado, W. Pathom-Aree and W. Beil, *J. Antibiot.*, 2008, **61**, 158-163.

37. A. K Sharma, V. Beniwal, R. Kumar, K. Thakur and R. Sharma, *Nat. Prod. J.*, 2015, **5**, 72-81.

38. Y.-L. Nie, Y.-D. Wu, C.-X. Wang, R. Lin, Y. Xie, D.-S. Fang, H. Jiang and Y.-Y. Lian, *Nat. Prod. Res.*, 2014, **28**, 2134-2139.

39. A. Denisiuk, V. Schubert, F. E. Wolter, E. Irran, P. Trouillas and R. D. Süssmuth, *Bioorg. Med. Chem.*, 2013, **21**, 3582-3589.

40. F. Brucoli, A. Natoli, P. Marimuthu, M. T. Borrello, P. Stapleton, S. Gibbons and A. Schätzlein, *Bioorg. Med. Chem.*, 2012, **20**, 2019-2024.

41. M. J. Frisch, G. W. Trucks, H. B. Schlegel, G. E. Scuseria, M. A. Robb, J. R. Cheeseman, G. Scalmani, V. Barone, B. Mennucci, G. A. Petersson, H. Nakatsuji, M. Caricato, X. Li, H. P. Hratchian, A. F. Izmaylov, J. Bloino, G. Zheng, J. L. Sonnenberg, M. Hada, M. Ehara, K. Toyota, R. Fukuda, J. Hasegawa, M. Ishida, T. Nakajima, Y. Honda, O. Kitao, H. Nakai, T. Vreven, J. A. Montgomery, J. E. P. Jr., F. Ogliaro, M. Bearpark, J. J. Heyd, E. Brothers, K. N. Kudin, V. N. Staroverov, R. Kobayashi, J. Normand, K. Raghavachari, A. Rendell, J. C. Burant, S. S. Iyengar, J. Tomasi, M. Cossi, N. Rega, J. M. Millam, M. Klene, J. E. Knox, J. B. Cross, V. Bakken, C. Adamo, J. Jaramillo, R. Gomperts, R. E. Stratmann, O. Yazyev, A. J. Austin, R. Cammi, C. Pomelli, J. W. Ochterski, R. L. Martin, K. Morokuma, V. G. Zakrzewski, G. A. Voth, P. Salvador, J. J. Dannenberg, S.

Dapprich, A. D. Daniels, Ö. Farkas, J. B. Foresman, J. V. Ortiz, J. Cioslowski and D. J. Fox, Gaussian 09, Revision D.01, Gaussian, Inc., Wallingford, CT, 2009.

42. K. Raghavachari and G. W. Trucks, *J. Chem. Phys.*, 1989, **91**, 1062-1065.

43. A. D. Becke, *Phys. Rev. A*, 1988, **38**, 3098-3100.

44. C. Lee, W. Yang and R. G. Parr, *Phys. Rev. B*, 1988, **37**, 785-789.

45. S. H. Vosko, L. Wilk and M. Nusair, *Can. J. Phys.*, 1980, **58**, 1200-1211.

46. L. A. Curtiss, P. C. Redfern, K. Raghavachari, V. Rassolov and J. A. Pople, *J. Chem. Phys.*, 1999, **110**, 4703-4709.

47. J. Tomasi, B. Mennucci and R. Cammi, *Chem. Rev.*, 2005, **105**, 2999-3094.

48. M. Cossi, N. Rega, G. Scalmani and V. Barone, *J. Comput. Chem.*, 2003, **24**, 669-681.

49. A. Boyer and M. Lautens, *Angew. Chem. Int. Ed.*, 2011, **50**, 7346-7349

Chapter 6

Conclusions and Future Research

6.1 Conclusions

In **Chapter 1**, green chemistry and renewable feedstocks were introduced. NAG, as the monomer of chitin (a form of oceanic biomass) and the main reactant in 3A5AF synthesis performed in the current Ph.D research, was described from its production and applications. As they form a significant component in biomass utilization studies, carbohydrates were also introduced. The transformation of biomass into useful chemicals (i.e. 5-HMF and 3A5AF) was reviewed, and the applications of these biomass-derived compounds were discussed. Different sorts of solvents were introduced, with ILs specifically discussed in detail since they are playing an increasingly important role in various chemical processes.

The review in **Chapter 2** demonstrated a collection of mechanisms proposed in conversion of carbohydrates (fructose, glucose, sucrose and glucose) to 5-HMF and the techniques used for investigation. There are mainly two proposed reactions routes (cyclic and acyclic) for the dehydration of fructose, and most of the studies reviewed support the cyclic route. The dehydration of glucose has been proposed to occur either directly through some intermediates (e.g. 3-DG) or through the isomerisation of glucose to fructose, the second route being more favored. Two pathways, enolization or 1,2-hydride shift, have been proposed for the isomerisation of glucose. Lewis acids have been widely used as catalysts in glucose conversion, and their coordination with glucose is a significant step in the whole process. The transformation of sucrose to 5-HMF has been proposed to proceed through its cleavage to form glucose and fructose. The conversion of cellulose starts with its hydrolysis to glucose. NMR spectroscopy and computational calculations are the two

most frequently used techniques in mechanistic research, and are often combined together for convincible results. Besides ^{1}H and ^{13}C, NMR spectroscopy of other elements (e.g. ^{17}O, ^{11}B) can also be performed. ^{13}C labelled carbohydrates can be used as reactants to track the locations of the labelled carbon atoms in the intermediates and products. Because of its easy-to-use and informative advantages, computational calculations have been used to analyze the energy changes during proposed reactions and the stability of intermediates. Besides these two approaches, other tools such as kinetic studies and UV-Vis spectroscopy have also been applied in some studies for mechanism investigation. Therefore, when similar research about biomass transformation is performed (such as that described in **Chapter 3**), one can refer to these relatively mature mechanisms and start the mechanistic study from these well-developed techniques.

In **Chapter 3**, the synthesis of 3A5AF from NAG in ILs was investigated. The 3A5AF yield was closely related to the acidity of the ILs and the addition of $B(OH)_3$ and NaCl. The 3A5AF yield was further improved through in situ extraction and multiple reaction runs of a single reaction mixture. Kinetic studies and NMR spectroscopy (^{1}H, ^{13}C and ^{11}B) were performed to investigate the reaction procedure and the intermediates involved. A mechanism different from the previous one in the work by Drover et al.[1] was proposed, and further studies (e.g. computational work) are needed for verification. The reusability of ILs was studied, and seawater was tried as the solvent in the reaction to replace NaCl. This study achieved decent yields of 3A5AF with moderate reaction temperature and time, increasing the availability of 3A5AF being studied as a promising platform chemical for renewable amines.

3A5AF is still a relatively new compound and as such little is known about its physical and chemical properties. Besides some studies on its synthesis via pyrolysis, there was no literature on its properties before the study described in **Chapter 4**. In this project, computational simulation and experimental analysis were combined to study some properties of 3A5AF, including its acidity in DMSO, its solubility in $scCO_2$, the intermolecular forces present within it and its reaction with a Grignard reagent. These findings will contribute to the design of reactions involving 3A5AF in future. For example, the dehydration of the hydroxyl functional group to form an alkene, which was found in the reaction of 3A5AF with CH_3MgBr (see **4.2.3.2**), will be well understood and expected for intermediates or products with similar structures.

The reactivity of 3A5AF was further explored in **Chapter 5**. The hydrolysis and reduction of 3A5AF were performed to obtain *N*-containing products, which were characterized through GC-MS, HRMS, NMR and IR spectroscopies. 3A5AF and the amine product (**5.1**) were tested for CO_2 absorption and antimicrobial screening, but negative results were obtained. Further studies on this biomass-derived heteroatom molecule should be performed.

6.2 Future Work

The dehydration of NAG represents a unique transformation of this molecule and also is novel in the field of carbohydrate transformations due to its nitrogen content. The product, 3A5AF, is a versatile renewable amide with great potential applications. So far the maximum yield of 3A5AF achieved was 62.3% (see **Chapter 3**), thus there is still scope to improve the efficiency of 3A5AF production. As was mentioned in **3.2.9**, it is promising to

use seawater as the replacement for NaCl (the additive) and water (the solvent). The influence of other minerals from seawater in 3A5AF synthesis should be investigated. $B(OH)_3$ can be added at the same time in order to increase the yield further. Microwave irradiation is a more controllable heating method compared to conventional heating,[2] and it can also be used to facilitate the production of 3A5AF. It is worth noting that microwave heating, long thought to be a purely academic pursuit, is being used industrially.[3]

In the early studies about NAG reactions, pyrolysis was performed to get 3A5AF.[4, 5] During pyrolysis, the reactant decomposes at high temperature in the absence of oxygen. The reaction temperature can reach above 1000 °C with a reaction time as short as 1- 10 s. In recent years pyrolysis has been widely used for the processing of biomass to get fuel-gas, bio-oil and biochar.[6-8] Usually there is no solvent used in pyrolysis so it is a "solvent-free" system, which reduces the pollution generated. Additives could be used to promote specific reactions, so I propose that the pyrolysis of NAG should be investigated with the addition of $B(OH)_3$ and NaCl. Furthermore, microwave irradiation and pyrolysis have been combined as an energy efficient technology in biomass utilization,[9, 10] which can also be tried in the future work towards the synthesis of 3A5AF or perhaps other novel nitrogen-containing products. Once a 3A5AF yield of 80% or higher can be obtained, or indeed a similarly good yield of another product, the scale of the synthesis could be enlarged for future industrial production and commercial applications.

Meanwhile, mechanistic studies are still needed for a better understanding of the NAG dehydration procedure and the design of reaction routes with higher 3A5AF yields obtained. Isotopic labelled starting materials can be used, such as ^{13}C labelled NAG and ^{35}Cl or ^{37}Cl

labelled NaCl. NMR analysis could be performed in situ to detect intermediates and to investigate the functions of B and Cl further. With such data in hand, more efficient additives can be designed for the achievement of higher 3A5AF yields. In addition, large scale reactions can be performed to isolate Chromogen I and III for identification. The proposed mechanism can be computationally simulated for determination of thermodynamic energy changes and the rate-limiting step.

The lack of information on 3A5AF properties is a barrier for further research about this compound. Although I have obtained data on its acidity and some other properties, studies on other basic physical properties, such as boiling point and solubility in water, should be carried out to get a clearer picture of 3A5AF. Chemical properties and applications of 3A5AF can be investigated through various types of reactions. For example, as discussed in **5.2.5**, there is a similarity in structure between 3A5AF and proximicin A, B and C (Figure 5-4), which have been studied as anticancer and antibiotic drugs.[11, 12] Therefore, it is promising to react 3A5AF as a precursor to a series of amido-furan compounds and study their pharmaceutical potential.

6.3 References

1. M. W. Drover, K. W. Omari, J. N. Murphy and F. M. Kerton, *RSC Adv.*, 2012, **2**, 4642-4644.

2. C. O. Kappe, *Chem. Soc. Rev.*, 2008, **37**, 1127-1139.

3. J.-F. Tremblay, *Chem. Eng. News*, 2016, **94**, 24-25.

4. R. A. Franich, S. J. Goodin and A. L. Wilkins, *J. Anal. Appl. Pyrolysis*, 1984, **7**, 91-100.

5. J. Chen, M. Wang and C.-T. Ho, *J. Agric. Food. Chem.*, 1998, **46**, 3207-3209.

6. M. Tripathi, J. Sahu and P. Ganesan, *Renew. Sust. Energ. Rev.*, 2016, **55**, 467-481.

7. A. Galadima and O. Muraza, *Energy Convers. Manage.*, 2015, **105**, 338-354.

8. A. V. Bridgwater, *Biomass Bioenergy*, 2012, **38**, 68-94.

9. C. Wu, V. L. Budarin, M. J. Gronnow, M. De Bruyn, J. A. Onwudili, J. H. Clark and P. T. Williams, *J. Anal. Appl. Pyrolysis*, 2014, **107**, 276-283.

10. F. Motasemi and M. T. Afzal, *Renew. Sust. Energ. Rev.*, 2013, **28**, 317-330.

11. F. Brucoli, A. Natoli, P. Marimuthu, M. T. Borrello, P. Stapleton, S. Gibbons and A. Schätzlein, *Bioorg. Med. Chem.*, 2012, **20**, 2019-2024.

12. F. E. Wolter, K. Schneider, B. P. Davies, E. R. Socher, G. Nicholson, O. Seitz and R. D. Süssmuth, *Org. Lett.*, 2009, **11**, 2804-2807.